Dissertation

submitted to the
Combined Faculties for the Natural Sciences and for Mathematics
of the

Ruperto-Carola University of Heidelberg, Germany

for the degree of

Doctor of Natural Sciences

put forward by

Rainer Stiele

born in Munich, Germany

Oral examination: 28th of April 2014

On the Thermodynamics and Phase Structure of Strongly-Interacting Matter in a Polyakov-loop–extended Constituent-Quark Model

Referees:

PD Dr. Jürgen Schaffner-Bielich

Prof. Dr. Jürgen Berges

On the Thermodynamics and Phase Structure of Strongly-Interacting Matter in a Polyakov-loop–extended Constituent-Quark Model

Abstract

Polyakov-loop–extended constituent-quark models are useful to investigate the chiral and (de)confinement phase structure and the thermodynamics of strongly-interacting matter. It is shown that taking into account the quark backreaction on the gauge-field dynamics as well as quantum and thermal fluctuations of quarks and mesons is crucial in such models to achieve results for order parameters and thermodynamics that are in line with non-perturbative calculations at vanishing chemical potential. The dependence of the results on remaining parameters is discussed. The investigations are extended to nonzero quark density and isospin. The impact of unquenching effects in the Polyakov-loop potential on the phase structure at non-vanishing quark densities is discussed. Predictions for thermodynamics at nonzero isospin are shown. Furthermore, the reliability of those models is tested by confronting its results with lattice data on the isospin dependence of the transition temperature. The phase structure of the three-dimensional temperature - isospin - quark density phase diagram is investigated. Moreover, the process of nucleation at small temperatures and large densities is investigated and the surface tension for the phase transition calculated. Some consequences of the results for the early Universe, for heavy-ion collisions, and for proto-neutron stars are discussed.

Über die Thermodynamik und Phasenstruktur stark wechselwirkender Materie in einem um den Polyakov-loop erweiterten Konstituentenquark-Modell

Zusammenfassung

Um den Polyakov-loop erweiterte Konstituentenquark-Modelle sind nützlich um die chirale Phasenstruktur und diejenige des Farbeinschlusses und die Thermodynamik stark wechselwirkender Materie zu erforschen. Es wird gezeigt, dass das Einbeziehen der Quarkrückwirkung auf die Eichfelddynamik, sowie von Quanten- und thermischen Fluktuationen von Quarks und Mesonen in solche Modelle entscheidend ist, um Ergebisse für Ordnungsparameter und die Thermodynamik zu erhalten, die im Einklang mit nicht störungstheoretischen Rechnungen bei verschwindendem chemischen Potential sind. Die Abhängigkeit der Ergebnisse von verbleibenden Parametern wird diskutiert. Die Untersuchungen werden zu nicht verschwindender Quarkdichte und Isospin erweitert. Die Auswirkungen von Unquencheffekten des Polyakov-loop Potentials auf die Phasenstruktur bei nicht verschwindenden Quarkdichten wird diskutiert. Vorhersagen für die Thermodynamik bei nicht verschwindendem Isospin werden gezeigt. Des Weiteren wird die Verlässlichkeit solcher Modelle getestet, in dem dessen Resultate Daten von Gitterrechnungen zur Isospinabhängigkeit der Übergangstemperatur gegenübergestellt werden. Die Phasenstruktur des dreidimensionalen Temperatur - Isospin - Quarkdichte Phasendiagramms wird untersucht. Ferner wird der Prozess der Nukleierung bei kleinen Temperaturen und großen Dichten eruiert und die Oberflächenspannung für den Phasenübergang berechnet. Einige Konsequenzen der Ergebnisse für das frühe Universum, für Schwerionenkollisionen und für Proto-Neutronensterne werden diskutiert.

Contents

1. Introduction

> «Un pays nouveau, un port magnifique,
> l'éloignement de la mesquine Europe, un nouvel
> horizon politique, une terre d'avenir et un passé
> presque inconnu qui invite l'homme d'étude à des recherches,
> une nature splendide et le contact avec
> des idées exotiques nouvelles.»
>
> From „Brasilien - Ein Land der Zukunft“ by Stefan Zweig

„Was die Welt im Innersten zusammenhält“, this was the topic of a lecture about elementary particles and fundamental forces that I attended at the event „Physik im Blick“ at Gießen University as a high school pupil. Now, a decade later, it's myself contributing to the investigations of the properties of strongly-interacting matter.

The determination of the properties of the elementary particles in the phase diagram of strongly-interacting matter at high temperatures and baryon densities is one of the major challenges of present high-energy physics research.

The thermodynamics of strongly interacting matter under such extreme conditions as shortly after the Big Bang [12–14], in high-energy heavy ion collisions [15–17], in the mechanism of supernovae explosions [18–21], and in the structure of compact stars [22–24] plays a major role in the understanding of these physical scenarios.

The possibility to probe such large temperatures and densities in current experiments at the Large Hadron Collider at CERN and the Relativistic Heavy Ion Collider at the Brookhaven National Laboratory, and especially in future experiments at the Facility for Antiproton and Ion Research at GSI and the Nuclotron-based Ion Collider Facility at the Joint Institute for Nuclear Research [25–29], calls for a detailed study of the transition between the low-temperature hadronic phase associated with confinement of massive constituent quarks and the high-temperature chirally symmetric quark-gluon plasma phase.

To interpret the data of these experiments and for theoretical predictions on the above discussed scenarios a thorough understanding and reliable description of the thermodynamics and equation of state of strongly-interacting matter is necessary. To approach this task different approaches exist.

Functional continuum methods are well suited for a combined study of the chiral and confining dynamics of quantum chromodynamics (QCD) at finite temperature and

density [30–35]. In recent years, much progress in this direction has been made within the functional renormalisation group (FRG) approach to QCD. However, to perform these non-perturbative calculations is highly non-trivial and computational time consuming such that they are limited so far to two quark-flavours in the chiral limit [36, 37].

A discretised version of QCD can be studied in Monte-Carlo calculations on a lattice. The latest generation of these calculations [38–42] are performed with physical quark masses and the results are extrapolated to the continuum. Nevertheless, there are still differences in the predicted equation of state. These type of calculations have been extended to non-vanishing isospin density [43–46] and can include the impact of magnetic fields [47–50]. But extensions to a non-vanishing (real) quark chemical potential remain a considerable obstacle due to the lack of an importance sampling procedure that is free of ambiguities in that case [51, 52].

Therefore, to obtain an adequate description of the hadron-quark phase transition and an equation of state at finite baryon density, low-energy effective models that capture the most important properties of strongly-interacting matter can be useful [53].

The Nambu–Jona-Lasinio model [54, 55] and Linear-σ model [56, 57] or Quark-Meson model [58–66] describe the strong interaction by meson exchange and include the generation of constituent-quark masses by spontaneous chiral symmetry breaking. In fact, these models emerge dynamically from first-principle QCD-flows at low energies. Their parameters that are defined at a certain infrared-scale can be extracted from a QCD RG-flow starting with the classical QCD action at a high (perturbative) ultraviolet scale. But these models do not account for confinement and therefore they fail in describing the QCD thermodynamics.

The inclusion of gluons can be obtained by coupling the constituent quarks to the gauge fields in form of the Polyakov-loop which results in the Polyakov-loop–extended Nambu–Jona-Lasinio [67–71] and Quark-Meson [72–78] models.

But on the mean-field level these models show nevertheless a sharper transition at zero densities than non-perturbative calculations as was shown in Ref. [73]. The proper renormalisation of the contribution of quantum fluctuations of quarks [75] and mesons [79] smoothens the transition. This effect gets enhanced by considering thermal fluctuations of quarks and mesons beyond one-loop with the help of the renormalisation-group flow equation [74, 76].

In these models for strongly-interacting matter the gauge potential is adjusted to lattice calculations of pure gauge theory [69, 71, 80, 81]. Such an analysis lacks the full inclusion of glue-matter dynamics to both the chiral as well as the (de)confinement physics. A first step towards the inclusion of the back-reactions of quarks on the gauge sector was done in Ref. [72] by estimating the change of the transition temperature of the Polyakov-loop potential when going from pure gauge theory to QCD.

In the functional renormalisation-group approach the pure gauge potential as well as

the glue part of the full effective potential in QCD can be calculated [36, 37, 82–84]. In the present work, these potentials are compared and a relation of both is extracted in Sec. 3.2.1 that allows to mimic the effect of the quark backreaction on the gauge sector.

Throughout this thesis this improvement of the Polyakov-loop potential from a pure gauge potential to the unquenched glue potential in full QCD is applied in the Polyakov-loop–extended Quark-Meson model with 2+1 quark flavours to which are also included thermal fluctuations of quarks and mesons and quantum fluctuations of quarks at one-loop order.

The results of this improved 2+1 flavour Polyakov-loop–extended Quark-Meson model for the temperature dependence of the quark condensates, the Polyakov loop and thermodynamic observables at vanishing chemical potential are compared to the results of latest non-perturbative lattice calculations [38–42] in Sec. 4.1. The impact of the different ingredients of the presented framework are discussed throughout this section and the robustness of the results is tested by analysing remaining parameter dependences.

In Sec. 4.2, the investigation of the phase structure of strongly-interacting matter in the presented framework is extended to non-vanishing quark chemical potential. It is explored how the different constituents of the model affect the phase structure and the applicability of such a model at nonzero densities is tested by comparison to results of non-perturbative calculations.

In all systems mentioned in the beginning, matter does not consist of equal amounts of protons and neutrons, i.e. one has a non-vanishing isospin density. Using Au or Pb beams in heavy ion collisions, the proton to neutron ratio is $\sim 2/3$. In astrophysical environments the initial proton fraction in supernovae is 0.4, reduces to 0.2 and finally reaches values of less than 0.1 in cold neutron stars. In the universe a large asymmetry in the lepton sector is allowed ($-0.38 < \mu_\nu/T < 0.02$) [85], which can shift the equilibrium conditions at the cosmological QCD transition [86]. Hence, in the description of the thermodynamics of strongly-interacting matter in all these scenarios of nature the impact of a non-zero isospin should not be overlooked.

One of the aspects in the extension of the phase diagram of strongly-interacting matter to nonzero isospin is the arising of a new phase. Charged pions couple to the isospin chemical potential and when this is equal to the in-medium pion mass there is the onset of pion condensation [87]. The running of the pion mass in the medium shifts the appearance of pion condensation to larger temperatures and densities.

To date, most of the calculations at non-vanishing isospin were done with only two quark flavours, neglecting strange quarks as relevant degrees of freedom at the energy scale of the chiral and deconfinement transition Furthermore, lattice calculations at nonzero isospin were performed so far only with unphysical heavy pion masses.

The extension of the Polyakov–Quark-Meson model to nonzero isospin is build in Sec. 2.3.1 and Chap. 3. The phase structure of strongly-interacting matter at non-

vanishing isospin before the onset of pion condensation is investigated in Sec. 4.3. The evolution of the order parameters and all relevant thermodynamic quantities with increasing isospin are calculated for 2+1 quark flavours and physical pion mass. The phase diagram for a nonzero isospin chemical potential is discussed and the impact of the pion mass on the curvature of the transition line is pointed out. For vanishing baryon chemical potential, the results for the isospin dependence of the pseudocritical temperature is compared to lattice data since in this case lattice calculations are free of the sign problem.

Testing the effective model with its parameters adjusted to provide a good description of lattice data at zero density in this fashion against lattice data at nonzero isospin is crucial to understand whether these models provide qualitative and quantitative accurate descriptions of the phase structure of strong interactions in general.

As discussed for example in Refs. [88–90], not only lattice QCD, but also effective models that possess gauge degrees of freedom do present the sign problem at nonzero quark chemical potential. This manifests in the appearance of an imaginary part of the in-medium effective potential. For such a complex function of complex variables, special care must be taken with respect to the meaning of a minimisation procedure that leads to the state of equilibrium of the system. Following an approach similar to the one in Ref. [90] in the context of the Polyakov–Nambu–Jona-Lasinio model, a change of variables is proposed in Sec. 3.3, followed by a simple approximation that renders the in-medium effective potential a real function of real variables at all quark chemical potentials. As a consequence, the effective potential in this approach possesses minima, as demanded for systems in equilibrium.

The computation of the surface tension and nucleation rates between two phases which are separated by a first-order phase transition, requires actually a precise definition and location of the minima of the potential. As discussed for example in Refs. [13, 91–98], the surface tension is a crucial parameter for the dynamics of a first-order phase transition in many scenarios of high-energy physics. A high surface tension can dynamically suppress a first-order phase transition that would be otherwise allowed if only the bulk equilibrium thermodynamics were considered. Its evaluation, however, is not available from first-principles QCD but can be performed in a relatively straightforward manner using effective models. In Secs. 5.1 and 5.2 the general computation of surface tensions in a first-order phase transition is reviewed. After that, it is discussed in Sec. 5.3 how to obtain an overestimate of the surface tension of a phase interface in the Polyakov–Quark-Meson model. The results for the surface tension are shown in Sec. 5.4 and the implications of these results are discussed.

Finally, in Sec. 6 are given the conclusions and the final discussions of the obtained results and possible continuations are outlined.

The results presented in this thesis or intermediate versions thereof are published in the following publications

[1] B. W. Mintz, R. Stiele, R. O. Ramos, and J. Schaffner-Bielich, "Phase Diagram and Surface Tension in the 3-flavor Polyakov-Quark-Meson Model," *Phys. Rev.* **D 87** (2013) 036004, arXiv:1212.1184 [hep-ph].

[2] L. M. Haas, R. Stiele, J. Braun, J. M. Pawlowski, and J. Schaffner-Bielich, "Improved polyakov-loop potential for effective models from functional calculations," *Phys. Rev.* **D 87** (2013) 076004, arXiv:1302.1993 [hep-ph].

[3] R. Stiele, E. S. Fraga, and J. Schaffner-Bielich, "Thermodynamics of (2+1)-flavor strongly interacting matter at nonzero isospin," *Phys. Lett.* **B 729** (2014) 72–78, arXiv:1307.2851 [hep-ph].

[4] T. K. Herbst, M. Mitter, J. M. Pawlowski, B.-J. Schaefer, and R. Stiele, "Thermodynamics of QCD at vanishing density," *Phys. Lett.* **B** (2014) arXiv:1308.3621 [hep-ph].

and are presented in the following proceedings

[6] B. W. Mintz, R. Stiele, R. O. Ramos, and J. Schaffner-Bielich, "Nucleation of quark matter in the PQM model," *AIP Conf. Proc.* **1520** (2012) 370–372.

[5] R. Stiele, L. M. Haas, J. Braun, J. M. Pawlowski, and J. Schaffner-Bielich, "QCD thermodynamics of effective models with an improved Polyakov-loop potential," *PoS* **ConfinementX** (2012) 215, arXiv:1303.3742 [hep-ph].

[7] R. Stiele and J. Schaffner-Bielich, "The QCD Phase Transition at finite Isospin," *PoS* **ConfinementX** (2012) 333.

[8] T. K. Herbst, M. Mitter, J. M. Pawlowski, B.-J. Schaefer, and R. Stiele, "Exploring the Phase Structure and Thermodynamics of QCD," *PoS* **QCD-TNT-III** (2014) 030, arXiv:1401.1735 [hep-ph].

2. Quantum Chromodynamics

2.1. Historical Review and Fundamental Properties of QCD

[1] The search for the basic building blocks of matter is a fundamental question for philosophers and scientists since millennia. The four classical elements of alchemy have already been replaced by the consideration of smallest indivisible particles of matter by the Greek philosopher Democritus around 450 B.C. who coined the term 'átomos'. In the first decade of the 20th century the gold foil experiment performed by H. Geiger and E. Marsden under the direction of E. Rutherford [103] lead to the discovery that what is considered as a atom in its scientific definition contains an atomic nucleus [104]. Still in the same decade it was the same E. Rutherford who performed the first fission of an nucleus in which he discovered the proton as one of the building blogs of nuclei and conceived the possible existence of neutrons [105]. The neutron was discovered as second constituent of nuclei by J. Chadwick, an associate of E. Rutherford in 1932 [106], for which he was awarded the Nobel prize in 1935.

The first step in the exploration of the strong interaction was done by H. Yukawa who investigated which interaction binds protons and neutrons inside a nucleus. His considerations have been that it has to be a force that is stronger than electromagnetism and that it has to have a short range to be able to explain the size of nuclei of a few fermi. H. Yukawa predicted in 1935 a 'medium-heavy' particle called meson which mediates this strong force. It creates between nucleons a Yukawa-potential $V_{\text{Yukawa}}(r) = -g^2 \exp(-mr)/r$, which is a screened Coulomb-potential [107]. Heisenberg's uncertainty principle $\Delta E \Delta t \geq 1$ allows to estimate the mass of this particle and its range of a few fermi corresponds to a mass of the order of 100 MeV.
Particle accelerators did not reach this energy scale at that time but researches tried to detect this particle in the cosmic rays that have been discovered by V. F. Hess in 1912 [108]. This led first to the discovery of the muon but its long range in matter ruled out that it participates in the strong interaction. D. H. Perkins and C. M. G. Lattes, G. P. S. Occhialini and C. F. Powell discovered in 1947 with the charged pions the first mesons in the microscopic inspection of photographic emulsions that they had exposed at high altitudes [109–111]. In 1948, E. Gardner, C. M. G. Lattes and their team first artificially produced pions at the Lawrence Berkeley National Laboratory [112]. Finally, H. Yukawa received the Nobel prize in 1949 for his theoretical prediction of the existence of mesons.

[1] The structure of this section is inspired by Refs. [99–101] with further information gained from Refs. [28, 102] and the given original references.

With the improvement of cyclotron accelerators to synchrotrons and the development of new particle detection techniques such as bubble chambers, photomultipliers and calorimeters, a hole zoo of resonances was observed in particle collisions at the leading accelerator facilities, the Lawrence Berkeley National Laboratory, the Brookhaven National Laboratory and the European Organization for Nuclear Research (CERN) in the 1950's and 60's. The detection of this zoo of hadrons imposed the question of a further substructure. To gain information about possible building blocks of these particles scientists classified them according to their properties such as electric charge and isospin as suggested by W. Heisenberg [113, 114] and E. Wigner [115] for the classification of nuclei and strangeness that was introduced by K. Nishijima and M. Gell-Mann in the 1950's [116–118].
With this criteria Y. Ne'eman and M. Gell-Mann could group the mesons and spin-1/2 baryons 1961 into octets [119, 120], a classification which M. Gell-Mann called the Eightfold Way. Applying the same principles of categorisation to baryons with spin 3/2 these form a decoupled. Combining the SU(2) symmetry group of isospin with the quantum number strangeness, M. Gell-Mann and G. Zweig independently found in the first half of the 1960's that this classification of the detected hadrons can be explained by composing them of constituent particles with an underlying SU(3) quantum number symmetry [121–124]. M. Gell-Mann coined the name quarks for these elementary particles and flavour for the distinguishing quantum number. This was the birth of the three lightest quark flavours, up, down and strange quarks. Mesons than consist of a quark and a antiquark and baryons contain three quarks. In 1969, M. Gell-Mann was awarded the Nobel prize for his contributions concerning the classification of elementary particles.
M. Gell-Mann considered that quarks could be fictitious constituents, while R. P. Feynman regarded them as obvious candidates for partons which he predicted to describe the character of the longitudinal momentum distributions in high energy hadron collisions in 1969 [125–127]. J. D. Bjorken and E. A. Paschos explained in the same year with the parton picture of hadrons the momentum-dependent scaling of the deep inelastic scattering cross section of electrons on nucleons [128]. Experimental evidence for the existence of quarks inside nucleons has been found throughout the second half of the 1960's at the Stanford Linear Accelerator Center. The deep inelastic scattering of electrons on protons and bound neutrons revealed the existence of three point-like centres of diffraction [129–131]. J. I. Friedman, Henry W. Kendall and Richard E. Taylor got honoured with the Nobel prize in 1990 for this finding.

As H. Yukawa investigated which force binds protons and neutrons inside nuclei, the question evolved to which interaction confined the quarks into nucleons. Evidence for an additional quantum number gave the observation of the resonances Δ^{++}, Δ^{-} and Ω^{-}. Its electric charge and decay products and total angular momentum of 3/2 oblige that they consist of three quarks of the same flavour with zero orbital angular momentum and all spins aligned, a state that contradicts Pauli's exclusion principle that no two

identical fermions may have the same quantum numbers. In 1964, O. W. Greenberg [132] and in 1965 M.-Y. Han and Y. Nambu [133] independently resolved the problem by proposing that quarks possess an additional SU(3) symmetry. M. Gell-Mann and H. Fritzsch phrased this observation in the first half of the 1970's in today's terms of a SU(3) gauge theory in which the three values that the quantum number could take are referred to as colours and the strong interaction is mediated by gluons that possess colour charge themselves [134]. Together with H. Leutwyler, they coined the term quantum chromodynamics (QCD) as the gauge theory of the strong interaction [135].
According to this theory all hadrons are colour-neutral states, meaning that the quark and antiquark of a meson carry a certain colour and its corresponding anti-colour and that the three quarks in baryons represent all three colours red, green and blue so that all hadrons are white. As a non-abelian gauge theory also the force mediators are charged and local gauge symmetry implies that these are massless as will be explained in the next section. Therefore, eight linear combinations are possible and gluons form a cloud octet. Because of the self-interaction of the gluons the force of the strong interaction increases at large distances.
The first experimental signature of the existence of gluons have been found in 1979 at the 'Doppel-Ring-Speicher' (DORIS) and 'Positron-Elektron-Tandem-Ring-Anlage' (PETRA) of the 'Deutsche Elektronen-Synchrotron' DESY in three jet events [136–138].

S. L. Glashow and J. D. Bjorken predicted a fourth quark flavour in 1964 [139] and the GIM mechanism developed in 1970 by S. L. Glashow, J. Iliopoulos and L. Maiani [140] to explain the suppression of flavour-changing neutral currents required the existence of this fourth quark flavour. These charm quarks were identified experimentally as the constituents of a newly observed meson in 1974 at the Stanford Linear Accelerator Center under B. Richter [141] and at the Brookhaven National Laboratory under S. Ting [142]. Both received the Nobel prize in 1976 for their discovery of this new, heavy particle.
The existence of a third generation of quarks was theorised in 1973 by M. Kobayashi and T. Maskawa to explain the observed charge-conjugation parity symmetry violation [143]. The bottom quark was discovered in 1977 at the Fermi National Accelerator Laboratory in a experiment led by L. M. Lederman, where proton-nucleus collisions produced the Υ-meson [144].
Finally, experimental evidence for the SU(6) flavour structure of QCD was found in 1995 by the observation of the top quark in proton-proton collisions at the Fermilab [145,146].

That the detection of the different quark flavours extended overall several decades can be attributed to the fact that their mass scales differ by several orders of magnitude. The current quark masses are given together with the numbers characterising the properties of strongly-interacting particles in Table 2.1. Today's standard model of particle physics compromises besides the elementary particles of the strong interaction also those of the electroweak interaction and their gauge bosons and the Higgs particle. It is depicted in Fig. 2.1.

Table 2.1.: Current quark masses and properties that characterise the strongly-interacting particles.

Flavour	Mass [MeV] [147]	Baryon number	Spin	Electric charge [e]	Isospin	Charm	Strange-ness	Top-ness	Bottom-ness
Up	$2.3^{+0.7}_{-0.5}$	1/3	1/2	+2/3	+1/2	0	0	0	0
Down	$4.8^{+0.5}_{-0.3}$	1/3	1/2	-1/3	-1/2	0	0	0	0
Strange	95 ± 5	1/3	1/2	-1/3	0	0	-1	0	0
Charm	$(1.275 \pm 0.025) \times 10^3$	1/3	1/2	+2/3	0	1	0	0	0
Bottom	$(4.18 \pm 0.03) \times 10^3$	1/3	1/2	-1/3	0	0	0	0	-1
Top	$(173.07 \pm 1.24) \times 10^3$	1/3	1/2	+2/3	0	0	0	1	0
Gluon	0	0	1	0	0	0	0	0	0

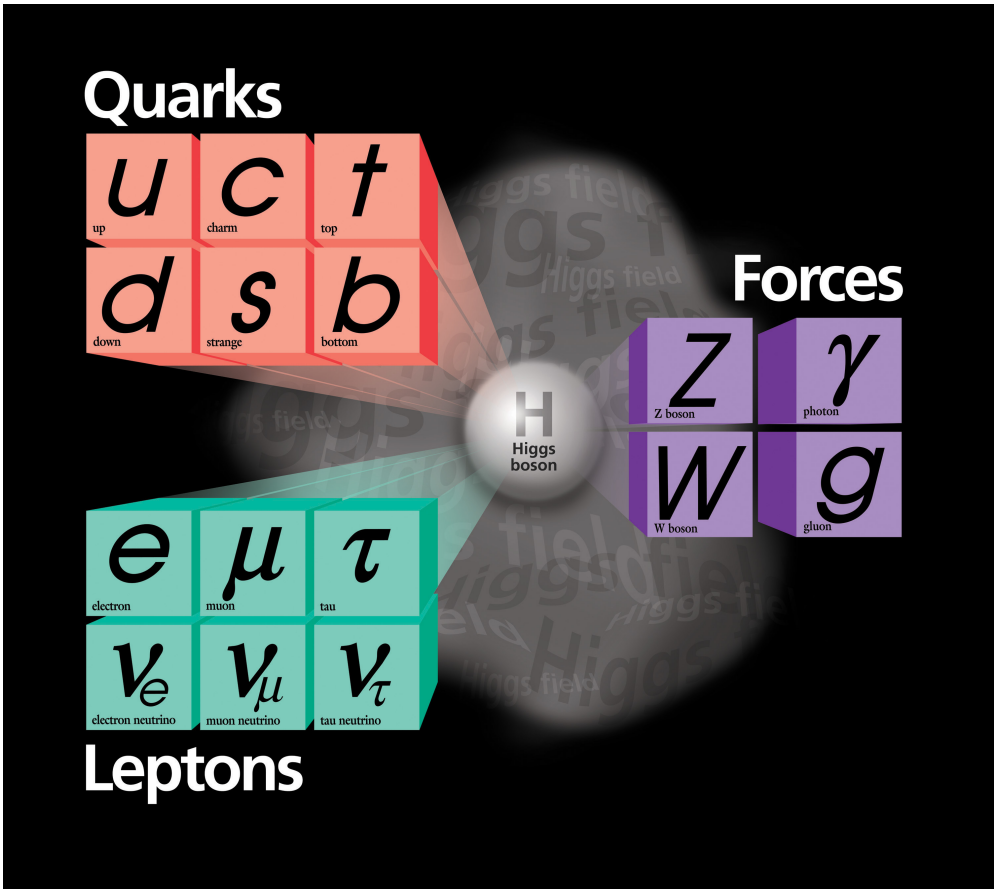

Figure 2.1.: Illustration of the standard model of particle physics. From Ref. [148] with courtesy of the Fermilab Visual Media Services.

The considerations of R. P. Feynman and J. D. Bjorken to describe the observations of deep inelastic scattering experiments implied that the nucleon constituents behave quasi free and interact only weakly inside a nucleon, so on very short distances or at very high momentum transfer. This was in opposition to the fact that the search for isolated quarks by that time didn't show any evidence which implies that at very long distances or small momentum transfer the strong interaction has to be very strong.
The former behaviour is known as asymptotic freedom which was discovered and described in 1973 by D. Gross and F. Wilczek [149–151] and independently by H. D. Politzer the same year [152, 153]. For their discovery, all three shared the Nobel Prize in physics in 2004. G. 't Hooft also noted the effect in 1972 but did not publish.
The variation of a coupling constant under changes of the scale can be understood as a consequence of shielding. In the vicinity of a charge the vacuum becomes polarised and when one approaches the source of the charge one penetrates the shielding cloud surrounding it and the effective charge one sees changes due to the loss of shielding. In case of the strong interaction this is a quantum effect and virtual quark-antiquark

pairs tend to screen the colour charge of a quark. But since gluons have colour charge themselves as well, also virtual gluons appear around a free quark that do not screen its field, but augment it. Getting closer to the central charge, one sees less and less of the effect of the vacuum. With decreasing distance the diminishing of the screening effect of the surrounding virtual quark-antiquark pairs increases the effective charge while the diminishing of the anti-screening effect of the surrounding virtual gluons weakens the effective charge. So virtual quarks-antiquark pairs and virtual gluons contribute opposite effects and which effect wins depends on the number of quark flavours and colour charges. In QCD, with three colours and six flavours anti-screening prevails and the theory is asymptotically free at short distances and large momentum transfer.
The variation of the theory's coupling constant is quantified in the β-function. In the lowest order in a renormalisation group expansion in the coupling constant the β-function is positive when the charge grows with shorter distances or negative when the charge decreases at short distances. Until 1973 only theories with the former behaviour of their β-function were known. D. Gross, H. D. Politzer and F. Wilczek discovered that non-abelian gauge theories allow for a negative beta function and concluded that the theory of colour charges had to be a of this type discovered by C. N. Yang and R. L. Mills in 1954 [154]. In lowest order in the coupling constant $\alpha_\mathrm{s} = g_\mathrm{s}^2/(4\pi)$ the β-function of the strong interaction is, see e.g. Ref. [102]

$$\beta \quad = \quad -\frac{g_\mathrm{s}^2}{48\pi^2}\,(11N_\mathrm{c} - 2N_\mathrm{f})\ . \tag{2.1}$$

So for any QCD-like theory with $N_\mathrm{f} < 5.5\,N_\mathrm{c}$ it is negative and the running coupling g_s decreases with increasing energy.

The finding that the strong coupling decreases towards high energies, justifies the application of perturbation theory for the theoretical description of high-energy scattering processes. On the other hand it implies that for small momenta the coupling tends towards a pole and a perturbative description breaks down. Therefore the long distance, strong-coupling behaviour which is thought to account for preventing the unbinding of quarks from hadrons, known as confinement cannot be addressed with perturbation theory. The running of the strong coupling shown in Fig. 2.2 illustrates the asymptotic free behaviour at large momentum transfers where it can be well described by perturbative QCD and its divergence at small energies.

At present there is no mathematical proof that QCD should be colour confining but the rise of the strong coupling constant with decreasing energy is compatible with it and a symmetry can be associated with confinement as will be discussed in detail in Sec. 2.2.2. But the confinement phenomenon is not sufficient to account for the observed mass spectrum of hadrons. This is characterised by light mesons that are much lighter than other hadrons. This observation can be attributed to spontaneous breaking of chiral symmetry at low energies. It justifies the effective description of the strong interaction at low energies via only weakly interacting pion degrees of freedom like H. Yukawa started the exploration of the strong interaction.

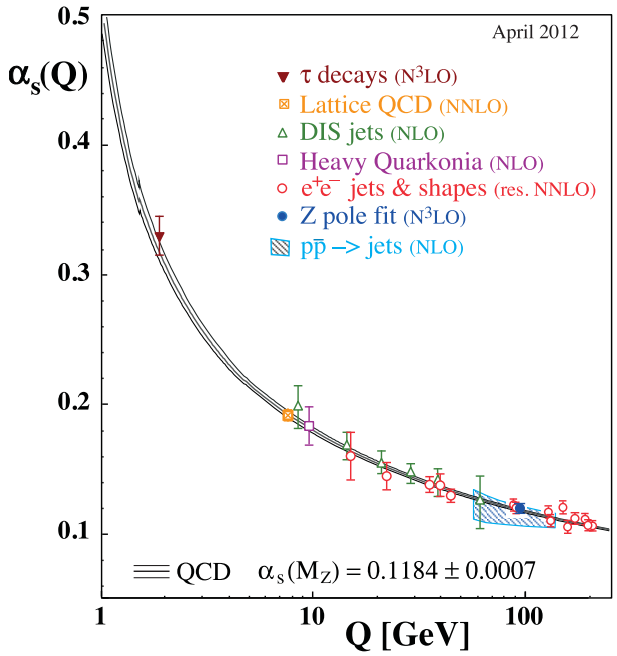

Figure 2.2.: Experimental data for the energy dependence of the strong coupling $\alpha_s = g_s^2/(4\pi)$ fitted with the 4-loop prediction of perturbation theory. From Ref. [147] with courtesy of the Particle Data Group.

In 1965 it was realised by R. Hagedorn that the application of a statistical thermal model to the particle production in heavy-ion collisions results in a resonance formation that grows exponentially towards a limiting temperature [155]. N. Cabibbo and G. Parisi suggested in 1975 that this exponential spectrum can be connected to a phase transition to a different phase where quarks are not confined [156]. In the late 1970s and beginning of the 80s investigations on space-time lattices of pure gauge theory and including quarks confirmed that at a certain temperature far before the asymptotic scenario the hadrons dissolve into a quark-gluon plasma [157–160]. It was as well realised in the 1970's that while a dilute system could be described in terms of hadronic degrees of freedom, with increasing density these extended composite particles would overlap and quarks and gluons would be free to roam in very dense systems [161–163].
From these two observations one can deduce a temperature-density phase diagram of strongly-interacting matter with one phase in which quarks are confined into massive hadrons and another phase of almost free, massless quarks and gluons as illustrated in Fig. 2.3. Two properties of strongly-interacting matter are entangled with these phases. One is the confinement of quarks into colour-singlet hadrons. The other one is quarks becoming massive which is connected to chiral symmetry breaking. So the question arises if these two transitions coincide and if they are linked over the whole phase diagram, at all temperatures and densities. Another question is the nature of the transition over the phase diagram, if it changes for large density and small temperature

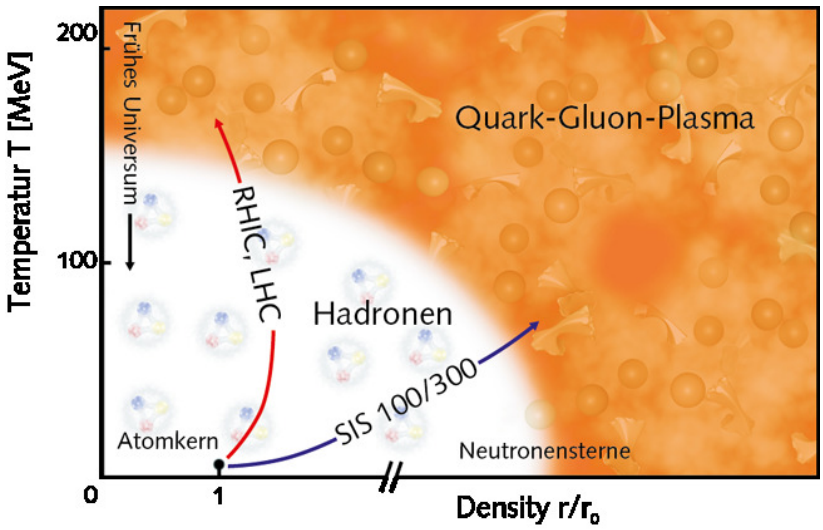

Figure 2.3.: Illustration of the temperature-density phase diagram of strongly-interacting matter. The abscissa is given in units of normal nuclear density ρ_0. It is expected that the quarks and their bonding particles, the gluons that are locked up inside massive hadrons at small temperature and/or density become liberated from confinement and move as free particles in a quark-gluon plasma at high temperature and/or density. From Ref. [164] with courtesy of the GSI Helmholtzzentrum für Schwerionenforschung GmbH.

compared to small density and large temperature. These are issues that will be addressed in the present work. A more detailed illustration of the phase diagram of strongly-interacting matter is shown in Fig. 2.4 in the plane of temperature and the quark chemical potential μ. At very high chemical potential and small temperature further phases could exist by effects like colour superconductivity and colour-flavour locking. These phenomena are beyond the scope of the present investigations. Inside the hadronic phase at small temperature and chemical potential is another phase transition that separates the vacuum that is characterised by vanishing baryon density from the nuclear matter phase. Different regions in the phase diagram have been, are and will be probed in nuclear collision experiments to find evidence of the phase transition from normal nuclear matter to a quark-gluon plasma and explore the nature of the transition and to investigate the properties of the quark-gluon plasma.

2.2. The QCD Lagrangian and its Symmetries

[2] The basic constituents of strongly-interacting matter are quarks and gluons. The quarks can be collected in a spinor in flavour space where each component is a spinor of N_c colour components. Free quarks obey a Lagrangian that is build up by a kinetic

[2] The line of argumentation of this section is inspired by that of Refs. [101, 166].

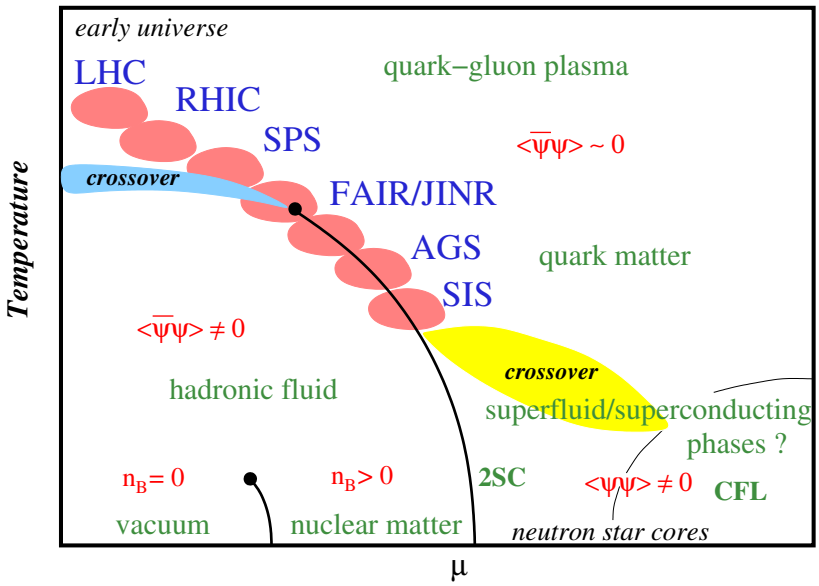

Figure 2.4.: Schema of the phase structure of strongly-interacting matter in the plane of temperature and quark chemical potential. After Ref. [165] with courtesy of B.-J. Schaefer.

term, a mass term and a chemical potential term

$$\bar{q}\,(\mathrm{i}\gamma_\mu\partial^\mu - m + \gamma_0\,\mu_f)\,q \quad , \tag{2.2}$$

where γ_μ denotes the Dirac matrices, the quark masses build up the diagonal matrix m and μ_f denotes the chemical potential of a quark flavour. In the Lagrangian the combination of the quark field q and antiquark field $\bar{q}$ has to be invariant under rotations in colour space

$$q\,(x) \to q'\,(x) = U(x)\,q\,(x) \qquad \text{with} \qquad U(x) = \exp\left(\mathrm{i}\,\epsilon_a(x)\,\frac{\lambda^a}{2}\right) \ , \tag{2.3}$$

where ϵ_a are the real parameters of the transformation and $\lambda^a/2$ are the N_c^2-1 hermitian generators of the gauge group SU(N_c). In the physical world with $N_\mathrm{c} = 3$, λ^a are the Gell-Mann matrices. Obviously, Eq. (2.2) is only invariant under this transformation if the transformation parameters are space-time–independent, i.e. under global SU(N_c) transformations. But the space-time dependence of the transformation parameters for a local transformation implies the necessity of a modification of Eq. (2.2) to ensure gauge invariance. The simple way out is to replace the partial derivative of the kinetic term by the covariant derivative

$$\mathcal{L}_\mathrm{q} = \bar{q}\,(\mathrm{i}\gamma_\mu D^\mu - m)\,q \qquad \text{with} \qquad D^\mu = \partial^\mu - \mathrm{i}\,g\,\frac{\lambda^a}{2}\,A_a^\mu + \delta^{\mu 0}\mu_f \ , \tag{2.4}$$

where g is the strong coupling constant and D_μ contains the $N_\mathrm{c}^2 - 1$ gauge fields of SU(N_c). In QCD with $N_\mathrm{c} = 3$ these gauge bosons are the gluons. Indeed the trans-

formation law of the gauge fields

$$A_\mu = \frac{\lambda^a}{2} A^a_\mu \quad \rightarrow \quad A'_\mu = U \left(A_\mu - \frac{\mathrm{i}}{g} U^\dagger \partial_\mu U \right) U^\dagger \tag{2.5}$$

ensures the gauge invariance of the Lagrangian (2.4).

Having introduced the gauge fields to the system one has to consider as well a kinetic and a mass term for these in the Lagrangian of QCD. But a mass term of the form $A_\mu A^\mu$ breaks gauge invariance explicitly and therefore, gauge fields have to be massless. The kinetic term of the vector gauge fields should contain the field strength tensor

$$F_{\mu\nu} \quad = \quad \partial_\mu A_\nu - \partial_\nu A_\mu \; . \tag{2.6}$$

But also in case of the gauge fields the most trivial ansatz for the kinetic term is not invariant under $\mathrm{SU}(N_\mathrm{c})$ transformations and the latter require the modification of the field strength tensor to

$$G^a_{\mu\nu} \quad = \quad \partial_\mu A^a_\nu - \partial_\nu A^a_\mu + g f^{abc} A^b_\mu A^c_\nu \; , \tag{2.7}$$

where f^{abc} denote the structure constants of the gauge group. The behaviour of this field strength tensor under a gauge transformation

$$G^a_{\mu\nu} \quad \rightarrow \quad G^a_{\mu\nu}{}' = U \, G^a_{\mu\nu} \, U^\dagger \tag{2.8}$$

implies that the colour trace

$$\mathcal{L}_\mathrm{g} \quad = \quad -\frac{1}{2} \, \mathrm{Tr_c} \, |G_{\mu\nu}| = -\frac{1}{4} \, G^a_{\mu\nu} \, G^{\mu\nu}_a \tag{2.9}$$

is a gauge invariant quantity which can be used as kinetic term for the gauge fields. This defines the Lagragian of pure gauge (Yang-Mills) theory. Having now gauge invariant kinetic and mass terms for the constituents of QCD, so quarks and gluons at hand, these can be collected to build up the Lagrangian of QCD

$$\mathcal{L}_\mathrm{QCD} \quad = \quad \bar{q} \left[\mathrm{i} \, \gamma_\mu \left(\partial^\mu - \mathrm{i} \, g A^\mu \right) - m + \gamma_0 \, \mu_f \right] q - \frac{1}{4} \, G^a_{\mu\nu} \, G^{\mu\nu}_a \; . \tag{2.10}$$

According to the principle of minimal coupling it only contains a coupling between quarks and gluons via the covariant derivative, so the coupling stems from the necessity of gauge invariance.

Besides the symmetry of the QCD Lagrangian (2.10) under $\mathrm{SU}(N_\mathrm{c})$ gauge transformations that was explicitly implied in its construction it is also interesting to study its behaviour under other transformations that characterise the properties of QCD.

A simple transformation is a global U(1) transformation which just multiplies the fields by a phase factor

$$q\,(x) \quad \rightarrow \quad q'\,(x) = \exp\left(\mathrm{i}\,\Theta\right) q\,(x) \;\; , \tag{2.11}$$

with $\Theta \in \mathbb{R}$. According to Noether's theorem, for every continuous transformation under which a Lagrangian is symmetric there exists a conserved current j_μ with corresponding conserved charge that is given by the space integral over the 0th component of the current. In case of the U(1) symmetry of QCD the conserved charge is the baryon number

$$B = \frac{1}{3}\int \mathrm{d}^3x\, \bar{q}\,(x)\,\gamma_0\, q\,(x) = \frac{1}{3}\int \mathrm{d}^3x\, q^\dagger q\ . \tag{2.12}$$

The vector current belonging to a global SU(N_f) symmetry is

$$V_\mu^a\,(x) = \bar{q}\,(x)\,\gamma_\mu\,\frac{\lambda^a}{2}\,q\,(x)\ , \tag{2.13}$$

with $\lambda^a/2$ as the $N_\mathrm{f}^2 - 1$ generators of the group SU(N_f), where λ^a are the Gell-Mann matrices for $N_\mathrm{f} = 3$. The divergence of this current

$$\partial^\mu V_\mu^a = \mathrm{i}\,\bar{q}\left[m, \frac{\lambda^a}{2}\right] q \tag{2.14}$$

only vanishes, so that the current (2.13) is conserved, if the quarks of all flavours are degenerated in mass because then the mass matrix is proportional to the unit matrix which commutates indeed with the generators of the group SU(N_f).
Therefore, the Lagrangian of strongly-interacting matter consisting only of up and down quarks and being isospin symmetric is symmetric under SU(N_f) vector transformations. Including the heavier strange quarks in $N_\mathrm{f} = 2+1$ the Lagrangian is no longer invariant to rotations in flavour space. Together with the even heavier quark flavours they break the flavour symmetry in QCD explicitly. Furthermore, Eqs. (2.13) and (2.14) show that the interaction between quarks and gluons is flavour-independent.

2.2.1. Chiral Symmetry

The energy range of the interesting phase structure of strongly-interacting matter is the low energy limit of QCD. Compared to the energy scale of the quark-hadron phase transition the masses of the five heaviest quark flavours are large and their dynamics can be neglected at these temperatures and densities. On the other hand, this scale is significantly larger than the masses of the light and strange quarks so that in a first approximation these can be assumed to be massless.

The Lagrangian in this so-called 'chiral limit' for reasons that become clear during the further discussion, is invariant under the following vector and axial-vector transformations in flavour space

$$q\,(x) \to q'\,(x) = \exp\left(\mathrm{i}\,\epsilon_a(x)\,\frac{\lambda^a}{2}\right) q\,(x)\ , \tag{2.15}$$

$$q\,(x) \to q'\,(x) = \exp\left(\mathrm{i}\,\gamma_5\,\epsilon_a(x)\,\frac{\lambda^a}{2}\right) q\,(x)\ , \tag{2.16}$$

with $\gamma_5 = \mathrm{i}\gamma_0\gamma_1\gamma_2\gamma_3$ in Minkowski space. The corresponding conserved vector and axial-vector currents are

$$V_\mu^a(x) = \bar{q}(x)\,\gamma_\mu\,\frac{\lambda^a}{2}\,q(x)\ , \tag{2.17}$$

$$A_\mu^a(x) = \bar{q}(x)\,\gamma_\mu\gamma_5\,\frac{\lambda^a}{2}\,q(x) \tag{2.18}$$

and the group structure of this symmetry of the Lagrangian of strongly-interacting matter in the chiral limit can be written as $\mathrm{SU}(3)_\mathrm{V} \otimes \mathrm{SU}(3)_\mathrm{A}$.
For another approach to this symmetry one can use the projection operators

$$P_\mathrm{R.L} = \frac{1}{2}\,(1 \pm \gamma_5) \tag{2.19}$$

to define right- and left-handed quarks as

$$q_\mathrm{R.L} = P_\mathrm{R.L}\,q \tag{2.20}$$

with which the Lagrangian in the chiral limit separates into independent contributions for left- and right-handed quarks

$$\mathcal{L}_\text{chiral limit} = \bar{q}_\mathrm{R}\mathrm{i}\gamma_\mu D^\mu q_\mathrm{R} + \bar{q}_\mathrm{L}\mathrm{i}\gamma_\mu D^\mu q_\mathrm{L} - \frac{1}{4}\,G_{\mu\nu}^a\,G_a^{\mu\nu}\ . \tag{2.21}$$

In this form one sees very well that this Lagrangian is invariant under separate transformations of right- and left-handed fermions

$$q_\mathrm{R,L}(x) \;\rightarrow\; q'_\mathrm{R,L}(x) = \exp\left(\mathrm{i}\,\epsilon_\mathrm{R,L}^a(x)\,\frac{\lambda^a}{2}\right) q_\mathrm{R,L}(x)\ . \tag{2.22}$$

So the symmetry group of chiral symmetry can be as well written as $\mathrm{SU}(3)_\mathrm{R} \otimes \mathrm{SU}(3)_\mathrm{L}$. The correspondence to vector and axial-vector symmetry can be shown explicitly using the conserved currents

$$j_\mathrm{R,L}^{a,\mu}(x) = \bar{q}_\mathrm{R,L}(x)\,\gamma^\mu\,\frac{\lambda^a}{2}\,q_\mathrm{R,L}(x) \tag{2.23}$$

and exploiting that the vector and axial-vector currents (2.17) and (2.18) can be written as linear combinations of these

$$V^{a,\mu}(x) = j_\mathrm{R}^{a,\mu}(x) + j_\mathrm{L}^{a,\mu}(x)\ , \tag{2.24}$$

$$A^{a,\mu}(x) = j_\mathrm{R}^{a,\mu}(x) - j_\mathrm{L}^{a,\mu}(x)\ . \tag{2.25}$$

The vector current (2.17) is of the same structure as that of the global $\mathrm{SU}(N_\mathrm{f})$ symmetry transformation (2.13), so for non-zero but degenerated quark masses it is still conserved and $\mathrm{SU}(2)_\mathrm{V}$ is a symmetry group of the Lagrangian of strongly-interacting matter. But the divergence of the axial-vector current takes the form

$$\partial_\mu A_a^\mu = \mathrm{i}\,\bar{q}\left\{m, \frac{\lambda^a}{2}\right\}\gamma_5\,q \tag{2.26}$$

which is non-vanishing for any non-zero quark masses. Therefore, a non-vanishing mass of a quark flavour breaks chiral symmetry explicitly which implies that the mass term in the Lagrangian mixes left- and right-handed quarks

$$\mathcal{L}_{\mathrm{QCD}} \quad = \quad \bar{q}_{\mathrm{R}} \mathrm{i} \gamma_\mu D^\mu q_{\mathrm{R}} + \bar{q}_{\mathrm{L}} \mathrm{i} \gamma_\mu D^\mu q_{\mathrm{L}} + \bar{q}_{\mathrm{R}}\, m\, q_{\mathrm{L}} + \bar{q}_{\mathrm{L}}\, m\, q_{\mathrm{R}} - \frac{1}{4}\, G^a_{\mu\nu}\, G^{\mu\nu}_a \ . \quad (2.27)$$

In general, a meson-like quark-antiquark state or quark condensate $\langle \bar{q} q \rangle$ mixes left- and right-handed quarks,

$$\langle \bar{q} q \rangle \quad = \quad \langle \bar{q}_{\mathrm{R}} q_{\mathrm{L}} \rangle + \langle \bar{q}_{\mathrm{L}} q_{\mathrm{R}} \rangle \ . \quad (2.28)$$

So, even though the Lagrangian itself is invariant under chiral transformations for massless quarks, the appearance of a non-vanishing quark condensate $\langle \bar{q} q \rangle$ breaks chiral symmetry spontaneously. Altogether, the quark condensate $\langle \bar{q} q \rangle$ is a order parameter for chiral symmetry breaking. The relation between quark masses, chiral symmetry and quark condensate can be exploited to explain the generation of constituent quark masses by spontaneous chiral symmetry breaking. The constituent quark mass of up and down quarks that are confined in protons or neutrons is of the order of one third of the mass of these nucleons, $\mathcal{O} \sim 300\,\mathrm{MeV}$ which is significantly larger than their current quark masses, $\mathcal{O} \sim \mathrm{MeV}$. While the non-zero current quark masses are responsible for explicit chiral symmetry breaking the constituent quark masses are dynamically generated by spontaneous chiral symmetry breaking, $m \sim \langle \bar{q} q \rangle$. This requires a mechanism that couples quarks to mesons which can be obtained by a Yukawa coupling.

With the spontaneous breaking of a symmetry comes along the appearance of a massless excitation in the particle spectrum which is called a 'Goldstone' boson. The additional explicit breaking of chiral symmetry by non-zero quark masses implies that these bosons are not massless. However, the current mass of the light up and down quarks is comparatively small, so that in this light quark sector axial-vector transformations are approximately symmetric and the axial-vector current is partially conserved. Therefore, the bosons belonging to spontaneous chiral symmetry breaking of light quarks are comparatively light compared to those associated to the heavier quark flavours.

2.2.2. Centre Symmetry

The opposite to the chiral limit of QCD is to consider all quarks as infinitely heavy so that one is left with the gluon dynamics. The Lagrangian then reduces to

$$\mathcal{L}_{\mathrm{YM}} \quad = \quad -\frac{1}{4}\, G^a_{\mu\nu}\, G^{\mu\nu}_a \ , \quad (2.29)$$

which represents the $\mathrm{SU}(N_\mathrm{c})$ pure gauge theory which is a 'Yang-Mills' theory. The corresponding partition function is

$$\mathcal{Z} = \mathrm{Tr}\left[\exp\left(-\beta H\right)\right] \qquad \text{or} \qquad \mathcal{Z} = \int \mathcal{D} A_\mu \exp\left(-\mathcal{S}\left[A_\mu\right]\right) \quad (2.30)$$

in the path integral formulation. So the Euclidean action reads

$$\mathcal{S}[A_\mu] \;=\; -\frac{1}{2}\int_0^\beta \mathrm{d}\tau \int \mathrm{d}^3x \;\mathrm{Tr}\,(G_{\mu\nu}\,G^{\mu\nu}) \tag{2.31}$$

where the gauge fields obey the periodic boundary condition

$$A_\mu(\tau+\beta,\vec{x}) \;=\; A_\mu(\tau,\vec{x})\ . \tag{2.32}$$

To the latter corresponds the following gauge transformation

$$U(\tau+\beta,\vec{x}) = h\,U(\tau,\vec{x})\ , \tag{2.33}$$

with h being an element of the gauge group $\mathrm{SU}(N_\mathrm{c})$ itself.
The transformation law of gauge fields (2.5) and the condition of gauge invariance of the Lagrangian restrict h to commute with the gauge fields. Elements of a group that commute with all elements of this group constitute the so-called centre of the group. So h has to be a member of the centre of $\mathrm{SU}(N_\mathrm{c})$, $h \in \mathbb{Z}(\mathrm{SU}(N_\mathrm{c}))$. These centre elements of $\mathrm{SU}(N_\mathrm{c})$ can be written as multiples of the N_c-dimensional unit matrix

$$h = z\mathbb{1} \qquad \text{with} \qquad z = \exp(2\pi\,\mathrm{i}\,n/N_\mathrm{c}) \qquad \text{and} \qquad n \in \{0,1,\ldots,N_\mathrm{c}-1\}\ . \tag{2.34}$$

So, a gauge symmetry under which the $\mathrm{SU}(N_\mathrm{c})$ pure gauge Lagrangian is invariant is centre symmetry.

Lifting the condition that the quarks are infinitely heavy they become dynamical fields again and one recovers the QCD Lagrangian (2.10). Under centre symmetry transformations quarks obey the transformation law (2.3) and furthermore, they fulfil anti-periodic boundary conditions

$$q(\tau+\beta,\vec{x}) \;=\; -q(\tau,\vec{x})\ . \tag{2.35}$$

This implies that quark fields transform under centre symmetry as

$$q'(\tau+\beta,\vec{x}) \;=\; -h\,U(\tau,\vec{x})\,q(\tau,\vec{x}) \tag{2.36}$$

$$\;=\; -z\,q'(\tau,\vec{x})\ . \tag{2.37}$$

This equation picks out a single centre element, namely $z = 1$ or $n = 0$, respectively. Hence, quarks are not symmetric under centre symmetry transformations and the presence of dynamical quarks breaks centre symmetry of the QCD Lagrangian explicitly.

For antiquarks the transformation law and anti-periodic boundary condition imply that they get multiplied with a factor $-z^\dagger$ under a centre symmetry transformation. Therefore, a quark-antiquark state obeys centre symmetry. The same is true for a state consisting of N_c quarks or N_c antiquarks for which a centre symmetry transformation is just a rotation by a multiple of 2π. Therefore, a hadronic phase where quarks and antiquarks are confined into mesons and baryons respects centre symmetry while deconfined quarks in a quark-gluon plasma phase break centre symmetry. Hence, the realisation or breaking of centre symmetry serves as an indication if strongly-interacting matter is confined or deconfined. Besides this explicit centre symmetry breaking by deconfined (anti-)quarks, the discussion of a order parameter for centre symmetry in Sec. 2.3.2 will reveal that it gets also spontaneously broken in the deconfined phase.

2.3. Effective Description of Symmetries

For any effective description of strongly-interacting matter it is important to capture the above discussed symmetries that reflect important properties of QCD, namely constituent quark masses and (de)confinement. In the 1960's, M. Gell-Mann and M. Levy and Y. Nambu and G. Jona-Lasinio made up the Linear-σ model [56, 57] and Nambu–Jona-Lasinio (NJL) model [54, 55] to describe spontaneous chiral symmetry breaking. For recent reviews of these models for QCD, see e.g. Refs. [60,167]. At non-zero temperature and quark density the former model can be extended to the Quark-Meson (QM) model. For centre symmetry the so-called Polyakov-loop can serve as an order parameter [157, 168, 169]. In this way, the Polyakov-loop extended versions of the NJL and QM models, PNJL [67–71] and PQM [4,72–74,76–78], take into account (de)confinement besides constituent quark masses.

2.3.1. Linear-σ Model

The quark condensate $\langle\bar{q}q\rangle$ represents a meson, so that one has to construct a Lagrangian for meson fields that describes spontaneous and explicit breaking of chiral symmetry and that reflects the above explained origin of explicit and spontaneous chiral symmetry breaking. Reference [57] found that it is governed by the following Lagrangian of the $N_\mathrm{f} = 3$ Linear-σ model

$$\begin{aligned}\mathcal{L}_\mathrm{m} &= \mathrm{Tr}\left(\partial_\mu\phi^\dagger\partial^\mu\phi\right) - m^2\mathrm{Tr}\left(\phi^\dagger\phi\right) - \lambda_1\left[\mathrm{Tr}\left(\phi^\dagger\phi\right)\right]^2 - \lambda_2\mathrm{Tr}\left[\left(\phi^\dagger\phi\right)^2\right] + \\ &\quad + c\left(\det\phi + \det\phi^\dagger\right) + \mathrm{Tr}\left[H\left(\phi + \phi^\dagger\right)\right] \ , \end{aligned} \tag{2.38}$$

where ϕ combines the scalar and pseudo-scalar meson fields

$$\phi = T_a\,\phi_a = \frac{\lambda_a}{2}\left(\sigma_a + \mathrm{i}\,\pi_a\right) \ . \tag{2.39}$$

The Gell-Mann matrices $\lambda_{1,\ldots,8}$ are completed by $\lambda_0 = \sqrt{\frac{2}{3}}\mathbb{1}$ as the nine generators of U(3). So the Lagrangian (2.38) covers besides chiral symmetry also U(1) transformations, U(3)=SU(3)⊗U(1). The U(1) transformation discussed in Sec. 2.2 under which the Lagrangian is symmetric is the vector transformation while the symmetry under axial-vector U(1) transformations is explicitly broken by the determinant terms in Eq. (2.38) and the coefficient c determines the strength of U(1) axial-symmetry breaking. It is the last term in Eq. (2.38), with $H = T_a\,h_a$ that breaks chiral symmetry explicitly.

Writing the matrix (2.39) explicitly out in its nine scalar and pseudo-scalar fields it consists of

$$T_a\,\varphi_a = \begin{pmatrix} \frac{\varphi_0}{\sqrt{6}} + \frac{\varphi_3}{2} + \frac{\varphi_8}{2\sqrt{3}} & \frac{\varphi_1}{2} - \mathrm{i}\frac{\varphi_2}{2} & \frac{\varphi_4}{2} - \mathrm{i}\frac{\varphi_5}{2} \\ \frac{\varphi_1}{2} + \mathrm{i}\frac{\varphi_2}{2} & \frac{\varphi_0}{\sqrt{6}} - \frac{\varphi_3}{2} + \frac{\varphi_8}{2\sqrt{3}} & \frac{\varphi_6}{2} - \mathrm{i}\frac{\varphi_7}{2} \\ \frac{\varphi_4}{2} + \mathrm{i}\frac{\varphi_5}{2} & \frac{\varphi_6}{2} + \mathrm{i}\frac{\varphi_7}{2} & \frac{\varphi_0}{\sqrt{6}} - \frac{\varphi_8}{\sqrt{3}} \end{pmatrix} \ , \tag{2.40}$$

with $\varphi_b \in \{\sigma_b, \pi_b\}$.

To implement spontaneous breaking of chiral symmetry one shifts the scalar meson fields by a vacuum expectation value $\bar{\phi} \equiv T_a\,\bar{\sigma}_a$ while the vacuum expectation value of the pseudo-scalar mesons is zero. Then the Lagrangian becomes [60]

$$\begin{aligned}\mathcal{L}_{\mathrm{m}} &= \frac{1}{2}\left[\partial_\mu\sigma_a\partial^\mu\sigma_a + \partial_\mu\pi_a\partial^\mu\pi_a - \sigma_a M^2_{s,ab}\sigma_b - \pi_a M^2_{p.ab}\pi_b\right] + \\ &+ \left(\mathcal{G}_{abc} - \frac{4}{3}\mathcal{F}_{abcd}\bar{\sigma}_d\right)\sigma_a\sigma_b\sigma_c - 3\left(\mathcal{G}_{abc} + \frac{4}{3}\mathcal{H}_{abcd}\bar{\sigma}_d\right)\pi_a\pi_b\sigma_c - \\ &- 2\mathcal{H}_{abcd}\sigma_a\sigma_b\pi_c\pi_d - \frac{1}{3}\mathcal{F}_{abcd}\left(\sigma_a\sigma_b\sigma_c\sigma_d + \pi_a\pi_b\pi_c\pi_d\right) - U\left(\bar{\sigma}\right)\ , \end{aligned} \tag{2.41}$$

where

$$M^2_{\mathrm{s},ab} = m^2\delta_{ab} - 6\mathcal{G}_{abc}\bar{\sigma}_c + 4\mathcal{F}_{abcd}\bar{\sigma}_c\bar{\sigma}_d\ , \tag{2.42}$$

$$M^2_{\mathrm{p},ab} = m^2\delta_{ab} + 6\mathcal{G}_{abc}\bar{\sigma}_c + 4\mathcal{H}_{abcd}\bar{\sigma}_c\bar{\sigma}_d\ , \tag{2.43}$$

$$U\left(\bar{\sigma}\right) = \frac{m^2}{2}\bar{\sigma}_a^2 - \mathcal{G}_{abc}\bar{\sigma}_a\bar{\sigma}_b\bar{\sigma}_c + \frac{1}{3}\mathcal{F}_{abcd}\bar{\sigma}_a\bar{\sigma}_b\bar{\sigma}_c\bar{\sigma}_d - h_a\bar{\sigma}_a\ , \tag{2.44}$$

with

$$\begin{aligned}\mathcal{G}_{abc} &= \frac{c}{6}\left[d_{abc} - \frac{3}{2}\left(\delta_{a0}d_{0bc} + \delta_{b0}d_{a0c} + \delta_{c0}d_{ab0}\right) + \right. \\ &\left. + \frac{9}{2}d_{000}\delta_{a0}\delta_{b0}\delta_{c0}\right]\ , \end{aligned} \tag{2.45}$$

$$\begin{aligned}\mathcal{F}_{abcd} &= \frac{\lambda_1}{4}\left(\delta_{ab}\delta_{cd} + \delta_{ad}\delta_{bc} + \delta_{ac}\delta_{bd}\right) + \\ &+ \frac{\lambda_2}{8}\left(d_{abn}d_{ncd} + d_{adn}d_{nbc} + d_{acn}d_{nbd}\right)\ , \end{aligned} \tag{2.46}$$

$$\mathcal{H}_{abcd} = \frac{\lambda_1}{4}\delta_{ab}\delta_{cd} + \frac{\lambda_2}{8}\left(d_{abn}d_{ncd} + f_{acn}f_{nbd} + f_{bcn}f_{nad}\right)\ , \tag{2.47}$$

where d_{abc} and f_{abc} are the structure constants of SU(3) that are symmetric or antisymmetric, respectively. These are given in App. B.

Equation (2.44) is the potential of the Linear-σ model at tree level and its derivative with respect to the scalar fields is

$$\frac{\partial U(\bar{\sigma})}{\partial\bar{\sigma}_a} = m^2\bar{\sigma}_a - 3\mathcal{G}_{abc}\bar{\sigma}_b\bar{\sigma}_c + \frac{4}{3}\mathcal{F}_{abcd}\bar{\sigma}_b\bar{\sigma}_c\bar{\sigma}_d - h_a\ . \tag{2.48}$$

The expectation values of the fields are minima of the potential so that $\partial U(\bar{\sigma})/\partial\bar{\sigma}_a = 0$ puts a necessary condition on the expectation values of the fields. To exclude other extrema than minima from the roots of Eq. (2.48) all eigenvalues of the Hessian matrix $\partial^2 U(\bar{\sigma})/\left(\partial\bar{\sigma}_a\partial\bar{\sigma}_b\right)$ have to be positive.

To ensure the quantum numbers of the vacuum in SU(3) only the condensates σ_0, σ_3 and σ_8 can be non-zero and the vacuum expectation value reduces to

$$\bar{\phi} = T_0\bar{\sigma}_0 + T_3\bar{\sigma}_3 + T_8\bar{\sigma}_8\ . \tag{2.49}$$

As a generalisation of Refs. [60,66] the potential (2.44) then takes the form

$$\begin{aligned} U\left(\bar{\sigma}_0,\bar{\sigma}_3,\bar{\sigma}_8\right) &= m^2\frac{\bar{\sigma}_0^2+\bar{\sigma}_3^2+\bar{\sigma}_8^2}{2}+\lambda_1\left(\frac{\bar{\sigma}_0^4+\bar{\sigma}_3^4+\bar{\sigma}_8^4}{4}+\frac{\bar{\sigma}_0^2\bar{\sigma}_3^2+\bar{\sigma}_0^2\bar{\sigma}_8^2+\bar{\sigma}_3^2\bar{\sigma}_8^2}{2}\right)+ \\ &+\lambda_2\left(\frac{\bar{\sigma}_0^4}{12}+\frac{\bar{\sigma}_3^4+\bar{\sigma}_8^4}{8}-\frac{\bar{\sigma}_0\bar{\sigma}_8^3}{3\sqrt{2}}+\frac{\bar{\sigma}_0^2\bar{\sigma}_3^2+\bar{\sigma}_0^2\bar{\sigma}_8^2}{2}+\frac{\bar{\sigma}_3^2\bar{\sigma}_8^2}{4}+\frac{\bar{\sigma}_0\bar{\sigma}_3^2\bar{\sigma}_8}{\sqrt{2}}\right)- \\ &-c\left(\frac{\bar{\sigma}_0^3}{3\sqrt{6}}-\frac{\bar{\sigma}_8^3}{6\sqrt{3}}-\frac{\bar{\sigma}_0\bar{\sigma}_3^2}{2\sqrt{6}}-\frac{\bar{\sigma}_0\bar{\sigma}_8^2}{2\sqrt{6}}+\frac{\bar{\sigma}_3^2\bar{\sigma}_8}{2\sqrt{6}}\right)- \\ &-h_0\bar{\sigma}_0-h_3\bar{\sigma}_3-h_8\bar{\sigma}_8\,. \end{aligned} \tag{2.50}$$

Its derivatives are given in App. B.

Coupling quarks to the mesons the masses of the quarks are generated dynamically by the Yukawa coupling to the mesons and therefore, the quark contribution (2.4) to the Lagrangian becomes

$$\mathcal{L}_{\mathrm{q}} = \bar{q}\left(\mathrm{i}\gamma_\mu D^\mu - g\,\phi_5\right)q\,. \tag{2.51}$$

ϕ_5 is defined similarly to ϕ but extended by a Lorentz structure

$$\phi_5 = \frac{\lambda_a}{2}\left(\sigma_a + \mathrm{i}\,\gamma_5\pi_a\right)\,, \tag{2.52}$$

where $\gamma_5 = \mathrm{i}\,\gamma_0\gamma_1\gamma_2\gamma_3$. Using Eqs. (2.40) and (2.49) this implies that the quark masses are

$$m_{\mathrm{u}} = g\left(\frac{\bar{\sigma}_0}{\sqrt{6}}+\frac{\bar{\sigma}_3}{2}+\frac{\bar{\sigma}_8}{2\sqrt{3}}\right)\,, \tag{2.53a}$$

$$m_{\mathrm{d}} = g\left(\frac{\bar{\sigma}_0}{\sqrt{6}}-\frac{\bar{\sigma}_3}{2}+\frac{\bar{\sigma}_8}{2\sqrt{3}}\right)\,, \tag{2.53b}$$

$$\Leftrightarrow\quad m_{\mathrm{l}} = \frac{m_{\mathrm{u}}+m_{\mathrm{d}}}{2} = g\left(\frac{\bar{\sigma}_0}{\sqrt{6}}+\frac{\bar{\sigma}_8}{2\sqrt{3}}\right)\,, \tag{2.53c}$$

$$m_{\mathrm{s}} = g\left(\frac{\bar{\sigma}_0}{\sqrt{6}}-\frac{\bar{\sigma}_8}{\sqrt{3}}\right)\,. \tag{2.53d}$$

So, it is the condensate $\bar{\sigma}_3$ that breaks the SU(2) isospin symmetry.

For the later discussion it is convenient to go from the SU(3) basis to that of the quark-flavour condensates. Using the result for the quark masses (2.53) these can be defined as

$$\bar{\phi} = \frac{1}{2}\begin{pmatrix} \bar{\sigma}_{\mathrm{u}} & 0 & 0 \\ 0 & \bar{\sigma}_{\mathrm{d}} & 0 \\ 0 & 0 & \sqrt{2}\bar{\sigma}_{\mathrm{s}} \end{pmatrix} \tag{2.54}$$

so that they are

$$\sigma_{\mathrm{u}} = \sqrt{\frac{2}{3}}\sigma_0 + \sigma_3 + \frac{\sigma_8}{\sqrt{3}}\,, \tag{2.55a}$$

$$\sigma_{\mathrm{d}} = \sqrt{\frac{2}{3}}\sigma_0 - \sigma_3 + \frac{\sigma_8}{\sqrt{3}}\,, \tag{2.55b}$$

$$\sigma_{\mathrm{s}} = \frac{\sigma_0}{\sqrt{3}} - \sqrt{\frac{2}{3}}\sigma_8\,. \tag{2.55c}$$

In these coordinates the self-interaction potential (2.50) of the meson fields reads

$$\begin{aligned} U\left(\bar{\sigma}_{\mathrm{u}}, \bar{\sigma}_{\mathrm{d}}, \bar{\sigma}_{\mathrm{s}}\right) = {} & \frac{\lambda_1}{4}\left[\left(\frac{\bar{\sigma}_{\mathrm{u}}^2 + \bar{\sigma}_{\mathrm{d}}^2}{2}\right)^2 + \bar{\sigma}_{\mathrm{s}}^4 + \left(\bar{\sigma}_{\mathrm{u}}^2 + \bar{\sigma}_{\mathrm{d}}^2\right)\bar{\sigma}_{\mathrm{s}}^2\right] + \frac{\lambda_2}{4}\left(\frac{\bar{\sigma}_{\mathrm{u}}^4 + \bar{\sigma}_{\mathrm{d}}^4}{4} + \bar{\sigma}_{\mathrm{s}}^4\right) + \\ & + \frac{m^2}{2}\left(\frac{\bar{\sigma}_{\mathrm{u}}^2 + \bar{\sigma}_{\mathrm{d}}^2}{2} + \bar{\sigma}_{\mathrm{s}}^2\right) - \frac{c}{2\sqrt{2}}\,\bar{\sigma}_{\mathrm{u}}\,\bar{\sigma}_{\mathrm{d}}\,\bar{\sigma}_{\mathrm{s}} - \\ & - \frac{h_{\mathrm{ud}}}{2}\left(\bar{\sigma}_{\mathrm{u}} + \bar{\sigma}_{\mathrm{d}}\right) - h_{\mathrm{s}}\,\bar{\sigma}_{\mathrm{s}}. \end{aligned} \tag{2.56}$$

In accord with the Vafa-Witten theorem [170] isospin symmetry of the vacuum is not broken and therefore only one single explicit symmetry breaking term for the up- and down-quark sector h_{ud} is considered, which implies $h_3 = 0$ in Eq. (2.50). The corresponding derivatives of the potential are given in App. B.

To see the effects introduced by isospin breaking it is convenient to separate the effect of the isospin-breaking condensate $\sigma_3 = (\sigma_{\mathrm{u}} - \sigma_{\mathrm{d}})/2$ from that of the average light quark condensate $\sigma_{\mathrm{l}} = (\sigma_{\mathrm{u}} + \sigma_{\mathrm{d}})/2$,

$$\begin{aligned} U\left(\bar{\sigma}_{\mathrm{l}}, \bar{\sigma}_{\mathrm{s}}, \bar{\sigma}_3\right) = {} & \frac{2\lambda_1 + \lambda_2}{8}\,\bar{\sigma}_{\mathrm{l}}^4 + \frac{\lambda_1 + \lambda_2}{4}\,\bar{\sigma}_{\mathrm{s}}^4 + \frac{2\lambda_1 + \lambda_2}{8}\,\bar{\sigma}_3^4 + \\ & + \frac{\lambda_1}{2}\,\bar{\sigma}_{\mathrm{l}}^2\bar{\sigma}_{\mathrm{s}}^2 + \frac{\lambda_1}{2}\left(\bar{\sigma}_{\mathrm{l}}^2 + \bar{\sigma}_{\mathrm{s}}^2\right)\bar{\sigma}_3^2 + \frac{3}{4}\lambda_2\,\bar{\sigma}_{\mathrm{l}}^2\bar{\sigma}_3^2 + \\ & + \frac{m^2}{2}\left(\bar{\sigma}_{\mathrm{l}}^2 + \bar{\sigma}_{\mathrm{s}}^2 + \bar{\sigma}_3^2\right) - \frac{c}{2\sqrt{2}}\left(\bar{\sigma}_{\mathrm{l}}^2 - \bar{\sigma}_3^2\right)\bar{\sigma}_{\mathrm{s}} - h_{\mathrm{l}}\bar{\sigma}_{\mathrm{l}} - h_{\mathrm{s}}\bar{\sigma}_{\mathrm{s}}\,. \end{aligned} \tag{2.57}$$

Its derivatives with respect to the condensates are given in App. B. The derivative of the potential with respect to the isospin-breaking condensate σ_3 shows that in order to preserve the isospin symmetry of the vacuum, i.e. $\bar{\sigma}_3 = 0$, explicit isospin symmetry breaking has to be avoided, i.e. $h_3 = 0$.

For the illustration that the Linear-σ potential describes spontaneous and explicit breaking of chiral symmetry it is advantageous to argue with the corresponding isospin symmetric potential for $N_{\mathrm{f}} = 2$,

$$U\left(\sigma, \vec{\pi}\right) = \frac{\lambda}{4}\left(\sigma^2 + \vec{\pi}^2 - v^2\right)^2 - h\sigma\,. \tag{2.58}$$

The coefficient λ has to be positive so that the potential is bounded from below and v can be considered as radius of the 'chiral circle'. A sketch of the potential is shown in

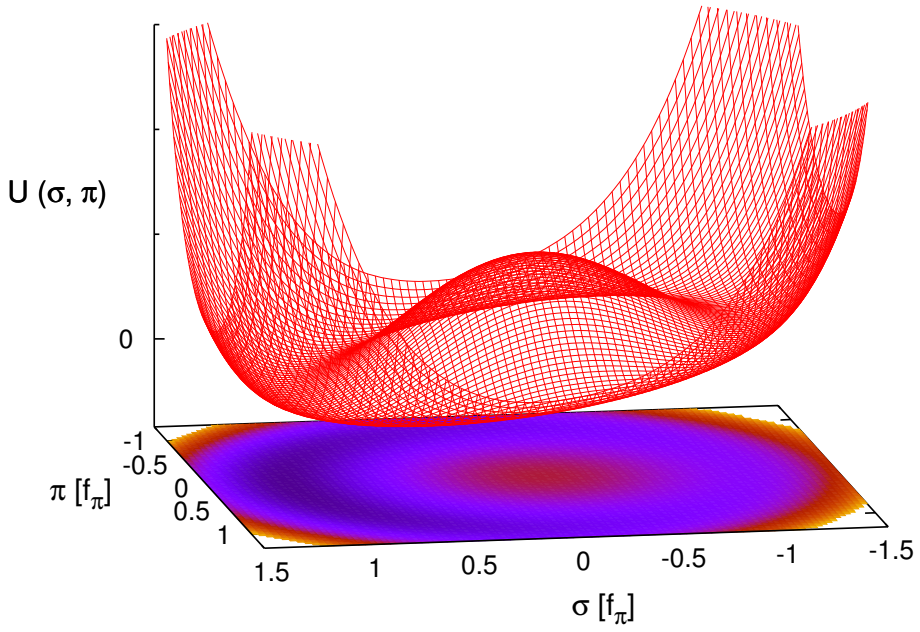

Figure 2.5.: Illustration of the Linear-σ potential for $N_\mathrm{f} = 2$ as a function of the fields σ and π.

Fig. 2.5. Indeed, it fulfils that the expectation value of the pseudo-scalar field vanishes, i.e. $\pi = 0$, that without explicit symmetry breaking the potential would be symmetric but that the scalar field σ takes a non-vanishing expectation value so that chiral symmetry is spontaneously broken and that the explicit symmetry breaking term singles out one specific minimum.

The determination of the parameters of the mesonic potential is discussed within its embedment in the Polyakov–Quark-Meson model in Sec. 3.1.

2.3.2. Polyakov-loop

Reducing the local gauge symmetry implied for the derivation of the QCD Lagrangian (2.10) to a global symmetry, the necessity of introducing gluon fields to achieve gauge invariance drops and with these the information about confinement gets lost. Nevertheless, it was shown in Sec. 2.2.2 that information about confinement can be taken into account via centre symmetry. The commonly used effective order parameter for (de)confinement is the expectation value of the traced Polyakov-loop operator,

$$\Phi \equiv \Phi\left[A\right] \quad = \quad \frac{1}{N_\mathrm{c}} \mathrm{Tr}_\mathrm{c} \left[P \exp\left(\mathrm{i}\, g \int_0^\beta \mathrm{d}\tau\, A_0\left(x_0\right) \right) \right] , \tag{2.59}$$

where P stands for path ordering, g denotes here the bare gauge coupling, $\beta = 1/T$ is the inverse of the temperature and A_0 is the temporal component of the gauge field A_μ [157]. What is commonly called Polyakov loop is then given by the thermal expectation value $\langle\Phi\rangle$. The Polyakov-loop operator itself is a Wilson loop in temporal direction

$$\mathcal{P} \quad = \quad P \exp\left(\mathrm{i}\, g \int_0^\beta \mathrm{d}\tau\, A_0\left(x_0\right)\right) \ . \tag{2.60}$$

With a gauge that ensures the time-independence of A_0, one can perform the integration easily and the path ordering becomes irrelevant [171, 172], so that $\mathcal{P} = \exp\left(\mathrm{i}\,\beta g A_0\right)$. In this form, it is trivial to see that the Polyakov-loop variable,

$$\Phi \quad = \quad \frac{1}{N_\mathrm{c}} \operatorname{Tr}_\mathrm{c} \mathcal{P} \tag{2.61}$$

is a complex scalar field $\Phi = \Phi_\mathrm{r} + \mathrm{i}\,\Phi_\mathrm{i}$. Furthermore, one can rotate the gauge field in the Cartan subalgebra $A_0^c = \frac{\lambda_3}{2} A_0^{(3)} + \frac{\lambda_8}{2} A_0^{(8)}$ [82]. Within this diagonal representation, one sees that the adjoint Polyakov-loop variable becomes simply $\bar{\Phi} = \Phi_\mathrm{r} - \mathrm{i}\,\Phi_\mathrm{i}$.

Under gauge transformations concerning centre symmetry, the Polyakov loop operator and its variable are multiplied with a centre element h, $\Phi \to h\Phi$. Therefore, the Polyakov-loop is an order parameter for centre symmetry [169].

The logarithm of the Polyakov loop $\langle\Phi\rangle$ can be associated to the negative of half of the free energy of a static quark-antiquark pair $F_{\mathrm{q}\bar{\mathrm{q}}}$ at infinite distance. When there are no dynamical quarks present and all gluons are confined the free energy is infinite which implies that the Polyakov loop vanishes in the confined phase of pure gauge theory. For this value, the Polyakov loop is symmetric under centre symmetry transformations.
Deconfinement is characterised by the appearance of free quarks or gluons. Therefore, the static quarks get screened and the free energy of the static quark-antiquark pair gets finite. This in turn implies a non-vanishing value of the Polyakov loop that is no longer symmetric under centre symmetry transformations and centre symmetry gets broken spontaneously.
Light, dynamical quarks and antiquarks can build a meson state with the static antiquark or quark, respectively in the 'confined' phase. This restricts the free energy of the static quark-antiquark pair meaning that the Polyakov loop takes a non-zero value already in the confined phase. This is the explicit breaking of centre symmetry as discussed in Sec. 2.2.2.
In the limit when the free energy of the static quark-antiquark pair vanishes the Polyakov loop becomes one, which restricts the domain of the Polyakov loop to $\langle\Phi\rangle \in [0, \ldots, 1]$.
At a non-zero quark chemical potential the screening of the static antiquark differs from that of the static quark and the Polyakov loop is a measures of the screening of the quark while the adjoint Polyakov loop $\bar{\Phi}$ tests this of the antiquark. In general, at a positive net quark density one can expect a stronger screening of the antiquark than the quark so that the adjoint Polyakov loop $\langle\bar{\Phi}\rangle$ should be larger than the Polyakov loop $\langle\Phi\rangle$.

In addition to the standard Polyakov loop $\langle \Phi[A] \rangle$, other order parameters for quark confinement have been introduced. The functional renormalisation group (FRG) calculations discussed in App. A and that will be applied in Sec. 3.2.1 consider an order parameter which is closely related to the Polyakov loop, namely $\Phi[\langle A_0 \rangle]$. In Polyakov-Landau-DeWitt gauge, it can be indeed shown that $\Phi[\langle A_0 \rangle]$ also is an order parameter, see Refs. [82, 172]. Here, $\langle A_0 \rangle$ is a constant element of the gauge group and denotes the ground state of the corresponding order-parameter potential. So this gluonic background is determined by the constant solution of the equations of motion. Such a solution can always be rotated in the Cartan subalgebra as well,

$$\langle A_\mu \rangle \quad = \quad \delta_{\mu 0} \left(\frac{\lambda_3}{2} \langle A_0^{(3)} \rangle + \frac{\lambda_8}{2} \langle A_0^{(8)} \rangle \right) , \tag{2.62}$$

with constant $\langle A_0^{(3,8)} \rangle$. The minima and maxima of the potential are accessed for $\langle A_0^8 \rangle = 0$, see Refs. [36, 82–84, 172]. Then this Polyakov-loop observable reads

$$\Phi[A_0] \quad = \quad \frac{1}{3} \left[1 + 2 \cos \left(\frac{\beta g}{2} A_0 \right) \right] \qquad \text{with} \qquad A_0 = \langle A_0^3 \rangle \, . \tag{2.63}$$

Both Polyakov-loop order parameters $\langle \Phi[A_0] \rangle$ and $\Phi[\langle A_0 \rangle]$ are related according to Jensen's inequality by

$$\Phi[\langle A_0 \rangle] \quad \geq \quad \langle \Phi[A_0] \rangle \, . \tag{2.64}$$

The potential of the Polyakov loop, $\mathcal{U}\big(\Phi, \bar{\Phi}; T\big)$ should mimic a background of gluons and controls the dynamics of the Polyakov loop.

First computations of the effective potential in gauge theories have been performed in the 80's at asymptotically high temperatures using perturbation theory [173–175] and in the strong coupling limit on a lattice [176]. In recent years, the non-perturbative Polyakov-loop potential has been studied using various different approaches [36, 37, 82–84, 172, 177–183]. First principle calculations of the potential are performed using different functional methods, mainly the FRG approach but as well Dyson-Schwinger equations and the 2PI-approach [82–84,172]. In Refs. [36,37] the Polyakov-loop potential in two flavour QCD in the chiral limit has been analysed. This computation includes the full back-coupling of the matter sector on the propagators of the gauge degrees of freedom via dynamical quark-gluon interactions [184–186].

A much simpler way to obtain an effective Polyakov-loop potential $\mathcal{U}\big(\Phi, \bar{\Phi}; T\big)$ is to construct a potential that respects all given symmetries and contains the spontaneous breaking of Z(3) symmetry if the system is in the deconfined phase [176, 187, 188]. The actual form and construction of the Polyakov-loop potential will be discussed in Sec. 3.2.

Overall, the Lagrangian of QCD (2.10) reduces in this effective description of the important symmetries of strongly-interacting matter that are chiral symmetry and centre

symmetry to

$$\begin{aligned}\mathcal{L}_{\mathrm{PQM}} &= \bar{q}\left[\mathrm{i}\,\gamma_\mu\left(\partial^\mu - \mathrm{i}A^\mu\delta_{\mu 0} + \mu_f\,\delta^{\mu 0}\right) - g\,\frac{\lambda_a}{2}\left(\sigma_a + \mathrm{i}\gamma_5\pi_a\right)\right]q + \\ &\quad + \frac{1}{2}\left(\partial_\mu\sigma_a\partial^\mu\sigma_a + \partial_\mu\pi_a\partial^\mu\pi_a\right) - \\ &\quad - U\left(\sigma_a,\pi_a\right) - \mathcal{U}\left(\Phi,\bar{\Phi};T\right)\ . \end{aligned} \tag{2.65}$$

To avoid a confusion of the coupling constants of quarks to gauge fields and to mesons, the former is absorbed into the definition of the gauge field, i.e. $gA^\mu \to A^\mu$ form here on. This Lagrangian defines the Polyakov-loop extended Quark-Meson model and will serve as basis to derive the grand-canonical potential of the PQM model in the next chapter.

3. The Polyakov–Quark-Meson Model

3.1. Formulation of the Polyakov–Quark-Meson Model

The particle content of the Polyakov–Quark-Meson model model are constituent quarks minimally coupled to gauge fields and coupled to mesons via a Yukawa-type term.

The starting point for the analysis of the system is the in-medium effective action of the theory. It is the space-time integral over the Lagrangian density

$$\mathcal{S}_{\mathrm{PQM}}\left[\sigma_a, \pi_a, A_0, q, \bar{q}; T, \mu_f\right] \;=\; \int_0^\beta \mathrm{d}\tau \int \mathrm{d}^3x \; \mathcal{L}^{\mathrm{E}}_{\mathrm{PQM}}\left[\sigma_a, \pi_a, A_0, q, \bar{q}; \mu_f\right] \; . \tag{3.1}$$

Here, it is referred to the definition of the action in the Euclidean metric. The Wick-rotation of the time coordinate leads to a flipped sign of the potential terms in the Euclidean formulation of the Lagrangian density $\mathcal{L}^{\mathrm{E}}_{\mathrm{PQM}}$ compared to that in Minkowski space-time in Eq. (2.65). The corresponding partition function is a path integral over all occurring fields

$$\mathcal{Z}_{\mathrm{PQM}} = \int \prod_a \mathcal{D}\sigma_a \int \prod_a \mathcal{D}\pi_a \int \mathcal{D}A_0 \int \mathcal{D}q \int \mathcal{D}\bar{q} \, \exp\left(-\mathcal{S}_{\mathrm{PQM}}\left[\sigma_a, \pi_a, A_0, q, \bar{q}\right]\right) \; . \tag{3.2}$$

The thermodynamic quantities and the behaviour of the order parameters of the theory can be derived from the thermodynamical effective potential. It is proportional to the logarithm of the partition function, with a prefactor that accounts for the normalisation of the space-time integral in the action,

$$\Omega_{\mathrm{PQM}}\left[\sigma_a, \pi_a, A_0, q, \bar{q}; T, \mu_f\right] \;=\; -\frac{T}{V} \ln \mathcal{Z}_{\mathrm{PQM}} \; . \tag{3.3}$$

Hence, it is a function of the order-parameters and thermodynamical control parameters. Characterising the system by its temperature, the chemical potentials of the quark flavours and the volume, the effective potential (3.3) is the grand-canonical potential. Normalising it by the volume, it is strictly speaking a density.

The difficultly in finding a final expression for the effective potential is performing the path integral over the fields. In order to evaluate it, an initial approximation is to refer to thermal equilibrium, which is described by homogeneous field configurations. In this mean-field approximation one ignores all the dynamics of the fields and excludes fluctuations. These can be again taken into account starting with the mean-field potential at some ultraviolet (UV) scale and considering the fluctuations in the flow towards the infrared (IR), see e.g. Refs. [4, 74, 76, 78].

In more detail, in the mean-field approximation a field $\phi = \bar{\phi} + \delta\phi$ is replaced by its spatially and temporally constant background $\bar{\phi}$, ignoring fluctuations $\delta\phi$. Doing this the path integral turns into an ordinary integral over the field,

$$\int \mathcal{D}\phi \, \exp\left(-\mathcal{S}\left[\phi\right]\right) \quad \rightarrow \quad \int \mathrm{d}\bar{\phi} \, \exp\left(-\mathcal{S}\left[\bar{\phi}\,\right]\right) \, . \tag{3.4}$$

Furthermore, the field configuration that contributes the most to the partition function is that that minimises the in-medium effective action or potential. All other extrema of the effective action are exponentially suppressed and give negligible contributions to the equilibrium thermodynamics of the system. This implies that the integral is trivially restricted to that mean-field which minimises the action

$$\int \mathrm{d}\bar{\phi} \, \exp\left(-\mathcal{S}\left[\bar{\phi}\,\right]\right) \quad \rightarrow \quad \exp\left(-\mathcal{S}\left[\bar{\phi}\,\right]\right) \, . \tag{3.5}$$

In the mean-field approximation of the PQM model this is how the meson and gluon fields are treated. Substituting the meson fields by their expectation values their derivative terms in the Lagrangian (2.65) vanish. The gauge fields are considered as constant background fields as well and therefore, one is left with an integration over the quark fields that keep their character as quantum fields,

$$\begin{aligned} \mathcal{Z}_{\mathrm{PQM}} &= \int \mathcal{D}\bar{q} \int \mathcal{D}q \exp\left\{ - \int \int_0^\beta \bar{q} \left[\mathrm{i}\,\gamma_\mu \left(\partial^\mu - \mathrm{i}\,A^\mu \delta_{\mu 0} + \mu_f\,\delta^{\mu 0} \right) - g\,\frac{\lambda_a}{2}\sigma_a \right] q + \right. \\ &\quad \left. + U\left(\sigma_a\right) + \mathcal{U}\left(\Phi, \bar{\Phi}; T\right) \, \mathrm{d}\tau \, \mathrm{d}^3x \right\} \qquad (3.6) \\ &= \exp\left\{ -\frac{V}{T} \left[U\left(\sigma_a\right) + \mathcal{U}\left(\Phi, \bar{\Phi}; T\right) \right] \right\} \int \mathcal{D}\bar{q}\,\mathcal{D}q \times \\ &\quad \times \exp\left\{ - \int_0^\beta \mathrm{d}\tau \int \mathrm{d}^3x \; \bar{q} \left[\mathrm{i}\,\gamma_\mu \left(\partial^\mu - \mathrm{i}\,A^\mu \delta_{\mu 0} + \mu_f\,\delta^{\mu 0} \right) - g\,\frac{\lambda_a}{2}\sigma_a \right] q \right\} . \qquad (3.7) \end{aligned}$$

Since the potential of the meson fields and the Polyakov-loop potential don't depend on the quark fields and are independent of space-time they can be put out of the path integral and the space-time integral can be performed trivially. This implies that he final expression of the grand-canonical potential (3.3) takes the form

$$\Omega\left(\sigma_a, \Phi, \bar{\Phi}; T, \mu_f\right) \;=\; U(\sigma_a) + \mathcal{U}\big(\Phi, \bar{\Phi}; T\big) + \Omega_{\mathrm{q\bar{q}}}\left(\sigma_a, A_0; T, \mu_f\right) \, . \tag{3.8}$$

The last term represents the constituent quark sector. It includes the coupling of the dynamical quarks to mesons via a Yukawa-type term and the minimal coupling to the background gauge field $\langle A_0 \rangle$. This coupling to the colour fields can be rewritten in terms of a coupling to the Polyakov-loop variable $\Phi[\langle A_0 \rangle]$.

The remaining integration over the fermions can be performed following the standard derivation [102] as Gaussian integral over Grassmann fields. This yields a determinant

which can be rewritten as a trace over a logarithm. Evaluating this trace in momentum-space within the Matsubara formalism one obtains within a 1-loop approximation

$$\begin{aligned}\Omega_{\mathrm{q\bar{q}}}\left(\sigma_a,\Phi,\bar{\Phi};T,\mu_f\right) = -2\sum_f \int \frac{\mathrm{d}^3k}{(2\pi)^3}\Big\{ N_{\mathrm{c}}E_f + \\ + T\ln\left[1+3\left(\Phi+\bar{\Phi}e^{-\left(E_f-\mu_f\right)/T}\right)e^{-\left(E_f-\mu_f\right)/T}+e^{-3\left(E_f-\mu_f\right)/T}\right] + \\ + T\ln\left[1+3\left(\bar{\Phi}+\Phi e^{-\left(E_f+\mu_f\right)/T}\right)e^{-\left(E_f+\mu_f\right)/T}+e^{-3\left(E_f+\mu_f\right)/T}\right]\Big\}\ . \quad (3.9)\end{aligned}$$

A detailed derivation is e.g. given in Refs. [101, 166]. The following discussion proceeds with the interpretation of Eq. (3.9). It includes the coupling of the dynamical quarks to the Polyakov-loop variable $\Phi[\langle A_0\rangle]$ and the mesons. The dependence on the quark condensates σ_a is implicit in the quasi-particle dispersion relation for the constituent quarks

$$E_f = \sqrt{k^2+m_f^2} \quad (3.10)$$

since the constituent quark masses are $m_f \propto g\sigma_f$.

The first term of the quark-antiquark contribution results from the negative energy states of the Dirac sea and is ultraviolet divergent. In the standard, no-sea mean-field (MF) approximation it is neglected [61] saying that it can be absorbed in the renormalisation of the vacuum since it has no explicit dependence on temperature and quark chemical potentials. However, this term can be normalised, e.g. in the dimensional regularisation scheme yielding a logarithmic correction that is implicitly medium-dependent via the quark condensates [75, 77, 79, 189, 190],

$$\Omega_{\mathrm{q\bar{q}}}^{\mathrm{vac}}\left(\sigma_a\right) = -2N_{\mathrm{c}}\sum_f \int \frac{\mathrm{d}^3k}{(2\pi)^3}\,E_f \quad = \quad -\frac{N_{\mathrm{c}}}{8\pi^2}\sum_f m_f^4\,\ln\left(\frac{m_f}{\Lambda}\right)\ . \quad (3.11)$$

The regularisation scale Λ corresponds to the UV scale of the renormalisation group (RG) flow equation. From the RG flow equation it can be inferred that the effective quark-antiquark potential has to change under a variation of this scale since it also plays the role of an IR scale, up to which fluctuations are integrated out [4, 74, 76, 78]. The origin of Λ in the flow equation makes clear that Eq. (3.11) includes that part of the quantum fluctuations of quarks related to momenta larger than the UV scale. Consequently one expects a significant contribution in particular for high temperature, large chemical potentials and large mass scales. Hence, it is interesting to study its impact on the $T-\mu$ phase diagram.

Note that in the extended mean-field (eMF) model that takes into account the fermionic sea contribution (3.11), this term contributes to the vacuum properties besides the mesonic potential $U(\sigma_a)$. This will become of importance in the latter adjustment of the parameters of the mesonic potential to meson masses in the vacuum, so at $T=\mu_f=0$.

The remaining part of Eq. (3.9) is the kinetic quark-antiquark contribution that is a

function of the thermodynamic variables

$$\Omega_{\mathrm{q\bar{q}}}^{\mathrm{th}}\left(\sigma_a,\Phi,\bar{\Phi};T,\mu_f\right)=-2T\sum_f\int\frac{\mathrm{d}^3k}{(2\pi)^3}\times$$
$$\times\left\{\ln\left[1+3\left(\Phi e^{-\left(E_f-\mu_f\right)/T}+\bar{\Phi}e^{-2\left(E_f-\mu_f\right)/T}\right)+e^{-3\left(E_f-\mu_f\right)/T}\right]+\right.$$
$$\left.+\ln\left[1+3\left(\bar{\Phi}e^{-\left(E_f+\mu_f\right)/T}+\Phi e^{-2\left(E_f+\mu_f\right)/T}\right)+e^{-3\left(E_f+\mu_f\right)/T}\right]\right\}\ . \quad (3.12)$$

The Quark-Meson model limit of the PQM model, that only covers chiral symmetry but does not contain any information about confinement, can be recovered for $\Phi=\bar{\Phi}\equiv 1$. Then the logarithms reduce to

$$3\times\ln\left[1-n_f\left(T,\mu_f\right)\right]\qquad\text{with}\qquad n_f\left(T,\mu_f\right)=\frac{1}{1+\exp\left[\left(E_f\pm\mu_f\right)/T\right]} \quad (3.13)$$

as the occupation numbers of free quarks and antiquarks, respectively.
Including the Polyakov loop, it is such that it takes small values in the confined phase and the logarithms take the form $\ln\{1+\exp\left[-3\left(E_f\pm\mu_f\right)/T\right]\}$. So, they take the same form of a free fermion gas but with an additional factor of 3. This indicates the dominance of states consisting of three quarks or antiquarks, respectively, that have the same quark number as a (anti-)baryon. Confinement is mimicked in a Polyakov-loop–extended constituent-quark model in this statistical sense. In the deconfined phase centre symmetry breaks spontaneously so that the Polyakov loop takes significantly larger values which implies that the single- and two (anti-)quark states contribute. For the limit $\Phi,\bar{\Phi}\to 1$ the logarithms take the form given in Eq. (3.13) which is a gas of non-interacting quarks and antiquarks in three colours.

The thermodynamic potential (3.8) is complemented by a potential energy for the expectation value of the Polyakov loop $\mathcal{U}\left(\Phi,\bar{\Phi};T\right)$ that will be derived in the following section and the tree-level contribution of the mesonic degrees of freedom $U(\sigma_a)$. In summary, the effective potential of the $N_\mathrm{f}=2+1$ Polyakov–Quark-Meson model reads

$$\Omega\left(\sigma_\mathrm{u},\sigma_\mathrm{d},\sigma_\mathrm{s},\Phi,\bar{\Phi};\,T,\mu_f\right)=U\left(\sigma_\mathrm{u},\sigma_\mathrm{d},\sigma_\mathrm{s}\right)+\Omega_{\mathrm{q\bar{q}}}^{\mathrm{vac}}\left(\sigma_\mathrm{u},\sigma_\mathrm{d},\sigma_\mathrm{s}\right)+$$
$$+\mathcal{U}\left(\Phi,\bar{\Phi};\,T\right)+\Omega_{\mathrm{q\bar{q}}}^{\mathrm{th}}\left(\sigma_\mathrm{u},\sigma_\mathrm{d},\sigma_\mathrm{s},\Phi,\bar{\Phi};\,T,\mu_f\right)\ . \quad (3.14)$$

It is a function of the order parameters for chiral symmetry in the light and strange quark sector and deconfinement of quarks and antiquarks. Additionally, it depends on the thermodynamic variables that are the temperature and the quark chemical potentials of each quark flavour.

In equilibrium, the expected values for the order parameters at given temperature and chemical potentials are those at the minimum of the effective potential. Therefore, a necessary condition are vanishing derivatives of the effective potential with respect to each order parameter,

$$\frac{\partial\Omega}{\partial\sigma_\mathrm{u}}=\frac{\partial\Omega}{\partial\sigma_\mathrm{d}}=\frac{\partial\Omega}{\partial\sigma_\mathrm{s}}=\frac{\partial\Omega}{\partial\Phi}=\frac{\partial\Omega}{\partial\bar{\Phi}}\quad=\quad 0\ . \quad (3.15)$$

This set of coupled equations are taken as equations of motion of the PQM model. Under which conditions that extremum which minimises the effective potential is indeed a global minimum of the effective potential is analysed in Sec. 3.3. In general, those solutions of the equations of motion are minima of the potential for which all eigenvalues of the Hessian matrix

$$\mathcal{H}_{ij} = \frac{\partial^2 \Omega}{\partial \psi_i \partial \psi_j} \qquad \text{with} \qquad \psi_i \in \left\{ \sigma_\mathrm{u}, \sigma_\mathrm{d}, \sigma_\mathrm{s}, \Phi, \bar{\Phi} \right\} \tag{3.16}$$

are positive.

The equations of motion (3.15) allow to analyse which values the order parameters take in dependence of temperature and quark chemical potentials. This implies the investigation of the phase structure of the PQM model. Furthermore, one can specifically map out the transition between phases where chiral and centre symmetry are only broken explicitly and those where spontaneous symmetry breaking occurs.

An order parameter for chiral symmetry that combines non-strange or light and strange condensates is the so-called subtracted condensate

$$\Delta_{\mathrm{l,s}} \quad = \quad \frac{\sigma_\mathrm{l} - \frac{h_\mathrm{l}}{h_\mathrm{s}} \sigma_\mathrm{s} \Big|_{T,\mu_f}}{\sigma_\mathrm{l} - \frac{h_\mathrm{l}}{h_\mathrm{s}} \sigma_\mathrm{s} \Big|_{T=\mu_f=0}} \, . \tag{3.17}$$

This quantity is better accessible in lattice simulations than the quark condensates themselves and hence will be used in Chap. 4 for the comparison of the behaviour of the chiral sector in the PQM model with lattice calculations.

The transition between the different phases is also reflected in thermodynamic quantities. These depend on if the degrees of freedom are massive or massless or if they are baryons and mesons or deconfined quarks and gluons. In difference to the order parameters these are also experimental accessible quantities and can be compared as well between different effective and non-perturbative descriptions of strongly-interacting matter. The starting point for the determination of thermodynamic quantities is the identification of the effective thermodynamical potential as the negative of the pressure

$$p = -\Omega \, , \tag{3.18}$$

where it is useful to remember from the definition of the effective potential (3.3) that it is normalised by the volume and therefore, a density. From the Euler equation for the energy follows the relation between all basic thermodynamic quantities that are the pressure p, the energy density ϵ, the entropy density s and the quark flavour densities n_f,

$$-p = \Omega \quad = \quad \epsilon - Ts - \sum_f \mu_f \, n_f \, . \tag{3.19}$$

Since the effective potential is a grand canonical potential these are mean densities. They can be derived from the effective potential by the Gibbs-Duhem relations

$$s = -\left.\frac{\partial\Omega}{\partial T}\right|_{\mu_f=\text{const}}, \quad n_f = -\left.\frac{\partial\Omega}{\partial\mu_f}\right|_{T=\text{const}} \quad \text{and} \quad \epsilon = Ts + \Omega + \sum_f \mu_f n_f \,. \tag{3.20}$$

The derivation of the effective potential (3.14) in the mean-field approximation implies that only thermal fluctuations of quarks (3.12) contribute to thermodynamics but it does not contain any thermal contribution of the mesons. To achieve a better description of the thermodynamics in the phase where mesons are the dominant degrees of freedom, the thermodynamics is augmented by the contribution of a gas of thermal mesons. The contribution to the pressure of each meson species is

$$p_{\phi_i} = \frac{1}{(2\pi)^3}\int_0^\infty \mathrm{d}^3k\,\frac{k^2}{3E_{\phi_i}}\,\frac{1}{e^{(E_{\phi_i}-\mu_{\phi_i})/T}-1} \qquad \text{with} \qquad E_{\phi_i} = \sqrt{k^2+m_{\phi_i}^2}\,. \tag{3.21}$$

The total contribution of the mesons to the pressure is accordingly $p_\phi = \sum_i p_{\phi_i}$ and overall

$$p = -\Omega + p_\phi\,. \tag{3.22}$$

The meson masses that enter to the dispersion relations of the mesons in Eq. (3.21) are medium dependent and are determined by the second derivatives of the thermodynamical potential with respect to the (pseudo-)scalar fields as will be discussed below. The medium dependence of the meson masses makes the pressure of the mesons p_ϕ strictly speaking to a field-dependent correction to the thermodynamical potential that contributes as well to the equations of motion, $\partial\Omega/\partial\psi_i - \partial p_\phi/\partial\psi_i$ and the (pseudo-)scalar masses themselves. In a lowest order approximation this correction is neglected, saying that the dynamics of the system is governed by the grand canonical potential Ω alone which determines the meson masses as well. An uncoupled meson gas with these meson masses is then added to thermodynamics as in Eq. (3.22). All thermodynamic quantities are derived from Eq. (3.22) ensuring the Gibbs-Duhem relation,

$$\epsilon = Ts - p + \sum_{N_f}\mu_f\, n_f\,, \quad s = \left.\frac{\partial p}{\partial T}\right|_{\mu_f=\text{const}} \quad \text{and} \quad n_f = \left.\frac{\partial p}{\partial\mu_f}\right|_{T=\text{const}}. \tag{3.23}$$

All contributions stemming from $\partial p_\phi/\partial\psi_i$ are neglected here consistently as well.

A remaining task is to determine the parameters of the model. The mesonic potential $U(\sigma_\mathrm{u},\sigma_\mathrm{d},\sigma_\mathrm{s})$ has seven parameters, that are the couplings m^2, λ_1, λ_2, the U(1) axial-vector symmetry breaking coefficient c and the explicit chiral symmetry breaking terms h_l, h_s and h_3. The quark contribution $\Omega_{\mathrm{q\bar{q}}}\left(\sigma_\mathrm{u},\sigma_\mathrm{d},\sigma_\mathrm{s},\Phi,\bar{\Phi};T,\mu_f\right)$ depends on the Yukawa coupling strength g between quarks and mesons. Furthermore, the values of the quark condensates $\sigma_\mathrm{u},\sigma_\mathrm{d},\sigma_\mathrm{s}$ in the vacuum have to be determined. Parameters of

the Polyakov-loop potential $\mathcal{U}\big(\Phi,\bar{\Phi};T\big)$ are independent of the other contributions and will be discussed together with the potential in Sec. 3.2.
The term that includes quantum fluctuations of the quarks above some UV scale Λ, $\Omega_{\mathrm{q\bar{q}}}^{\mathrm{vac}}\left(\sigma_{\mathrm{u}},\sigma_{\mathrm{d}},\sigma_{\mathrm{s}}\right)$ seems to introduce additionally a dependence on this scale. But this dependence cancels neatly with that of the parameters of the mesonic potential that are adjusted to vacuum properties to which the vacuum quark-term contributes as well. This is shown explicitly in the further discussion. Therefore, the PQM model is independent of the regularisation scale and includes all quantum fluctuations of the quarks. In an FRG calculation the Λ-independence can be directly computed from the flow and follows from the invariance of the effective action at vanishing cutoff scale under a variation of Λ, see the reviews [30–35, 37, 191–193].

The parameters of the mesonic potential can be adjusted to vacuum properties of mesons. A starting point for the description of the vacuum in the PQM model are the equations of motion (3.15). In the vacuum, i.e. $T=\mu_f=0$ only the mesonic potential and the quark quantum-fluctuations contribute,

$$\left.\frac{\partial\Omega}{\partial\psi_i}\right|_{T=\mu_f=0} \;=\; \frac{\partial U}{\partial\psi_i}+\frac{\partial\Omega_{\mathrm{q\bar{q}}}^{\mathrm{vac}}}{\partial\psi_i}\;. \tag{3.24}$$

To implement isospin symmetry of the vacuum, i.e. $\sigma_3(T=\mu_f=0)=0$, $\partial\Omega/\partial\sigma_3|_{T=\mu_f=0}=0$ is the related equation. The contribution of the mesonic potential is given in Eq. (B.7) and is

$$\frac{\partial U}{\partial\bar{\sigma}_3} \;=\; m^2\,\bar{\sigma}_3+\lambda_1\left(\bar{\sigma}_{\mathrm{l}}^2+\bar{\sigma}_{\mathrm{s}}^2\right)\bar{\sigma}_3+\frac{3}{2}\lambda_2\,\bar{\sigma}_{\mathrm{l}}^2\bar{\sigma}_3+\frac{2\lambda_1+\lambda_2}{2}\,\bar{\sigma}_3^3+\;\frac{c}{\sqrt{2}}\,\bar{\sigma}_3\bar{\sigma}_{\mathrm{s}}-h_3\;. \tag{3.25}$$

In the standard mean-field model this is the only contribution and isospin symmetry of the vacuum, i.e. $\sigma_3(T=\mu_f=0)=0$, implies $h_3=0$. The derivatives of the quark quantum-fluctuations contribution with respect to the (pseudo-)scalar fields are in general

$$\frac{\partial\Omega_{\mathrm{q\bar{q}}}^{\mathrm{vac}}}{\partial\varphi_a}=-\frac{N_{\mathrm{c}}}{16\pi^2}\sum_f m_f^2\,m_{f,a}^2\,\left[4\ln\left(\frac{m_f}{\Lambda}\right)+1\right]\qquad\text{with}\qquad m_{f,a}^2=\frac{\partial m_f^2}{\partial\varphi_a}\;, \tag{3.26}$$

with $\varphi_a\in\{\sigma_a,\pi_a\}$. So the dependence on the meson fields enters via the dynamically generated quark masses (2.52). In App. B are summarised the derivatives of the squared quark masses with respect to the meson fields. The flipped sign in $m_{d,3}^2$ compared to $m_{u,3}^2$ is such that $\partial\Omega_{\mathrm{q\bar{q}}}^{\mathrm{vac}}/\partial\sigma_3=0$ for $\sigma_3=0$ as well. So, the condition of isospin symmetry of the vacuum implies no explicit isospin-symmetry breaking, $h_3=0$ and the expectation value of the chiral condensate σ_3 vanishes in the vacuum so that the up and down quark condensates σ_{u} and σ_{d}, take the same value in the vacuum.
The values of the light and strange quark condensates in the vacuum can be determined by decay constants f_a corresponding to pseudoscalar fields π_a. They follow from the partially conserved axial-vector current as [60]

$$f_a=d_{aab}\,\bar{\sigma}_b\;, \tag{3.27}$$

and are given explicitly in App. B. The pion decay constant can be identified by the three degenerate decay constants $f_1 = f_2 = f_3$. For $\sigma_3 = 0$, four more decay constants take the same value, $f_4 = f_5 = f_6 = f_7$ so that they can be identified as the kaon decay constant f_K. For the values that the light and strange quark condensates take in the vacuum this implies

$$\bar{\sigma}_\mathrm{l} = \bar{\sigma}_\mathrm{u} = \bar{\sigma}_\mathrm{d} = f_\pi \,, \tag{3.28}$$

$$\bar{\sigma}_\mathrm{s} = \frac{2f_\mathrm{K} - f_\pi}{\sqrt{2}} \,. \tag{3.29}$$

In the next step, the Yukawa coupling between quarks and (pseudo-)scalar mesons can be fixed by choosing a constituent mass of the light quarks in the vacuum,

$$g = \frac{m_\mathrm{l}}{f_\pi} \,. \tag{3.30}$$

The couplings of the mesonic potential and the axial-vector breaking coefficient can be adjusted to the meson masses in the vacuum. The masses of the scalar and pseudoscalar mesons in the PQM model are the second derivatives of the potential with respect to the (pseudo-)scalar fields.

$$m^2_{i,ab} = \frac{\partial^2 \Omega\left(\bar{\sigma}, \bar{\pi}\right)}{\partial\varphi_{i,a}\partial\varphi_{i,b}} = m^2_{i,ba} \,. \tag{3.31}$$

In the vacuum, only the mesonic contribution and the contribution of the quark quantum-fluctuations contribute to the meson masses. But in general, the meson masses are medium dependent via the thermal quark fluctuations. The second derivatives of the quark quantum-fluctuations contribution with respect to the (pseudo-)scalar fields are

$$\frac{\partial^2 \Omega^\mathrm{vac}_{\mathrm{q\bar{q}}}}{\partial\varphi_a\partial\varphi_b} = -\frac{N_\mathrm{c}}{16\pi^2}\sum_f \left\{ m^2_{f,a}\, m^2_{f,b} \left[4\ln\left(\frac{m_f}{\Lambda}\right) + 3\right] + m^2_{f,ab} \left[4\ln\left(\frac{m_f}{\Lambda}\right) + 1\right]\right\}$$

$$\text{with} \qquad m^2_{f,ab} = \frac{\partial^2 m_f^2}{\partial\varphi_a\partial\varphi_b} \,, \tag{3.32}$$

where besides the first order derivatives of the quark masses with respect to the meson fields $m^2_{f,a}$, also the second order derivatives $m^2_{f,ab}$ enter. These are also given in App. B. Equations (2.42) and (2.43) give the contributions of the mesonic potential to the scalar and pseudoscalar meson masses since they can be written as second derivatives of the potential (2.44), e.g.

$$M^2_{s,ab} = \frac{\partial^2 U\left(\bar{\sigma}\right)}{\partial\bar{\sigma}_a\partial\bar{\sigma}_b} = M^2_{s,ba} \,. \tag{3.33}$$

They are explicitly given in App. B.
It is important to notice that the contributions (2.42) and (2.43) of the mesonic potential as well as the contributions of the quantum-fluctuations of quarks (3.32) to the

meson masses have off-diagonal components. In the mass matrix defined by the second derivatives of the potential as in Eq. (3.31), the $0-3-8$ components mix and this sector has to be diagonalised to obtain a mass matrix of the physical states,

$$\begin{pmatrix} \tilde{m}^2_{i,00} & 0 & 0 \\ 0 & \tilde{m}^2_{i,33} & 0 \\ 0 & 0 & \tilde{m}^2_{i,88} \end{pmatrix} = R^T \begin{pmatrix} m^2_{i,00} & m^2_{i,03} & m^2_{i,08} \\ m^2_{i,03} & m^2_{i,33} & m^2_{i,38} \\ m^2_{i,08} & m^2_{i,38} & m^2_{i,88} \end{pmatrix} R \,. \tag{3.34}$$

With the rotation matrix

$$\begin{aligned} R &= \begin{pmatrix} \cos\theta_i & 0 & -\sin\theta_i \\ 0 & 1 & 0 \\ \sin\theta_i & 0 & \cos\theta_i \end{pmatrix} \begin{pmatrix} \cos\varphi_i & -\sin\varphi_i & 0 \\ \sin\varphi_i & \cos\varphi_i & 0 \\ 0 & 0 & 1 \end{pmatrix} = \\ &= \begin{pmatrix} \cos\theta_i\cos\varphi_i & -\cos\theta_i\sin\varphi_i & -\sin\theta_i \\ \sin\varphi_i & \cos\varphi_i & 0 \\ \sin\theta_i\cos\varphi_i & -\sin\theta_i\sin\varphi_i & \cos\theta_i \end{pmatrix} \end{aligned} \tag{3.35}$$

the entries of the diagonalised matrix become

$$\begin{aligned} \tilde{m}^2_{i,00} &= \left(m^2_{i,00}\cos^2\theta_i + m^2_{i,88}\sin^2\theta_i + 2m^2_{i,08}\sin\theta_i\cos\theta_i\right)\cos^2\varphi_i + \\ &\quad + m^2_{i,33}\sin^2\varphi_i + 2\left(m^2_{i,03}\cos\theta_i + m^2_{i,38}\sin\theta_i\right)\sin\varphi_i\cos\varphi_i \,, && \text{(3.36a)} \\ \tilde{m}^2_{i,33} &= \left(m^2_{i,00}\cos^2\theta_i + m^2_{i,88}\sin^2\theta_i + 2m^2_{i,08}\sin\theta_i\cos\theta_i\right)\sin^2\varphi_i + \\ &\quad + m^2_{i,33}\cos^2\varphi_i - 2\left(m^2_{i,03}\cos\theta_i + m^2_{i,38}\sin\theta_i\right)\sin\varphi_i\cos\varphi_i \,, && \text{(3.36b)} \\ m^2_{i,88} &= m^2_{i,00}\sin^2\theta_i + m^2_{i,88}\cos^2\theta_i - 2m^2_{i,08}\sin\theta_i\cos\theta_i && \text{(3.36c)} \end{aligned}$$

with the mixing angles

$$\begin{aligned} \tan(2\theta_i) &= \frac{2m^2_{i,08}}{m^2_{i,00} - m^2_{i,88}} \,, && \text{(3.37a)} \\ \tan(2\varphi_i) &= \frac{2\left(m^2_{i,03}\cos\theta_i + m^2_{i,38}\sin\theta_i\right)}{m^2_{i,00}\cos^2\theta_i - m^2_{i,33} + m^2_{i,88}\sin^2\theta_i + 2m^2_{i,08}\sin\theta_i\cos\theta_i} \,. && \text{(3.37b)} \end{aligned}$$

Note that for isospin symmetry, i.e. $\bar{\sigma}_3 = 0$ as in the vacuum the above results simply reduce to that of Refs. [60, 66, 190].
From the mass hierarchy and number of degenerated components, the mass eigenstates can be associated with physical mesons as given in Table 3.1. Since the couplings and the axial-vector symmetry breaking coefficient of the mesonic potential are adjusted to the meson masses in the vacuum, where $\sigma_3 = 0$, solving of selected meson masses for these parameters is the same as in Refs. [60, 66, 190].

Finally, the coefficients of the chiral symmetry explicitly breaking terms remain to be determined. This can be done by solving the equations of motion corresponding to the light and strange quarks in the vacuum for them. Also this is analogous to Refs. [60, 66, 190] for a isospin-symmetric vacuum.

Table 3.1.: Association between the mass eigenstates of the diagonalised matrix $\partial^2\Omega/\left(\partial\varphi_{i,a}\partial\varphi_{i,b}\right)$ and physical mesons.

$\tilde{m}^2_{s,00}$	$m^2_{s,11}=m^2_{s,22}$	$\tilde{m}^2_{s,33}$	$m^2_{s,44}=m^2_{s,55}$	$m^2_{s,66}=m^2_{s,77}$	$\tilde{m}^2_{s,88}$
$m^2_{f_0(500)}$	$m^2_{a_0^+}=m^2_{a_0^-}$	$m^2_{a_0^0}$	$m^2_{\kappa^+}=m^2_{\kappa^-}$	$m^2_{\kappa^0}=m^2_{\bar{\kappa}^0}$	$m^2_{f_0(1370)}$
$\tilde{m}^2_{p,00}$	$m^2_{p,11}=m^2_{p,22}$	$\tilde{m}^2_{p,33}$	$m^2_{p,44}=m^2_{p,55}$	$m^2_{p,66}=m^2_{p,77}$	$\tilde{m}^2_{p,88}$
$m^2_{\eta'}$	$m^2_{\pi^+}=m^2_{\pi^-}$	$m^2_{\pi^0}$	$m^2_{K^+}=m^2_{K^-}$	$m^2_{K^0}=m^2_{\bar{K}^0}$	m^2_{η}

Table 3.2.: Values of decay constants of pseudoscalar mesons and meson masses in the vacuum according to Ref. [147], to which the parameters of the mesonic potential are adjusted, as well as the chosen value of the constituent quark mass of the light (up and down) quarks that is used to fix the quark-meson Yukawa coupling.

Constant	f_π	f_K	m_π	m_K	m_η	$m_{\eta'}$	m_σ	m_l
Value [MeV]	92	110	138	495	548	958	400-600	300

The values of the pion and kaon decay constants and of meson masses in the vacuum to which the parameters of the mesonic potential and the vacuum expectation values of the quark condensates are adjusted are listed in Table 3.2. Note that in the determination of the parameters only the sum of the squared masses of the η- and η'-mesons, $m_\eta^2+m_{\eta'}^2$ enters.

The mass of the resonance $f_0\,(500)$ is not exactly known. The most recent compilation of the Particle Data Group [147] considers that it can vary between 400 MeV and 550 MeV. Usually, the resonance $f_0\,(500)$ is considered as the chiral partner of the pion, so as the σ-meson [147]. To keep the notation short this labelling is adopted in the following and $m_\sigma = (400-600)\,\mathrm{MeV}$ is considered to be a reasonable parameter range. Note however that in Ref. [194] it was demonstrated that within an extended quark-meson model that includes vector and axial-vector meson fields, the resonance $f_0\,(1370)$ was identified as the non-strange scalar quarkonium state.

As canonical value for the constituent mass of light quarks $m_\mathrm{l} = 300\,\mathrm{MeV}$ is taken, which results according to Eq. (2.53) in $m_\mathrm{s} \simeq 417\,\mathrm{MeV}$ for the constituent mass of strange quarks.

To the thermal contribution of mesons to the thermodynamics in Eq. (3.21) enter the meson masses (3.31) in the medium. To these do not only contribute the derivatives of the mesonic potential (2.42) and (2.43) and the contribution of quantum fluctuations of

quarks (3.32) but as well the derivatives of the potential of thermal quark fluctuations (3.12) with respect to the meson fields. For the QM model these derivatives are given in Ref. [66] but for the PQM model they are not yet available in the literature and are derived in App. B.

Now, there all contributions at hand required for calculations with the PQM model except of that ingredient that is improved in this work. This is the potential of the order parameter for deconfinement, the Polyakov loop. How its general form can be deduced by the considerations of centre symmetry given in Sec. 2.3.2 is explained in the next section. There are serval forms of the potential that are widely used. The adjustment of their parameters and the quality of their description of pure gauge theory is compared and discussed. How the Polyakov-loop potential for the PQM model can be improved by considering the effect of the backreaction of quarks onto the gauge fields is discussed in Sec. 3.2.1.

Since the Polyakov loop and its conjugate are in general complex variables, the effective potential of the PQM model has an imaginary part as well. This is shown explicitly in Sec. 3.3 and different ways to circumvent this 'sign problem' are discussed. To define a potential which equilibrium states are minima of the effective potential is of importance for the calculation of quasi-equilibrium properties in Chap. 5.

3.2. The Polyakov-loop Potential

First computations of the effective potential in gauge theories have been performed in the 80's at asymptotically high temperatures using perturbation theory [173–175] and in the strong coupling limit on a lattice [176]. In recent years, the non-perturbative Polyakov-loop potential has been studied using various different approaches [36,37,82–84,172,177–183]. First principle calculations of the potential are performed using different functional methods, mainly the functional RG approach but as well Dyson-Schwinger equations and the 2PI-approach [82–84, 172]. In Refs. [36, 37] the Polyakov-loop potential in two flavour QCD in the chiral limit has been analysed. This computation includes the full back-coupling of the matter sector on the propagators of the gauge degrees of freedom via dynamical quark-gluon interactions [184–186].

A much simpler way to obtain an effective Polyakov-loop potential $\mathcal{U}\big(\Phi,\bar{\Phi};T\big)$ is to construct a potential that respects all given symmetries and contains the spontaneous breaking of Z(3) symmetry if the system is in the deconfined phase [176, 187, 188].

The simplest terms that lead to a real potential, respect centre symmetry and are able to describe spontaneous symmetry breaking is a combination of terms of second and forth order $\mathcal{U} \sim p_2\Phi\bar{\Phi}+p_4\left(\Phi\bar{\Phi}\right)^2$. The combination $\Phi\bar{\Phi}$ is also invariant under $U(1)$ transformations. But the potential governing centre symmetry should not introduce any additional symmetries. Therefore, the potential has also to contain terms that break the global symmetry down from $O(2)$ to $Z(3)$. The simplest real term that is invariant under $Z(3)$ but breaks $U(1)$ and is symmetric under charge conjugation is $\left(\Phi^3+\bar{\Phi}^3\right)$.

The only scale to give the potential its correct dimension is the temperature[1], $\mathcal{U} \sim T^4$. The above mentioned terms form the minimal content of a Polyakov-loop potential and the easiest ansatz is a polynomial [69, 168]

$$\frac{\mathcal{U}_{\text{poly}}\left(\Phi,\bar{\Phi},t\right)}{T^4} = p_2(t)\,\Phi\bar{\Phi} + p_3\left(\Phi^3+\bar{\Phi}^3\right) + p_4\left(\Phi\bar{\Phi}\right)^2 . \tag{3.38}$$

The coefficient of the forth order term has be positive so that the potential is bounded from below for large Φ and $\bar{\Phi}$. The coefficient p_2 has to be temperature dependent to realise the transition to a phase where $Z(3)$ symmetry is spontaneously broken. For the later use, this temperature dependence is written here in terms of a reduced temperature $t = (T - T_\text{c})/T_\text{c}$ where $T_\text{c} = T_0$ is in this case the transition temperature of the Polyakov-loop potential. A negative cubic term forces the nature of the transition to be of first order that would be of second order otherwise.

The ansatz for the Polyakov-loop potential can be enhanced by including the term that arrises if one integrates out the SU(3) group volume in the generating functional for the Euclidean action. This integration can be performed via the so-called Haar measure and takes the form of the Jacobian determinant $J\left(\Phi,\bar{\Phi}\right)$. Its logarithm adds as an effective potential to the action in the generating functional [197],

$$\begin{aligned}
&\int \mathcal{D}A \int \mathcal{D}\bar{q} \int \mathcal{D}q \, \exp\left(-S\right) \\
&\qquad \sim \int \prod_{j=1,2,4,5,6,7} \mathrm{d}A_j \int \mathrm{d}A_3 \int \mathrm{d}A_8 \int \mathrm{d}\bar{q} \int \mathrm{d}q \, \exp\left(-S\right) \\
&\qquad = \int \mathcal{D}A_3 \int \mathcal{D}A_8 \int \mathcal{D}\bar{q} \int \mathcal{D}q \, J\left(A_3, A_8\right) \exp\left(-S'\right) \\
&\qquad = \int \mathcal{D}A_3 \int \mathcal{D}A_8 \int \mathcal{D}\bar{q} \int \mathcal{D}q \, \exp\left[-S' + \ln J\left(A_3, A_8\right)\right] .
\end{aligned} \tag{3.39}$$

The explicit computation of the SU(3) Haar measure that leads to the functional dependence of J on Φ and $\bar{\Phi}$ results from integrating out the six non-diagonal Lie algebra directions while keeping the two diagonal elements $A^{3,8}$ that build up Φ. This function already breaks the $U(1)$ symmetry and with a positive coefficient the logarithm bounds the potential from below for large Φ and $\bar{\Phi}$, so that one can drop the cubic and forth order terms of the polynomial while the kinetic part $\sim \Phi\bar{\Phi}$ remains [68, 71],

$$\frac{\mathcal{U}_{\log}\left(\Phi,\bar{\Phi},t\right)}{T^4} = p_2(t)\,\Phi\bar{\Phi} + l(t)\ln\left[1 - 6\Phi\bar{\Phi} + 4\left(\Phi^3+\bar{\Phi}^3\right) - 3\left(\Phi\bar{\Phi}\right)^2\right] . \tag{3.40}$$

This potential is also qualitatively consistent with the leading order result of the strong coupling expansion [198, 199]. An additional feature of the logarithmic term is that the potential diverges for $\Phi, \bar{\Phi} \to 1$ thus limiting the Polyakov loop to be always smaller

[1] When the Polyakov loop is coupled to quarks in the PQM model, the quark chemical potentials μ_f can be adopted as another scale to set the dimension of the potential [195, 196]. But then the Polyakov loop would contribute to the quark densities, $\partial\mathcal{U}/\partial\mu_f \neq 0$.

than one, reaching this value only asymptotically as $T \to \infty$. This is consistent with the domain of the Polyakov loop found by its relation to the free energy of a static quark-antiquark pair in Sec. 2.3.2.

Reference [81] went beyond a minimal content for the Polyakov-loop potential and kept the higher order terms of the polynomial parametrisation of the Polyakov-loop potential and added the logarithmic term to consider the group volume additionally,

$$\begin{aligned} \frac{\mathcal{U}_{\text{polylog}}\left(\Phi,\bar{\Phi},t\right)}{T^4} &= p_2(t)\,\Phi\bar{\Phi} + p_3(t)\left(\Phi^3+\bar{\Phi}^3\right) + p_4(t)\left(\Phi\bar{\Phi}\right)^2 + \\ &\quad + l(t)\ln\left[1 - 6\Phi\bar{\Phi} + 4\left(\Phi^3+\bar{\Phi}^3\right) - 3\left(\Phi\bar{\Phi}\right)^2\right] . \end{aligned} \tag{3.41}$$

Furthermore, they consider all coefficients as temperature depend.

In Refs. [69,71,80] the temperature dependence of the coefficients c of the polynomial and logarithmic parametrisations is parametrised as a polynomial

$$c\,(t) = \sum_n \frac{C_n}{(1+t)^n} , \tag{3.42}$$

where $t = (T - T_\text{c})/T_\text{c}$ defines a reduced temperature and $T_\text{c} = T_0$ is in this case the transition temperature of the Polyakov-loop potential.
The coefficients of the polynomial-logarithmic parametrisation were defined in Ref. [81] in a more complex way,

$$p_i\,(t) = \left[P_0^{(i)} + \frac{P_1^{(i)}}{1+t} + \frac{P_2^{(i)}}{(1+t)^2}\right] \Bigg/ \left[1 + \frac{P_3^{(i)}}{1+t} + \frac{P_4^{(i)}}{(1+t)^2}\right] \tag{3.43}$$

and

$$l(t) = \frac{L_0}{(1+t)^{L_1}}\left[1 - e^{L_2/(1+t)^{L_3}}\right] . \tag{3.44}$$

The number of independent parameters of the different parametrisations can be reduced by imposing some general constraints. One condition is that the Polyakov-loop variables approach unity for large temperatures. A necessary condition for the expectation values of the Polyakov loops is $\partial\mathcal{U}/\partial\Phi = \partial\mathcal{U}/\partial\bar{\Phi} = 0$. This leads to the following constraints on the parameters:

$$\mathcal{U}_{\text{poly}}: \quad P_0 + 3p_3 + 2p_4 = 0 , \tag{3.45a}$$

$$\mathcal{U}_{\log}: \quad L_0 = 0 , \tag{3.45b}$$

$$\mathcal{U}_{\text{polylog}}: \quad P_0^{(2)} + 3P_0^{(3)} + 2P_0^{(4)} = 0 . \tag{3.45c}$$

To fix further parameters one applies and restricts the Polyakov-loop potential to pure gauge (Yang-Mills) theory. The non-presence of dynamical quarks restricts the Polyakov-loop variable to be real, $\Phi = \bar{\Phi}$ as will be explained in Sec. 3.3. Then the expectation

value of the Polyakov loop is a root of

$$\frac{\partial \mathcal{U}_{\text{poly}}}{T^4 \partial \Phi} = 2p_2(t)\,\Phi + 6p_3\Phi^2 + 4p_4\Phi^3 \,, \tag{3.46a}$$

$$\frac{\partial \mathcal{U}_{\log}}{T^4 \partial \Phi} = 2p_2(t)\,\Phi + l(t)\,\frac{-12\Phi + 24\Phi^2 - 12\Phi^3}{1 - 6\Phi^2 + 8\Phi^3 - 3\Phi^4} \,, \tag{3.46b}$$

$$\frac{\partial \mathcal{U}_{\text{polylog}}}{T^4 \partial \Phi} = 2p_2(t)\,\Phi + 6p_3(t)\,\Phi^2 + 4p_4(t)\,\Phi^3 + l(t)\,\frac{-12\Phi + 24\Phi^2 - 12\Phi^3}{1 - 6\Phi^2 + 8\Phi^3 - 3\Phi^4} \,. \tag{3.46c}$$

and thus it is given by

$$\Phi_{\min} = 0 \quad \bigvee \quad \begin{array}{l} \Phi^{\text{poly}}_{\min} = \frac{-3p_3 \pm \sqrt{9{p_3}^2 - 8p_2(t)p_4}}{4p_4} \\ \Phi^{\log}_{\min} = \frac{p_2(t) \pm \sqrt{4\,{p_2}^2(t) - 18\,p_2(t)l(t)}}{3p_2(t)} \end{array} \tag{3.47a}$$

At the transition scale of the Polyakov-loop potential T_0 a first order phase transition is required. This implies $\mathcal{U}\left(\Phi = 0, t = 0\right) = 0 = \mathcal{U}\left(\Phi_{\min} \neq 0, t = 0\right)$ and results in the following condition:

$$\mathcal{U}_{\text{poly}}: \qquad \left(P_0 + 2\,p_4\right)^2 - 9\,p_4 \sum_n P_n = 0 \,, \tag{3.48a}$$

$$\mathcal{U}_{\log}: \qquad \sum_n L_n = 0.216 \sum_n P_n \,, \tag{3.48b}$$

If a reliable prediction of the value of the Polyakov-loop at the phase transition would be available it would further constrain the parameters,

$$\Phi^{\text{poly}}_{\text{t=0}} = \frac{P_0 + 2p_4 + \sqrt{\left(P_0 + 2p_4\right)^2 - 8\,p_4 \sum_n P_n}}{4p_4} \,, \tag{3.49a}$$

$$\Phi^{\log}_{\text{t=0}} = \frac{\sum_n P_n - \sqrt{4\left(\sum_n P_n\right)^2 - 18 \sum_n P_n \sum_m L_m}}{3\sum_n P_n} \,, \tag{3.49b}$$

Furthermore, a gas of quarks and gluons should approach the Stefan-Boltzmann limit as $T \to \infty$. The pressure of $N_{\text{c}} - 1$ non-interacting, massless gluons is

$$p_{\text{SB}}/T^4 = \left(N_{\text{c}}^2 - 1\right)\pi^2/45 \,. \tag{3.50}$$

Since $p = -\mathcal{U}$ this implies in turn for the parameters of the parametrisations

$$\mathcal{U}_{\text{poly}}: \qquad P_0 - p_4 = -\frac{8\pi^2}{15} \,, \tag{3.51a}$$

$$\mathcal{U}_{\log}: \qquad P_0 = -\frac{8\pi^2}{45} \,, \tag{3.51b}$$

$$\mathcal{U}_{\text{polylog}}: \qquad P_0^{(2)} + 2P_0^{(3)} + P_0^{(4)} = -\frac{8\pi^2}{45} \,. \tag{3.51c}$$

Table 3.3.: Parameters of the different parametrisations of the Polyakov-loop potential for fits to the lattice Yang-Mills simulations [200, 201] and [202, 203].

	P_0	P_1	P_2	P_3	p_3	p_4
Poly-BNL [80]	-0.765	-0.48	1.15	1.425	-2.223	3.72
Poly-TUM [69]	-3.375	0.975	-1.3125	3.72	-0.125	1.875
	P_0	P_1	P_2	L_3		
Log [71]	-1.755	1.235	-7.6	-1.75		
Poly-Log [81]	$P_0^{(2)}$	$P_1^{(2)}$	$P_2^{(2)}$	$P_3^{(2)}$	$P_4^{(2)}$	
	22.07	-75.7	45.03385	2.77173	3.56403	
	$P_0^{(3)}$	$P_1^{(3)}$	$P_2^{(3)}$	$P_3^{(3)}$	$P_4^{(3)}$	
	-25.39805	57.019	-44.7298	3.08718	6.72812	
	$P_0^{(4)}$	$P_1^{(4)}$	$P_2^{(4)}$	$P_3^{(4)}$	$P_4^{(4)}$	
	27.0885	-56.0859	71.2225	2.9715	6.61433	
	L_0	L_1	L_2	L_3		
	-0.32665	-82.9823	3.0	5.85559		

The remaining open parameters are determined in Refs. [69, 71, 80, 81] by fitting both the lattice data for pressure, entropy density and energy density and the evolution of the Polyakov loop $\langle\Phi\rangle$ on the lattice in pure gauge theory. Reference [81] adjusted their parameters in addition to lattice data of the longitudinal and transverse Polyakov-loop susceptibilities.
The different parameter sets are summarised in Table 3.3. Reference [81] uses with not less than 19 parameters a huge parameter set compared to the other parametrisations to adjust the potential to the results of Yang-Mills theory. Note that in Ref. [80] the polynomial of p_2 contains all summands up to $n = 6$. To harmonise it with the parametrisation of Ref. [69] the parameter P_3 is adjusted in Ref. [1] to account for the higher order coefficients.

The results for the above discussed quantities that characterise the Polyakov-loop potential are given in Table 3.4. Some differences become apparent. First, the polynomial potential with the parameters of Ref. [80] converges only towards $\sim 85\,\%$ of the Stefan-Boltzmann limit and the polynomial-logarithmic parametrisation reaches only $\sim 93\,\%$ of this high temperature expectation. Second, for the polynomial potential with the parameters of Ref. [69] the Polyakov-loop expectation value at the phase transition is a order of magnitude smaller than for the other parametrisations. The most accurate result for this number is $\Phi_{t=0} = 0.354 \pm 0.008$ [81] calculated on a $64^3 \times 8$ lattice and is

Table 3.4.: Numbers characterising the Polyakov-loop potential. It should be $\Phi_{T\to\infty} = 1$, $(\mathcal{U}/p_{\mathrm{SB}})_{T\to\infty} = 1$ and $\mathcal{U}(\Phi_{t=0}) = 0$.

	$\Phi_{t=0}$	$\mathcal{U}/T^4(\Phi_{t=0})$	$\Phi_{T\to\infty}$	$(\mathcal{U}/p_{\mathrm{SB}})_{T\to\infty}$
Poly-BNL	0.599	5.66×10^{-4}	0.9993	0.852
Poly-TUM	0.072	-4.05×10^{-6}	1.0	0.997
Log	0.449	-8.84×10^{-4}	1.0	1.0
Poly-Log	0.348	-1.18×10^{-4}	1.0	0.933

of the order like in the other parametrisations of the Polyakov-loop potential.

The Polyakov-loop potentials for the different parametrisations and parameter sets[2] are compared in Fig. 3.1. They are displayed for different relative temperatures and are compared to the FRG glue potential where these data are available. At temperatures below the transition temperature all potentials have a global minimum at $\Phi = 0$ but the form and slope of the potential varies considerably between the different parametrisations at non-zero values of the Polyakov loop. But this is the region of the potential that is probed when the Polyakov loop is coupled to dynamical quarks, so in the Polyakov–Quark-Meson model. Hence, one has to expect different results for the Polyakov-loop expectation value and contribution of the Polyakov-loop potential in the fully coupled theory. This dependence of the results of the Polyakov–Quark-Meson model on the parametrisation of the Polyakov-loop potential will be analysed in Sec. 4.1.4.

In the confined phase all potentials are characterised by the identical minimum $(\Phi, \mathcal{U}(\Phi)) = (0, 0)$. The minimum of the deconfined phase at a non-zero value of Φ does not show this uniqueness between the different parametrisations. The value of the Polyakov loop at which it becomes the global minimum close to T_0[3] differs significantly between the different parametrisations as quantified in Table 3.4.

But Fig. 3.1 shows another important difference between the different parametrisations. The barrier between the two minima at the transition temperature differs significantly in its width and height between the different parametrisations. This affects nucleation in Yang-Mills theory and in Sec. 5.4.2 will be discussed how one can account partially for the impact of these different barriers on nucleation within the Polyakov–Quark-Meson model and how they influence the result of the surface tension.

Finally, at temperatures above the transition temperature not only the location of the absolute minimum differs between the different parametrisations but also the depths of

[2] In the following the notion 'different parametrisations' will include the different parameters sets of the polynomial parametrisation.

[3] Unfortunately, not all parametrisations are tuned such that their critical temperature agrees exactly with the parameter T_0.

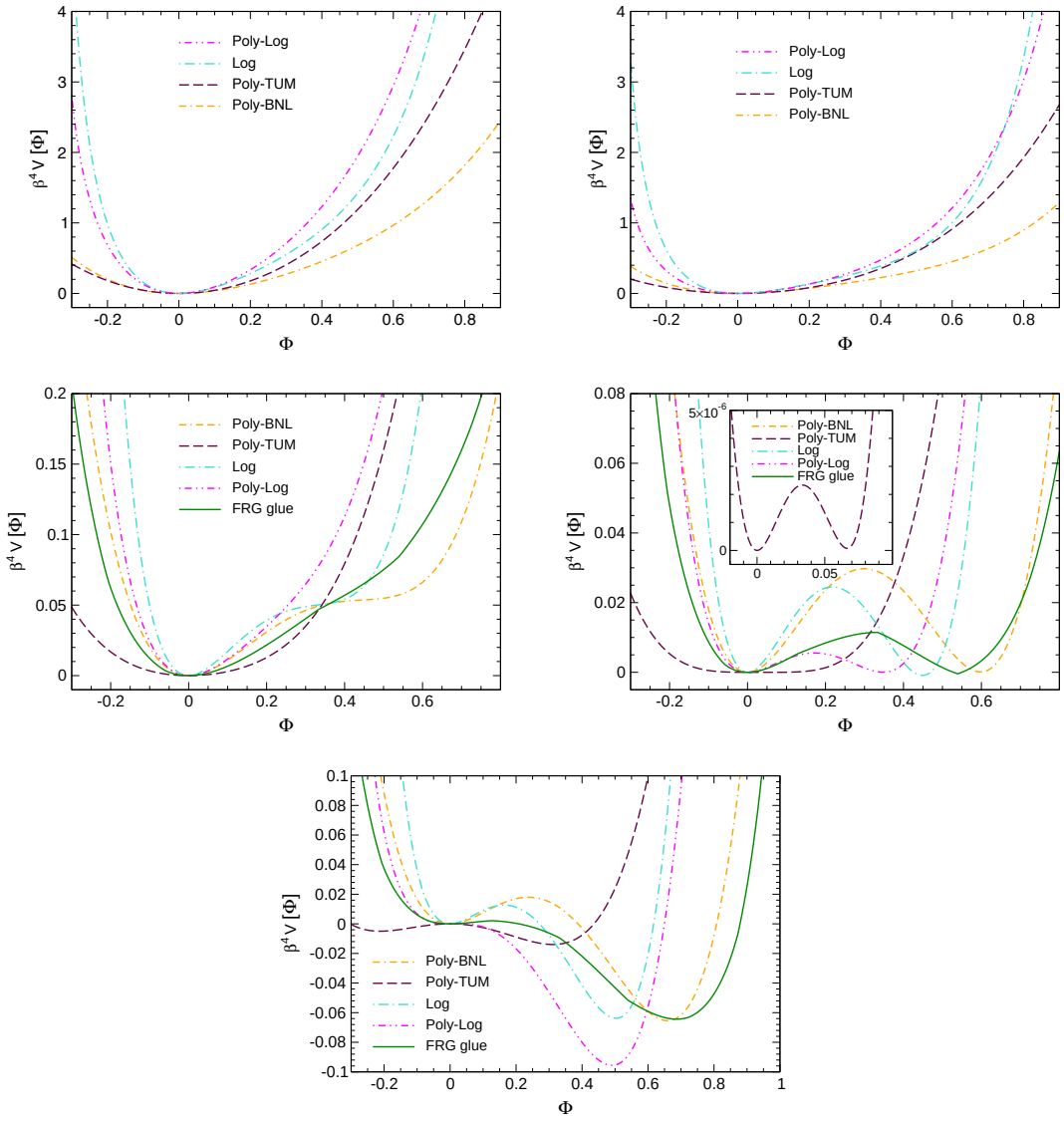

Figure 3.1.: Different parametrisations of the Polyakov-loop potential compared to the FRG glue potential at different temperatures: $t = -0.4$ (top left), $t = -0.25$ (top right), $t = -0.05$ (centre left), $t = 0$ (centre right), $t = 0.05$ (bottom). Note that the abscissae of the parametrisations is the expectation value of the Polyakov loop $\langle \Phi [A_0] \rangle$ while that of the FRG glue potential is $\Phi [\langle A_0 \rangle]$ with $\Phi [\langle A_0 \rangle] \geq \langle \Phi [A_0] \rangle$. See Sec. 2.3.2 for details.

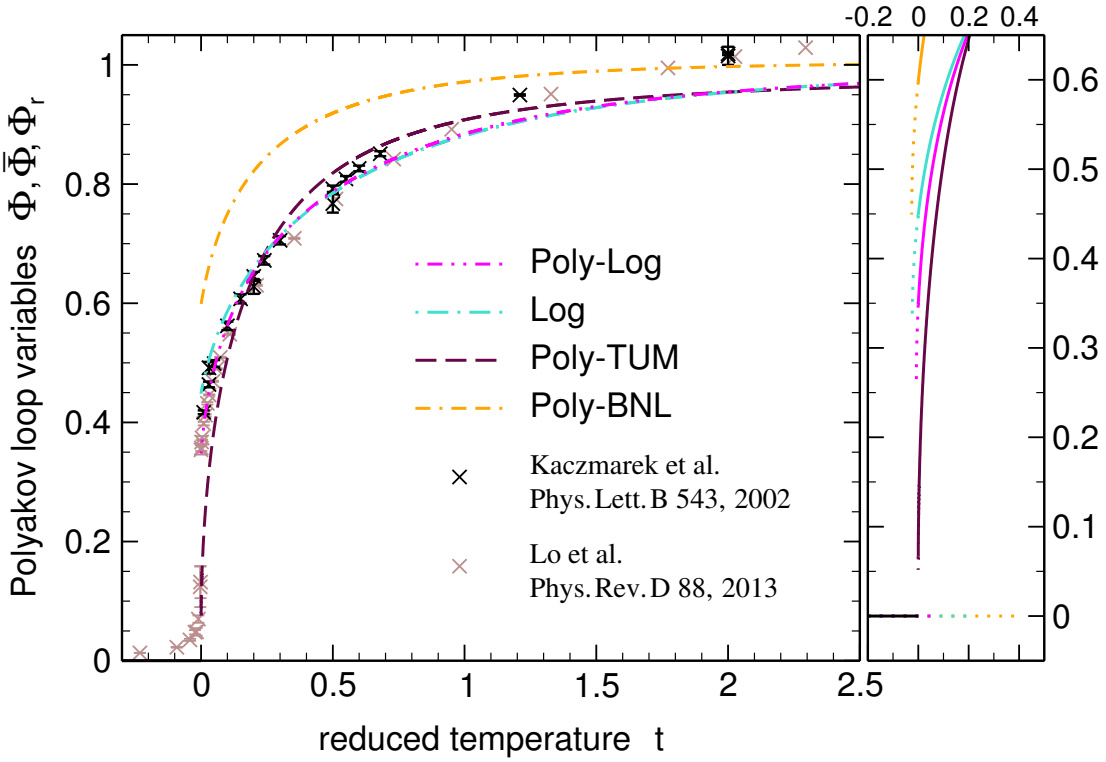

Figure 3.2.: Polyakov loop as a function of the temperature in pure-gauge theory for the different parametrisations of the Polyakov-loop potential, compared to corresponding lattice results taken from Refs. [81, 200].

the potentials. This has an effect on the thermodynamics that is quantified in Figs. 3.3 and 3.4 for pure gauge theory.

But to begin with, Fig. 3.2 shows the Polyakov loop as a function of the temperature in pure $SU(3)$ Yang-Mills theory or, equivalently the location of the global minimum of the Polyakov-loop potential. The data points are results for the renormalised Polyakov loop in lattice simulations of Yang-Mills theory. Those of Ref. [200] have been obtained with a spatial lattice extent of 32 and temporal size of 4 and 8 and Ref. [81] used a $64^3 \times 8$ lattice.

The confined phase is characterised by centre symmetry and, therefore the Polyakov loop vanishes for all parametrisations below the transition temperature.[4] The temperature dependence of the Polyakov loop differs between the different parametrisations above the transition temperature. The logarithmic and polynomial-logarithmic parametrisations only deviate slightly from each other for $\Phi \lesssim 0.7$ and follow closely the lattice data up to $\Phi \lesssim 0.9$. At larger temperature the lattice data rise more rapidly and exceed unity while the parametrisations that include the Haar measure are restricted to $\Phi < 1$.

[4] This is not the case for the lattice data due to the finite volume of the lattice. A finite volume prohibits a first order phase transition and at fixed temporal lattice extent the renormalised Polyakov loop in the confined phase shows a $1/\sqrt{V}$ volume dependence, see e.g. Ref. [81].

The polynomial parametrisation of Ref. [69] undershoots the lattice data for $\Phi \lesssim 0.6$, exceeds them for $0.6 \lesssim \Phi \lesssim 0.9$ and shows a shallow evolution for larger temperatures falling below the logarithmic and polynomial-logarithmic parametrisations for $t \gtrsim 2$. The polynomial parametrisation of Ref. [80] shows the largest deviation of the Polyakov loop from the lattice data. The deconfined phase starts with the largest value for the Polyakov loop of all parametrisations. It rises fast towards unity and therefore, exceeds the other parametrisations for all temperatures and is the closest to the lattice data at $t \approx 2$.
The right part of Fig. 3.2 shows a zoom into the transition region. Here, the different starting values of the Polyakov loop in the deconfined phase for the different parametrisations are easy to identify. The polynomial-logarithmic and logarithmic parametrisations start with $\Phi \approx 0.35$ and $\Phi \approx 0.45$, respectively and are the closest to the starting values of the lattice data they are fitted to: $(t, \Phi) = (0, 0.354 \pm 0.008)$, [81], $(t, \Phi) = (0.01, 0.420 \pm 0.003)$, [200]. The value of the Polyakov loop where the deconfined phase becomes the dominant minimum of the polynomial potential of Ref. [80] is of the same order as these lattice data but exceeds them: $\Phi \approx 0.60$. The other extreme is the polynomial parametrisation of Ref. [69]. This potential features a comparatively week first order phase transition to a value for Φ of ~ 0.07. Hence, even with the same height of the barrier between the two coexisting minima at the transition as the other parametrisations the probability to tunnel from one minimum to the other is significantly larger for the polynomial potential of Ref. [69]. How this affects nucleation within the Polyakov–Quark-Meson model will be quantified in Sec. 5.4.2.
The dotted lines in the right part of Fig. 3.2 show the extent of the metastable region where a local minimum coexists. Also this quantity varies considerably between the different parametrisations of the Polyakov-loop potential. The parameterisations that show the broader and taller barrier between the two minima at the transition have also a larger extent of the metastable region. Hence, the polynomial parametrisation of Ref. [69] has a negligible metastable region ($-1 \times 10^{-4} \lesssim t \lesssim 9 \times 10^{-4}$). The one of the polynomial-logarithmic parametrisation ($-0.008 \lesssim t \lesssim 0.062$) is significantly smaller than the one of the logarithmic parametrisation ($-0.02 \lesssim t \lesssim 0.21$) since the barrier of the polynomial-logarithmic parametrisation is much shorter at a similar width as the one of the logarithmic parametrisation. The metastable region of the polynomial potential of Ref. [80] extends from $t \approx -0.03$ to $t \approx 0.40$. In general, the metastable region has an asymmetric extent. The minimum at $\Phi = 0$ persists in a larger temperature range above the transition than the metastable minimum of the deconfined phase below the transition temperature. This asymmetry is also suggested in the FRG result of the glue potential in Fig. 3.1.

While Fig. 3.2 reveals the temperature dependence of the location of the minimum of the Polyakov loop potential, Fig. 3.3 shows the depths of the global minimum ($p = -\mathcal{U}$) as a function of the temperature. At $\Phi = 0$ the pressure of the Polyakov-loop poten-

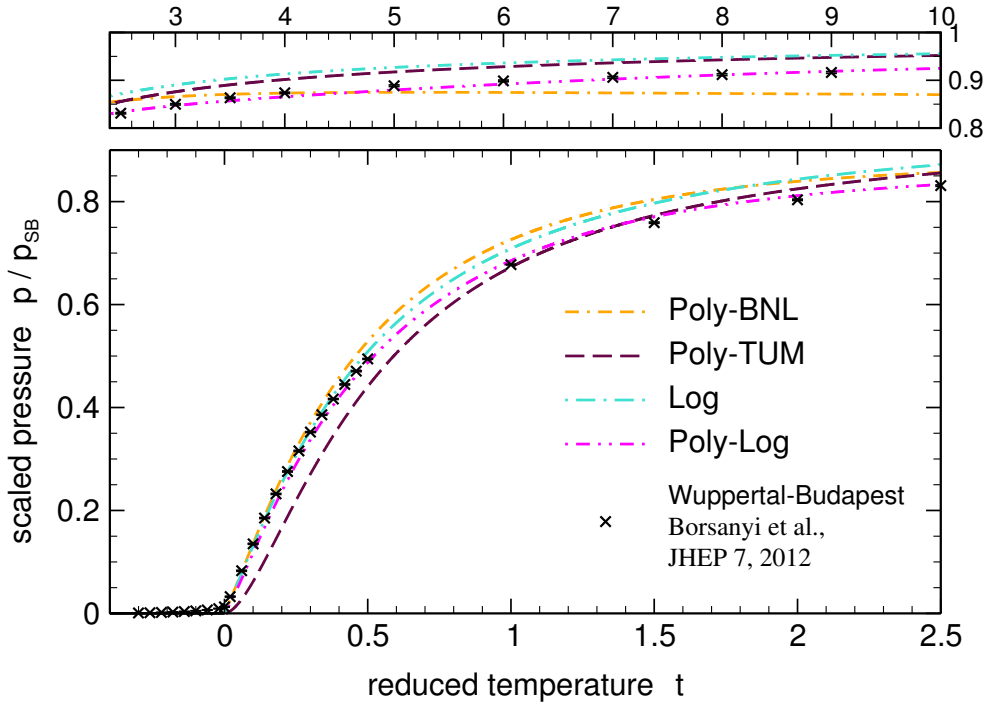

Figure 3.3.: Scaled pressure as a function of the reduced temperature in the pure-gauge sector for the different parametrisations of the Polyakov-loop potential, compared to corresponding lattice results taken from Ref. [203].

tial vanishes. The continuum extrapolated lattice results of Ref. [203][5] show a slight increase of the pressure already below the transition temperature up to $\sim 1.3\,\%$ of the Stefan-Boltzmann limit. This can be attributed to the thermal excitation of glueballs and is reproduced in Ref. [203] within a glueball resonance model including a Hagedorn spectrum. These are additional ingredients of the gauge sector that are not governed by centre symmetry. The confinement of gluons into glueballs can be associated with the breaking of scale symmetry in the confined phase [204–206]. In an extension of the present work a potential for the dilaton field that is the order parameter for scale symmetry can be added to the Polyakov-loop potential to include also this property of the gauge sector.[6]

For the evolution of the pressure of the different parametrisations relative to the lattice data qualitatively similar conclusions hold as for the temperature dependence of the Polyakov loop. In the deconfined phase the minimum of the polynomial parametrisation of Ref. [69] is considerably less deep than the lattice data suggest. It reaches the lattice result at $\sim 68\,\%$ of the Stefan-Boltzmann limit and exceeds the data from there on. The polynomial potential of parametrisation [80] has the largest slope of the temperature

[5] The continuum limit can be achieved by performing an $1/N_t \to 0$ extrapolation on the data at a set of fixed physical temperatures.

[6] This implies that the parameters of the Polyakov-loop potential have to be readjusted such that both potentials together reproduce the thermodynamics of lattice Yang-Mills theory.

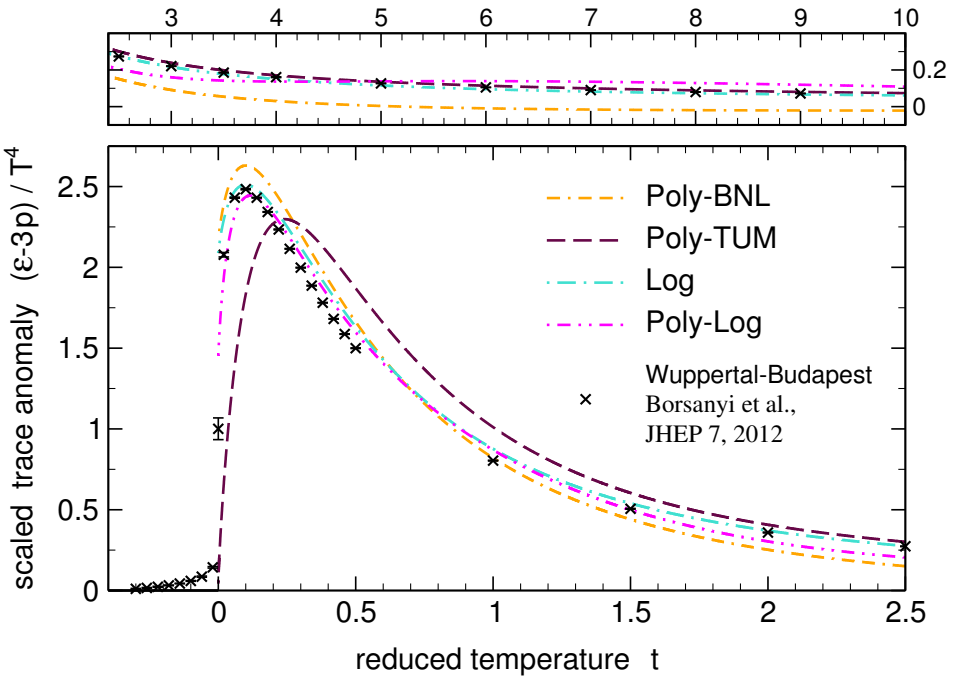

Figure 3.4.: Scaled trace anomaly as a function of the reduced temperature in the pure-gauge sector for the different parametrisations and parameter sets of Table 3.3, compared to corresponding lattice results taken from Ref. [203].

dependence of the pressure for $0 < t \lesssim 0.6$ in comparison to those potentials that consider the Haar measure. It only deviates slightly from the lattice data up to $\sim 50\,\%$ of the Stefan-Boltzmann pressure before exceeding them more visibly and showing a shallow evolution at even larger temperatures. The depth of the polynomial-logarithmic potential at its minimum is very precisely adjusted to the lattice Yang-Mills pressure of Ref. [203] over the whole temperature range. While it slightly underestimates the pressure for $p \lesssim 0.5\, p_{\mathrm{SB}}$, the logarithmic potential is the closest to the lattice data in this range above the transition temperature.

For the sake of completeness, the upper part of Fig. 3.3 shows the high temperature convergence of the pressure. While this tests the description of pure gauge theory by the Polyakov-loop potentials their behaviour in this temperature range is not relevant for predictions on the QCD phase transition at a much lower scale. The polynomial-logarithmic potential reaches $\sim 92\,\%$ of the Stefan-Boltzmann pressure at $t_{\mathrm{YM}} = 10$ and coincides with the lattice data in this temperature regime. The result of the logarithmic potential and the polynomial parametrisation of Ref. [69] exceeds them and they converge towards $0.95\, p_{\mathrm{SB}}$ in the shown region. The polynomial parametrisation of Ref. [80] fails to describe the high temperature convergence of the depth of the gauge potential. Instead of converging towards the Stefan-Boltzmann limit its pressure reaches a maximum of $\sim 0.87\, p_{\mathrm{SB}}$ at $t_{\mathrm{YM}} \approx 6.2$ and slightly decreases from there on.

While the pressure of a theory probes the depths of the minimum of a potential, the entropy density $s = -\partial\Omega/\partial T$ tests its temperature dependence. For the evolution of the entropy and energy density ($\epsilon = Ts - p$) with temperature qualitatively the same conclusions hold as for the discussion of the pressure. To avoid a tedious discussion the comparison of the entropy and energy density of the different parametrisations of the Polyakov-loop potential and its comparison to lattice data is transferred to App. B.

Here, the discussion proceeds with the combined quantity $\epsilon - 3p$. If this is nonzero it deviates from the trace of the energy momentum tensor of an ideal gas for which reason this quantity is also called trace anomaly or interaction measure. Figure 3.4 shows the result of the dimensionless trace anomaly as a function of the temperature for the different parametrisations of centre symmetry breaking. Here, the conclusions drawn from the evolution of the pressure about the minimum of the different potentials appear even clearer. The development of the centre symmetry breaking minimum in the polynomial potential of Ref. [69] lags behind the lattice data and the other potentials what leads to an offset of the maximum of the interaction measure towards larger temperatures. Only at temperatures more than two times larger than the transition scale of the Polyakov-loop potential this potential approaches the trace anomaly of lattice gauge theory. The other potentials scatter close around the lattice data. Those potentials that include the Haar measure are the closest to the data points. The maximum of the trace anomaly of the polynomial potential [80] overshoots the lattice data by $\sim 6\,\%$ and the polynomial-logarithmic potential shows a slight offset of the maximum towards larger temperatures. None of the parametrisations reproduces the temperature dependence of the depth of the potential at the transition temperature on the lattice $\left(t, (\epsilon - 3p)/T^4\right) = (0, 1.0008 \pm 0.0672)$. The polynomial potential of Ref. [69] clearly underestimates it (0.0423), while the polynomial parametrisation of Ref. [80] (2.1785), the logarithmic potential (2.0885) and the polynomial logarithmic potential (1.4519) overshoot it.

To summarise this discussion one can conclude that the polynomial parametrisation of the Polyakov-loop potential with the parameter set of Ref. [69] is the least suited to reproduce with its location, depth and temperature dependence of the depth of its minimum the lattice data of the Polyakov loop and the thermodynamics of pure gauge theory. Using instead the parameter set of Ref. [80] only the Polyakov loop is too much off compared to the lattice data but the thermodynamics is reasonable for temperatures up to $t \sim 6$. Only the parametrisations of the Polyakov-loop potential that respect the Haar measure lead to a satisfying agreement of all above discussed observables with the results of lattice simulations.[7] How these different potentials adjusted more or less precisely to the deconfined phase of Yang-Mills theory prove their value in the Polyakov–Quark-Meson Model to describe the QCD phase transition will be analysed in Chaps. 4

[7] Reference [81] showed that the logarithmic potential can't reproduce their lattice result for the curvature $\delta^2\mathcal{U}/\delta\Phi^2$ above the transition temperature and they fitted the parameters of the polynomial-logarithmic parametrisation to reproduce also these data.

Table 3.5.: Transition scale of the Polyakov-loop potential T_0 in the presence of N_f massless quark flavours and in the physical case with massive strange quarks with a current strange quark mass of 95 MeV [147], according to Eq. (3.53).

N_f	0	1	2	3	$2+1$
T_0 [MeV]	270	239	208	178	182

and 5.

The construction of the Polyakov-loop potential $\mathcal{U}$ and the fitting of its parameters entails that it models the pure gauge potential $\mathcal{U}_{\rm YM}\left(t_{\rm YM}\right)/T^4$. The transition scale of the Polyakov-loop potential entering the reduced temperature is accordingly the critical temperature of pure gauge theory, $T_0^{\rm YM} = 270\,\text{MeV}$. However, in full dynamical QCD, one important effect of fermionic matter fields is to change the scale $\Lambda_{\rm QCD}$ to which the transition temperature of the Polyakov-loop potential is linked to. To consider this aspect of the backreaction of quarks to the gauge sector, Ref. [72] estimated the running coupling of QCD by consistency with hard thermal loop perturbation theory calculations [185,207] and they mapped the effect to an N_f-dependent modification of the expansion coefficients of the Polyakov-loop potential. Their result of the N_f-dependent decrease of T_0 is given in Table 3.5. This accounts partially for the unquenching of the pure gauge Polyakov-loop potential to an effective glue potential in QCD.

Besides the flavour dependency of the transition scale of the glue sector, one can consider its dependence on the quark density. Such a dependency has to be expected in view of a $\mu_{\rm q}$-dependent colour screening effect due to quarks. In Ref. [72] a $\mu_{\rm q}$-dependent small correction to the running coupling was motivated by using HTL/HDL theory and by comparison to the one found in FRG calculations [36]. The description presented in Refs. [72,78] can be generalised to allow for different chemical potentials for each quark flavour,

$$T_0\left(\mu_f\right) = m_\tau e^{-1/\left(\alpha_0 b\left(\mu_f\right)\right)} \qquad \text{with} \qquad b\left(\mu_f\right) = \bar{b}\left(N_f\right) - b_\mu \sum_{N_f} \frac{\mu_f^2}{m_\tau^2} \frac{\tilde{T}_0^2}{\tilde{T}_0^2 + m_f^2} \tag{3.52}$$

and $b_\mu \simeq 16/\pi$. The parameter $\bar{b}$ can account for the dependence on the number of quark flavours. For the results presented in Table 3.5 the following N_f dependence was chosen

$$\bar{b}\left(N_f\right) \;=\; \frac{1}{6\pi}\left[11 N_{\rm c} - 2\sum_{N_f} \frac{\tilde{T}_0^2}{\tilde{T}_0^2 + m_f^2}\right] . \tag{3.53}$$

The pure gauge limit ($N_f = 0$) allows to fix the running coupling at a UV-scale of

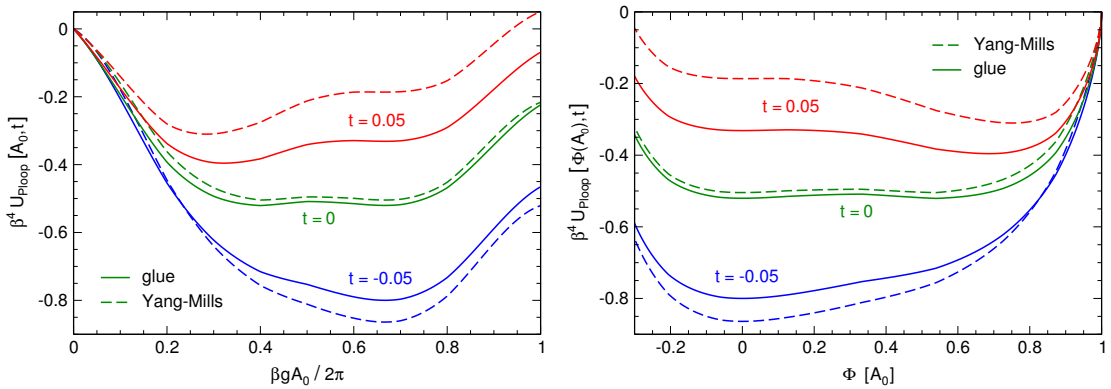

Figure 3.5.: Comparison of the SU(3) Yang-Mills [82–84] and glue effective potentials [36, 37] as functions of the background gauge field $A_0 = \langle A_0^3 \rangle$ (left, from Ref. [2]) and of the related order parameter $\Phi[\langle A_0 \rangle]$ (right) for several reduced temperatures. The form of the potentials is very similar, however, the temperature scale changes. Only the glue part of the full effective potential is shown here and compared to the Yang-Mills potential.

$m_\tau \simeq 1.777$ GeV to $\alpha_0 \simeq 0.303$. The impact of massive quarks is suppressed by their current quark mass m_f relative to the critical temperature of one massless flavour $\tilde{T}_0$.

3.2.1. The Polyakov-loop Potential with Functional Methods in Pure Gauge Theory and Full QCD

So far, the Polyakov-loop potential is an approximation to the Yang-Mills glue potential. However, in Polyakov-loop extended models for (full) QCD, this Polyakov-loop potential has to be replaced by the QCD glue potential effectively generated by pure gluodynamics. It is therefore beneficial to amend the pure gauge Polyakov-loop potential by utilising available information on the potential stemming from the gauge degrees of freedom in the presence of dynamical quarks. Using the functional renormalisation group (FRG) approach outlined in App. A, Refs. [82–84] calculated the non-perturbative Polyakov-loop potential of pure gauge theory and Refs. [36,37] the QCD analogue taking into account the backreaction of the quark degrees of freedom on the gluon propagators. Figure 3.5 compares the effective potential of SU(3) Yang-Mills theory as obtained in Refs. [82–84] with the Polyakov-loop potential of the glue sector [36, 37][8]. The latter includes also the quark part of the gluonic vacuum polarisation but does not include the fermionic part of the full QCD potential. The respective reduced temperature scales of

[8] In these references they considered the Polyakov-loop potential which has been computed by considering two quark flavours with vanishing current masses. The strange quark has been ignored. Corrections resulting from the inclusion of a strange quark are expected to be subleading in these studies [2].

both potentials are

$$t_{\mathrm{glue}} = \frac{T - T_{\mathrm{cr}}^{\mathrm{glue}}}{T_{\mathrm{cr}}^{\mathrm{glue}}} \qquad \text{and} \qquad t_{\mathrm{YM}} = \frac{T - T_{\mathrm{cr}}^{\mathrm{YM}}}{T_{\mathrm{cr}}^{\mathrm{YM}}} \ . \tag{3.54}$$

The order parameters $\langle A_0 \rangle$ and $\Phi[\langle A_0 \rangle]$ show a first-order phase transition for both, the glue potential and the Yang-Mills potential. One sees in Fig. 3.5 a shift between both potentials for a given nonzero reduced temperature or in other words, the temperature scale of the various Yang-Mills potentials and the glue potentials differ. These differences are induced by the matter fluctuations altering the propagators of the gauge fields. One observes furthermore that although the temperature scales are different, the shape of the order-parameter potentials is not. This observation can be exploited to estimate how the temperature of a given pure gauge Polyakov-loop potential has to be modified to be closer to the unquenched glue potential. For a quantitative comparison of the potentials one needs to define a measure,

$$\int_0^{2\pi/\beta} \mathrm{d}A_0 \left| \mathcal{U}_{\mathrm{YM}}\left(A_0\right) - \mathcal{U}_{\mathrm{glue}}\left(A_0\right) \right|^2 \ . \tag{3.55}$$

The comparison of the potentials then yields the translation of the two temperature scales: given a reduced QCD temperature t_{glue}, the related Yang-Mills temperature t_{YM} is that which minimises Eq. (3.55). This leads to

$$t_{\mathrm{YM}}(t_{\mathrm{glue}}) \approx 0.57\, t_{\mathrm{glue}} \ . \tag{3.56}$$

This relation between pure gauge and unquenched glue potential is displayed in Fig. 3.6. Strictly speaking, this approximation holds only for small and moderate temperatures, as at high scales the slope of Eq. (3.56) saturates, where one reaches the perturbative limit and the potentials reach their asymptotic form. In fact, one should expect that the results for the reduced temperatures agree at (very) high temperatures where the quark degrees of freedom are parametrically suppressed. The relation (3.56) serves together with the absolute temperature scales $T_{\mathrm{cr}}^{\mathrm{glue}}$ and $T_{\mathrm{cr}}^{\mathrm{YM}}$ in the definition of the reduced temperatures (3.54) as an important input for Polyakov-loop model studies. In Refs. [82–84] they got $T_{\mathrm{cr}}^{\mathrm{YM}} = 276\,\mathrm{MeV}$ which is in quantitative agreement with the results from lattice studies $T_0^{\mathrm{YM}} = 270\,\mathrm{MeV}$. In Refs. [36,37] where they considered two quark flavours with vanishing current masses they obtained $T_{\mathrm{cr}}^{\mathrm{glue}} = 203\,\mathrm{MeV}$. Note that this is not the critical temperature obtained from the full effective potential including pure quark loops but only from the contribution stemming from the glue part of the potential for two massless quark flavours. But in Ref. [36] the absolute temperature scale was not computed in a chiral extrapolation with physical quark masses. Hence, throughout this work the glue critical temperature will be considered as a free parameter in the range

$$180\,\mathrm{MeV} \lesssim T_{\mathrm{cr}}^{\mathrm{glue}} \lesssim 270\,\mathrm{MeV} \ . \tag{3.57}$$

The upper limit is the critical temperature of Yang-Mills theory and the lower limit is the estimate of Ref. [72] given in Table 3.5. For the chemical potential dependence of

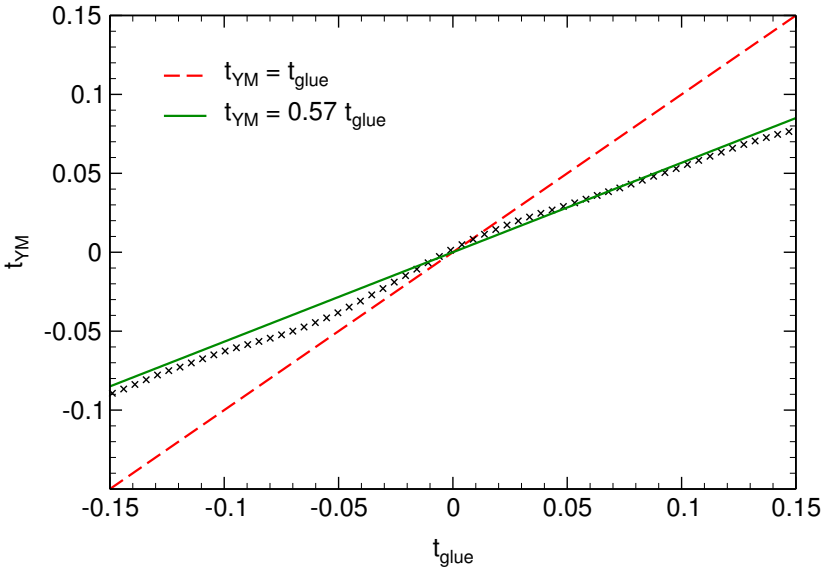

Figure 3.6.: Relation between the two temperature scales of pure Yang-Mills theory [82–84] and the glue part of the study [36,37] including the backreaction of the quarks on the gauge fields. The solid (green) line is a fit to the numerical data (black crosses) in the range around the transition temperatures. A clear deviation from linear behaviour with slope one (dashed red line), i.e., from pure Yang-Mills theory, can be recognised. From Ref. [2].

$T_{\mathrm{cr}}^{\mathrm{glue}}$ the estimation (3.52) of Ref. [72] can be applied.

To summarise this section, one can conclude that the thitherto use of the model potentials $\mathcal{U}$ incorporates several approximations and deficiencies. Firstly, a Yang-Mills potential is used instead of the glue potential. Secondly, it only models the Polyakov-loop potential in Yang-Mills theory by using the location of its absolute minimum and the value at the minimum. Below T_0 this basically provides no information about the potential. Thirdly, the potential has to be known as a function of $\Phi[\langle A_0 \rangle]$ as the coupling to the matter sector is described in this variable as will be discussed in Sec. **??**. Strictly speaking, $\Phi\left[\langle A_0 \rangle\right] \approx \langle \Phi \rangle$ is only valid in the Gaußian approximation but in general it is $\Phi[\langle A_0 \rangle] \geq \langle \Phi \rangle$ up to renormalisation issues [82,172]. In this work the first approximation is resolved by using the relation between pure gauge and glue effective potential (3.56). This allows to convert the Yang-Mills potential for the Polyakov loop to a glue potential of full QCD,

$$\frac{\mathcal{U}_{\mathrm{glue}}}{T^4}\left(\Phi, \bar{\Phi}, t_{\mathrm{glue}}\right) = \frac{\mathcal{U}_{\mathrm{YM}}}{T_{\mathrm{YM}}^4}\left(\Phi, \bar{\Phi}, t_{\mathrm{YM}}(t_{\mathrm{glue}})\right) , \tag{3.58}$$

with $t_{\mathrm{YM}}(t_{\mathrm{glue}})$ in Eq. (3.56). The absolute temperature scale is then determined by the value of the transition temperature (3.57). The resolution of the other two approximations remains for the future.

3.3. The Sign Problem in the Polyakov–Quark-Meson Model

Given the temperature T and the quark chemical potentials μ_f, the effective potential (3.14) is then given as a function of the order parameters of the model. In thermal equilibrium, the field configurations that contribute the most to the partition function are those that minimise the in-medium effective potential (or the in-medium effective action, for non-homogeneous systems). All other extrema of the effective action are exponentially suppressed and give negligible contributions to the equilibrium thermodynamics of the system. Only with equilibrium states described by minima of the effective potential one can calculate quasi-equilibrium properties of the system, such as the surface tension and nucleation rate in a first-order phase transition, as will bee done in Chap. 5. The calculation of these properties explicitly demands not only the localisation of the minima of the effective potential, but also the precise form of the potential between them.

The one-loop effective potential of the PQM model at finite temperature and quark chemical potential, as defined in Eq. (3.14), is in general a complex function of complex variables. Therefore, it can have no minima and, as it stands, it cannot provide a standard description for a thermodynamical system in equilibrium. Finally, it only makes sense to identify the extrema of a function with maxima, minima and saddle-points if it is a real function of real variables. In order to make this statement clearer, it is helpful to identify the real and imaginary parts of the effective potential at finite T and μ_f. Thus, one must write down the effective potential in terms of these real variables only. To this end one can start with a change of variables in the potential by introducing the real and imaginary parts of the Polyakov-loop variables as

$$\Phi_\mathrm{r} \equiv \frac{\Phi + \bar{\Phi}}{2} \quad \text{and} \quad \Phi_\mathrm{i} \equiv \frac{\Phi - \bar{\Phi}}{2\mathrm{i}}. \tag{3.59}$$

The parametrisations of the Polyakov-loop potential (3.38), (3.40) and (3.41) can be rewritten as functions of the real variables Φ_r and Φ_i as

$$\frac{\mathcal{U}_\mathrm{poly}\left(\Phi_\mathrm{r}, \Phi_\mathrm{i}, t\right)}{T^4} = p_2(t)\left(\Phi_\mathrm{r}^2 + \Phi_\mathrm{i}^2\right) + 2p_3\left(\Phi_\mathrm{r}^3 - 3\Phi_\mathrm{r}\Phi_\mathrm{i}^2\right) + p_4\left(\Phi_\mathrm{r}^2 + \Phi_\mathrm{i}^2\right)^2 , \tag{3.60a}$$

$$\frac{\mathcal{U}_\mathrm{log}\left(\Phi_\mathrm{r}, \Phi_\mathrm{i}, t\right)}{T^4} = p_2(t)\left(\Phi_\mathrm{r}^2 + \Phi_\mathrm{i}^2\right) + \\ + l(t)\ln\left[1 - 6\left(\Phi_\mathrm{r}^2 + \Phi_\mathrm{i}^2\right) + 8\left(\Phi_\mathrm{r}^3 - 3\Phi_\mathrm{r}\Phi_\mathrm{i}^2\right) - 3\left(\Phi_\mathrm{r}^2 + \Phi_\mathrm{i}^2\right)^2\right] , \tag{3.60b}$$

$$\frac{\mathcal{U}_\mathrm{polylog}\left(\Phi_\mathrm{r}, \Phi_\mathrm{i}, t\right)}{T^4} = p_2(t)\left(\Phi_\mathrm{r}^2 + \Phi_\mathrm{i}^2\right) + 2p_3(t)\left(\Phi_\mathrm{r}^2 - 3\Phi_\mathrm{r}\Phi_\mathrm{i}^2\right) + p_4(t)\left(\Phi_\mathrm{r}^2 + \Phi_\mathrm{i}^2\right)^2 + \\ + l(t)\ln\left[1 - 6\left(\Phi_\mathrm{r}^2 + \Phi_\mathrm{i}^2\right) + 8\left(\Phi_\mathrm{r}^3 - 3\Phi_\mathrm{r}\Phi_\mathrm{i}^2\right) - 3\left(\Phi_\mathrm{r}^2 + \Phi_\mathrm{i}^2\right)^2\right] . \tag{3.60c}$$

Let us now turn to the contribution from the quarks at finite temperature and chemical potentials. Once Φ and $\bar{\Phi}$ are complex-valued variables, the potential (3.12) can take complex values. To make this statement explicit $\Omega^{\rm th}_{\rm q\bar{q}}$ can be rewritten as a function of real variables. Dropping the flavour indices to keep the notation simpler, one can define

$$z_+ \equiv 1 + 3\left(\Phi + \bar{\Phi}e^{-(E-\mu)/T}\right)e^{-(E-\mu)/T} + e^{-3(E-\mu)/T}, \tag{3.61}$$

and

$$z_- \equiv 1 + 3\left(\bar{\Phi} + \Phi e^{-(E+\mu)/T}\right)e^{-(E+\mu)/T} + e^{-3(E+\mu)/T}, \tag{3.62}$$

such that Eq. (3.12) can now be written as

$$\Omega^{\rm th}_{\rm q\bar{q}} = -2T\sum_{f={\rm u,d,s}}\int\frac{{\rm d}^3k}{(2\pi)^3}\ln\left(z_+z_-\right)\ . \tag{3.63}$$

After using Eq. (3.59) and performing some straightforward manipulations, one can see that the argument of the logarithm in Eq. (3.63) is complex, that is,

$$z_+z_- = R + {\rm i}I, \tag{3.64}$$

where

$$\begin{aligned} R \equiv\ & 1 + e^{-3(E-\mu)/T} + e^{-3(E+\mu)/T} + e^{-6E/T} + \\ & + 6\,\Phi_{\rm r}\,e^{-E/T}\left[\cosh\left(\frac{\mu}{T}\right) + e^{-E/T}\cosh\left(\frac{2\mu}{T}\right)\right] + \\ & + 6\,\Phi_{\rm r}\,e^{-4E/T}\left[\cosh\left(\frac{2\mu}{T}\right) + e^{-E/T}\cosh\left(\frac{\mu}{T}\right)\right] + \\ & + 9\left(\Phi_{\rm r}^2 + \Phi_{\rm i}^2\right)\left(1 + e^{-2E/T}\right)e^{-2E/T} + 18\left(\Phi_{\rm r}^2 - \Phi_{\rm i}^2\right)e^{-3E/T}\cosh\left(\frac{\mu}{T}\right) \end{aligned} \tag{3.65}$$

and

$$\begin{aligned} I \equiv\ & 6\,\Phi_{\rm i}\,e^{-E/T}\left[\sinh\left(\frac{\mu}{T}\right) - e^{-E/T}\sinh\left(\frac{2\mu}{T}\right)\right] + \\ & + 6\,\Phi_{\rm i}\,e^{-4E/T}\left[e^{-E/T}\sinh\left(\frac{\mu}{T}\right) - \sinh\left(\frac{2\mu}{T}\right)\right] - \\ & - 36\,\Phi_{\rm r}\,\Phi_{\rm i}\,\sinh\left(\frac{\mu}{T}\right)e^{-3E/T}\ . \end{aligned} \tag{3.66}$$

The complex argument of the logarithm can be written in polar form, $R + {\rm i}\,I = \rho e^{{\rm i}\theta}$, with

$$\rho \equiv \sqrt{R^2 + I^2} \quad \text{and} \quad \theta \equiv \arctan\left(I/R\right)\ , \tag{3.67}$$

so that the potential can be cast in a manifestly complex form,

$$\Omega^{\rm th}_{\rm q\bar{q}} = \Omega^{\rm R}_{\rm q\bar{q}} + {\rm i}\,\Omega^{\rm I}_{\rm q\bar{q}}\ , \tag{3.68}$$

where

$$\Omega^{\mathrm{R}}_{\mathrm{q\bar{q}}} \equiv -2T \sum_{f=\mathrm{u,d,s}} \int \frac{\mathrm{d}^3k}{(2\pi)^3} \ln\rho \tag{3.69}$$

and

$$\Omega^{\mathrm{I}}_{\mathrm{q\bar{q}}} \equiv -2T \sum_{f=\mathrm{u,d,s}} \int \frac{\mathrm{d}^3k}{(2\pi)^3} \theta \tag{3.70}$$

The imaginary part (3.70) is the manifestation of the fermion sign problem in the context of the Polyakov–Quark-Meson model already at the one-loop level. Note that it is very closely related to the sign problem in lattice QCD, in the so-called matrix model and in the PNJL model [52, 88–90]. An important aspect of Eq. (3.70) is that it vanishes for $\mu_f = 0$, so that the effective potential becomes real and free of the sign problem. Furthermore, Eq. (3.70) is odd in Φ_{i}, while the real part (3.69) is even in Φ_{i}. This means that one must have $\langle\Phi_{\mathrm{i}}\rangle = 0$, i.e., $\langle\Phi\rangle = \langle\bar{\Phi}\rangle$ for $\mu_f = 0$, which is a well-known result.

In order to make the sign problem in the PQM model explicit, let us write the grand partition function for the model in the mean-field approximation

$$\mathcal{Z} = \int \mathrm{D}\vec{\Psi} \exp\left[-\frac{V}{T}\Omega(\vec{\Psi})\right] , \tag{3.71}$$

where V is the volume of the space and $\vec{\Psi} = (\sigma_{\mathrm{u}}, \sigma_{\mathrm{d}}, \sigma_{\mathrm{s}}, \Phi_{\mathrm{r}}, \Phi_{\mathrm{i}})$ formally represents the (real) order parameters.

Notice from Eqs. (3.60) and (3.68) that the imaginary part of the quark contribution is odd in Φ_{i} and all the other contributions to the effective potential are even in Φ_{i}. So one can split the effective potential in a Φ_{i}-odd part that coincides with $\Omega^{\mathrm{I}}_{\mathrm{q\bar{q}}}$ and a Φ_{i}-even part. The functional integral is to be performed for every possible (real) value that Φ_{i} can assume. One can organise the sum such that the contributions for a given Φ_{i} and its negative $-\Phi_{\mathrm{i}}$ are assembled. After a few simple manipulations, one finds

$$\begin{aligned} \mathcal{Z} &= \int_{\Phi_{\mathrm{i}}\in\mathbb{R}} \mathrm{D}\vec{\Psi} \exp\left[-\frac{V}{T}\left(\Omega_{\Phi_{\mathrm{i}}-even} + \mathrm{i}\Omega^{\mathrm{I}}_{\mathrm{q\bar{q}}}\right)\right] \\ &= \int \mathrm{D}\vec{\Psi} \exp\left[-\frac{V}{T}\Omega_{\Phi_{\mathrm{i}}-even}\right] \cos\left[-\frac{V}{T}\Omega^{\mathrm{I}}_{\mathrm{q\bar{q}}}\right] . \end{aligned} \tag{3.72}$$

The integrand in the partition function (3.72) is not positive defined, as a sound Boltzmann factor should be. Recall that the integrand of the partition function (the density matrix elements) corresponds to a sort of probability density, which must be non-negative. This is not true for the grand-partition function (3.72) and one can conclude that the Polyakov–Quark-Meson model has the sign problem at the mean-field level for a finite chemical potential. If one insists in writing the partition function (3.72) in the same form as (3.71), one ends up with

$$\Omega = \Omega_{\Phi_{\mathrm{i}}-even} - \frac{T}{V}\ln\left[\cos\left(\frac{V}{T}\Omega^{\mathrm{I}}_{\mathrm{q\bar{q}}}\right)\right] , \tag{3.73}$$

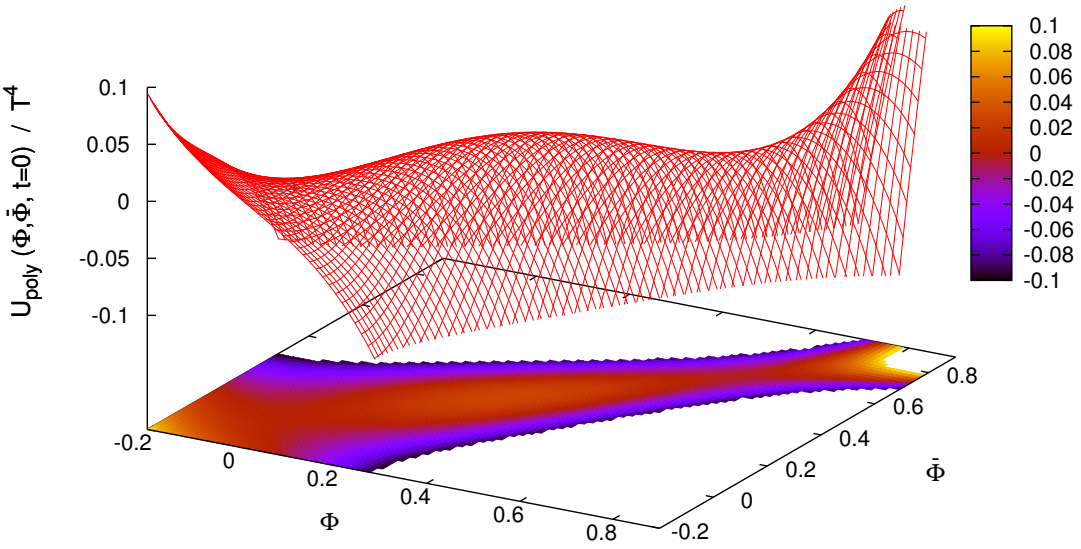

Figure 3.7.: Polynomial Polyakov-loop potential [80] at $t = 0$ as a function of real coordinates Φ and $\bar{\Phi}$. One recognises its saddle-point structure and that it is unbounded for $\left(\Phi, \bar{\Phi}\right) \to (0, \infty), (\infty, 0)$.

This function is not physically acceptable as an effective potential. First, it is a volume-dependent effective potential and therefore, it is not intensive and second, it is not defined in the thermodynamical limit $V \to \infty$.

The standard approach in the literature to circumvent the sign problem of the PQM model is to restrict the Polyakov-loop variables Φ and $\bar{\Phi}$ to be two independent, real variables. But by this approach, the effective potential has no minima, but only saddle-points. The state of thermodynamical equilibrium is then chosen among the extrema of the effective potential as the one with the lowest value of the potential. The chosen point is then not a minimum, but a saddle-point of the effective potential. This 'saddle-point' approach is particularly troublesome for the evaluation of the surface tension and thus of the nucleation rate in the region of the phase diagram of the model where a first-order phase transition separates two phases. It can be easily seen that the effective potential is unbounded from below. Just consider $\Phi = 0$ in Eqs. (3.38), (3.40) or (3.41) and one can realise that the Polyakov loop potential is unbounded from below for $\bar{\Phi} \to \infty$ [72]. This is illustrated together with the saddle point structure of the potential in Fig. 3.7.

Another possibility to avoid the sign problem, as indicated in Ref. [90] is to treat the imaginary part of the effective potential perturbatively in an expansion in powers of T/V. In the first order of the approximation (which the authors of Ref. [90] identify

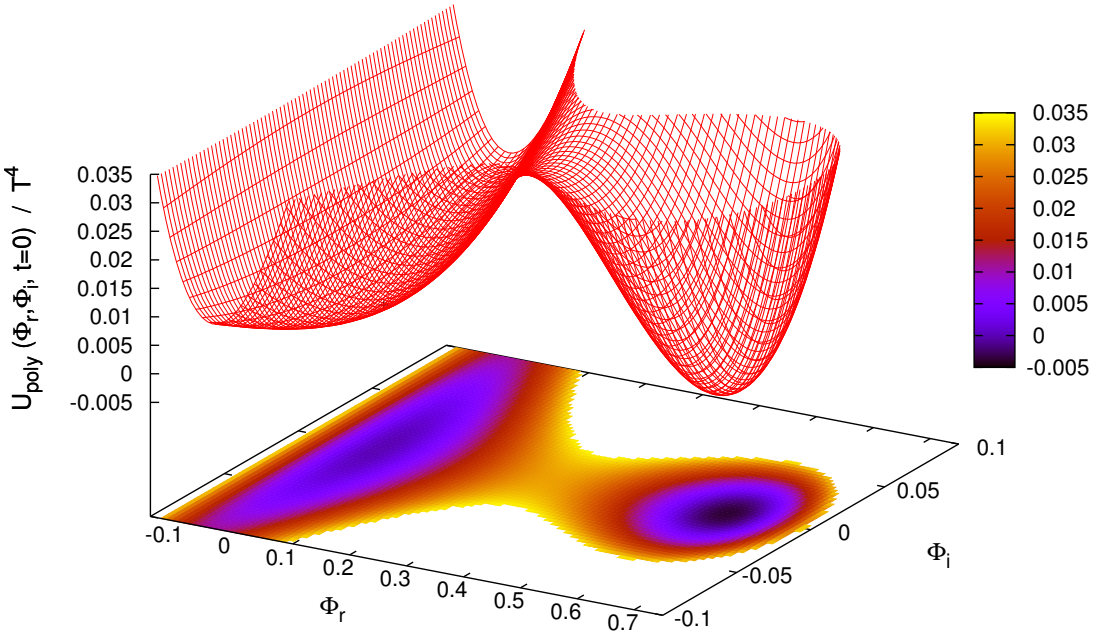

Figure 3.8.: Polynomial Polyakov-loop potential [80] at $t = 0$ as a function of real coordinates Φ_r and Φ_i.

with the mean-field approximation), one simply ignores the imaginary part (3.70) of the effective potential at finite chemical potentials. Ignoring $\Omega^{\mathrm{I}}_{\mathrm{q\bar{q}}}$ is equivalent to taking the modulus of the Dirac determinant that is tacitly present in Eq. (3.72). However, if one neglects $\Omega^{\mathrm{I}}_{\mathrm{q\bar{q}}}$, the expectation value of Φ_i is zero due to the even parity of $\mathcal{U}$ and $\Omega^{\mathrm{R}}_{\mathrm{q\bar{q}}}$ with respect to Φ_i. As a consequence, the difference $\langle\bar{\Phi} - \Phi\rangle = 0$, which is in disagreement with complex Langevin [208] and Monte-Carlo simulations [51, 52]. In spite of this setback, the approach presented here can be understood as an approximation scheme that has the strong theoretical advantage of dealing with the well-established minimisation procedure for finding the state of equilibrium, as can be seen in Fig. 3.8.

4. Thermodynamics and Phase Structure

4.1. Order Parameters and Thermodynamics at zero Chemical Potentials

In this section results of sophisticated lattice QCD calculations are used to adjust the uncertain parameters of the Polyakov–Quark-Meson model. More precisely, the parameters will be chosen such that results for basic observables of strongly-interacting matter at zero quark densities are reproduced. This allows to achieve a reliable basis for the subsequent investigations at nonzero quark and isospin densities. The impact of the parameters within their uncertainties is discussed in the following subsections. Information on the method of lattice calculations can be found e.g. in Refs. [28, 102] or in the reviews [209, 210] or in the detailed literature [211, 212].
For an explicit crosscheck of the model and the numerics the pseudocritical temperatures for deconfinement and chiral symmetry restoration where compared to those calculated in Refs. [66, 72, 73, 77] using their parameter sets.

The uncertainties of the Polyakov–Quark-Meson model include the parametrisation of the Polyakov-loop potential, the transition temperature of the Polyakov-loop potential and the mass of the σ-meson. The different parametrisations of the Polyakov-loop potential that will be discussed are (3.38), (3.40) and (3.41) with the parameters of Table 3.3. As discussed around Eq. (3.57), the glue critical temperature is expected to be in the range $180\,\mathrm{MeV} \lesssim T_{\mathrm{cr}}^{\mathrm{glue}} \lesssim 270\,\mathrm{MeV}$. Usually, the chiral partner of the pion is identified with the experimentally measured resonance $\mathrm{f}_0\,(500)$ with mass $m_{\mathrm{f}_0} = (400 - 550)$ MeV [147]. Note however that in Ref. [194] it was demonstrated that within an extended quark-meson model that includes vector and axial-vector mesons the resonance $f_0(1370)$ was identified as the nonstrange scalar quarkonium state. Within the present work, $m_\sigma = (400 - 600)\,\mathrm{MeV}$ will be considered as parameter range for the mass of the σ-meson. The scalar coupling between quarks and (pseudo-)scalar mesons g is kept fixed such that the constituent mass of the light quarks is $m_{\mathrm{l}} = 300\,\mathrm{MeV}$ according to Eq. (3.30). The impact of varying the Yukawa coupling on the evolution of the order parameters and equation of state is e.g. investigated in Refs. [10, 213].

The equilibrium states of the system are solutions of the equations of motion (3.15). For zero quark chemical potentials $\mu_f = 0$ they are indeed minima of the effective

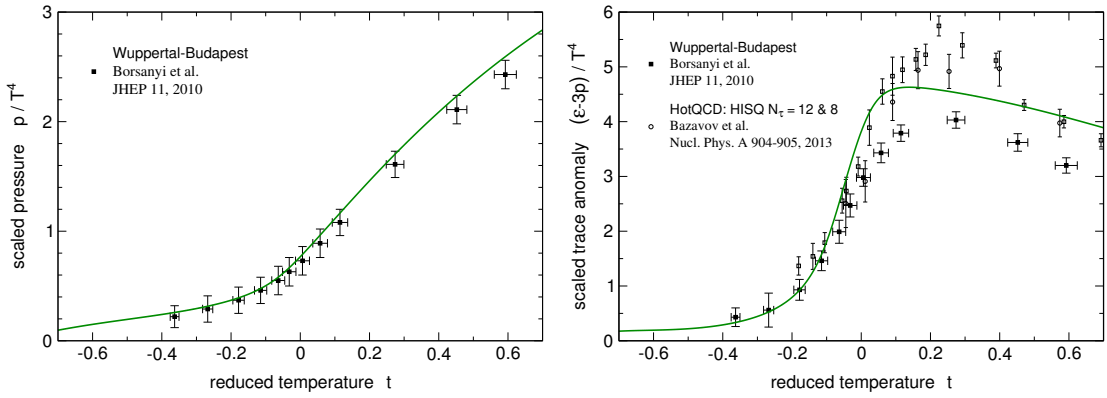

Figure 4.1.: Scaled pressure p/T^4 (left) and trace anomaly $(\epsilon - 3p)/T^4$ (right) as a function of temperature at $\mu_f = 0$. The results are compared to the lattice calculations of Refs. [39, 41].

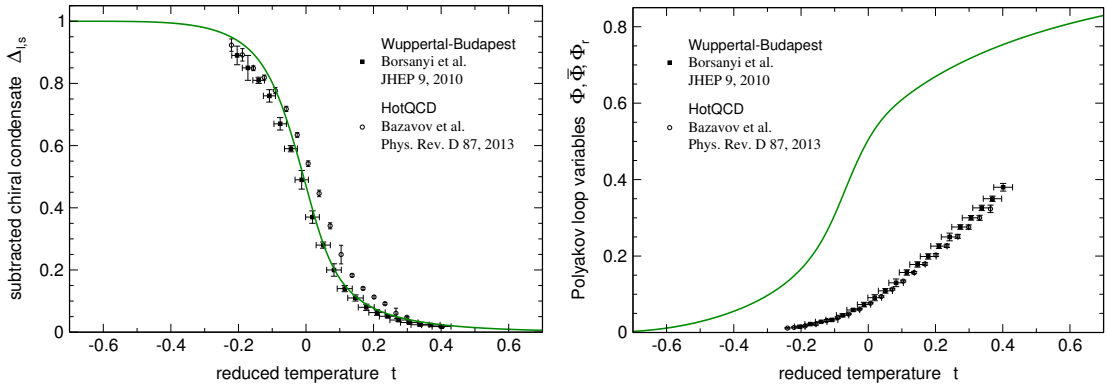

Figure 4.2.: The subtracted chiral condensate $\Delta_{\mathrm{l,s}}$ (left) and the Polyakov-loop expectation value Φ (right) as a function of temperature at $\mu_f = 0$. The results are compared to the lattice calculations of Refs. [38, 42].

potential as shown in Sec. 3.3 and the 'saddle-point' approach and the 'minimisation' procedure discussed in that section lead to identical results.

Figures 4.1 and 4.2 show those results for thermodynamics and order parameters that are the closest to the results of lattice calculations. These are achieved using the polynomial Polyakov-loop potential (3.38) with the parameters of Ref. [80] with a transition scale of $T_{\mathrm{cr}}^{\mathrm{glue}} = 270\,\mathrm{MeV}$ and $m_\sigma = 400\,\mathrm{MeV}$ as mass of the σ-meson.

The lattice results to which the results are compared to are the continuum extrapolations of the Wuppertal-Budapest collaboration of Refs. [38, 39] using the 'stout' action and those of the HotQCD collaboration using the highly improved staggered quark (HISQ) action, with a temporal lattice extent of $N_\tau = 12$ (open circles) and $N_\tau = 8$ (open squares) [41] and continuum extrapolated [42], all with physical quark masses.

The results for the chiral order parameter and thermodynamics either agree quantitatively with the lattice results or are at least within the trend of the data. A big differ-

Table 4.1.: Pseudocritical temperatures on the lattice for the crossover transition at $\mu_f = 0$. They are determined by the peak position of the temperature derivatives of the subtracted chiral condensate $\Delta_{\mathrm{l,s}}$.

	Wuppertal-Budapest	HotQCD	
	[38]	continuum [42]	$N_\tau = 12$ & 8 [40]
T_c [MeV]	157 ± 3	154 ± 9	159 ± 3 & 163 ± 3

ence is seen in the Polyakov-loop expectation value. The lattice data shows a smoother transition with significant smaller values. However, at least a part of this discrepancy originates in the inherent approximations which are still present: the derivation of the Polyakov–Quark-Meson model entails that the Polyakov-loop variable in the thermal fermionic determinant (3.12) is $\Phi\left[\langle A_0 \rangle\right]$ and not $\langle \Phi\left[A_0\right] \rangle$ as used in the Polyakov-loop potentials $\mathcal{U}$ and computed on the lattice. However, the continuum definition serves as an upper bound for the lattice one, $\Phi\left[\langle A_0 \rangle\right] \geq \langle \Phi \rangle$ as discussed in Sec. 2.3.2.

The abscissæ of the figures are in units of the reduced temperature of full QCD $t = (T - T_\mathrm{c})/T_\mathrm{c}$. This choice allows to compare the overall shape of the observables and thereby the proper inclusion of the relevant dynamics independent of a possible mismatch of the pseudocritical temperature T_c that is scaled out. To have a unique criterion for lattice and model calculations the pseudocritical temperature of the crossover transition are determined by the peak of the susceptibility of the subtracted chiral condensate. Table 4.1 summarises the hereby defined pseudocritical temperatures for the lattice calculations. The chiral transition temperature of the model calculation is $T_\mathrm{c} = 164\,\mathrm{MeV}$ and $T_\mathrm{d} = 153\,\mathrm{MeV}$ for the Polyakov-loop related transition. These values coincide with the transition range on the lattice, $(144 - 170)$ MeV [38] defined by the peaks and inflection points of various observables.

In summary, the parameters have been adjusted in this section in order to reproduce lattice results at zero quark densities. The important ingredients to achieve compatibility with lattice data for the order parameters and thermodynamics are given by the inclusion of quark quantum fluctuations (3.11), to unquench the Polyakov-loop potential by including the quark backreaction via relation (3.58) and to consider the contribution of thermal meson fluctuations (3.21). This setting constitutes an adequate framework to investigate the phase structure of strongly interacting matter at nonzero quark and isospin densities and to test the applicability of the model at nonzero densities.

Before the study will be extended to nonzero chemical potentials in the following sections, the impact of the before mentioned ingredients is illustrated and the influence of the parameters within their uncertainties is discussed.

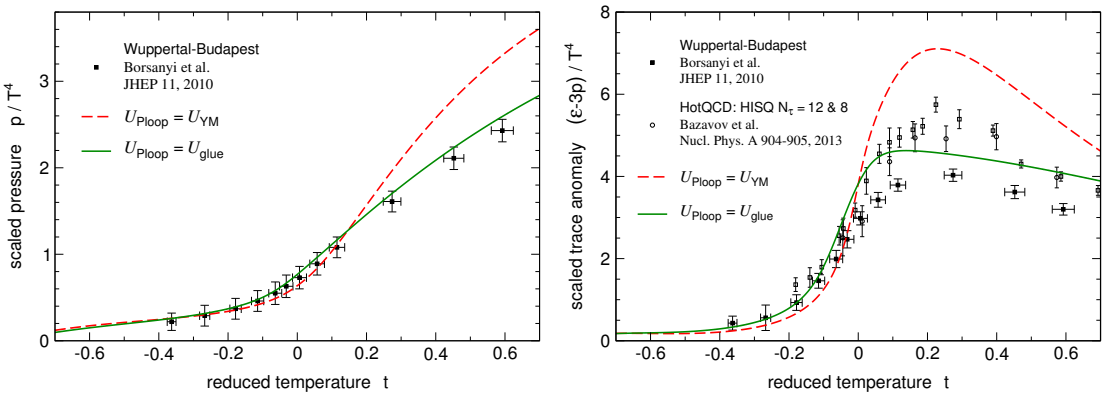

Figure 4.3.: Scaled pressure p/T^4 (left) and trace anomaly $(\epsilon - 3p)/T^4$ (right) as a function of temperature at $\mu_f = 0$. The red dashed line is the result using as Polyakov-loop potential the pure Yang-Mills potential, the full green line is the case for the unquenched glue potential. The results are compared to the lattice calculations of Refs. [39, 41].

4.1.1. Impact of Unquenching the Polyakov-loop potential

An important improvement of the Polyakov-loop extended Quark-Meson model is the unquenching of the Polyakov-loop potential (3.58) by using the relation between pure gauge and glue effective potential (3.56) that is extracted from renormalisation group calculations.

The enhancement of the Polyakov-loop potential smoothes the phase transition significantly. This can be seen in the comparison of thermodynamics and order parameters using the Yang-Mills and the unquenched Polyakov-loop potential as displayed in Figs. 4.3 and 4.4. Unquenching the Polyakov-loop potential brings the effective model in close agreement with the lattice calculations. This improvement holds in the low as well as in the high temperature phase.

One can see in the interaction measure that is shown on the right of Fig. 4.3 that the unquenched glue potential leads to a emergence of the quark degrees of freedom in a larger temperature interval and its amplitude is in better agreement with lattice results. By applying the unquenched glue potential, the Polyakov loop is shifted differently in the two phases as one sees on the right of Fig. 4.4. This could also be anticipated in Figs. 3.5 and 3.6 and Eq. (3.56). So, the Polyakov-loop variables are shifted to higher expectation values in the confined phase and to lower values in the deconfined phase. This shift in the respective phases is what leads to a overall smoother transition, not only of the Polyakov-loop. The evolution of the Polyakov loop when the unquenched potential is considered has also the advantage that its expectation value is shifted to a value of ~ 0.5 at $t = 0$ which is a reasonable criterion to define a transition between the confined phase and the quark gluon plasma in case of a crossover.
The adjustment of the Polyakov-loop potential from the pure gauge potential to the unquenched glue potential does not only affect the Polyakov-loop but also quarks and

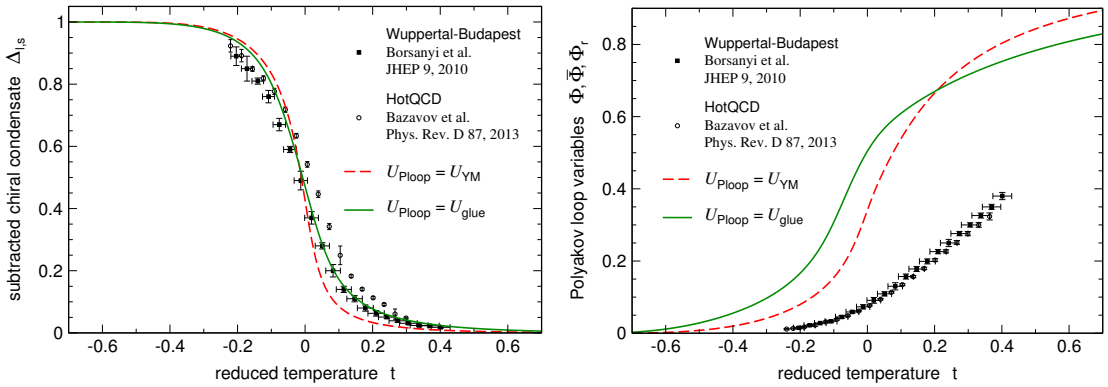

Figure 4.4.: The subtracted chiral condensate $\Delta_{\rm l,s}$ (left) and the Polyakov-loop expectation value Φ (right) as a function of temperature at $\mu_f = 0$. The red dashed line is the result using as Polyakov-loop potential the pure Yang-Mills potential, the full green line is the case for the unquenched glue potential. The results are compared to the lattice calculations of Refs. [38, 42].

mesonic degrees of freedom because of their nontrivial coupling to the gauge field. Therefore, on the left of Fig. 4.4 it is shown how the subtracted chiral condensate is affected by unquenching the Polyakov-loop potential. The results of the PQM model using as Polyakov-loop potential the pure gauge potential and the glue potential show that the adjustment of the Polyakov-loop potential leads also to a smoother chiral transition and to a further agreement with the result of lattice calculations.

Using the unquenched Polyakov-loop potential the chiral transition temperature is $T_{\rm c} = 164\,\text{MeV}$ and $T_{\rm d} = 153\,\text{MeV}$ for the Polyakov-loop related transition. These values coincide well with the transition range on the lattice, $(144 - 170)$ MeV [38]. In contrast to this the pseudocritical temperature $T_{\rm c} \sim T_{\rm d} \approx 188\,\text{MeV}$ achieved with the pure gauge Polyakov-loop potential exceeds this range. So, applying the quark-improved Polyakov-loop potential not only smoothes the transition but leads as well to an important reduction of the pseudocritical temperature.

In summary, adjusting the Polyakov-loop potential from a pure gauge potential to the unquenched glue potential in full QCD by applying Eqs. (3.58) and (3.56) improves the description of the chiral and (de)confinement phase transition with effective models.

4.1.2. Impact of Mesonic Fluctuations

To achieve a better description of the thermodynamics in the phase where chiral symmetry is broken, the thermodynamics has been augmented by the contribution of a gas of thermal mesons. For the meson masses the in-medium masses are taken. The evolution of the masses for the calculation presented in Figs. 4.1 and 4.2 at $\mu_f = 0$ for the lightest mesons, the pions and the σ-meson are shown in Fig. 4.5.

The mass of the pions stays practically constant at its vacuum value $m_\pi = 138\,\text{MeV}$

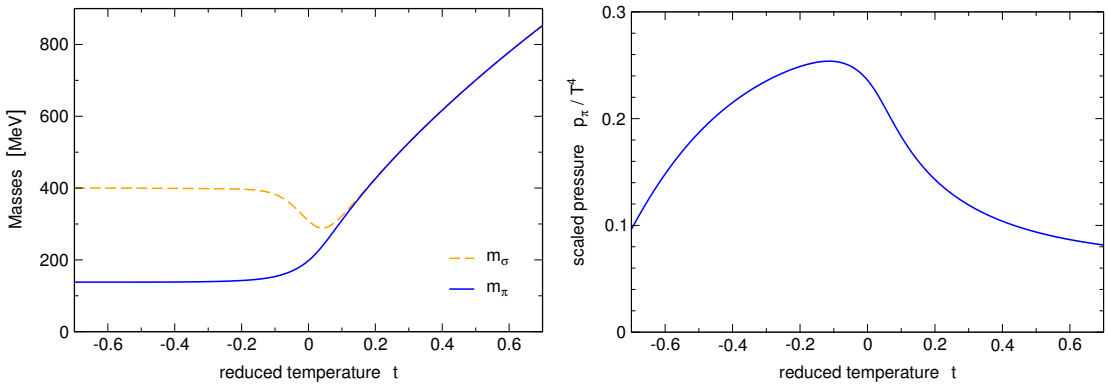

Figure 4.5.: The in-medium masses of pions m_π and the σ-meson (left) and the scaled pressure p_π/T^4 of a gas of thermal pions (right) as a function of temperature at $\mu_f = 0$. The polynomial parametrisation of the Polyakov-loop potential with the parameters of Ref. [80] with a transition scale of $T_{\rm cr}^{\rm glue} = 270\,\text{MeV}$ and $m_\sigma = 400\,\text{MeV}$ as vacuum mass of the σ-meson is used.

in the chirally broken phase. Therefore, the gas of thermal pions represents a significant contribution to thermodynamics for $t \lesssim 0$ as shown in the right part of Fig. 4.5. With the effective restoration of chiral symmetry the mass of the pions rises linearly with temperature and the contribution of the thermal pion gas to thermodynamics diminishes accordingly. Physically, the mesonic degrees of freedom dissolve with the onset of deconfinement and there are no pions in the deconfined phase that contribute to thermodynamics. This aspect of deconfinement is not covered by centre symmetry restoration. The mass of the second lightest meson, the σ-meson is larger than m_π in the chirally broken phase as can be seen in Fig. 4.5. This justifies to only consider the contribution of a gas of thermal pions but no other mesons.

To illustrate how the total pressure is build up, Fig. 4.6 shows the contributions of quarks and mesons separately. For $t \lesssim 0$ the mesons represent a significant contribution to thermodynamics and are those degrees of freedom that allow compatibility with lattice data. For $t \gtrsim 0$ the pressure of quarks alone coincides better with lattice results than the total pressure with the inclusion of the mesonic contribution. Indeed a proper inclusion of deconfinement would dissolve the mesonic degrees of freedom for $t \gtrsim 0$. The increase of the pion masses in the chirally restored phase leads to a decrease of the mesonic contribution to thermodynamics but this suppression is not enough. A melting of the mesonic degrees of freedom when centre symmetry gets broken would further improve the description of the deconfined phase. Work in this direction has been put forward in Ref. [196].

The inclusion of quantum fluctuations of mesons in a renormalisation group framework would not further improve the agreement for the order parameters and thermodynamics, as is shown in Figs. 4.7 and 4.8.

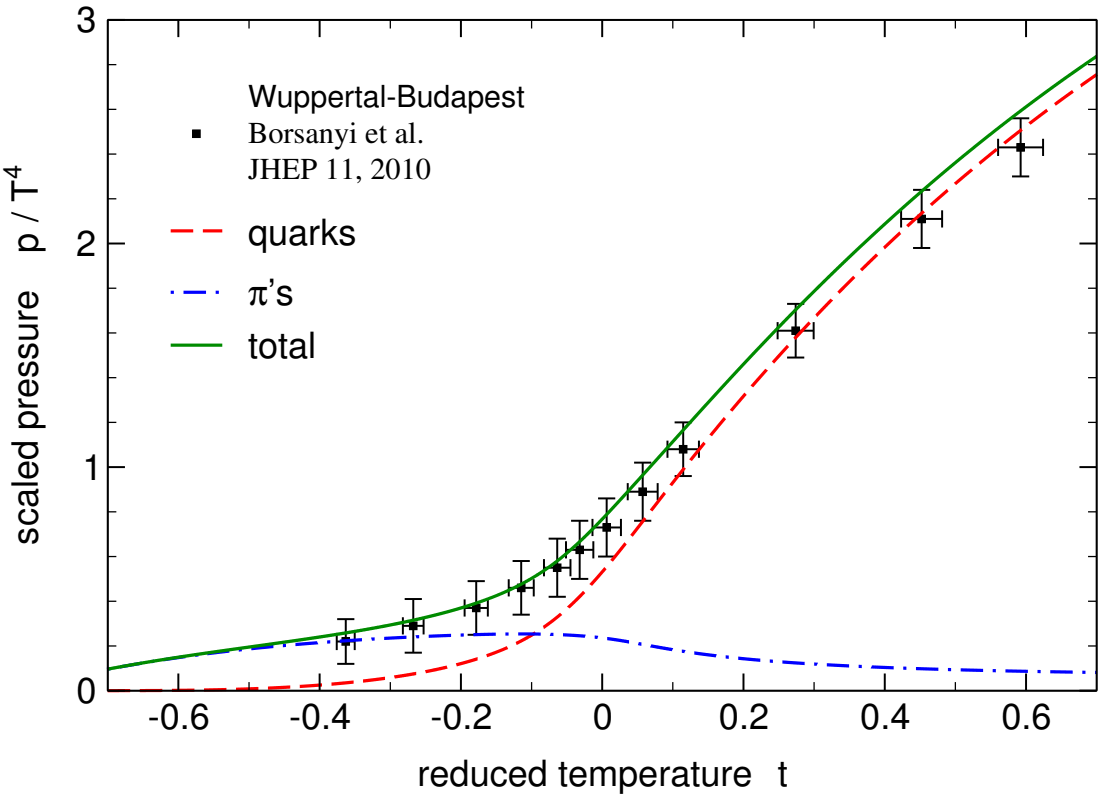

Figure 4.6.: Contributions of mesons and quarks to the scaled pressure p/T^4 as a function of temperature at $\mu_f = 0$. The results are compared to the lattice calculation of Ref. [39].

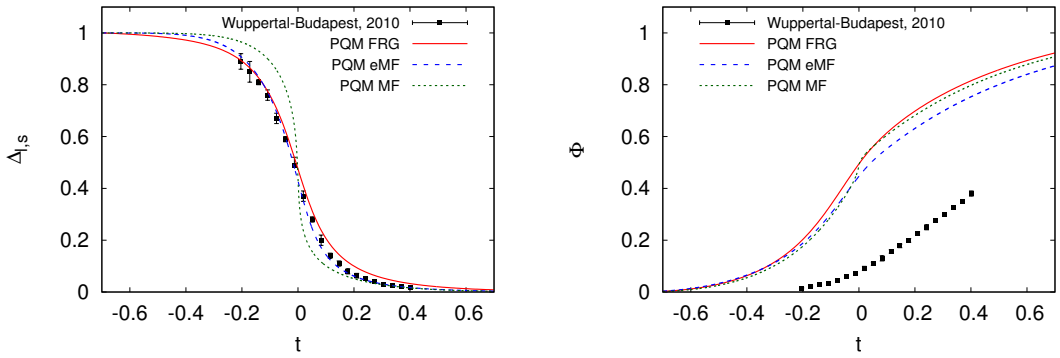

Figure 4.7.: Comparison of the temperature dependence of the subtracted chiral condensate (left) and Polyakov loop (right) in a mean-field, extended mean-field and FRG calculation. The results are compared to the lattice result of the Wuppertal-Budapest collaboration, [38]. From Ref. [4].

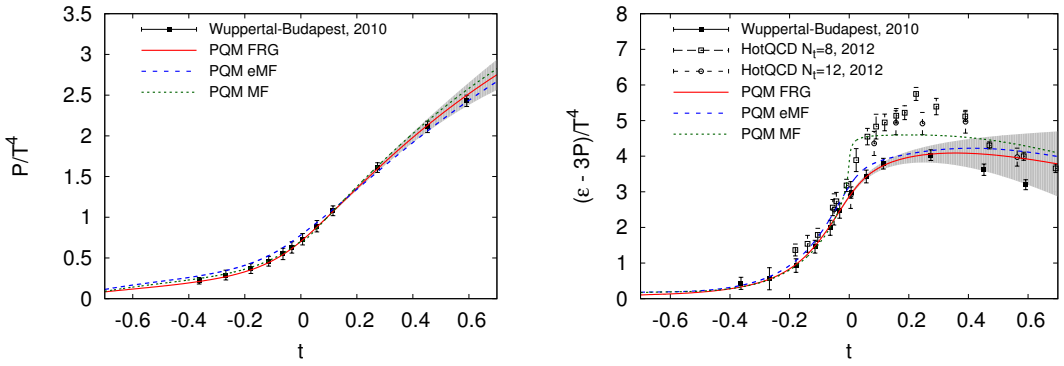

Figure 4.8.: Comparison of the temperature dependence of the pressure (left) and interaction measure (right) in a mean-field, extended mean-field and FRG calculation. The results are compared to the lattice result of Refs. [39, 41]. From Ref. [4].

4.1.3. Impact of Quantum Fluctuations of Quarks

A proper renormalisation of the one-loop contribution from quarks [75, 77, 79, 189, 190] leads to the contribution of fermionic quantum fluctuations (3.11) to the in-medium effective potential. In the so-called extended mean-field (eMF) analysis this term is taken into account while in standard mean-field (MF) calculations it was traditionally neglected.

Figures 4.9 and 4.10 show the impact of neglecting the fermionic quantum fluctuations. Keeping the parameters fixed as in the extended mean-field calculation this has tremendous implications. The transition becomes considerably steeper and even changes its natures to a first order transition. The liberation of quark degrees of freedom in a smaller temperature interval in the mean-field calculation is overlaid in the pressure by the missing contribution (3.11). The critical temperature $T_c = T_d = 144\,\mathrm{MeV}$ is very low.

Changing the parameters within their uncertainties one can achieve also within the standard mean-field analysis a result that is closer to the best extended mean-field calculation and in better agreement with the lattice results. Those results are presented in Figs. 4.11 and 4.12. The standard mean-field calculation is performed using the logarithmic parametrisation of the Polyakov-loop potential with a transition scale of $T_{\mathrm{cr}}^{\mathrm{glue}} = 210\,\mathrm{MeV}$ and $m_\sigma = 500\,\mathrm{MeV}$ as vacuum mass of the σ-meson. This leads to a pseudocritical temperature of $T_c = 158\,\mathrm{MeV}$ which is in very good agreement with lattice calculations.

The pressure shown on the left of Fig. 4.11 shows that the transition is marginally steeper in the standard mean-field calculation. A quantitative probe of this slight deviation is the interaction measure which tests not only the free energy or minimum of the potential but contains as well information about its temperature derivative. In the right part of Fig. 4.11 are compared the results for the trace anomaly. Even though the agreement of

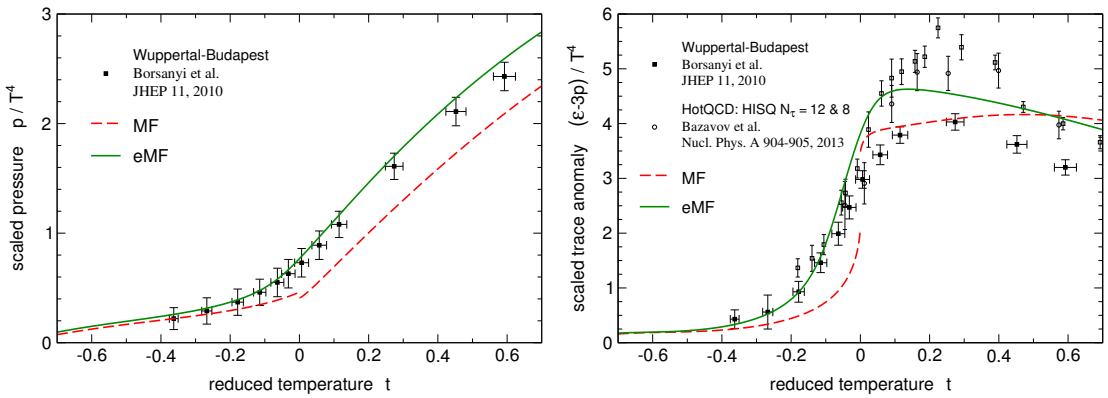

Figure 4.9.: Scaled pressure p/T^4 (left) and trace anomaly $(\epsilon - 3p)/T^4$ (right) as a function of temperature at $\mu_f = 0$. The red dashed line is the result without fermionic quantum fluctuations at one loop and the full green line is the case including these. The results are compared to the lattice calculations of Refs. [39, 41].

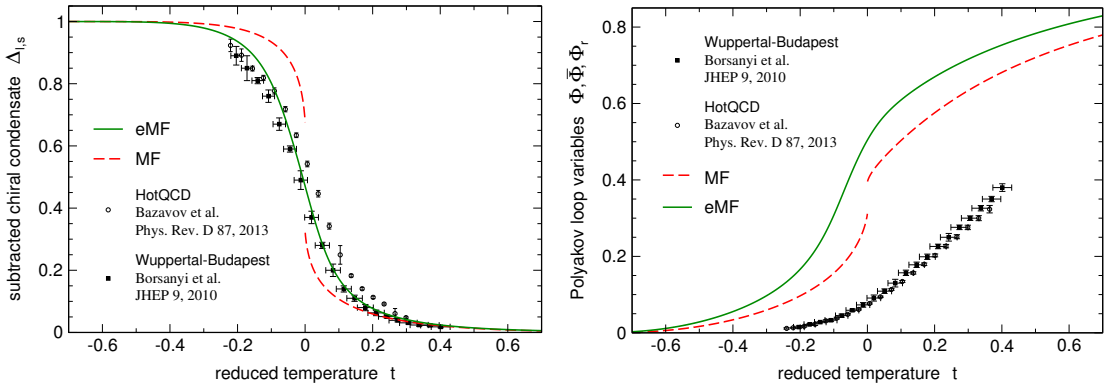

Figure 4.10.: The subtracted chiral condensate $\Delta_{l,s}$ (left) and the Polyakov-loop expectation value Φ (right) as a function of temperature at $\mu_f = 0$. The red dashed line is the result without fermionic quantum fluctuations at one loop and the full green line is the case including these. The results are compared to the lattice calculations of Refs. [38, 42].

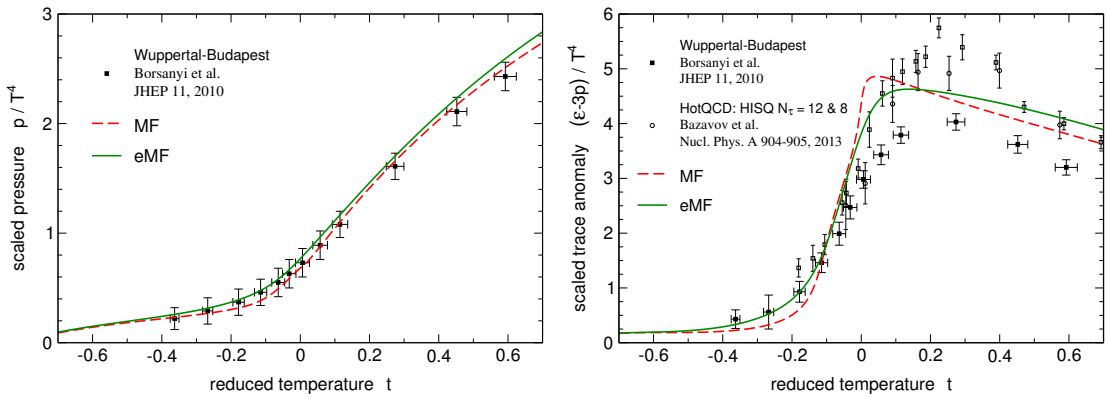

Figure 4.11.: Scaled pressure p/T^4 (left) and trace anomaly $(\epsilon - 3p)/T^4$ (right) as a function of temperature at $\mu_f = 0$. The red dashed line is the best result without fermionic quantum fluctuations at one loop and the full green line is the case including these. The results are compared to the lattice calculations of Refs. [39, 41].

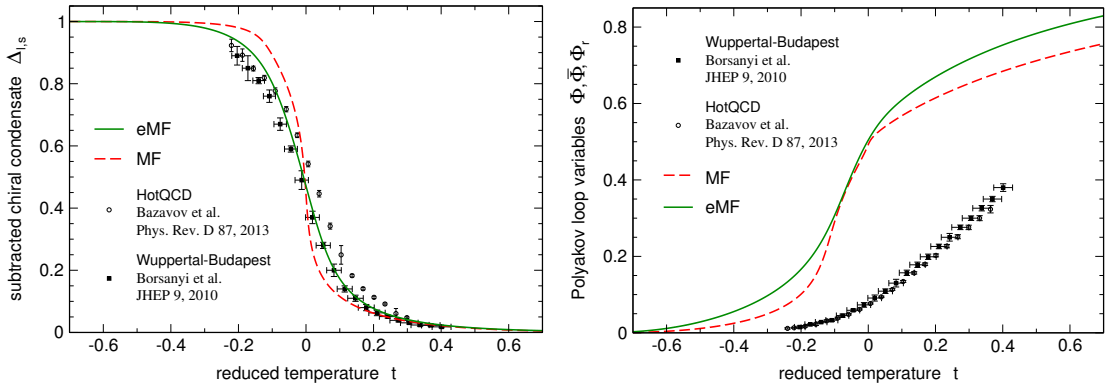

Figure 4.12.: The subtracted chiral condensate $\Delta_{l,s}$ (left) and the Polyakov-loop expectation value Φ (right) as a function of temperature at $\mu_f = 0$. The red dashed line is the best result without fermionic quantum fluctuations at one loop and the full green line is the case including these. The results are compared to the lattice calculations of Refs. [38, 42].

the normalised pressure of the effective model and the lattice calculation is remarkably close the slight differences get more visible in the trace anomaly. The amplitude is in good agreement with lattice results, nevertheless the transition in the effective model without vacuum-loop contribution is steeper. The results of the order parameters show as well a steeper change in the transition region in the standard mean-field calculation as is shown in Fig. 4.12.

4.1.4. Dependence on the Parametrisation of the Polyakov-loop Potential

In Polyakov-loop extended chiral models one uncertainty in the gluonic sector is the parametrisation of the Polyakov-loop potential. Ideally, the Polyakov-loop potential of full QCD from first principal calculations should be applied but this is not yet directly applicable. So one chooses a parametrisation of the Polyakov-loop potential and fits its parameters to available pure gauge lattice data as discussed in Sec. 3.2. In Figs. 3.2, 3.3 and 3.4 it was demonstrated that the different approximations of the potential show already significant differences for pure Yang-Mills theory. However, in this manner only the region close to the minimum is constrained but not the overall shape. That can differ considerably as shown in Fig. 3.1. But when the Polyakov-loop is coupled to the matter sector, regions away from the minimum are probed and one should not expect to find exactly the same results with different versions of the potential. So here is considered the uncertainty that comes along with the different parametrisations and parameter sets.

For the comparison of the different parametrisations of the Polyakov-loop potential a σ-meson mass of 400 MeV and a transition temperature of the Polyakov-loop potential of $T_{\mathrm{cr}}^{\mathrm{glue}} = 270\,\mathrm{MeV}$ is chosen.

The normalised pressure displayed in Fig. 4.13 shows the steepest rise in the transition region for the polynomial parametrisation with the parameters of Ref. [80] (Poly-BNL potential). This is in accord with the description of pure Yang-Mills theory discussed in Sec. 3.2. Overall, the difference in the results for the scaled pressure for the different parametrisations is not large around the transition region.

As seen before, the differences are more pronounced in the interaction measure which is shown in Fig. 4.14. The slopes of the curves are similar for the polynomial potential [80] and logarithmic parametrisation but with a larger amplitude in the case of the Poly-BNL potential. This originates from the description of pure Yang-Mills theory as seen in Fig. 3.4. The normalised trace anomaly with the polynomial parametrisation of Ref. [69] continues to increase above the transition temperature. This is a feature of the offset of the maximum of the trace anomaly in Yang-Mills theory seen in Fig. 3.4. This offset is also seen in calculations with the PQM model using the Yang-Mills Polyakov-loop potential [5, 73]. The overall reduction of the amplitude in the transition region with the unquenched Polyakov-loop potential leads to the behaviour seen in Fig. 4.14.

The evolution of the Polyakov-loop shown in Fig. 4.15 reveals that the onset of the transition in the confined phase is the steepest with those potentials that include a

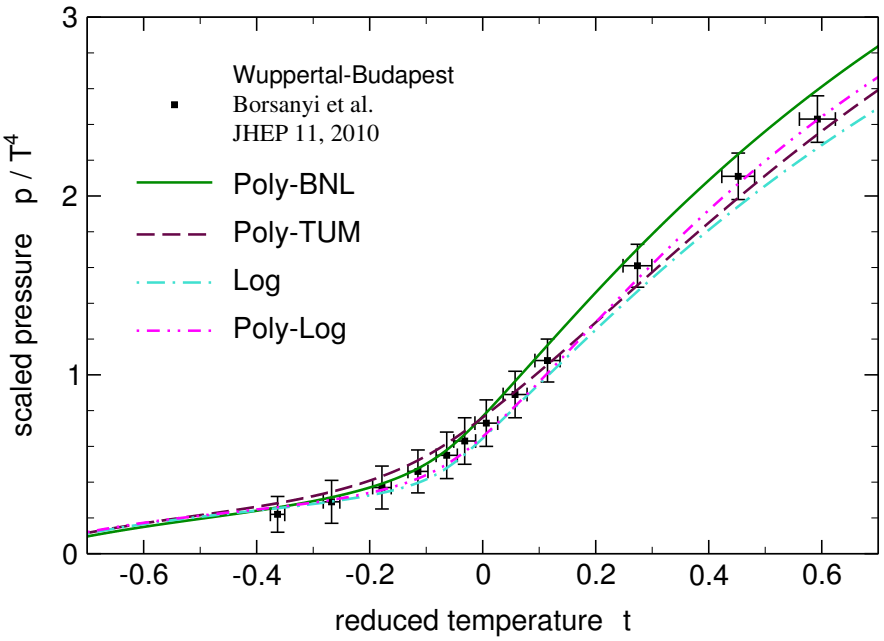

Figure 4.13.: Scaled pressure p/T^4 as a function of temperature at $\mu_f = 0$ for the different parametrisations of the Polyakov-loop potential. The results are compared to the lattice calculation of Ref. [39].

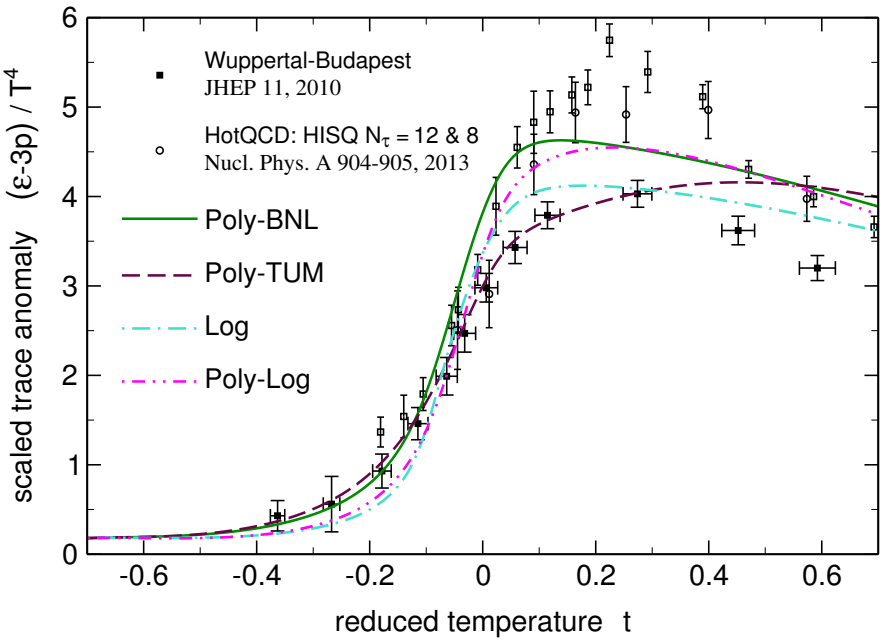

Figure 4.14.: Scaled trace anomaly $(\epsilon - 3p)/T^4$ as a function of temperature at $\mu_f = 0$ for the different parametrisations of the Polyakov-loop potential. The results are compared to the lattice calculations of Refs. [39, 41].

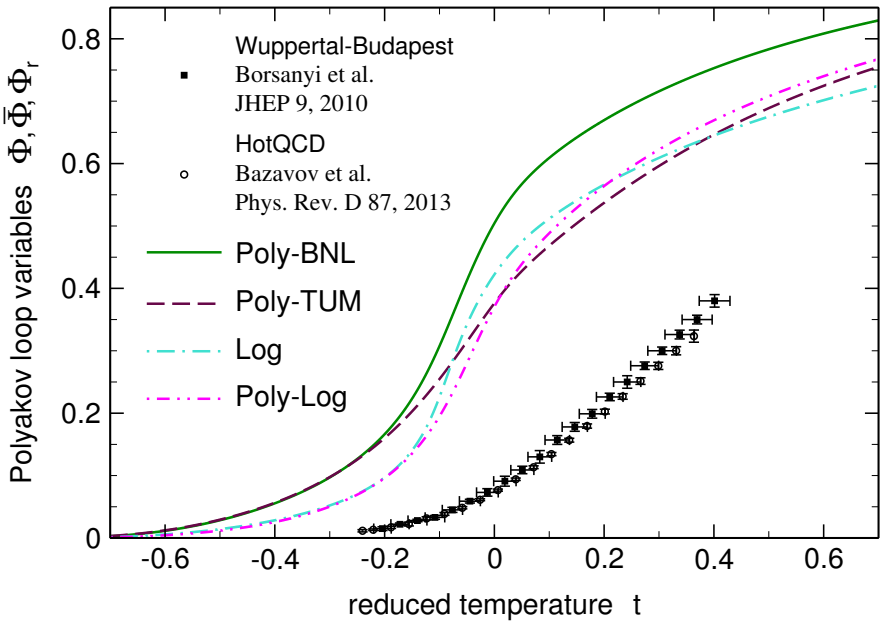

Figure 4.15.: The Polyakov-loop expectation value Φ as a function of temperature at $\mu_f = 0$ for the different parametrisations of the Polyakov-loop potential. The results are compared to the lattice calculations of Refs. [38, 42].

logarithmic term. The polynomial potential [69] leads to the smoothest evolution of the Polyakov loop. Note that the Polyakov-loop expectation values for the calculations with the polynomial parametrisation are normalised such that they tend towards unity at infinite temperature. Overall, the differences in the Polyakov-loop variables due to the different parametrisations are so large that it should be considered before making quantitative statements.

Nevertheless, the differences in the glue sector due to the different parametrisations are considerably smaller in the evolution of the subtracted chiral condensate. This is shown on the left of Fig. 4.16. As for the Polyakov-loop, the polynomial parametrisation [69] leads to the smoothest evolution.

In all quantities shown in Figs. 4.13, 4.14, 4.15 and 4.16 it can be seen that using the polynomial-logarithmic potential the results follow those with the logarithmic potential below T_c and run towards the results with the polynomial potentials in the chirally restored and deconfined phase.

The slightly stronger transition in the gluonic sector for the polynomial parametrisation [80] shifts the pseudocritical temperature to a smaller value compared to the other potentials as seen in Table 4.2. Only the result with the polynomial Polyakov-loop potential [80] coincide with the transition range on the lattice, $(144 - 170)$ MeV [38] that is defined by the peaks and inflection points of various observables.

With the other Polyakov-loop potentials one can achieve pseudocritical temperatures that are closer to the transition region on the lattice when changing the other uncer-

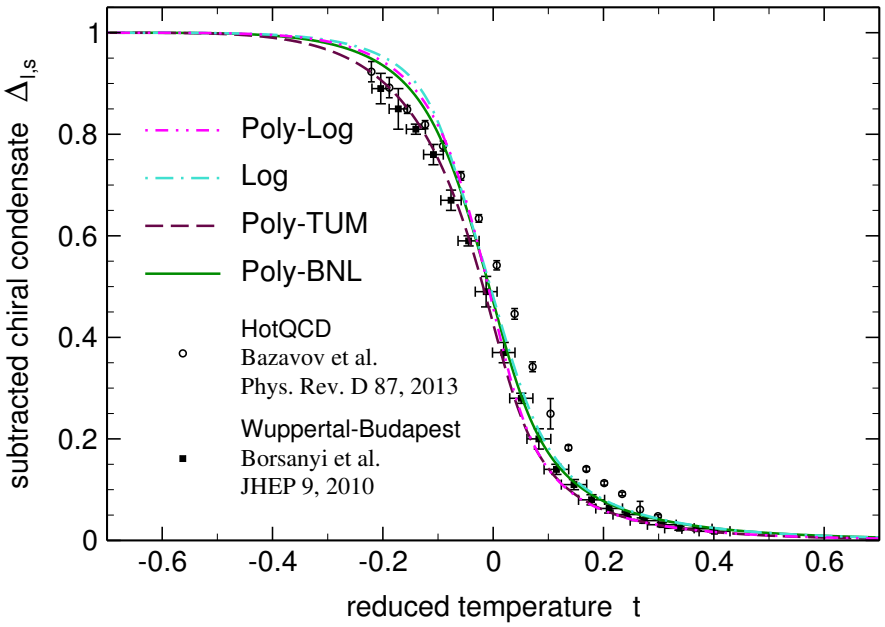

Figure 4.16.: The subtracted chiral condensate $\Delta_{\mathrm{l,s}}$ as a function of temperature at $\mu_f = 0$ for the different parametrisations of the Polyakov-loop potential. The results are compared to the lattice calculations of Refs. [38, 42].

Table 4.2.: Pseudocritical temperatures for the crossover transition at $\mu_f = 0$ with different parametrisations and parameter sets of the Polyakov-loop potential. They are determined by the peak position of the chiral susceptibility $\partial\Delta_{\mathrm{l,s}}/\partial T$ and of the temperature derivative of the Polyakov loop $\partial\Phi/\partial T$. As transition temperature of the Polyakov-loop potential $T_{\mathrm{cr}}^{\mathrm{glue}} = 270\,\mathrm{MeV}$ is used and $m_\sigma = 400\,\mathrm{MeV}$ as vacuum mass of the σ-meson.

	Poly-BNL	Poly-TUM	Log	Poly-Log
T_{c} [MeV]	164	183	180	188
T_{d} [MeV]	153	176	165	180

Table 4.3.: Pseudocritical temperatures for the best results for the crossover transition at $\mu_f = 0$ with the different parametrisations and parameter sets of the Polyakov-loop potential presented in Figs. 4.17, 4.18, 4.19 and 4.20. They are determined by the peak position of the chiral susceptibility $\partial\Delta_{\mathrm{l,s}}/\partial T$ and of the temperature derivative of the Polyakov loop $\partial\Phi/\partial T$. As vacuum mass of the σ-meson $m_\sigma = 400\,\mathrm{MeV}$ is used.

	Poly-BNL	Poly-TUM	Log	Poly-Log
$T_{\mathrm{cr}}^{\mathrm{glue}}$ [MeV]	270	240	240	240
T_{c} [MeV]	164	176	175	179
T_{d} [MeV]	153	166	152	165

tainties to bring thermodynamics and order parameters to the closest agreement with lattice data. This can be achieved by reducing the transition scale of the unquenched Polyakov-loop potential to $T_{\mathrm{cr}}^{\mathrm{glue}} = 240\,\mathrm{MeV}$ for the polynomial parametrisation [69] and those parametrisations that consider the $SU(3)$ group volume. This reduces the pseudocritical temperatures as well as can be seen in Table 4.3. Still, only the transition region with the polynomial Polyakov-loop potential [80] is a subset of the transition range of the lattice calculation [38] while the others now have an intersection with the lattice result. Using a polynomial Polyakov-loop potential, the chiral and deconfinement transitions lie closer to each other than with those that include a logarithm.

Figures 4.17, 4.18, 4.19 and 4.20 show those results with all parametrisations of the Polyakov-loop potential that are closest to the results of lattice calculations. The evolution of the pressure and chiral condensate agree well which each other and the only characteristic is that with the polynomial Polyakov-loop potential [69] the transition is the smoothest. The results of the interaction measure and Polyakov loop show a larger sensitivity on the form of the Polyakov-loop potential. The logarithmic Polyakov-loop potential leads to the steepest increase of the Polyakov loop. Characteristics of the interaction measure are that the polynomial Polyakov-loop potential [69] leads to a significant offset of the maximum and that with the polynomial-logarithmic potential the decrease of the trace anomaly in the chirally restored and deconfined phase is the largest
.

In conclusion, the differences due to the different parametrisations of the the Polyakov-loop potential are so large that they should be considered before making quantitative statements. Further input to constrain the form of the potential or a potential from first principal calculations are important to improve the reliability of results of effective models.

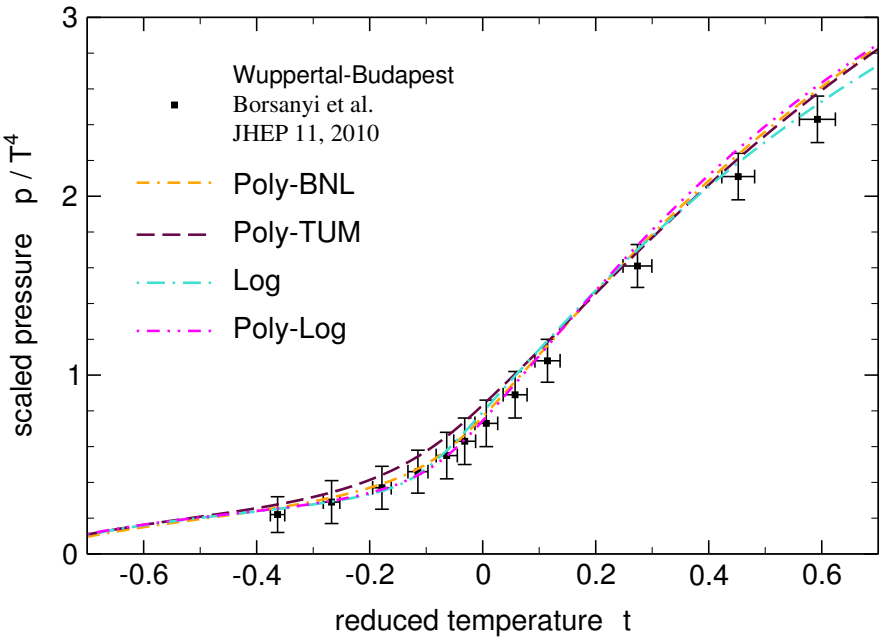

Figure 4.17.: Best results for the scaled pressure p/T^4 as a function of temperature at $\mu_f = 0$ for the different parametrisations of the Polyakov-loop potential. The results are compared to the lattice calculation of Refs. [39].

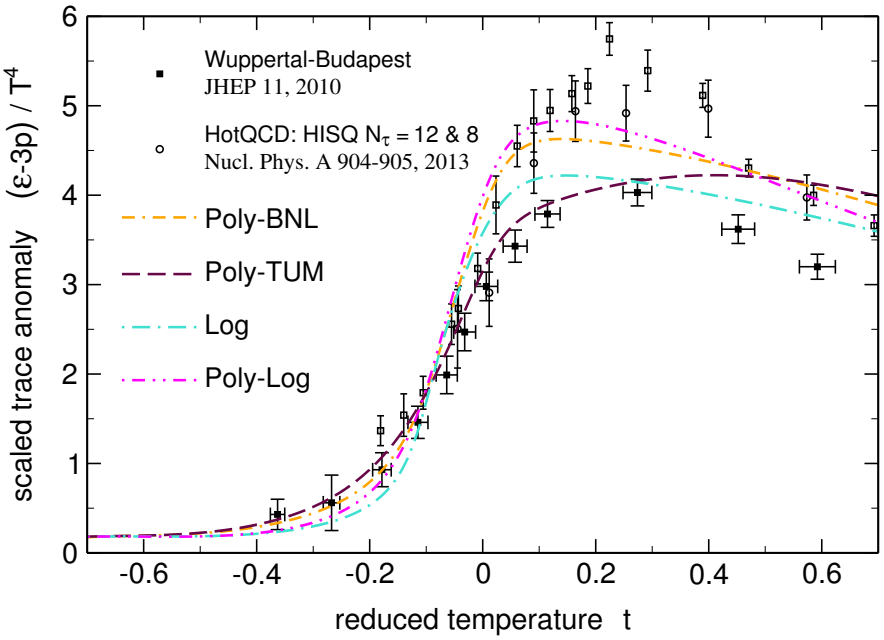

Figure 4.18.: Best results for the scaled trace anomaly $(\epsilon - 3p)/T^4$ as a function of temperature at $\mu_f = 0$ for the different parametrisations of the Polyakov-loop potential. The results are compared to the lattice calculations of Refs. [39, 41].

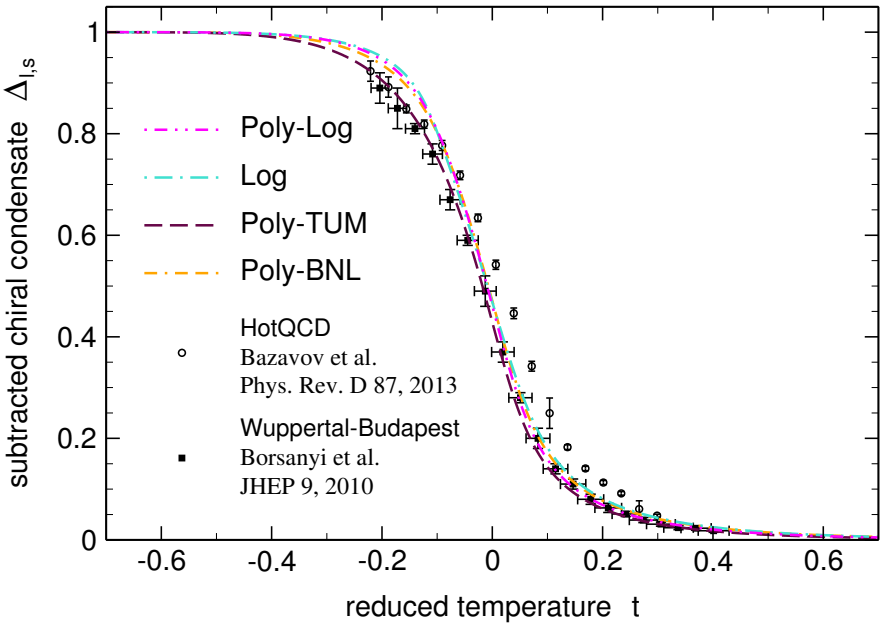

Figure 4.19.: Best results for the subtracted chiral condensate $\Delta_{l,s}$ as a function of temperature at $\mu_f = 0$ for the different parametrisations of the Polyakov-loop potential. The results are compared to the lattice calculations of Refs. [38, 42].

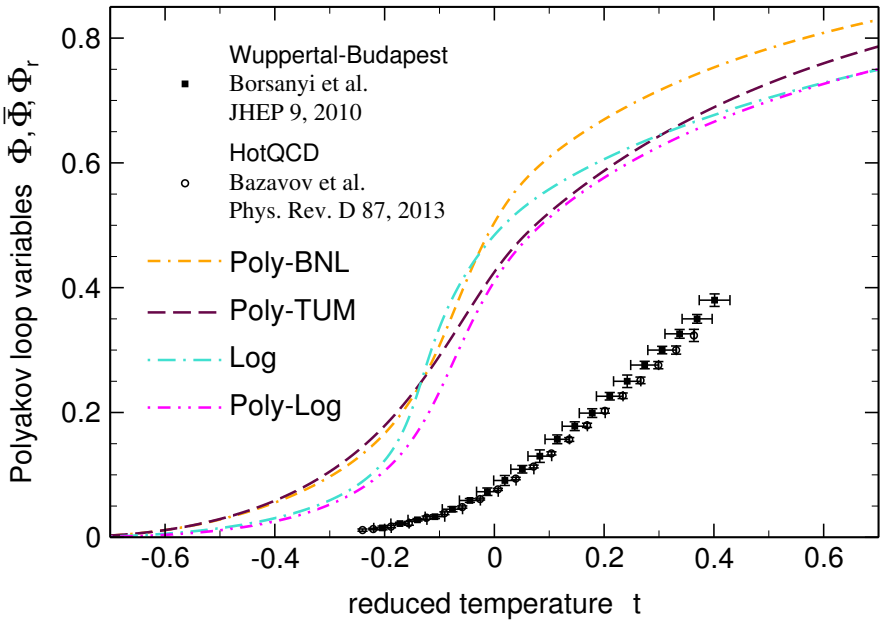

Figure 4.20.: Best results for the Polyakov-loop expectation value Φ as a function of temperature at $\mu_f = 0$ for the different parametrisations of the Polyakov-loop potential. The results are compared to the lattice calculations of Refs. [38, 42].

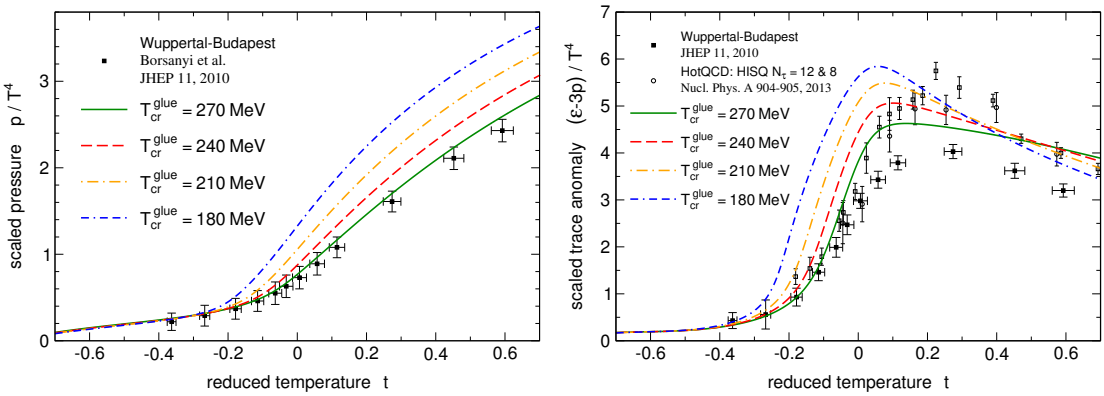

Figure 4.21.: Scaled pressure p/T^4 (left) and trace anomaly $(\epsilon - 3p)/T^4$ (right) as a function of temperature at $\mu_f = 0$ for four different glue critical temperatures. The results are compared to the lattice calculations of Refs. [39, 41].

4.1.5. Dependence on the Glue Critical Temperature

The second uncertainty in the gluonic sector is the transition temperature of the unquenched Polyakov-loop potential. It is not yet uniquely defined so that it is considered as a parameter. According to the discussion in Sec. 3.2.1 around Eq. (3.57) it is expected to be in the interval $(180 - 270)$ MeV.

For the investigation of the impact of $T_{\mathrm{cr}}^{\mathrm{glue}}$ the polynomial parametrisation of the Polyakov-loop potential with the parameters of Ref. [80] and a vacuum σ-meson mass of $m_\sigma = 400\,\mathrm{MeV}$ is used.

All quantities shown in Figs. 4.21 and 4.22 show that the transition sets on already at smaller relative temperatures when the critical temperature of the unquenched Polyakov-loop potential is lowered. This is due to a broadening of the transition range with decreasing glue critical temperature while the pseudocritical temperature defined by the chiral susceptibility remains on the upper end. The respective pseudocritical temperatures are summarised in Table 4.4.

The the best agreement with lattice results and a transition region that is in accordance with the lattice result is achieved for $T_{\mathrm{cr}}^{\mathrm{glue}} = 270\,\mathrm{MeV}$. But for all glue critical temperatures is the chiral pseudocritical temperature in the transition region of lattice calculations.

Another aspect that one sees in Fig. 4.21 is that the slope of the trace anomaly becomes smaller above T_{c} with increasing critical scale of the Polyakov-loop potential. This behaviour has two reasons. First, the transition range diminishes for larger critical temperatures of the glue potential, so that the impact of the emergence of the quark degrees of freedom is larger close above T_{c}. Second, the saturation scale of the adjustment between pure gauge potential and unquenched glue potential, i.e., the upper limit of validity of Eq. (3.56), is closer to the transition scale for larger critical temperatures of the Polyakov-loop potential.

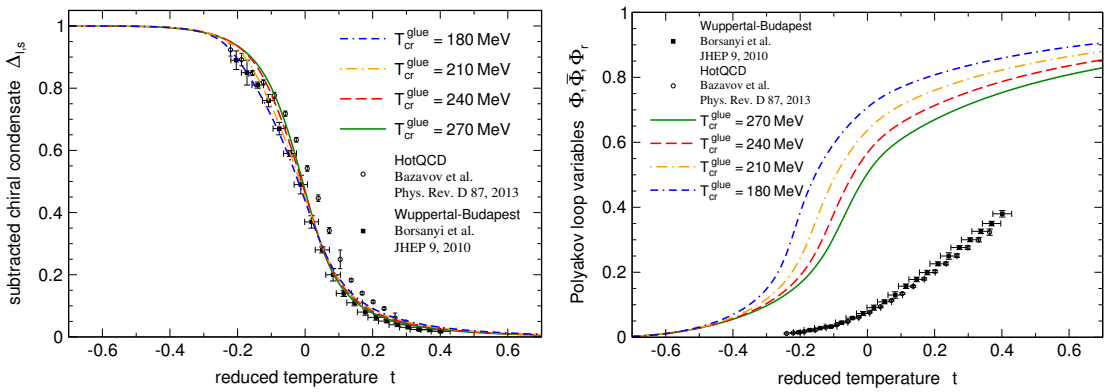

Figure 4.22.: The subtracted chiral condensate $\Delta_{\mathrm{l,s}}$ (left) and the Polyakov-loop expectation value Φ (right) as a function of temperature at $\mu_f = 0$ for four different glue critical temperatures. The results are compared to the lattice calculations of Refs. [38, 42].

Table 4.4.: Pseudocritical temperatures for the crossover transition at $\mu_f = 0$ for four different glue critical temperatures. They are determined by the peak position of the chiral susceptibility $\partial\Delta_{\mathrm{l,s}}/\partial T$ and of the temperature derivative of the Polyakov loop $\partial\Phi/\partial T$. The polynomial Polyakov-loop potential with the parameters of Ref. [80] and $m_\sigma = 400\,\mathrm{MeV}$ as vacuum mass of the σ-meson is used.

$T_{\mathrm{cr}}^{\mathrm{glue}}$ [MeV]	180	210	240	270
T_{c} [MeV]	151	155	159	164
T_{d} [MeV]	119	131	142	153

Figure 4.22 shows the dependence of the evolution of the Polyakov-loop expectation values on the critical temperature of the Polyakov-loop potential. The magnitude of the transition increases when the transition temperature of the Polyakov-loop potential is lowered and the transition regions is shifted towards smaller relative temperatures. So the onset of deconfinement is shifted further away from T_c with decreasing critical temperature of the Polyakov-loop potential. This is a natural consequence, as decreasing the scale of the Polyakov-loop potential leads to a relative shift of the glue part towards a lower scale in the full theory.

Due to the nontrivial coupling between Polyakov loop, quarks and mesons, the onset of deconfinement at lower temperatures with decreasing critical temperature of the Polyakov-loop potential shows its impact also in the chiral condensate. It deviates at relative smaller temperatures from its vacuum value when the transition temperature of the Polyakov-loop potential is lowered. This effect gets enhanced due to the simultaneous lowering of the pseudocritical temperature. Apart from that, the chiral condensate shows only a very mild dependence on the transition temperature of the glue potential.

As discussed in the previous section one can also achieve results for the evolution of thermodynamics and the order parameters that are consistent with the lattice data for $T_{\mathrm{cr}}^{\mathrm{glue}} = 240\,\mathrm{MeV}$ if on choses one of the other parametrisations of the Polyakov-loop potential. But then the transition range shows less overlap with that of lattice calculations as was shown in Table 4.3.

For even lower glue critical temperatures no consistency with lattice data can be found within the presented framework, also not if changing the remaining uncertainty which is the mass of the scalar meson σ.

4.1.6. Dependence on the Sigma-Meson Mass

An uncertainty in the mesonic sector of chiral models is the vacuum value of the mass of the σ-meson. Usually, the chiral partner of the pion is identified with the experimentally measured resonance $\mathrm{f}_0\,(500)$ which is rather broad, $m_{\mathrm{f}_0} = (400 - 550)$ MeV [147]. Note however that in Ref. [194] it was demonstrated that within an extended quark-meson model that includes vector and axial-vector interactions the resonance $f_0(1370)$ was identified as the nonstrange scalar quarkonium state. Here, $m_\sigma = (400 - 600)\,\mathrm{MeV}$ is considered as parameter range for the mass of the σ-meson.

To investigate the role of the mass of the scalar meson σ the polynomial parametrisation of the Polyakov-loop potential with the parameters of Ref. [80] and a transition scale of $T_{\mathrm{cr}}^{\mathrm{glue}} = 270\,\mathrm{MeV}$ is used in the following.

The change of the pressure for an increasing mass of the σ-meson is opposite to the case of an increasing glue critical temperature (Fig. 4.21). Therefore, to get agreement with the pressure of the lattice calculation for a σ-meson masses of 500 MeV and 600 MeV one would have to choose an even larger critical temperature of the glue potential. So the lower the mass of the σ-meson, the smaller the transition temperature of the glue potential has to be in order to reproduce the lattice results. This is due to the fact that

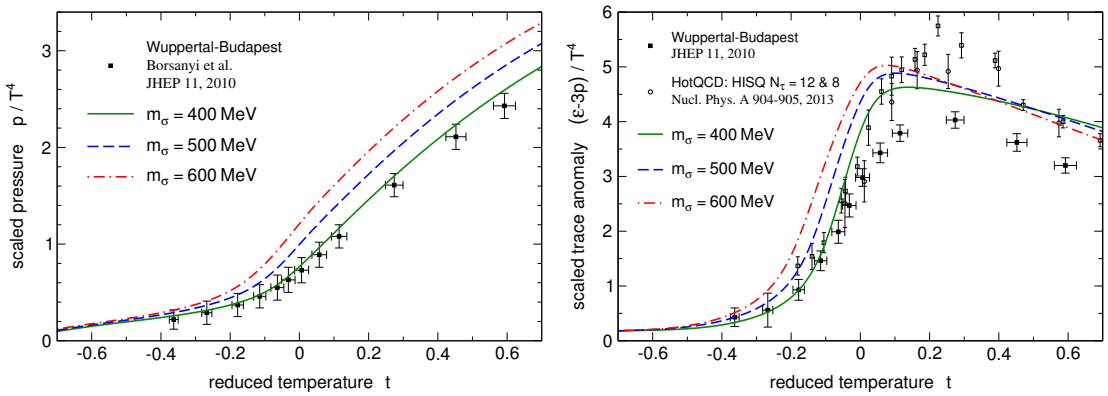

Figure 4.23.: Scaled pressure p/T^4 (left) and trace anomaly $(\epsilon - 3p)/T^4$ (right) as a function of temperature at $\mu_f = 0$ for three different values of the mass of the σ-meson. The results are compared to the lattice calculations of Refs. [39, 41].

Table 4.5.: Pseudocritical temperatures for the crossover transition at $\mu_f = 0$ for three different masses of the σ-meson. They are determined by the peak position of the chiral susceptibility $\partial\Delta_{l,s}/\partial T$ and of the temperature derivative of the Polyakov loop $\partial\Phi/\partial T$. The polynomial Polyakov-loop potential with the parameters of Ref. [80] and a transition scale of $T_{\rm cr}^{\rm glue} = 270\,\text{MeV}$ is used.

m_σ [MeV]	400	500	600
$T_{\rm c}$ [MeV]	164	175	187
$T_{\rm d}$ [MeV]	153	156	158

a decrease in the mass of the σ-meson lowers the scale of the chiral transition as can be seen in Table 4.5 and Ref. [66]. So the scale of the (de)confinement transition has to decrease as well. Note that the combination of $m_\sigma = 400\,\text{MeV}$ and $T_{\rm cr}^{\rm glue} = 270\,\text{MeV}$ leads to a transition region that fits to the one of lattice calculations.

The results of the trace anomaly and chiral and (de)confinement order parameters for different σ-meson masses show that the transition region broadens for a larger mass of the σ-meson.

The observation that a larger mass of the σ-meson requires also a larger glue critical temperature to achieve consistency with lattice results implies that with the other Polyakov-loop potentials one can get results that match the lattice data for $m_\sigma = 500\,\text{MeV}$ with $T_{\rm cr}^{\rm glue} = 270\,\text{MeV}$. This is shown in Figs. 4.25 and 4.26 where the polynomial-logarithmic form of the Polyakov-loop potential is used. But even if the evolution of the observables for $m_\sigma = 500\,\text{MeV}$ is then consistent with the lattice data, the transition range moves further away from the lattice result as can be seen from the

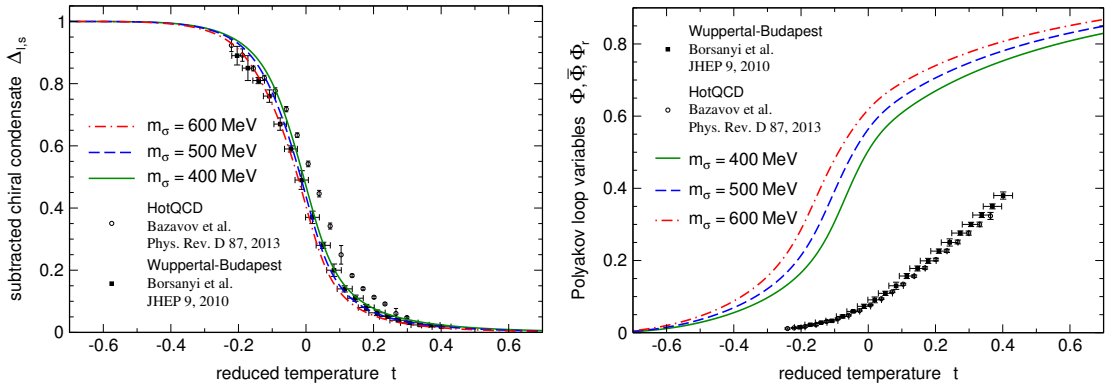

Figure 4.24.: The subtracted chiral condensate $\Delta_{l,s}$ (left) and the Polyakov-loop expectation value Φ (right) as a function of temperature at $\mu_f = 0$ for three different values of the mass of the σ-meson. The results are compared to the lattice calculations of Refs. [38, 42].

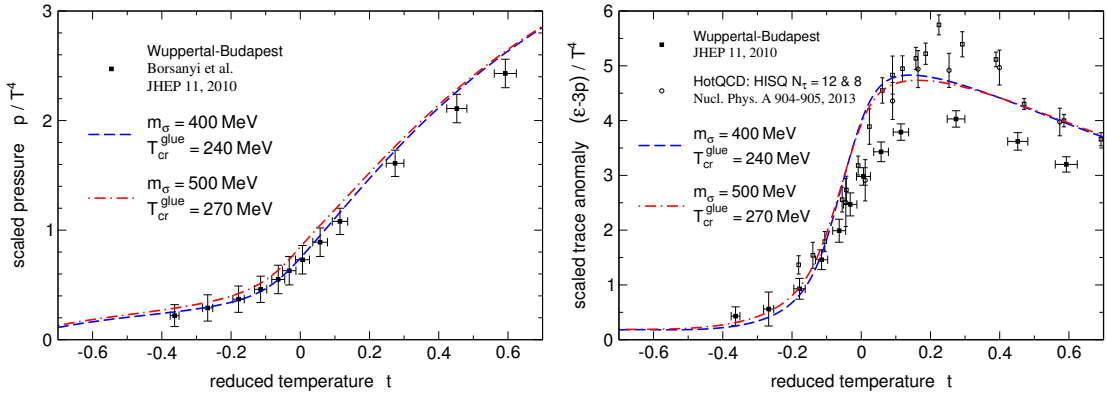

Figure 4.25.: The best results for the scaled pressure p/T^4 (left) and trace anomaly $(\epsilon - 3p)/T^4$ (right) as a function of temperature at $\mu_f = 0$ for different values of the mass of the σ-meson. The results are compared to the lattice calculations of Refs. [39, 41].

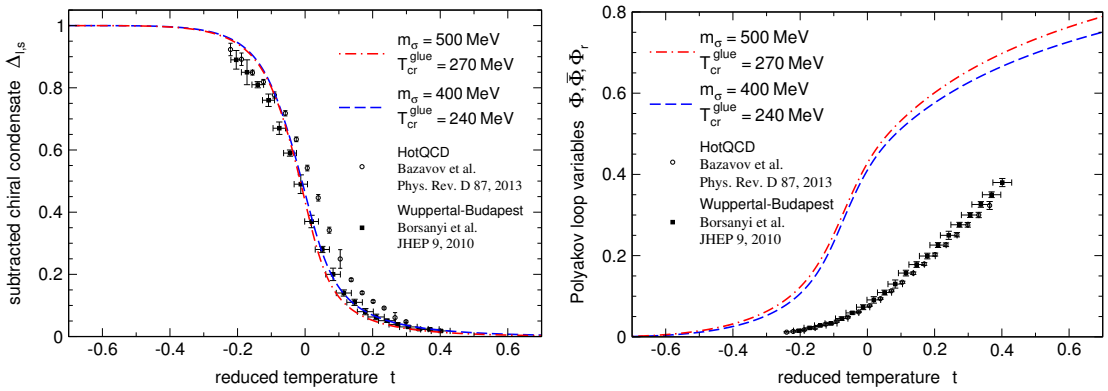

Figure 4.26.: The best results for the subtracted chiral condensate $\Delta_{\mathrm{l,s}}$ (left) and the Polyakov-loop expectation value Φ (right) as a function of temperature at $\mu_f = 0$ for different values of the mass of the σ-meson. The results are compared to the lattice calculations of Refs. [38, 42].

Table 4.6.: Pseudocritical temperatures for the crossover transition at $\mu_f = 0$ for different combinations of σ-meson masses and glue critical temperatures. They are determined by the peak position of the chiral susceptibility $\partial\Delta_{\mathrm{l,s}}/\partial T$ and of the temperature derivative of the Polyakov loop $\partial\Phi/\partial T$. The polynomial-logarithmic parametrisation of the Polyakov-loop potential is used.

$(m_\sigma, T_{\mathrm{cr}}^{\mathrm{glue}})$ [MeV]	(400, 240)	(500, 270)
T_{c} [MeV]	179	197
T_{d} [MeV]	165	183

values in Table 4.6.

In summary, in this section the impact of the improvements of the presented framework and the robustness of the results has been tested by the analyses of the impact of the different ingredients and the dependence on the parametrisation and the transition temperature of the Polyakov-loop potential as well as the σ-meson mass. A parameter-dependence of the results has been found, which can not be ignored in a quantitative analysis. To be more specific, when varying the glue critical temperature and the mass of the scalar σ-meson one observes that a larger glue critical temperature has a similar effect on the results as a decrease of the mass of the σ-meson.

Comparing the impact of the different ingredients and the parameter dependences discussed in this section unquenching the Polyakov-loop potential has the biggest impact on the nature of the transition and is most important to bring Polyakov-loop extended

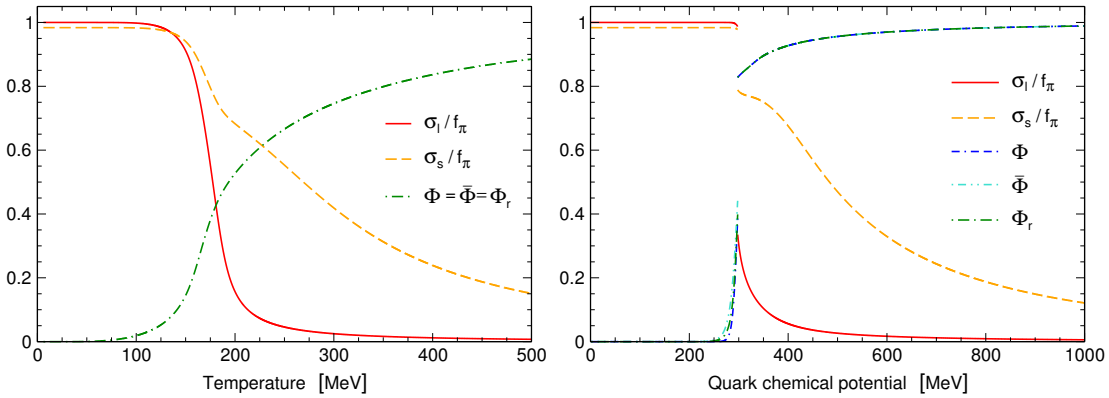

Figure 4.27.: Evolution of the chiral condensates and the Polyakov loop with increasing temperature at vanishing density (left) and with increasing quark chemical potential at a temperature of 10 MeV (right).

chiral models to qualitative agreement with results of lattice calculations at zero quark chemical potentials.

4.2. Thermodynamics and Phase Structure at nonzero Quark Chemical Potentials

In the previous section the unquenching of the Polyakov-loop potential showed to be an important improvement for the description of the phase structure and thermodynamics at zero quark chemical potentials with Polyakov-loop extended chiral models.

Now, the applicability of this improved Polyakov–Quark-Meson model will be tested at nonzero quark chemical potentials. The impact of unquenching the Polyakov-loop potential onto the phase diagram will be discussed as well as the differences between those combinations of the parameters that have been adjusted to lattice data at zero chemical potentials throughout the previous subsections.

The results presented in the following are obtained using the polynomial-logarithmic Polyakov-loop potential. They correspond to the magenta dashed–double-dotted line in Figs. 4.17 to 4.20 for zero chemical potentials. Why a parametrisation is chosen that limits the Polyakov loop to be always smaller than one will become clear during the discussion.

The evolution of the order parameters with increasing quark chemical potential at a small temperature is qualitatively different than that at small chemical potentials with increasing temperature as is shown in Fig. 4.27. At low temperatures, the order parameters have a discontinuity at some finite chemical potential which signals a first-order phase transition.

Displayed are the results for the expectation values of the light and strange chiral condensates σ_l and σ_s normalised by the vacuum value of the nonstrange condensate

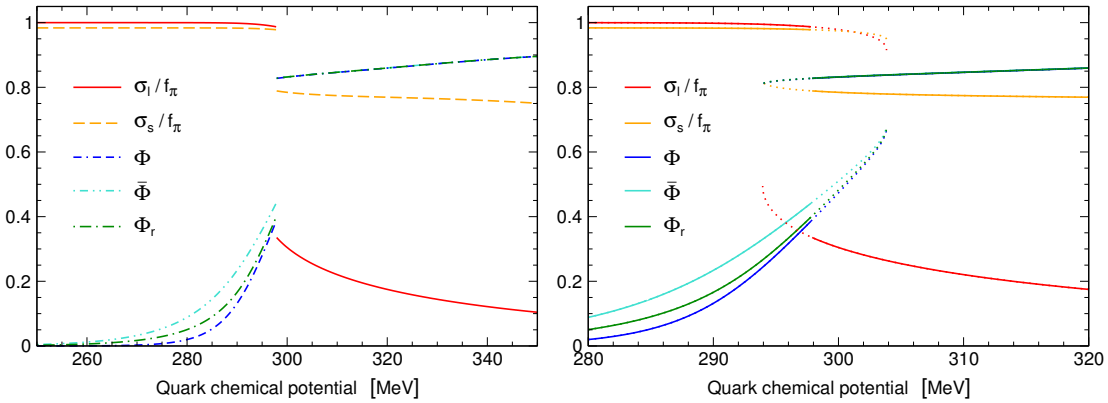

Figure 4.28.: Zoom into the transition region for the evolution of the chiral condensates and the Polyakov loop with increasing quark chemical potential at a temperature of 10 MeV. The left figure shows the differences between the 'saddle-point' approach and the 'minimisation' procedure and the right figure indicates the extension of the metastable region.

$\langle \sigma_l \rangle_{\rm vac} = f_\pi$ as well as of the Polyakov loop variables in the 'saddle-point' approach and the 'minimisation' model. Figure 4.27 shows that solving the sign problem of the PQM model by neglecting the imaginary part of the effective potential leads qualitatively to the same results as circumventing the sign problem by assuming that the Polyakov-loop variables are two independent, real quantities. That even the quantitative differences between $(\Phi, \bar{\Phi})$ and $\Phi_{\rm r}$ are small shows the zoom into the transition region shown in Fig. 4.28. The real part $\Phi_{\rm r}$ of the in general complex Polyakov loop takes values that are in between the real variables Φ and $\bar{\Phi}$ with $\left(\bar{\Phi} - \Phi\right) \geq 0$ and visible differences exist only in the confined phase. Important to observe is as well that the chiral fields take the same values independent of the realisation of the glue sector.

The right part of Fig. 4.28 is a further zoom into the transition region and shows in addition the extension of the metastable region and how the order parameters in the one minimum evolve while it coexists as a local minimum. The extension and asymmetry of the metastable region will be analysed further later on.

The impact of a quark-backreaction onto the Polyakov-loop potential at finite quark densities is shown in Fig. 4.29. The upper panels are results obtained with the unquenched Polyakov-loop potential while for the results in the lower part a pure Yang-Mills Polyakov-loop potential has been used. Obviously, using the quark-enhanced Polyakov-loop potential the chiral and (de)confinement transition remain linked at small temperatures and large quark chemical potentials.
The question is whether the use of the same functional relation between pure Yang-Mills and glue effective potential found in the transition region for zero chemical potentials is justified at small temperatures and large quark chemical potentials. At small temperatures and zero density one should actually expect that Yang-Mills and effective glue potential become asymptotically the same. So the question specifies to if the impact of

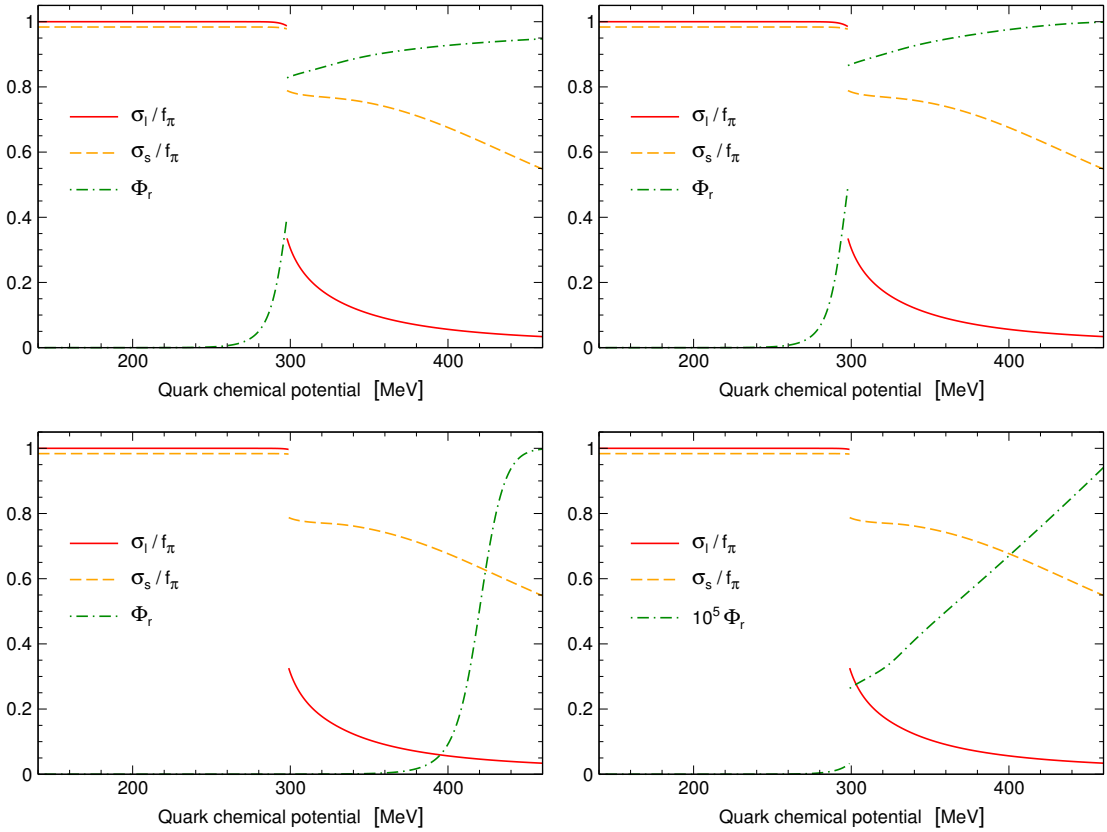

Figure 4.29.: Evolution of the chiral condensates and the Polyakov loop with increasing quark chemical potential at a temperature of 10 MeV with the unquenched Polyakov-loop potential with a density independent $T_{\mathrm{cr}}^{\mathrm{glue}}$ (top left), with $T_{\mathrm{cr}}^{\mathrm{glue}}(\mu_f)$ (top right), with the Yang-Mills Polyakov-loop potential with $T_{\mathrm{cr}}^{\mathrm{YM}}(\mu_f)$ (bottom left) and with a density independent $T_{\mathrm{cr}}^{\mathrm{YM}}$ (bottom right).

quarks to the Polyakov-loop potential at small temperatures and chemical potentials of the order of the critical one can be approximated by their impact at zero density and temperatures around the pseudocritical temperature.
The pure Yang-Mills Polyakov-loop potential does as such not contain any direct dependence on quark densities and therefore, the Polyakov-loop remains at its vacuum value ~ 0 at small temperatures when the quark chemical potential is increased as is shown in the lower right part of Fig. 4.29. Only the coupling to quarks and mesons leads to an extremely small variation.
One way to include a density-dependent matter backreaction onto the Polyakov-loop potential is to consider the chemical potential dependence of its transition temperature [72, 78] as generalised in Eq. (3.52). This implies that the transition scale of the Polyakov-loop potential decreases with increasing chemical potential. This in turn lowers the pseudocritical temperature of the crossover transition of the Polyakov-loop at a large chemical potential towards the critical temperature of the chiral first order transition. This is shown in the lower left panel of Fig. 4.29 and Refs. [72, 76–78]. With the inclusion of meson fluctuations in a renormalisation group framework this backreaction is enough to see the chiral and (de)confinement transitions remaining linked at large chemical potentials as shown in Refs. [76, 78].
Therefore, the coincidence of the chiral and (de)confinement transition at large chemical potentials with the unquenched Polyakov-loop potential is qualitatively a welcome feature. Taking additionally into account the chemical potential dependence of the glue critical temperature shows then a minor impact as can be seen in comparing the upper right and upper left figures of Fig. 4.29. The consequence of adjusting $T_{\rm cr}^{\rm glue}$ with $\mu_{\rm q}$ is as for the Yang-Mills Polyakov-loop potential to move the Polyakov-loop to larger values at a given chemical potential.
Interestingly enough, the evolution of the chiral order parameters is perfectly independent of the realisation of the Polyakov-loop potential as is shown in Fig. 4.29, except of a 1 % decrease of the chiral condensates just before the transition when the unquenched Polyakov-loop potential is used.

Even the qualitative impact of unquenching the Polyakov-loop potential, that it links chiral and (de)confinement transition is reasonable its quantitative magnitude remains in question. While pure gauge theory allows to adjust parametrisations of the Polyakov-loop potential to the minimum of the potential and the PQM model at zero densities but nonzero temperature probes regions of the Polyakov-loop potential away from the minimum, the PQM model at large quark chemical potentials probes the form of the Polyakov-loop potential far away from the minimum. The impact of applying relation (3.56) to unquench the Polyakov-loop potential is such that the Polyakov-loop becomes unbound at small temperatures and large chemical potentials for polynomial parametrisations. Only the limitation of the Polyakov loop to be smaller than one when the Haar measure is considered avoids this artificial behaviour.

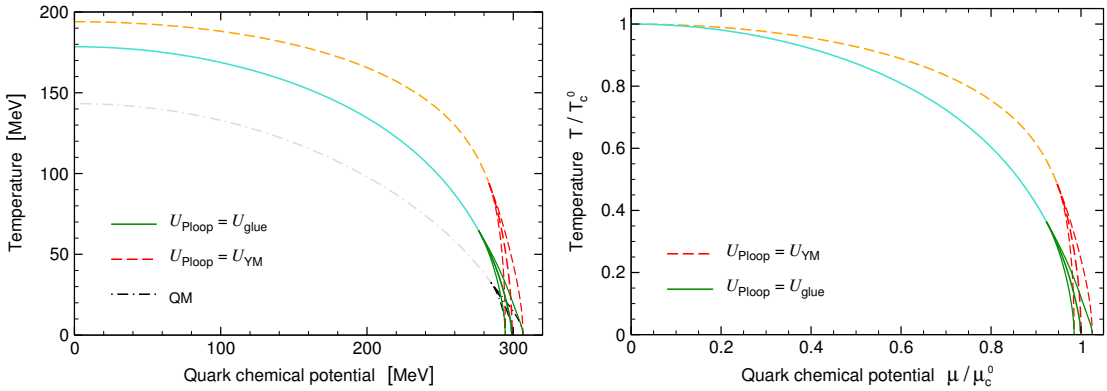

Figure 4.30.: Phase diagram with the Yang-Mills Polyakov-loop potential and the unquenched one, in absolute units (left) and relative units (right). The (lighter) crossover lines are the pseudocritical values of the subtracted chiral condensate. The thiner, outer lines around the first-order transition lines retrace the extension of the metastable regions.

Having found a crossover at small chemical potentials and a first-order transition at small temperatures, the next step is to investigate the complete $T - \mu_q$ phase diagram considering the before mentioned observations.

The phase diagram of the PQM model is shown in Fig. 4.30. The effect of unquenching the Polyakov-loop potential onto the phase diagram is displayed by the comparison of the results using the Yang-Mills Polyakov-loop potential and its quark-enhanced counterpart. The (lighter) crossover lines are the pseudocritical values of the subtracted chiral condensate. These results are obtained using the polynomial-logarithmic Polyakov-loop potential with a density-independent critical temperature of 240 MeV and $m_\sigma = 400\,\mathrm{MeV}$ as adjusted to lattice results at zero density.

For all values of the quark chemical potential $\mu_q = \mu_u = \mu_d = \mu_s$, unquenching the Polyakov-loop potential has the consequence of lowering the transition temperature which has its origin in the effect of lowering the transition scale of the Polyakov-loop. In the zero temperature limit $T \to 0$ the Polyakov-loop potential becomes independent of its variables $\mathcal{U}(\Phi_r, \Phi_i; T = 0) = 0\ \forall (\Phi_r, \Phi_i)$ since gluon excitations are entirely independent of the quark chemical potential and therefore, the phase structure is that of the Quark-Meson model that is shown as well in Fig. 4.30.

With all uncertainties adjusted to lattice data at zero quark chemical potential, there remains a region at large chemical potentials where the phase transition is discontinuous and the order parameters show a jump. The thiner, outer lines around the first-order transition line retrace the extension of the metastable region, so to which extent the one phase remains as local minimum while the system is in the other phase which is the global minimum. The coordinates of the critical endpoints (CEP) are $(T, \mu)_{CEP} = (65, 276)$ MeV with the unquenched Polyakov-loop potential and $(94, 283)$ MeV with the Yang-Mills potential. So the main effect of including the quark backreaction onto the gluons is to lower the temperature of the CEP at a similar chemical potential.

At these large values of the quark or baryon chemical potential ($\mu_\mathrm{b} = 3\mu_\mathrm{q}$), baryons are the relevant degrees of freedom that are not contained in the PQM model. To implement baryons as bound states of quarks and diquarks using the Fadeev and Bethe-Salpeter equations, see e.g. Refs. [214–217], to the PQM model remains for future work. Even this region of the phase diagram at large chemical potentials and small temperatures is speculative within the present model, general methods to analyse the properties of this region will be derived in the next chapter.

An important aspect of the phase diagram at small chemical potentials is the curvature of the transition line. This can also be extracted from lattice calculations that are hampered at nonzero quark chemical potentials due to the sign problem. In the right part of Fig. 4.30 the transition lines are normalised by the respective pseudocritical temperatures at zero density, T_c^0 and the critical chemical potential at zero temperature, μ_c^0 to allow for a comparison of the curvatures. One sees that applying the unquenched Polyakov-loop potential lowers the pseudocritical temperature relatively stronger with increasing chemical potential such that the curvature of the phase transition line increases.

It is a general observation that in effective models the pseudocritical temperature drops faster with increasing baryon chemical potential compared to the results of functional [218] and lattice [219] calculations. This discrepancy is not cured by unquenching the Polyakov-loop potential. One ingredient that brings the result of the curvature of the crossover line closer to the one of nonperturbative calculations is the inclusion of meson fluctuations in a renormalisation group framework [76, 78]. In Ref. [220] it was shown that including repulsive vector interactions can lead to a slope of the phase transition line that agrees with the result of lattice calculations. But one should be aware that by including the vector meson exchange, the model fails to describe lattice results of quark number susceptibilities as was shown in Refs. [221, 222]. Therefore, it is important to overcome the later failure to investigate the impact of vector interactions onto the curvature of the crossover line and the nature of the transition at large chemical potentials.

The influence of lowering the critical temperature of the Polyakov-loop potential with increasing density according to Eq. (3.52) has a smaller effect on the phase diagram than applying Eq. (3.58) to unquench the Polyakov-loop potential, as can can be seen in the comparison of Figs. 4.30 and 4.31. To illustrate the impact on the curvature of the transition line, in the right part of Fig. 4.31 the square of the chemical potential is chosen as abscissa. In this unit the pseudocritical temperature follows a straight line for small values of the chemical potential. Lowering the glue critical temperature with increasing chemical potential has the impact of decreasing the pseudocritical temperature such that the curvature of the transition line gets larger. The location of the critical endpoint is lowered further in temperature to $(T, \mu)_\mathrm{CEP} = (47, 280)$ MeV when the glue critical temperature is decreased with growing chemical potential.

The analysis of how well the different parametrisations of the Polyakov-loop potential

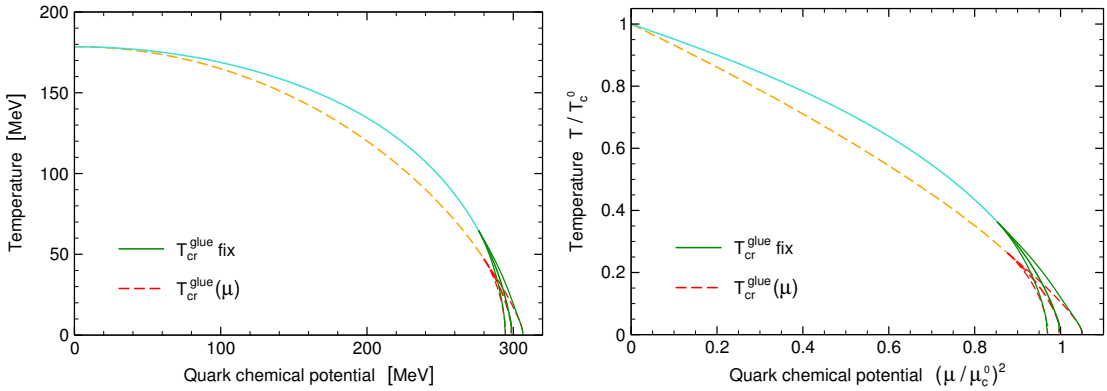

Figure 4.31.: Phase diagram for a constant critical scale of the unquenched Polyakov-loop potential and with the density dependence of Eq. (3.52), in absolute units (left) and relative units (right).

are adjusted to lattice data of Yang-Mills theory in Chap. 3.2 and the investigation of the impact of the parametrisations on the evolution of order parameters and thermodynamics at zero chemical potentials when the potential is coupled to quarks and mesons in Sec. 4.1.4, showed that the results show similar qualitative behaviour (except of the trace anomaly of pure gauge theory and the full model with the parameters of Ref. [69] in the polynomial parametrisation) but differ quantitatively. Figures 4.32 and 4.33 compare the phase diagrams for the different parametrisations using the parameters as they were determined in Sec. 4.1.4 to get as close as possible to the lattice results for the order parameters, thermodynamics and pseudocritical temperatures. Characteristics are the lower pseudocritical temperatures with the parameters of Ref. [80] in the polynomial Polyakov-loop potential and that the polynomial-logarithmic Polyakov-loop potential leads to larger transition temperatures from medium chemical potentials on. The former observation is the result that only this potential allowed to achieve a pseudocritical temperature that corresponds well to the lattice result together with a relative evolution of the analysed observables that matches the lattice data. The overall shape of the phase boundaries is similar and only the critical endpoint with the polynomial-logarithmic Polyakov-loop potential shows a larger deviation than the difference between the other parametrisations. The coordinates are summarised in Table 4.7. The extensions of the metastable regions for the different parametrisations of the Polyakov-loop potential will be compared below. The fact that the Polyakov loop is unbounded with the unquenched polynomial Polyakov-loop potentials at small temperatures and large chemical potentials does not affect negatively the phase structure nor the location of the critical end point.

In Sec. 4.1.3 it was shown that also omitting the contribution of fermionic quantum fluctuations (3.11), one can achieve results for thermodynamics, order parameters and the pseudocritical temperature at zero density that are in close agreement with lattice results as long as the unquenched Polyakov-loop potential is considered. One could

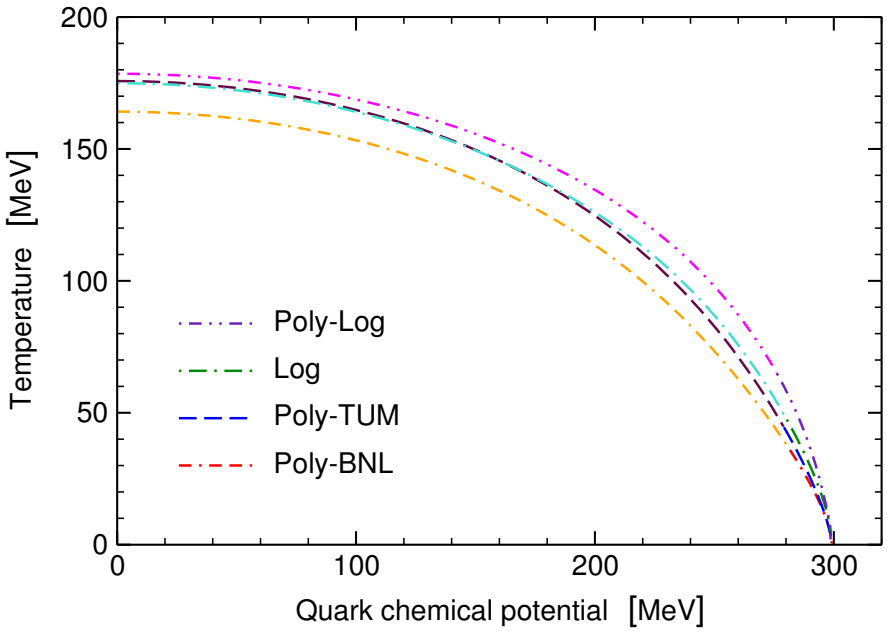

Figure 4.32.: Phase diagram for the different parametrisations of the Polyakov-loop potential, in absolute units.

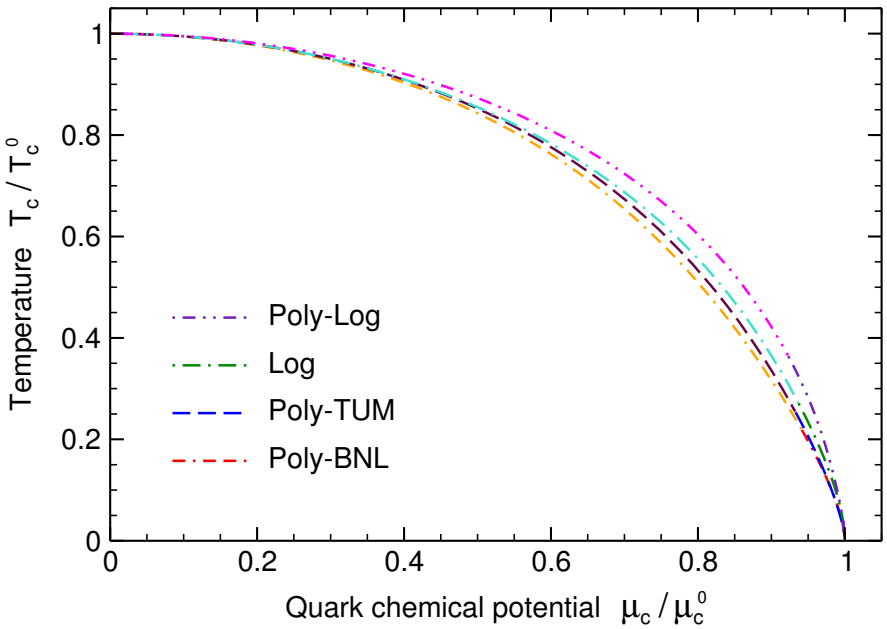

Figure 4.33.: Phase diagram for the different parametrisations of the Polyakov-loop potential, in relative units.

Table 4.7.: Temperature and quark chemical potential coordinates of the critical end points found with the different parametrisations and parameter sets of the Polyakov-loop potential.

	Poly-BNL	Poly-TUM	Log	Poly-Log
$T_{\mathrm{cr}}^{\mathrm{glue}}$ [MeV]	270	240	240	240
$(T,\mu)_{\mathrm{CEP}}$ [MeV]	$(36, 282)$	$(45, 279)$	$(47, 280)$	$(65, 276)$

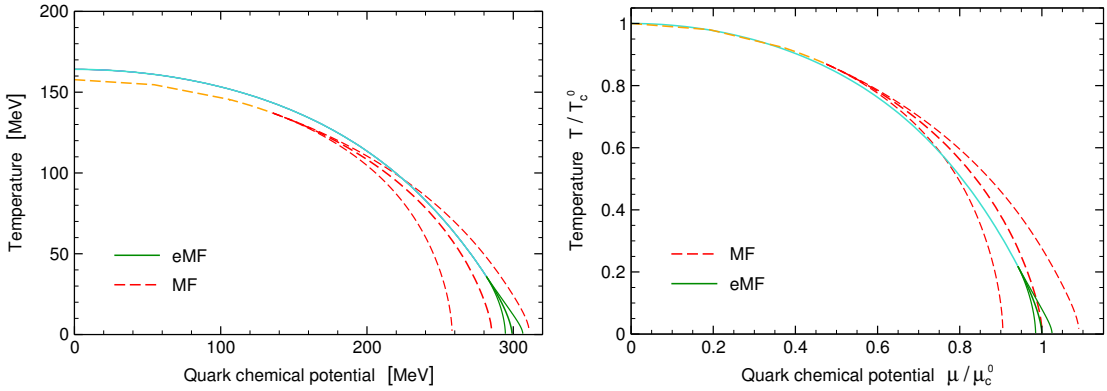

Figure 4.34.: Phase diagram with and without fermionic quantum fluctuations at one loop, in absolute units (left) and relative units (right).

recognise in Figs. 4.11 and 4.12 that the crossover in this standard mean-field analysis is nevertheless slightly steeper that in the extended mean-field calculation that includes the fermionic quantum fluctuations at one loop order. However, even the difference in the steepness of the transition at zero chemical potentials is small, neglecting the fermionic quantum fluctuations has tremendous implications on the location of the critical endpoint and the extent of the metastable region. The phase diagrams corresponding to the MF and eMF model adjusted at zero density in Figs. 4.11 and 4.12 are compared in Fig. 4.34. The curvature of the phase transition line is similar in both cases with a slightly larger curvature from medium chemical potentials on when the fermionic vacuum loop is taken into account. But the location of the critical endpoint is shifted to much smaller values of the chemical potential when the field-dependent normalisation term of the one-loop contribution from quarks is neglected, as was previously observed in Ref. [77] using the Yang-Mills Polyakov-loop potential. Its coordinates are $(T,\mu)_{\mathrm{CEP}} = (137, 135)$ MeV. The location of the critical end point at a smaller chemical potential entails that the transition is steeper at larger chemical potentials and the extent of the metastable region therefore much larger. Hence, it will be important to consider the impact of the fermionic quantum fluctuations in the analysis of the first-order transition region in Chap. 5.

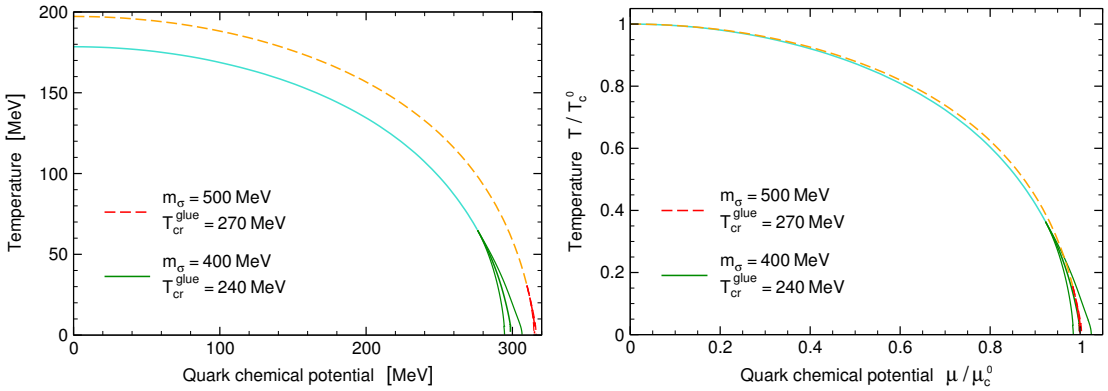

Figure 4.35.: Phase diagram for different combinations of masses of the σ-meson and glue critical temperatures, in absolute units (left) and relative units (right).

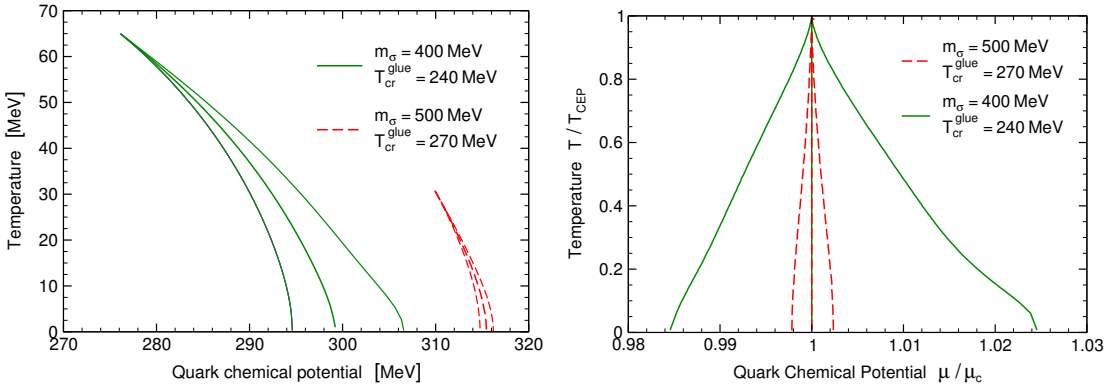

Figure 4.36.: Metastable regions of the PQM model for different combinations of masses of the σ-meson and glue critical temperatures. Their extension is compared in absolute units (left) and with respect to the transition line (μ_c) and the temperature of the critical end point T_{CEP} (right).

In Figs. 4.26 and 4.25 of Sec. 4.1.6 it was shown that different combinations of the mass of the σ-meson and glue critical temperatures lead to a relative evolution of thermodynamics and order parameters that is consistent with lattice data. At zero density the effect of changing these parameters within their uncertainty is to shift the transition region. This implication is also seen over the hole phase diagram as is shown in Fig. 4.35. Once the axis are normalised as on the right side of Fig. 4.35 the location of the transition lines agree but the location of the critical endpoint is sensitive to the parameters. For $m_\sigma = 500\,\text{MeV}$ and $T_{\text{cr}}^{\text{glue}} = 270\,\text{MeV}$ the critical endpoint is shifted to $(T, \mu)_{\text{CEP}} = (30, 310)$ MeV. So the first order region as well as the extent of the metastable region shrink when the mass of the σ-meson and the glue critical temperature are increased. The later observation can be seen in more detail in Fig. 4.36 which displays the metastable region in detail on the left and analyses its relative extent on the right.

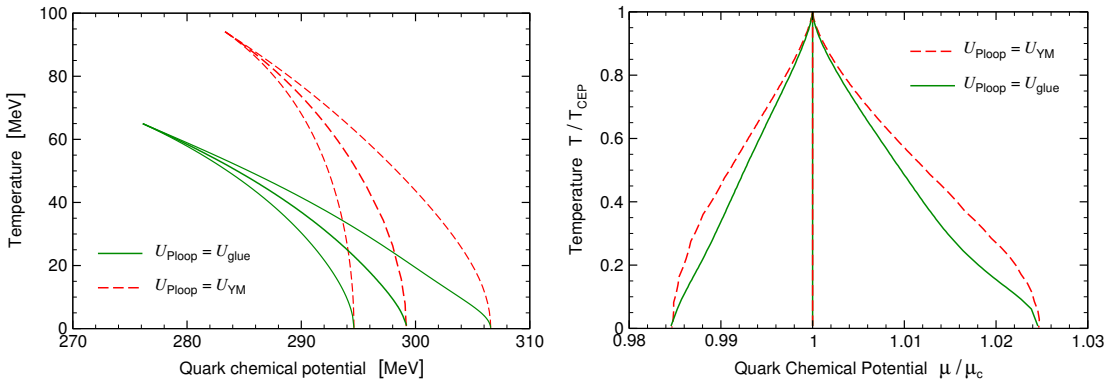

Figure 4.37.: Metastable regions of the PQM model with the Yang-Mills Polyakov-loop potential and the unquenched one. Their extension is compared in absolute units (left) and with respect to the transition line (μ_c) and the temperature of the critical end point T_{CEP} (right).

In general, the two minima of the potential that are degenerate on the coexistence line persist as a global and a metastable local minimum in some region of the phase diagram around the phase transition line. Going away from the coexistence line, the intervening maximum approaches the local minimum until these two extrema meet and form an inflection point that defines the spinodal line.

Figure 4.37 compares the extension of the metastable region that is limited by the spinodal lines using the unquenched Polyakov-loop potential and the Yang-Mills potential. The absolute location of the critical endpoint and therefore of the metastable region differs except for the lowest temperatures when the Polyakov-loop independent Quark-Meson limit is reached. But the relative extent is similar as is shown on the right side of Fig. 4.37. Here, the from changes from a convex shape with the Yang-Mills Polyakov-loop potential to a concave form when the matter backreaction to the Polyakov-loop potential is considered.

The zoom into metastable regions achieved with different parametrisations and parameter sets of the Polyakov-loop potential shown in Fig. 4.38 shows in more detail that the critical endpoint with the polynomial-logarithmic glue potential deviates from the location of the critical endpoint calculated with the other Polyakov-loop potentials. But once the metastable regions are corrected for the different coordinates of the critical endpoints, all parametrisations and parameter sets lead to an extent of the metastable region that is largely independent of the form of the Polyakov-loop potential. This is shown in Fig. 4.39. Furthermore, one finds that the degree of metastability that can be reached is relatively modest. The extent of the metastable region shows an asymmetry for the lowest temperatures in which the spinodal line in the chirally restored and deconfined phase has a larger distance to the coexistence line than the spinodal in the chirally restored and confined phase. This observation on the asymmetric extent of the metastable region holds as well for the description of Yang-Mills theory with the different Polyakov-loop potentials as could be seen in the right part of Fig. 3.2 and in

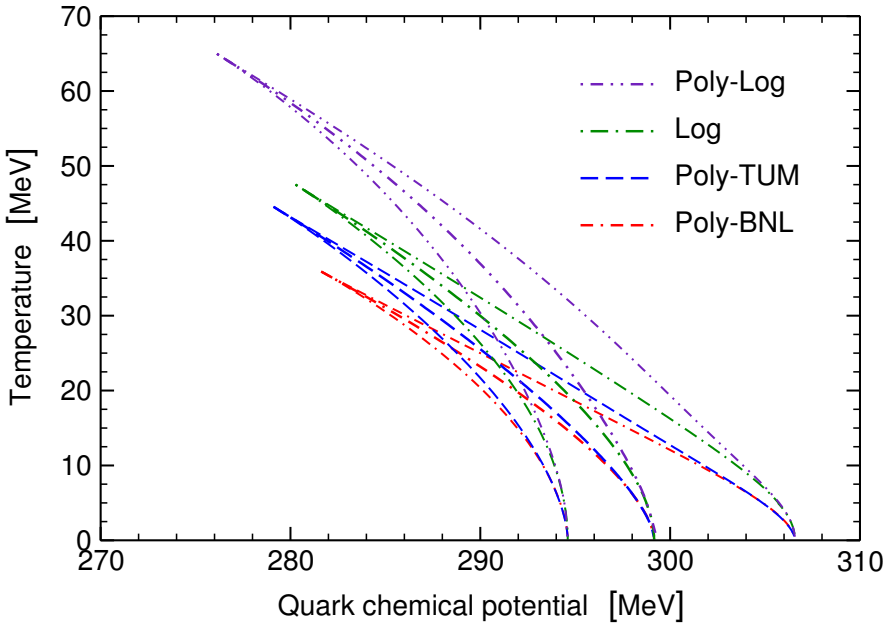

Figure 4.38.: Metastable regions of the PQM model for the different parametrisations of the Polyakov-loop potential.

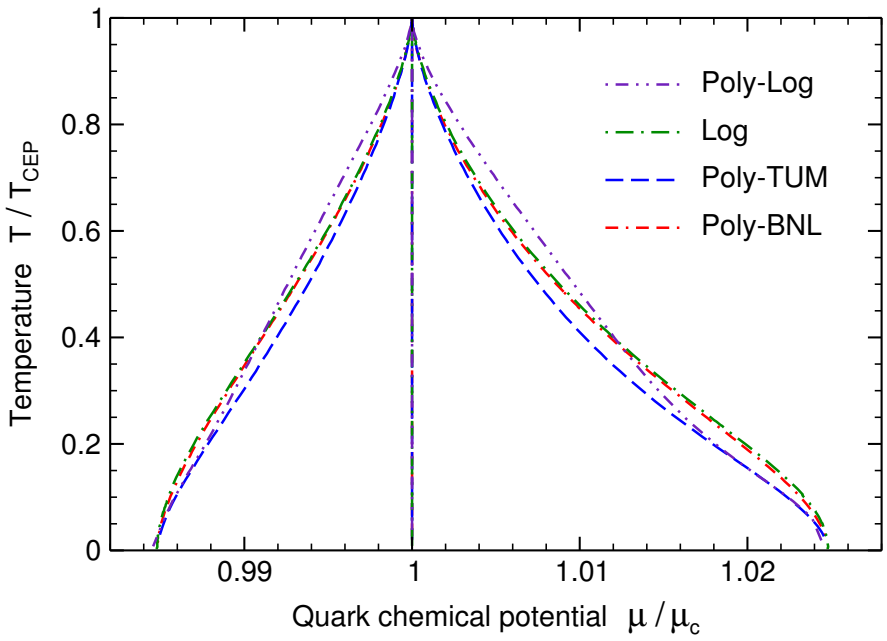

Figure 4.39.: Metastable regions of the PQM model for the different parametrisations of the Polyakov-loop potential. Their extension is compared with respect to the transition line (μ_c) and the temperature of the critical end point T_{CEP}.

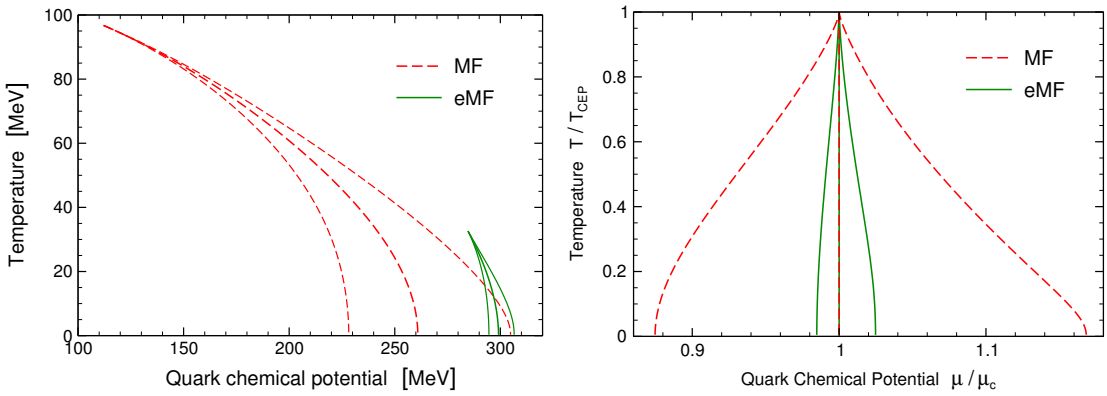

Figure 4.40.: Metastable regions of the QM model with and without fermionic quantum fluctuations at one loop. Their extension is compared in absolute units (left) and with respect to the transition line (μ_c) and the temperature of the critical end point T_{CEP} (right).

the pure chiral Quark-Meson model as is shown in Fig. 4.40.

To analyse the impact of the fermionic vacuum loop contribution (3.11) onto the location and extent of the metastable region, Fig. 4.40 shows results for the Quark-Meson model. Neglecting centre symmetry has the advantage that different choices of the Polyakov-loop potential, glue critical temperature and for the mass of the σ-meson as in Fig. 4.34 don't interfere with the effect of considering or not the medium independent contribution of the quark loop. The left part of Fig. 4.40 confirms the observation that fermionic vacuum fluctuations are crucial for the nature of the phase transition at large densities. The region of the phase diagram where the transition is discontinuous is significantly larger when the fermionic quantum fluctuations to the in-medium effective potential are neglected. Furthermore, the transition is much stronger at small temperatures and large chemical potentials in that case. Therefore, it is important to consider the effect of fermionic vacuum fluctuations when investigating systems that probe the low temperature and high density region of the phase diagram like compact stars and supernova explosions, see e.g. Refs. [9, 10]. Important for the properties of the transition in these systems is as well the extent of the meltable region. The right part of Fig. 4.40 entails that it differs significantly between the mean-field and extended mean-field analysis.

In summary, in the present study the biggest impact on the nature of the transition at large densities and small temperatures have the fermionic vacuum fluctuations. For the position of the transition line unquenching the Polyakov-loop potential has the biggest effect, even if the backreaction of the quarks onto the gluons is considered as density independent. So considering the quark-enhanced Polyakov-loop potential proved to be decisive to find results for the phase structure at zero density that agree with results of lattice calculations, the curvature of the transition line of the PQM model

with the unquenched Polyakov-loop potential remains larger than in nonperturbative functional and lattice calculations. This entails that the density dependence of the quark backreaction has to analysed in more detail and further ingredients to the effective model have to considered, such as repulsive interactions by exchange of vector mesons and meson fluctuations.

In Chap. 5 the properties of the phase transition in the high density and low temperature region of the phase diagram will be analysed. But before, the application of the model at nonzero isospin will allow for another and more detailed test of the reliability of Polyakov-loop extended chiral models in systems containing other control parameters besides the temperature.

4.3. Thermodynamics and Phase Structure at nonzero Isospin

In this section the phase structure of strongly interacting matter at nonvanishing isospin will be investigated. Vanishing quark chemical potential but nonzero isospin has the advantage that the results can be compared directly to lattice data since this case is free of the sign problem [51, 52].

In the description of strongly interacting matter in its natural environment isospin should not be overlooked. Using Au or Pb beams in heavy ion collisions, the proton to neutron ratio is $\sim 2/3$. In astrophysical environments the initial proton fraction in supernovae is 0.4, reduces to 0.2 and finally reaches values of less than 0.1 in cold neutron stars. In the universe a large asymmetry in the lepton sector is allowed ($-0.38 < \mu_\nu/T < 0.02$) [85], which can shift the equilibrium conditions at the cosmological QCD transition [86]. Hence, in all systems mentioned above matter does not consist of equal amounts of protons and neutrons, i.e. one has a nonvanishing isospin density.

Effective chiral models, combined with the different versions of the Polyakov-loop potential, usually have their parameters adjusted to provide a good description of lattice data at zero density. Testing the model built in this fashion against lattice data at nonzero isospin is crucial to understand whether such an effective model provides qualitative and quantitative accurate descriptions of the phase structure of strong interactions in general, when also other control parameters besides the temperature are involved.

To date, most of the calculations at nonvanishing isospin were done with only two quark flavours, neglecting strange quarks as relevant degrees of freedom at the energy scale of the chiral and deconfinement transition [43–45, 223–237]. Furthermore, lattice calculations at nonzero isospin were performed so far only with unphysical heavy quark masses [43–45]. The impact of the quark mass on the deconfining critical temperature at nonzero isospin was investigated in Refs. [223, 224], using a framework that combines chiral perturbation theory to describe the low-energy sector with the phenomenological fuzzy bag model for high energies, showing that quark masses play a relevant role.

Previously, there have also been investigations with the hadron resonance gas model [238], the O(2N)-symmetric ϕ^4-theory [239], the Nambu–Jona-Lasinio model [225–233, 240], the Quark-Meson model [234], and its Polyakov-loop extended versions [235–237].

One of the aspects in the extension of the phase diagram to nonzero isospin is the arising of a new phase. Charged pions couple to the isospin chemical potential and at $\mu_\mathrm{I} = \mu_\mathrm{u} - \mu_\mathrm{d} = m_\pi$ there is the onset of pion condensation [87]. The running of the pion mass in the medium shifts the appearance of pion condensation to larger temperatures and densities. Depending on the analysed region of isospin, temperature and quark chemical potential, pion condensation must be taken into account [43, 44, 223, 224, 227–235, 239, 240] or not [45, 225, 226, 237, 238].

The omission of pion condensation in the presented framework limits the upper value of isospin chemical potential that can considered to moderate isospin chemical potential values.

In difference to two-flavour investigations, in the case of 2+1 quark flavours one has to choose the quark chemical potential of strange quarks as well. In the case of supernovae and in the early universe there exists a local β-equilibrium with respect to weak flavour-mixing interactions so that $\mu_\mathrm{s} = \mu_\mathrm{d}$. In heavy ion collisions no net strangeness can be produced and the strange quark chemical potential has to be adjusted accordingly. However, the case that can be considered in lattice calculations avoiding the sign problem corresponds to the choice $\mu_\mathrm{s} = 0$. Therefore, for $\mu_\mathrm{u} = -\mu_\mathrm{d}$ results for the case with vanishing strange chemical potential will be shown which corresponds in this limit also to the heavy ion case of zero net strangeness. Differences to $\mu_s = \mu_d$ will be briefly discussed. The result for nonvanishing light quark chemical potential will be presented for astrophysical environments ($\mu_\mathrm{s} = \mu_\mathrm{d}$).

Figure 4.41 shows the impact of moderate isospin on the temperature dependence of the order parameters and thermodynamics at vanishing quark chemical potential. One can see from the plot that a nonzero isospin brings the transition to smaller temperatures. Furthermore, although the chiral condensate decreases appreciably, the pressure hardly rises and the maximum of the interaction measure experiences a certain increase. Qualitatively, this dependence of the chiral condensate and pseudocritical temperature on the isospin is also seen in the lattice calculation of Ref. [43]. Furthermore, one observes that the chiral condensate gets smaller with increasing isospin for all temperatures. This means a shrinking of the 'chiral circle' of the tilted Mexican hat potential with increasing isospin due to an increasing contribution of the thermal quark fluctuations. At a isospin chemical potential beyond the onset of pion condensation an additional effect would be a rotation from the chiral condensate to the pion condensate [231].

This is also reflected in Fig. 4.42 where the evolution of the order parameters (left) and all relevant thermodynamic quantities (right) as functions of the isospin chemical potential for vanishing quark chemical potential and at the pseudocritical temperature $T_\mathrm{c}\,(\mu_\mathrm{I} = 0)$ (therefore, the order parameters start at around 0.5) are shown. One can see that the chiral condensate of the light quarks decreases for increasing isospin chemical

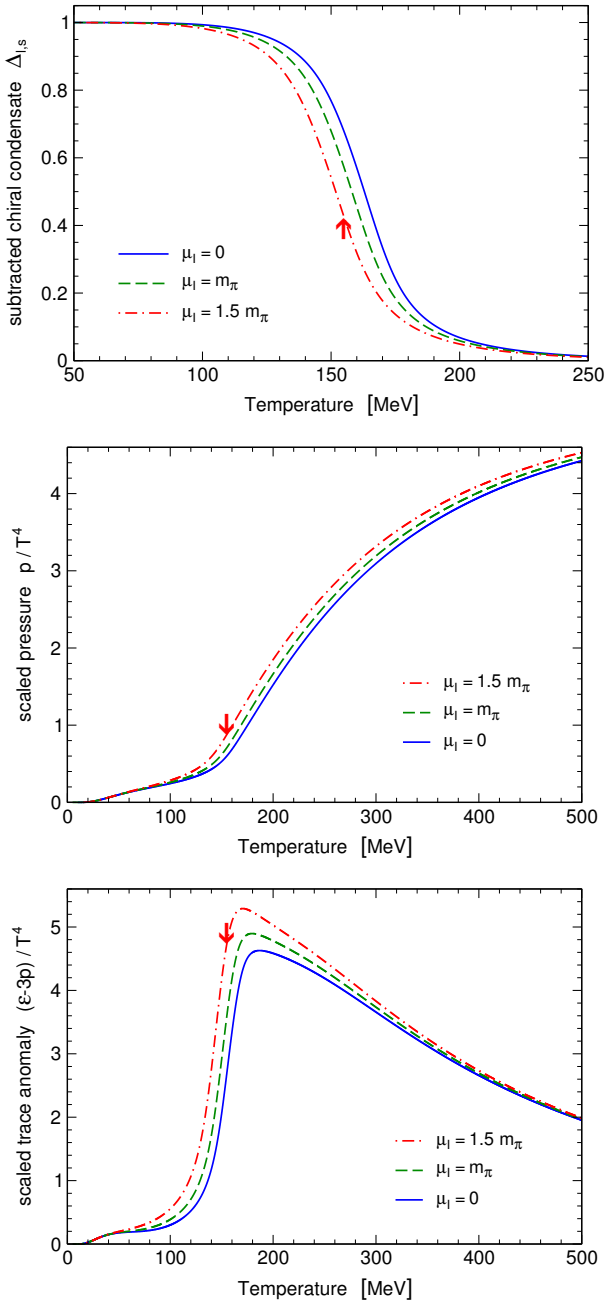

Figure 4.41.: Subtracted chiral condensate, normalised pressure and trace anomaly as functions of the temperature for different isospin at vanishing net quark density. The arrow indicates from which temperature on the in-medium pion mass exceeds the isospin chemical potential in the calculation with $\mu_I = 1.5 m_\pi$ where $m_\pi = 138\,\mathrm{MeV}$ is the vacuum pion mass. From Ref. [3].

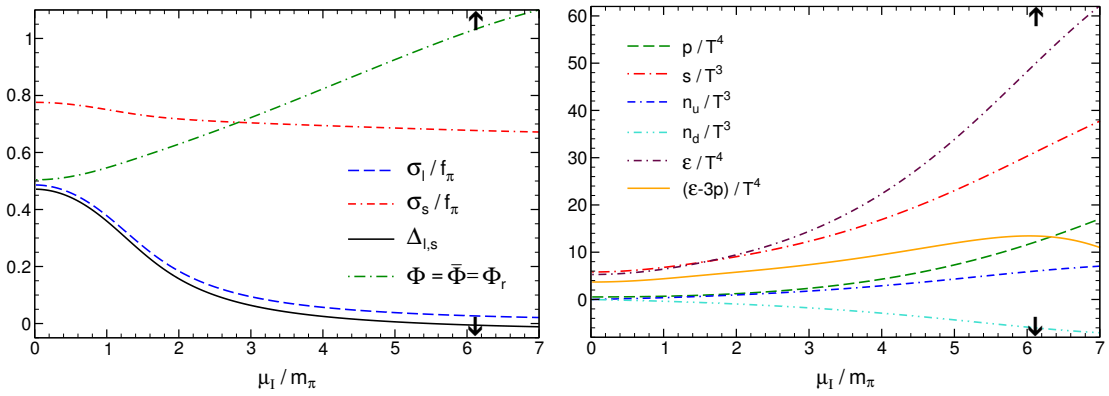

Figure 4.42.: Order parameters (left) and thermodynamic quantities (right) as functions of the isospin at $T_c\,(\mu_I = 0)$ and vanishing quark density. The arrows indicate from where on the isospin chemical potential exceeds the in-medium pion mass. From Ref. [3].

potential. On the other hand, chiral symmetry tends to remain broken in the strange quark sector, since the strange quark chemical potential is zero. Only the nonzero temperature reduces the strange chiral condensate and the coupling to the light quarks induces a slight decrease of this condensate for increasing isospin chemical potential. The Polyakov-loop observables $(\Phi, \bar{\Phi})$ and Φ_r coincide at vanishing quark chemical potential. The different impact of a finite chemical potential of the up quarks μ_u onto Φ and $\bar{\Phi}$ in Eq. (3.12) is just the opposite of the effect of the down quarks with $\mu_d = -\mu_u$. This restriction onto $\Phi = \bar{\Phi}$ at nonzero isospin but vanishing quark density implies that the sign problem is not present in this case. In the right part of Fig. 4.42 one sees that the pressure and the trace anomaly change moderately with isospin at vanishing quark chemical potential but the energy density is more sensitive to the variation in isospin.

The dependence of the phase structure on the isospin chemical potential is shown in the phase diagram of Fig. 4.43. It shows the decrease of the pseudocritical temperature with the isospin chemical potential at vanishing quark chemical potential. The results are confronted to the recent lattice simulation of Ref. [45] and to results of Ref. [223] where the authors combine chiral perturbation theory, including nucleons, for the low-energy sector with the phenomenological fuzzy bag model at high energy. The pseudocritical temperatures of the lattice calculation [45] and of the model calculation [223] are that of the deconfinement transition. For the PQM model calculation the deconfinement transition line coincides with the chiral transition presented in Fig. 4.43. Note that in all model calculations the pseudocritical temperatures are linear functions when plotted against μ_I^2 in agreement with lattice data [43, 45].

All these calculations are performed with different pion masses. To correct for the effect of the pion mass onto the abscissae of the temperature-isospin phase diagram, the isospin chemical potential can be normalised by the individual pion masses. So pion condensation at zero temperature where no medium modifications are present sets in

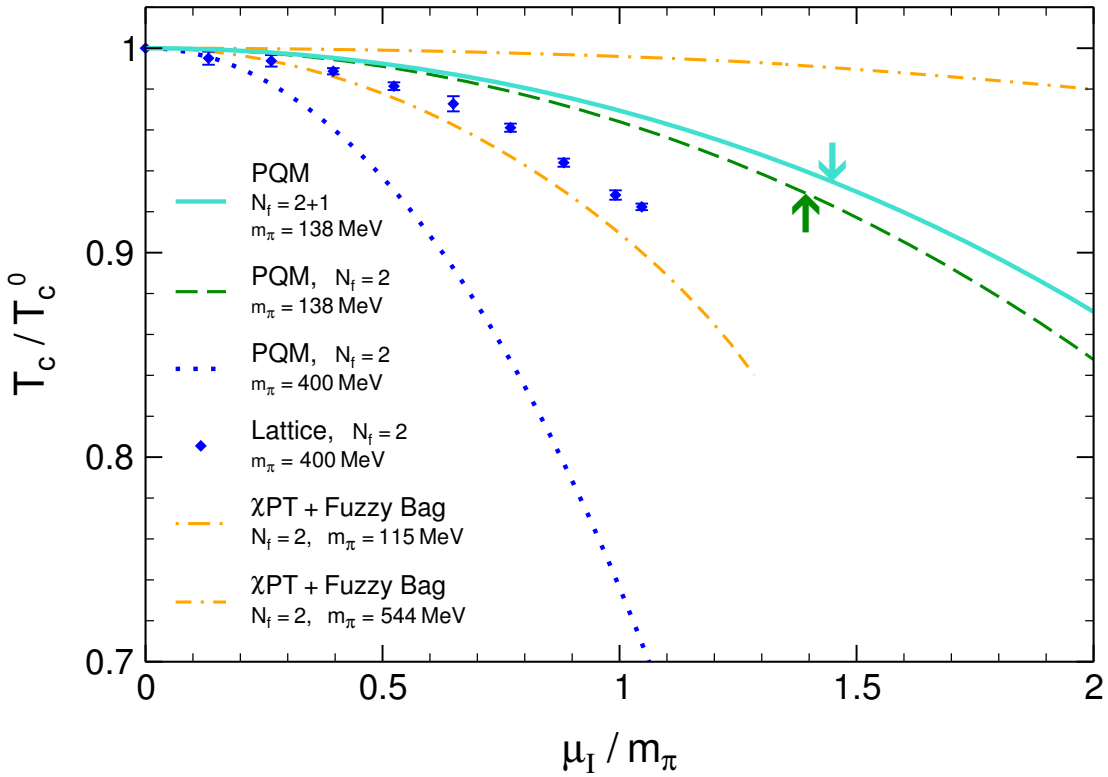

Figure 4.43.: Phase diagram at vanishing net quark density and nonzero isospin. The results are compared to the lattice calculation of Ref. [45] and the model calculation of Ref. [223].

at the same point $\mu_I = m_\pi$ in all calculations. This removes a general offset between calculations with different pion masses. One observes that in the range before the onset of pion condensation the curvature of the transition line is much more sensitive to the pion mass than to the number of quark flavours.

The arrows in Fig. 4.43 indicate the points on the phase transition lines where the isospin chemical potential exceeds the in-medium pion mass, so that condensation of charged pions should no longer be neglected. The upper line of Ref. [223] includes a range where a superfluid pion condensate is present (short dot-dashed line), but the curvature of the transition line is hardly affected by this correction. The lattice calculation, on the other hand, is performed for values of the isospin chemical potential below the onset of pion condensation.

Figure 4.43 contains results for $2+1$ and 2 flavours and physical pion mass (light blue, solid curve and green, dashed curve) and for 2 flavours and $m_\pi = 400$ MeV (dark blue, dotted curve), the latter being more appropriate to compare to the currently available lattice data [45]. In the case with $m_\pi = 400\,\mathrm{MeV}$, the dependence of the nucleon mass on the pion mass is considered according to Ref. [241] and therefore, the scalar coupling g is increased by a factor of 1.25. The coupling λ is also adjusted to preserve the mass difference $m_\sigma^2 - m_\pi^2$ in the vacuum.

The results for 2 flavours and $m_\pi = 400$ MeV (dark blue, dotted line in Fig. 4.43) show a decrease with μ_I that is significantly larger than the one obtained on the lattice. This corresponds to the observation that the pseudocritical temperature drops faster with increasing quark chemical potential in low-energy effective models compared to functional methods [218] and the lattice [219] as discussed in the previous section. Further ingredients that can alleviate this discrepancy are repulsive vector interactions [220] and the inclusion of meson fluctuations [76, 78]. Besides this investigation at nonvanishing isospin, Polyakov-loop extended chiral models seem to face difficulties describing lattice data also when one considers the dependence of the critical temperature on quark masses or on a magnetic field, see e.g. Refs. [242, 243].
Some studies compared the curvature of the crossover line along the isospin and light quark chemical potential axes within their calculations. While in older investigations the pseudocritical temperatures are almost identical along both axes [43, 225, 238], Ref. [45] found a difference of about 10 % of the slope parameters. The framework applied here implies the former result. To address this issue thermal fluctuations of the pion fields should be considered which remains for future work [11].

The results presented here and those of Ref. [223] at two different pion masses illustrate the impact of the pion mass on the phase transition line. A larger pion mass increases the curvature of the transition line significantly. Hence, the solid line in Fig. 4.43 provides a lower limit of the pseudocritical temperature at nonzero isospin chemical potential for the case of $2 + 1$ quark flavours and physical quark masses. Results from the lattice in the physical limit would be very helpful to constrain further the applicability of effective chiral models at nonzero densities.

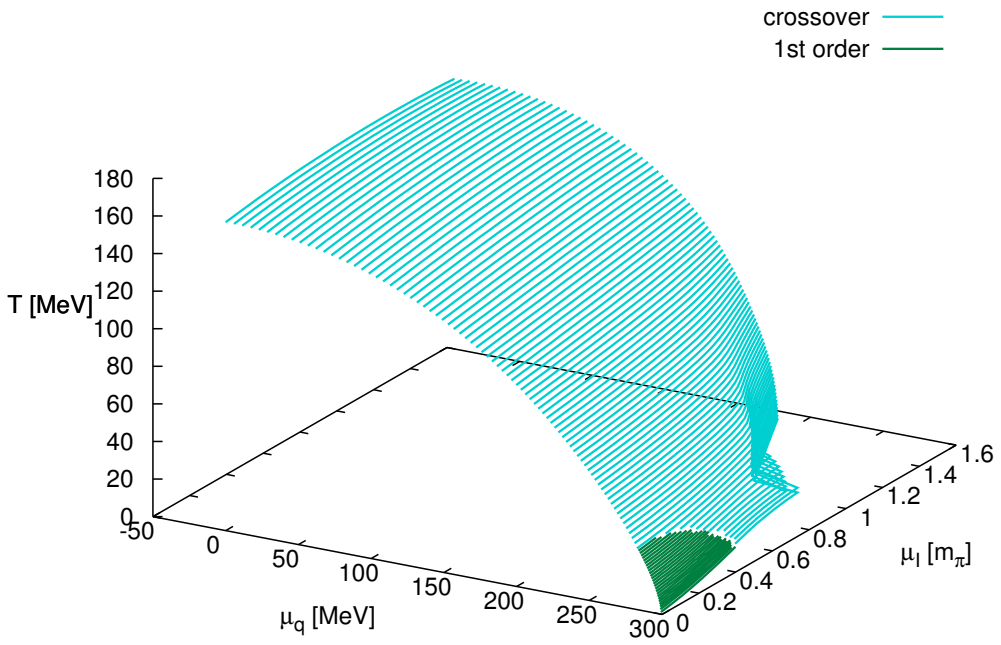

Figure 4.44.: Phase diagram, three dimensional in temperature, quark chemical potential and isospin space.

The impact of the pion mass on the transition line is much larger than that of adding strange quarks to the system. The pseudocritical temperatures for $N_\mathrm{f} = 2$ lie relatively close but below the $N_\mathrm{f} = 2 + 1$ result and the transition temperatures only deviate by two percent just before the onset of pion condensation.

An effect of similar magnitude and in the same direction has a nonvanishing strange quark density with $\mu_\mathrm{s} = \mu_\mathrm{d}$, as is the case in the astrophysical and cosmological scenarios. It increases the curvature of the transition line. For instance, the value of the transition temperature in the region just before the onset of pion condensation becomes two percent smaller.

The plot in Fig. 4.44 shows the global, three dimensional phase diagram. The kink in the phase transition surface at small temperatures, large quark chemical potential and moderate isospin is due to the splitting of the chiral transition in the up and down quark sectors. When a nonzero value for the chiral condensate σ_3 arises the evolution of the condensates of up quarks ($\sigma_\mathrm{u} = \sigma_\mathrm{l} + \sigma_3$) and down quarks ($\sigma_\mathrm{d} = \sigma_\mathrm{l} - \sigma_3$) splits around the average light quark condensate $\sigma_\mathrm{l} = (\sigma_\mathrm{u} + \sigma_\mathrm{d})/2$ as is discussed below in Fig. 4.47. Since the transition surface in Fig. 4.44 is defined by the peak of the susceptibility of the subtracted chiral condensate, the transition shifts depending on the dominant contribution. A criterion that would lead to a smooth transition surface would be to use the half-value of the condensates.

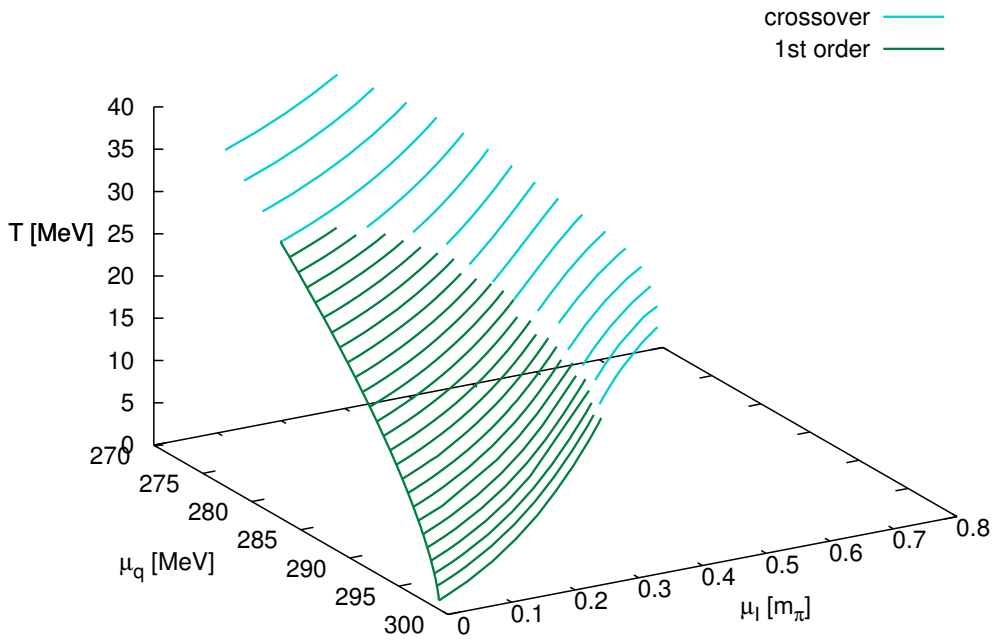

Figure 4.45.: First order region of the three dimensional phase diagram in temperature, quark chemical potential and isospin space.

At zero isospin there remains a small region at large quark chemical potential where the transition is of first order that is shown in more detail in Fig. 4.45. This first-order region shrinks with increasing isospin. With growing isospin the quark chemical potential of the down quarks gets reduced and therefore, the phase transition gets weaker. The critical endpoint disappears at not so large values of the isospin chemical potential: from an isospin chemical potential of $\mu_{\mathrm{I}} \approx 80\,\mathrm{MeV}$ on, the transition is a smooth crossover for all quark chemical potentials.

In the case of a quark-hadron phase transition during the evolution of a supernova [19,244,245], the system evolves from a hadronic phase with $\mu_{\mathrm{I}} = \mu_{\mathrm{charge}} \approx 100\,\mathrm{MeV}$ and $T \approx 50\,\mathrm{MeV}$ to a quark phase with $\mu_{\mathrm{I}} \sim T \sim \mathcal{O}\,(1\,\mathrm{MeV})$. So, within the uncertainties of the present description, at large quark chemical potential the phase transition in supernovae could be of first order, which would have several observable implications. One observable signal would be a second peak in the neutrino signal dominated by the emission of antineutrinos and with a significant change in the energy of emitted neutrinos [18, 246].

That a nonvanishing isospin can have an impact even on the nature of the phase transition is shown in Fig. 4.46. While it is of first order at small temperature and large quark density at zero isospin it becomes again a crossover at large enough isospin. So the reduction of the down quark chemical potential with increasing isospin ($\mu_{\mathrm{d}} =$

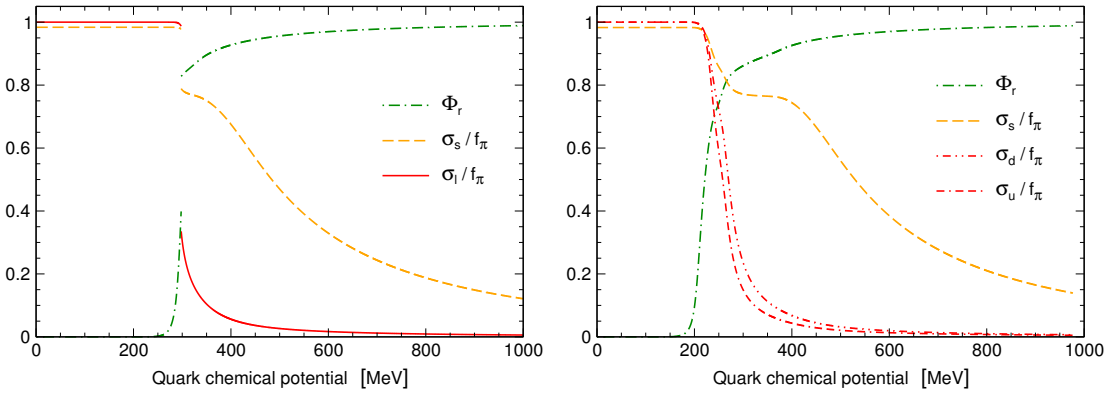

Figure 4.46.: Evolution of the chiral condensates and the Polyakov loop at a temperature of 10 MeV with increasing quark chemical potential at vanishing isospin (left) and at a isospin chemical potential of $\mu_\mathrm{I} = \mu_\mathrm{u} - \mu_\mathrm{d} = m_\pi = 138\,\mathrm{MeV}$.

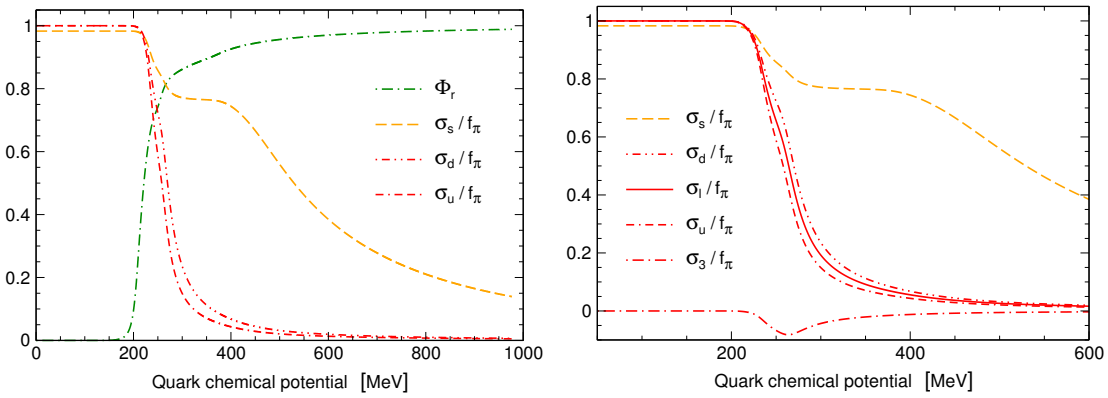

Figure 4.47.: Evolution of the chiral condensates and the Polyakov loop at a temperature of 10 MeV with increasing quark chemical potentials at a isospin chemical potential of $\mu_\mathrm{I} = \mu_\mathrm{u} - \mu_\mathrm{d} = m_\pi = 138\,\mathrm{MeV}$.

$\mu_\mathrm{l} - \mu_\mathrm{I}/2)$[1] is not compensated by the simultaneous further increase of the up quark chemical potential ($\mu_\mathrm{u} = \mu_\mathrm{l} + \mu_\mathrm{I}/2$). The difference of the chemical potentials of up and down quarks leads to a splitting in the evolution of the chiral condensates of up and down quarks. To compensate for the isospin chemical potential the down quark sector requires a larger average quark chemical potential so that chiral symmetry gets restored. This implies that the decrease of the chiral condensate of the down quark sector is shifted towards larger quark chemical potentials compared to the up quark chiral condensate.

In terms of the meson fields σ_0, σ_3 and σ_8 the splitting of the chiral condensates of up and down quarks is created due to a nonvanishing expectation value of σ_3 in the transition region. This is shown on the right of Fig. 4.47. While the chiral condensate σ_3 takes a nonzero value the evolution of the condensates of up quarks ($\sigma_\mathrm{u} = \sigma_\mathrm{l} + \sigma_3$)

[1] With $\mu_\mathrm{l} = (\mu_\mathrm{u} + \mu_\mathrm{d})/2$ being the average chemical potential of the light quarks.

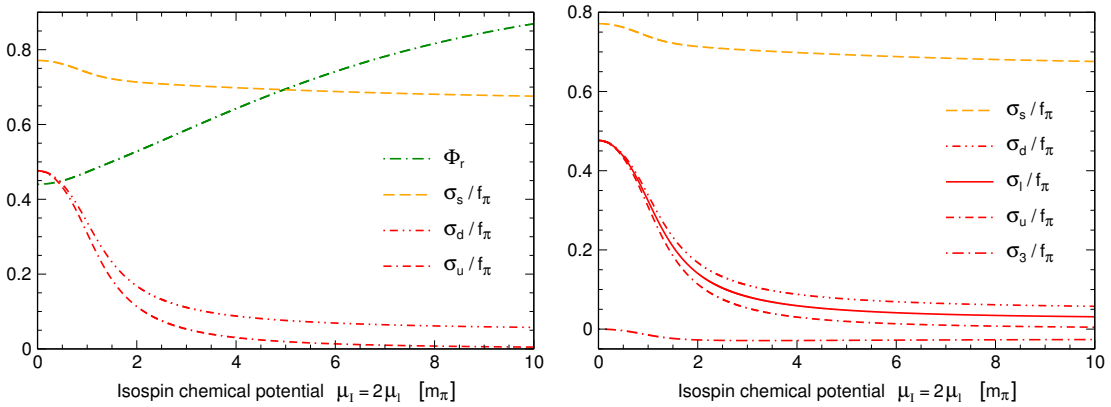

Figure 4.48.: Evolution of the chiral condensates and the Polyakov loop at the pseudocritical temperature with increasing up quark chemical potential at vanishing down quark chemical potential, so along $\mu_\mathrm{I} = 2\mu_\mathrm{l}$. The nonvanishing value of the condensate σ_3 (shown additionally on the right) induces the splitting of the chiral condensates of up and down quarks and their deviation from the average light quark condensate.

and down quarks ($\sigma_\mathrm{d} = \sigma_\mathrm{l} - \sigma_3$) splits around the average light quark condensate $\sigma_\mathrm{l} = (\sigma_\mathrm{u} + \sigma_\mathrm{d})\,/\,2$.

The splitting between the light chiral condensates becomes enhanced if one considers the evolution of the order parameters along $\mu_\mathrm{l} = \mu_\mathrm{I}/2$, so at vanishing chemical potential of down quarks but increasing up quark chemical potential. This is displayed in Fig. 4.48. With increasing isospin the difference in the chiral condensates of up and down quarks develops and increases. The quark chemical potential drives chiral symmetry restoration in the up quark sector but the vanishing chemical potential of down quarks implies a residual symmetry breaking in the down quark sector.

Assuming local β-equilibrium with respect to weak flavour-mixing interactions so that $\mu_\mathrm{s} = \mu_\mathrm{d}$ not only the down quark chemical potential vanishes but also $\mu_\mathrm{s} = 0$ so that a change in the strange chiral sector is only induced due to the coupling to the chiral condensates of the light quarks and the Polyakov loop and the chiral condensate in the strange sector tends to stay constant.

In conclusion, this section presents predictions on the dependence of order parameters and thermodynamics on a isospin chemical potential for 2+1 quark flavours and physical quark masses. The investigation of the three dimensional temperature - isospin chemical potential - quark chemical potential phase diagram showed that it is important to consider the isospin of a system to determine the nature of the phase transition, especially at low temperatures and large quark chemical potential. The comparison of the isospin dependence of the curvature of the phase transition line with recent lattice data confirmed the conclusion of Sec. 4.2 that the model in its here presented form faces difficulties describing nonperturbative results for the transition temperature when one

considers further dimensions besides the temperature as nonvanishing quark chemical potential, isospin or magnetic fields [243]. Possible improvements on this situation can be the inclusion of repulsive vector interactions, considering meson fluctuations within the renormalisation group framework and investigating the medium dependence of the quark-backreaction on the Polyakov-loop potential.

5. Nucleation

5.1. Homogeneous Thermal Nucleation

The dynamics of a first-order phase transition at small metastability as found in the PQM model in Sec. 4.2, can be described by phenomenological droplet nucleation models [91, 247–250]. In such a family of models, the transition between a metastable and a stable phase takes place by the appearance and growth of domains (droplets or bubbles) of the stable phase inside the metastable phase. The phase conversion is finished when these domains grow and coalesce completely. In any case, a minimum-sized bubble is needed for the beginning of the phase transition, as can be inferred from the following heuristic argument. The bulk free energy density of the metastable phase, often called 'false vacuum', is by definition higher than that of the stable phase, the 'true vacuum'. Therefore, the conversion of a given fraction of the system into the stable phase makes the bulk free energy of the whole system lower. However, given that such a conversion takes place within a connected domain of the system, most likely in a spherical bubble [251], an interface is needed in order to separate the stable interior from the metastable exterior of this domain. Once the creation of an interface represents an energy cost, the mechanism of phase conversion through bubble nucleation settles a competition between the free energy gain from the phase conversion of the bulk and the energy cost from the creation of an interface. Roughly, one can say that the free energy shift due to the appearance of a spherical bubble of the stable phase of radius R inside a metastable system is

$$\begin{aligned} \Delta F_{\rm b} &= \left[\frac{4\pi}{3}R^3 f_{\rm stable} + 4\pi R^2 f_{\rm wall}\right] - \left[\frac{4\pi}{3}R^3 f_{\rm metastable}\right] \\ &= \frac{4\pi}{3}R^3 \Delta f + 4\pi R^2 f_{\rm wall}\ , \end{aligned} \tag{5.1}$$

where $f_{\rm stable}$ and $f_{\rm metastable}$ are, respectively, the bulk free energy densities of the stable and metastable phases, and $f_{\rm wall}$ is the surface energy density of the bubble wall, that is, the surface tension of the interface between the two phases. This formula clearly shows the competition between bulk (negative) and surface (positive) contributions. Notice that the shift in the bulk free energy, $\Delta f \equiv f_{\rm stable} - f_{\rm metastable} < 0$ is proportional to the volume of the bubble, while the surface free energy cost is proportional to its area. For the nucleation of small bubbles, the energy cost is higher than the energy gain. Therefore, small bubbles shrink. On the other hand, a very large bubble represents a large bulk energy gain, which is higher than the surface energy cost in creating the

bubble. As a consequence, large bubbles tend to grow even more and to occupy the whole system, completing the phase transition. Consequently, this energy competition implies the existence of a so-called 'critical bubble': any bubble smaller than the critical bubble will shrink and any larger bubble will grow and drive the phase conversion. For this reason, the critical bubble is the crucial object in the theory of dynamical first-order phase transitions of slightly metastable systems.

The appearance of a bubble, critical or not of the stable phase inside a metastable system is a natural consequence of the never-ending thermal and quantum fluctuations of any thermodynamical system sufficiently close to a first-order phase transition. As just discussed, each bubble created by these fluctuations may grow or shrink, depending on its energy budget with regard to a homogeneous metastable phase. One should also have in mind that larger fluctuations (like a critical bubble) should be less common than smaller ones. Although small bubbles are frequently created, they rapidly disappear and do not contribute to the process of phase conversion with the exception in a weak first-order phase transition, when coalescing subcritical fluctuations [252, 253] can complete the phase transition without the nucleation of critical bubbles. Only those fluctuations that have a size equal to or larger than the critical bubble have a decisive role. The smallest and therefore the most probable among them is the critical bubble. This means that the mean time that it takes for random fluctuations to create a critical bubble is the shortest time scale for the creation of a lasting domain of the stable phase, which is the dynamical seed of the phase conversion.

Assume that the system is in a metastable state in quasi-equilibrium with a reservoir with intensive coordinates generically represented by $\mathcal{R}$ such as temperature, quark chemical potentials, etc. Being metastable, bubbles of the stable phase with different sizes randomly appear and subsequently disappear. This process keeps happening until a critical bubble is nucleated and the phase conversion effectively starts. It can be shown by different approaches that the rate at which critical bubbles are nucleated per unit time, per unit volume can be expressed in the form [91, 92, 247, 254, 255]

$$\Gamma\left(\mathcal{R}\right) \;=\; \mathcal{P}(\mathcal{R})\,\exp\left[-\frac{\Delta F_{\rm b}(\mathcal{R})}{T}\right]\,, \tag{5.2}$$

where T is the temperature of the system in equilibrium with the reservoir. The prefactor $\mathcal{P}(\mathcal{R})$ corresponds to the probability for a critical bubble-like field fluctuation $\phi_{\rm b}$ to be generated and grow [91–93]. The exponential factor in Eq. (5.2) is a Boltzmann factor in which $\Delta F_{\rm b}(\mathcal{R})$ is the shift of free energy as compared to the homogeneous metastable phase due to the formation of a critical bubble. It can be easily shown that $\Delta F_{\rm b}(\mathcal{R})$ can be cast as in Eq. (5.1) for a small degree of metastability, where the thin-wall approximation is valid [256] and where it is proportional to $f_{\rm wall}^3/(\Delta f)^2$. In spite of the general importance of the prefactor in Eq. (5.2), its specific form is not crucial for the nucleation rate at a small degree of metastability. Close to the coexistence of both phases, it shows a proportionality to $f_{\rm wall}^{7/2}/\Delta f$, so that the nucleation rate is strongly dominated by the exponential factor [92]. For this reason, it will be enough to focus on

the free energy shift $\Delta F_{\rm b}$ in the following.

The process of bubble nucleation in an impurity-free environment is called 'homogeneous nucleation'. In this work we shall only consider the process of homogeneous nucleation, which is not the most common in natural environments, such as in a boiling liquid. In such cases, the presence of impurities can drastically accelerate the nucleation of bubbles, and the process is called 'inhomogeneous nucleation' which is also the case when subcritical thermal fluctuations can dominate [252, 253]. The process of inhomogeneous nucleation can be orders of magnitude faster than homogeneous nucleation because impurities, like dust often reduce the free energy cost for the formation of a critical bubble, raising the probability for its formation [257, 258]. This will not be considered here for two reasons. First, the following approach will underestimate the nucleation rate and inhomogeneities could only increase this rate, and second, the used approach will be kept as simple as possible.

5.2. The coarse-grained Free Energy for a single scalar Order-Parameter

As discussed in Refs. [93, 256, 259, 260], the nucleation rate of critical bubbles can be calculated from the microphysics using semiclassical methods in Euclidean thermal field theory. It is important to consider the effective action in the problem of bubble nucleation, and not simply the effective potential, since a critical bubble is clearly a non-homogeneous field configuration. A simple model to discuss the derivation of the free energy shift due to the formation of a critical bubble is the Euclidean Lagrangian density for a single scalar order-parameter field called ϕ,

$$\mathcal{L}_{\rm E} \;=\; \frac{1}{2}\left(\partial_\mu \phi\right)^2 + V\left(\phi\right) \;. \tag{5.3}$$

In this simple model, one assumes that the order parameter for a system in thermodynamical equilibrium is given by the expectation value of ϕ. In general, it depends on the properties of the reservoir, such as its temperature or chemical potential, which are here generally denoted by $\mathcal{R}$. The corresponding action is

$$S_{\rm E}\left(\phi, \mathcal{R}\right) \;=\; \int_0^\beta {\rm d}\tau \int {\rm d}^3x \, \mathcal{L}_{\rm E}\left[\phi(\vec{x}, \tau)\right] \;. \tag{5.4}$$

In the high-temperature limit, $\beta \equiv 1/T \to 0$, the imaginary time dependence of the order parameter can be neglected [259] and therefore, one can make the approximation

$$S_{\rm E}\left(\phi, \mathcal{R}\right) \;\equiv\; \frac{F(\phi, \mathcal{R})}{T} \;, \tag{5.5}$$

where one identifies

$$F(\phi, \mathcal{R}) = \int {\rm d}^3x \, \left[\frac{1}{2}\left(\nabla\phi\right)^2 + V_{\rm eff}\left(\phi, \mathcal{R}\right)\right] \;, \tag{5.6}$$

with the coarse-grained free energy of the system. Notice that the coarse-grained free energy is a sort of dimensionally reduced effective action, so that the tree-level potential $V(\phi)$ must be replaced by the medium-dependent effective potential $V_{\text{eff}}(\phi, \mathcal{R})$. In full thermodynamical equilibrium, the minimisation of the coarse-grained free energy, which is equivalent to the minimisation of the Euclidean action is achieved by a constant field configuration $\phi(\vec{x}) = \phi_0$ so that the gradient term vanishes and $V_{\text{eff}}(\phi_0, \mathcal{R})$ must be a global minimum of V_{eff}.

The possibility of a metastable state arises when V_{eff} develops some local minimum other than the global minimum at $\phi = \phi_0$. In this framework, a metastable state is described by a constant field configuration ϕ_{f} that is a local minimum of V_{eff}. For this reason, this second minimum is often called a 'false vacuum' of the potential, while the global minimum is called the 'true vacuum' of the theory, $\phi_{\text{t}} \equiv \phi_0$. A bubble is then represented as a non-homogeneous spherically symmetric field configuration $\phi(r)$ such that [94, 95, 256]

$$\lim_{r\to\infty} \phi(r) = \phi_{\text{f}} \quad \text{and} \quad \frac{\mathrm{d}\phi}{\mathrm{d}r}(0) = 0 \,, \tag{5.7}$$

where ϕ_{f} is the value of the order-parameter field at the false vacuum. That is, away from the centre of the bubble, the system is in the metastable phase. But, in the vicinity of its centre, the field configuration should be close to the stable minimum but not necessarily exactly on it.

The critical bubble is a saddle point field configuration ϕ_{b} that extremises the functional F, i.e., it solves the Euler-Lagrange equation

$$\frac{\delta F(\phi, \mathcal{R})}{\delta\phi(\vec{x})} = 0 \quad \Rightarrow \quad \nabla^2\phi(\vec{x}) - \frac{\partial V_{\text{eff}}}{\partial\phi}[\phi(\vec{x})] = 0 \,. \tag{5.8}$$

It can be shown [251] for a wide class of Lagrangians, including Eq. (5.3), that the smallest value of F indeed corresponds to a spherically symmetric solution of Eq. (5.8), $\phi(r)$, so that the equation to be solved is therefore the non-linear ordinary differential equation

$$\frac{\mathrm{d}^2\phi(r)}{\mathrm{d}r^2} + \frac{2}{r}\frac{\mathrm{d}\phi(r)}{\mathrm{d}r} = \frac{\partial V_{\text{eff}}}{\partial\phi}[\phi(r)] \,, \tag{5.9}$$

with the boundary conditions (5.7).

The coarse-grained free energy associated with a spherical bubble ϕ_{b} is then

$$F_{\text{b}} = 4\pi\int_0^\infty \mathrm{d}r\, r^2 \left\{\frac{1}{2}\left[\frac{\mathrm{d}\phi_{\text{b}}(r)}{\mathrm{d}r}\right]^2 + V_{\text{eff}}[\phi_{\text{b}}(r)]\right\} \,, \tag{5.10}$$

which directly follows from Eq. (5.6).

Once the solution for Eqs. (5.9) and (5.7) is found, that is, the critical bubble profile $\phi_{\text{crit}}(r)$, the shift in the coarse-grained free energy due to the appearance of a critical bubble,

$$\Delta F_{\text{b}}(\mathcal{R}) = F(\phi_{\text{crit}}, \mathcal{R}) - F(\phi_{\text{f}}, \mathcal{R}) \,, \tag{5.11}$$

needed in the nucleation rate (5.2), can be readily calculated.

For a generic effective potential V_{eff}, the solution of Eq. (5.9) with boundary conditions (5.7) cannot be obtained analytically. However, an approximate solution can be found when the system is very close to the coexistence line, so that it is slightly metastable and the thin-wall approximation [254, 256, 259] is applicable. Within these limits, the coarse-grained free energy shift (5.11) can be well approximated by the expression

$$\Delta F_{\text{b}}(\mathcal{R}) \quad = \quad \frac{16\pi}{3}\frac{\Sigma^3}{\left(\Delta V_{\text{eff}}\right)^2} \,, \tag{5.12}$$

where

$$\Sigma\left(\mathcal{R}\right) \quad \equiv \quad \int_0^\infty \mathrm{d}r \left[\frac{\mathrm{d}\phi_{\text{crit}}(r)}{\mathrm{d}r}\right]^2 \,, \tag{5.13}$$

is the surface tension of the critical bubble interface between the phases. Notice that the surface tension is calculated directly from the critical bubble solution ϕ_{crit}. It must be so because the surface tension must contain information about how the system reacts to inhomogeneities, e.g. a wall. That is, any description of a critical bubble has to take into account more than just the bulk thermodynamics. This is the reason why the coarse-grained free energy (5.6) is needed in the formalism for bubble nucleation.

The quantity $\Delta V_{\text{eff}} = V_{\text{eff}}\left(\phi_{\text{t}}\right) - V_{\text{eff}}\left(\phi_f\right)$ is the difference between the bulk free energy in the two homogeneous vacua. In the grand canonical potential, it can be identified as $\Delta V_{\text{eff}}\left(\mathcal{R}\right) \equiv -\Delta p\left(\mathcal{R}\right)$, i.e. minus the difference of pressures between the two phases. Using the thin-wall approximation, the surface tension integral (5.13) can be calculated without solving for the profile. After changing variables from r to ϕ, one finds

$$\Sigma\left(\mathcal{R}\right) = \int_{\phi_{\text{t}}}^{\phi_{\text{f}}} \mathrm{d}\phi \, \sqrt{2V_{\text{eff}}(\phi, \mathcal{R})} \,, \tag{5.14}$$

so that only the effective potential $V_{\text{eff}}(\phi, \mathcal{R})$ is needed to calculate $\Sigma(\mathcal{R})$ in the thin-wall approximation. Notice that V_{eff} is normalised so that its global minimum is located at $\phi = \phi_{\text{t}} = 0$. Exactly at the coexistence points, where the thin-wall approximation is exact, the minima are degenerate with $V_{\text{eff}} = 0$.

As a last remark, one should notice that the surface tension cannot be correctly defined unless ϕ_{t} and ϕ_{f} are actual minima of the effective potential. This a further motivation for the minimisation approach discussed in Sec. 3.3.

5.3. The coarse-grained Free Energy for the Polyakov–Quark-Meson Model

In order to calculate the free energy shift $\Delta F_{\text{b}}(\mathcal{R})$ due to the nucleation of a critical bubble within the Polyakov–Quark-Meson Model model, one first needs to define the coarse-grained free energy functional and then identify an order parameter.

Just as in the case of a single order-parameter, the coarse-grained free energy of the PQM model has its origin in the in-medium effective action of the theory. In the PQM model, the Lagrangian density of the chiral fields directly leads to a kinetic term of the form $|\nabla\phi|^2$. The kinetic term for the Polyakov loop variable, however, is not determined a priori. If one considers the Polyakov loop order parameters Φ and $\bar{\Phi}$ as independent variables at finite chemical potentials a simple assumption for the kinetic term is [168]

$$\mathcal{L}_{\rm kin}\left(\Phi_{\rm r},\Phi_{\rm i}\right) \;=\; \frac{\kappa^2}{2}\left(\partial_\mu\Phi\right)^2+\frac{\kappa^2}{2}\left(\partial_\mu\bar{\Phi}\right)^2 \;. \tag{5.15}$$

Effective models cannot do much more than estimate the value of the kinetic parameter κ. From dimensional arguments, it is estimated to be $\kappa^2 = N_{\rm c}\,T_0^2/g_{\rm s}^2$ [80, 168]. For $N_{\rm c}=3$ and assuming $\alpha_{\rm s}=g_s^2/4\pi\simeq 0.3$, one finds $\kappa\simeq 0.9\,T_0$, which is of the order of magnitude of the only scale in the glue part of the model, the transition temperature T_0. Another consistent approach is to consider as an input the surface tension of the pure gauge SU(3) theory calculated through lattice Monte-Carlo simulations [261, 262] and in an effective matrix model [179], $\Sigma_{\rm SU(3)}\simeq 0.02\,T_0^3$. With a given parametrisation of the Polyakov-loop potential, the parameter κ can then be fitted from the value of the surface tension at $T=T_0$ using Eq. (5.14). The implications of this second approach in order to fix the parameter κ will be discussed in Sec. 5.4.2.

The coarse-grained free energy for the $N_{\rm f}=2+1$ PQM model can be written as

$$\begin{aligned}\mathcal{F}\left(\sigma_0,\sigma_3,\sigma_8,\Phi,\bar{\Phi};\mathcal{R}\right) = \int \mathrm{d}^3x\,\Bigg[&\frac{1}{2}\left(\nabla\sigma_0\right)^2+\frac{1}{2}\left(\nabla\sigma_3\right)^2+\frac{1}{2}\left(\nabla\sigma_8\right)^2+\\ &+\frac{\kappa^2}{2}\left(\nabla\Phi\right)^2+\frac{\kappa^2}{2}\left(\nabla\bar{\Phi}\right)^2+\Omega\left(\sigma_0,\sigma_3,\sigma_8,\Phi,\bar{\Phi};\mathcal{R}\right)\Bigg] \;.\end{aligned} \tag{5.16}$$

As discussed above, the critical bubble is a solution of the four coupled Euler-Lagrange equations that arise from the functional (5.16). There is no general procedure to solve this set of coupled equations, even though some ansatz solutions can be eventually tried for very simple effective potentials [263].

There are two possible ways in which one can tackle the problem. The first is, of course, to numerically solve the four equations that follow from the extremisation of $\mathcal{F}$ simultaneously. The exact solution will define a path in the four-dimensional space of order parameters. Notice, however, that this path is in general not in the 'valley' that connects the two minima, as can be intuitively seen from the inverted potential mechanical analog.

The approach applied in the following will lead to an overestimate of the surface tension or, equivalently, to an underestimate of the nucleation rate. According to Eq. (5.2), the higher the free energy shift of the critical bubble, the lower is the nucleation rate, at least as long as the thin-wall approximation is valid. Now consider that the exact critical bubble solution is found. Consider also a small deviation from it that follows a different path in the order-parameter space. Once the true critical bubble is a saddle point solution in a functional space, one expects that the distorted path will have a higher

value of ΔF as compared with the true bubble. Hence, one can artificially constrain the configuration path to a given arbitrary line that connects the two vacua in the space of order parameters. This path will give an overestimate of the free energy and, therefore, of the surface tension. The simplest choice is, of course, a straight line that connects both minima.[1] For example, let $\sigma_{\mathrm{l}}^{(1)}$ and $\sigma_{\mathrm{l}}^{(2)}$ be the values of the σ_{l} order-parameter in the two minima of Ω close to the coexistence line. The interpolation

$$\sigma_0 = \xi\sigma_0^{(1)} + (1-\xi)\,\sigma_0^{(2)} \tag{5.17a}$$

is such that for $0 \leq \xi \leq 1$, the value of σ_{l} varies from one minimum to the other. If the same function ξ is used to parametrise the path followed by the remaining order parameters,

$$\sigma_3 = \xi\sigma_3^{(1)} + (1-\xi)\,\sigma_3^{(2)}\,, \tag{5.17b}$$
$$\sigma_8 = \xi\sigma_8^{(1)} + (1-\xi)\,\sigma_8^{(2)}\,, \tag{5.17c}$$
$$\Phi = \xi\Phi^{(1)} + (1-\xi)\,\Phi^{(2)} \tag{5.17d}$$
$$\bar{\Phi} = \xi\bar{\Phi}^{(1)} + (1-\xi)\,\bar{\Phi}^{(2)}\,, \tag{5.17e}$$

then this path is a straight line in the four-dimensional order parameter space.

It is then natural to define the four-dimensional order-parameter for the PQM model as

$$\vec{\Psi} = \left(\sigma_0, \sigma_3, \sigma_8, \kappa\Phi, \kappa\bar{\Phi}\right)\,. \tag{5.18}$$

It can be easily shown from Eqs. (5.17) and (5.18) that if one writes the coarse-grained free energy (5.16) in terms of the field ξ, it assumes the form

$$\tilde{\mathcal{F}}\left(\xi,\mathcal{R}\right) = \int \mathrm{d}^3x \left[\frac{h^2}{2}\left(\nabla\xi\right)^2 + \tilde{\Omega}\left(\xi,\mathcal{R}\right)\right]\,, \tag{5.19}$$

where

$$h^2 = \left(\vec{\Psi}_0 - \vec{\Psi}_1\right)^2 \tag{5.20}$$
$$= \left(\Delta\sigma_0\right)^2 + \left(\Delta\sigma_3\right)^2 + \left(\Delta\sigma_8\right)^2 + \left(\kappa\Delta\Phi\right)^2 + \left(\kappa\Delta\bar{\Phi}\right)^2 \tag{5.21}$$
$$= \frac{1}{2}\left(\Delta\sigma_{\mathrm{u}}\right)^2 + \frac{1}{2}\left(\Delta\sigma_{\mathrm{d}}\right)^2 + \left(\Delta\sigma_{\mathrm{s}}\right)^2 + \left(2\kappa\Delta\Phi_{\mathrm{r}}\right)^2 - \left(2\kappa\Delta\Phi_{\mathrm{i}}\right)^2\,, \tag{5.22}$$

and $\tilde{\Omega}\left(\xi,\mathcal{R}\right)$ is the projection of the effective potential $\Omega(\vec{\Psi},\mathcal{R})$ along the straight line defined by Eqs. (5.17). Notice that the coarse-grained free energy $\tilde{\mathcal{F}}$ is formally equivalent to the single field coarse-grained free energy (5.6) and one can now consider ξ as

[1] In the whole range of interest in the $T-\mu$ plane, always either one or two minima have been found. The case of three or more minima, which is not encountered, would lead to a much more complicated analysis.

a scalar order-parameter. As a result, the surface tension in the PQM model can be overestimated by

$$\Sigma\left(\mathcal{R}\right) \;=\; h\int_0^1 \mathrm{d}\xi\,\sqrt{2\tilde{\Omega}(\xi;\mathcal{R})}\,, \tag{5.23}$$

where the domain of integration ranges from one minimum of Ω and thus of $\tilde{\Omega}$ to the other along a straight line path in the four-dimensional order-parameter space.

Notice that a path other than a straight line in the space of order parameters would not lead to a simple coarse-grained free energy with the same form as Eq. (5.19). In the general case, even the definition of the surface tension should be reformulated. This problem remains for future work.

5.4. Results

The derivation of an overestimate of the surface tension for bubble nucleation within the thin-wall approximation, Eq. (5.23) shows that it is determined by two contributions. On the one hand by the distance between the two degenerate minima in the space of the order parameters, i.e. the factor h and on the other hand by the shape of the effective potential along the straight line that connects both minima.

To discuss how the different contributions to the Polyakov–Quark-Meson Model build up the result of the surface tension, Sec. 5.4.1 presents the results within the Quark-Meson Model and Sec. 5.4.2 discusses the effects of the Polyakov-loop extension.

5.4.1. Nucleation within the Quark-Meson Model

The PQM model reduces to the Quark-Meson Model that governs only chiral symmetry breaking and restoration by fixing $(\Phi_\mathrm{r},\Phi_\mathrm{i})\equiv(1,0)$ at all temperatures and densities. This implies that the coarse-grained free energy and the estimate of the surface tension become independent of the kinetic parameter κ of the Polyakov-loop order parameters,

$$\Sigma_\mathrm{QM}^\mathrm{SU(3)}\left(T,\mu_\mathrm{l},\mu_\mathrm{s}\right) \;=\; \sqrt{\left(\Delta\sigma_\mathrm{l}\right)^2+\left(\Delta\sigma_\mathrm{s}\right)^2}\int_0^1 \mathrm{d}\xi\,\sqrt{2\tilde{\Omega}(\xi;T,\mu_\mathrm{l},\mu_\mathrm{s})}\,. \tag{5.24}$$

The contribution of the light quark sector is already present in the SU(2) Quark-Meson Model, where the overestimate of the surface tension simply reduces to

$$\Sigma_\mathrm{QM}^\mathrm{SU(2)}\left(T,\mu_\mathrm{l}\right) \;=\; \int_{\sigma_\mathrm{l}^{(1)}}^{\sigma_\mathrm{l}^{(2)}} \mathrm{d}\sigma_\mathrm{l}\,\sqrt{2\Omega(\sigma_\mathrm{l};T,\mu_\mathrm{l})}\,. \tag{5.25}$$

Hence, differences in the surface tension of the two-flavour and 2+1–flavour Quark-Meson model arise due to a possible modification of the degenerate values of the light chiral condensate, the additional dimension of the strange chiral condensate and a possible modification of the effective potential along the straight line connecting the minima.

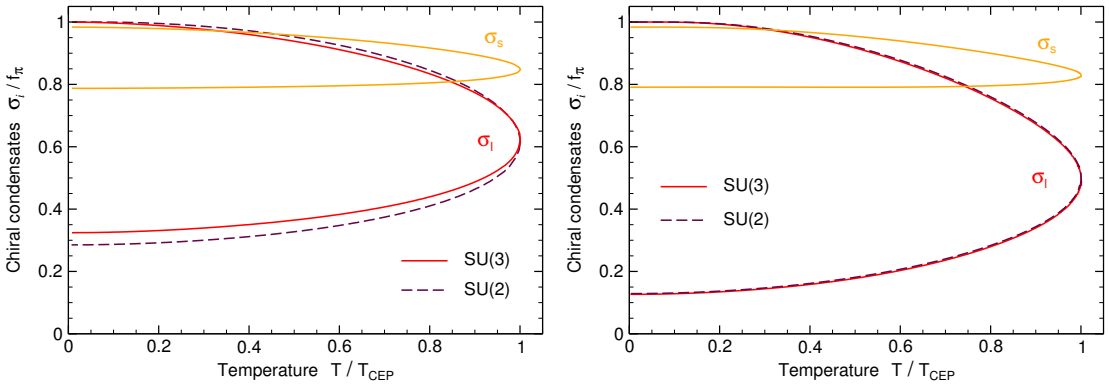

Figure 5.1.: Degenerate values of the chiral condensates σ_l and σ_s along the first-order transition line in the two and 2+1–flavour Quark-Meson model. The left figure is the result with the fermionic quantum fluctuations at one loop and the right figure is the case without these.

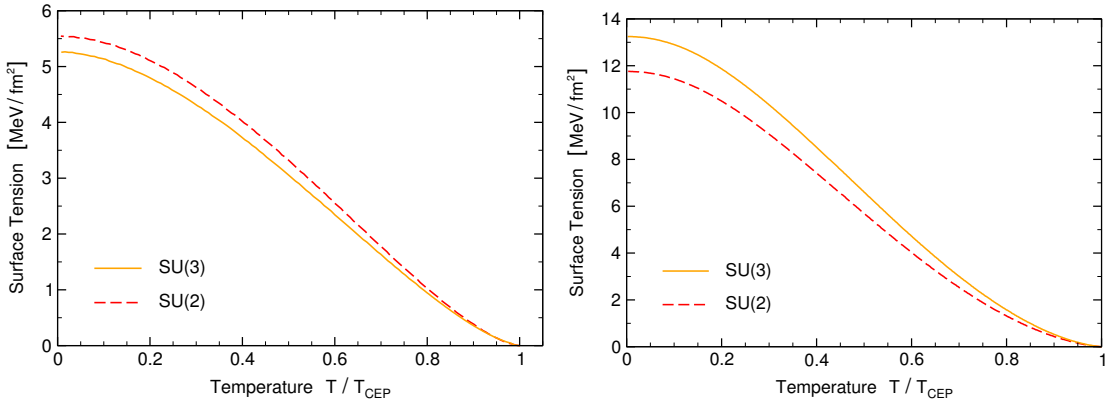

Figure 5.2.: Surface tension along the coexistence line in the two and 2+1–flavour Quark-Meson model with (left) and without (right) fermionic vacuum loop contribution.

To investigate the impact of the values of the chiral condensates, Fig. 5.1 shows the degenerate values that the chiral order parameters take at the first-order phase transition. Notice that the minima merge smoothly at the critical end point. In the Quark-Meson model without the fermionic quantum fluctuations, adding strange quarks to the system doesn't affect the light chiral condensate at the phase transition. Consequently, extending the analysis from two to 2+1 quark flavours, the jump in the strange chiral condensate at the transition adds an additional dimension to the path between the minima and the surface tension increases accordingly. This is shown on the right hand side of Fig. 5.2.

As for the temperature and density dependence of the order parameters and thermodynamics and for the phase structure, taking into account the fermionic quantum fluctuations (3.11) has also a severe impact on the result for the surface tension. Comparing the values of the chiral condensates in the minima at the phase transition one

sees that the transition becomes weaker in the light quark sector when fluctuations are considered while the strange chiral condensate is hardly affected. This is because the vacuum loop has the largest effect on the evolution of the order parameters in the transition region as could be seen in Figs. 4.11 and 4.12 and the first order transition is that that restores chiral symmetry in the light quark sector but the chiral condensate of the strange quarks takes large values at both sides of the phase transition line. The left panel of Fig. 5.1 illustrates also that the main effect of the fermionic vacuum loop to weaken the transition is to shift the chirally restored phase of the light quarks to larger values of the light chiral condensate.

Even though the vacuum loop contribution of the strange quarks does not change the values of the strange chiral condensate at the discussed transition it has the effect of further weakening the transition in the light quark sector as can be seen in Fig. 5.1. This counteracts partially the increase of the factor h in the surface tension when strange quarks are taken into account. But the upper limit on the surface tension presented in Fig. 5.2 is even smaller for the 2+1 quark flavour Quark-Meson model than in the two-flavour calculation. This observation is opposite to the build-up of the surface tension when the fermionic vacuum loop contribution is neglected. This is because the contribution of fermionic quantum fluctuations at one loop order

$$\Omega^{\mathrm{vac}}_{\mathrm{q\bar{q}}} \quad \sim \quad - \sum_{f=\mathrm{u,d,s}} m_f^4 \ln\left(m_f\right) \ , \tag{5.26}$$

decreases the thermodynamical potential and the height of the barrier at the first-order phase transition and each quark flavour leads to a further decrease that is even larger the heavier the quark species are.

In general, Fig. 5.2 shows the overestimate of the surface tension in the thin-wall approximation of the QM model along the first-order transition line. The temperature dependence of the surface tension and its value at zero temperature without fermionic quantum fluctuations is similar to the results found in Refs. [264, 265], which considered the two-flavour Quark-Meson and Nambu–Jona-Lasinio models, respectively. Including the fermionic quantum fluctuations to the model the zero-temperature value of the surface tension decreases by a factor 2-3 and the hierarchy of the two-flavour and 2+1–flavour result changes.

5.4.2. Nucleation within the Polyakov–Quark-Meson Model

With the Polyakov-loop extension of the Quark-Meson model, the system contains another order parameter, the Polyakov loop and the effective potential gets an additional contribution, the Polyakov-loop potential $\mathcal{U}$. Therefore, the Polyakov loop adds an additional contribution to the distance between the degenerate minima at the phase transition, so to the factor h in Eq. (5.22). Another effect of the Polyakov-loop extension onto this quantity can be the modification of the values of the chiral condensates at the minima compared to the Quark-Meson model.

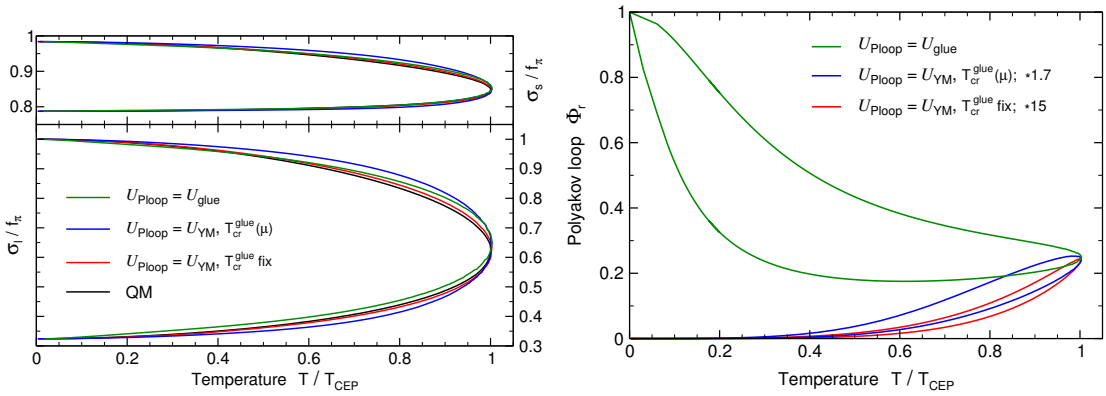

Figure 5.3.: Degenerate values of the chiral condensates σ_l and σ_s (left) and the Polyakov loop Φ_r (right) along the first-order transition line. Compared are the results of the PQM model with the Yang-Mills Polyakov-loop potential with constant and density dependent critical scale and with the unquenched Polyakov-loop potential with constant $T_\mathrm{cr}^\mathrm{glue}$. Note that the results for the Polyakov loop are scaled as given in the label so that they start out at similar values at the critical endpoint.

The left part of Fig. 5.3 shows how the values of the chiral condensates of the degenerate minima at the phase transition are altered by the coupling to the Polyakov-loop. This result shows a slight dependence if and which kind of back coupling of the quarks onto the quenched Polyakov-loop potential is considered. With the Yang-Mills Polyakov-loop potential with constant transition scale the values of the chiral condensates are hardly altered compared to the Quark-Meson model result. Lowering the critical temperature of this potential with increasing density increases the gap between the values of the chiral condensates in the degenerate minima. This is not the case when the unquenched Polyakov-loop potential with constant critical scale is considered but it shifts the values of the condensates somewhat to larger values. The latter observation can be attributed to the close link of (de)confinement and chiral transition. The values that the Polyakov loop takes in the degenerate minima at the transition are much more sensitive to the kind of Polyakov-loop potential as is shown on the right of Fig. 5.3. As discussed in detail in the discussion of Fig. 4.29, the (de)confinement and chiral transition of the light quarks remain linked in the low temperature and high density region of the phase diagram with the unquenched Polyakov-loop potential. The opposite behaviour occurs with the pure Yang-Mills Polyakov-loop potential with which the Polyakov loop takes only very small values at temperatures far below the critical scale of the Polyakov-loop potential. An intermediate behaviour for the Polyakov loop is observed with the chemical potential dependence of the transition temperature of the Polyakov-loop potential (3.52). Close to the critical endpoint the Polyakov loop takes at the phase transition values of the same order as with the unquenched Polyakov-loop potential but nevertheless the (de)confinement transition decouples from the chiral phase transition of the light quarks at even smaller temperatures.

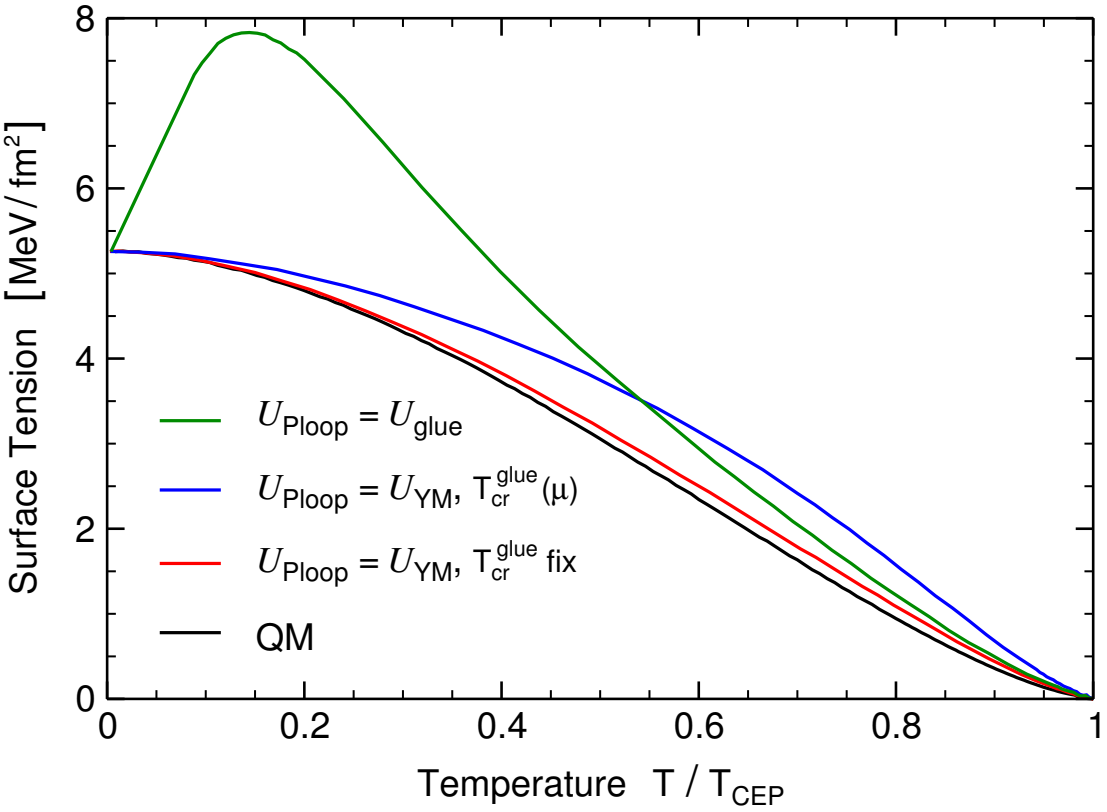

Figure 5.4.: Surface tension along the coexistence line. Compared are the results of the PQM model with the Yang-Mills Polyakov-loop potential with constant and density dependent critical scale and with the unquenched Polyakov-loop potential with constant $T_{\rm cr}^{\rm glue}$.

These results are obtained with the polynomial-logarithmic parametrisation of the Polyakov-loop potential with the best fit parameters of Sec. 4.1.4. Figure 5.4 presents the corresponding results of the surface tension.[2] The Polyakov-loop extension of the pure chiral Quark-Meson model leads to an increase of the surface tension. Nevertheless, the zero temperature limit is the same since gluon excitations are independent of the quark chemical potential in this limit, $\mathcal{U}\left(\Phi_{\rm r},\Phi_{\rm i};T=0\right)=0\;\forall\left(\Phi_{\rm r},\Phi_{\rm i}\right)$. Except than very close to the critical endpoint, $\Delta\sigma_{\rm l}$ is much lager than $\Delta\Phi_{\rm r}$, $\Delta\Phi_{\rm i}$ and $\Delta\sigma_{\rm s}$ so that the order of magnitude of the surface tension is set by the two-flavour Quark-Meson model. The maximum in the surface tension with the unquenched Polyakov-loop potential is the result of the increasing strength of the (de)confinement transition that comes along with the stronger transition in the chiral sector at larger chemical potentials and the tendency that a (de)confinement crossover transition sets on at chemical potentials slightly below the chiral first-order transition.

To compare the results with the different parametrisations of the Polyakov-loop po-

[2]The kinetic parameter κ of the Polyakov-loop in Eq. (5.22) is adjusted via the pure gauge surface tension as discussed in detail below, $\kappa\simeq 0.818\,T_0$.

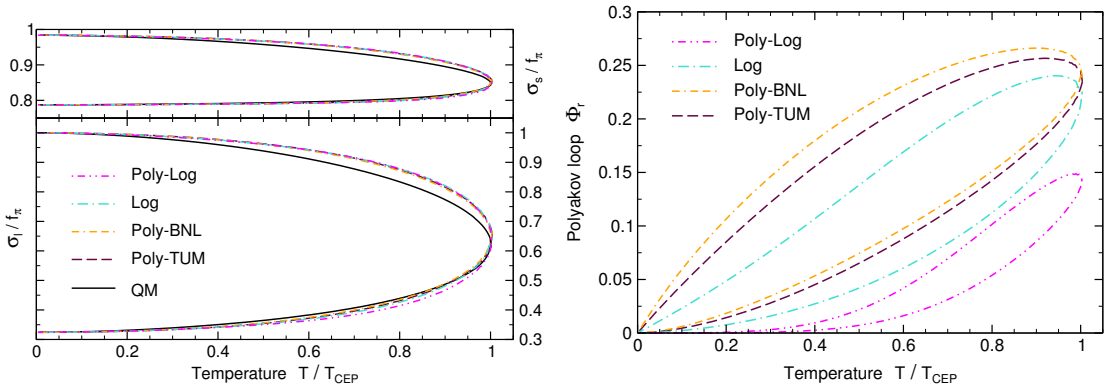

Figure 5.5.: Degenerate values of the chiral condensates σ_l and σ_s (left) and the Polyakov loop Φ_r (right) along the first-order transition line for the different parametrisations of the Polyakov-loop potential.

tential, the Yang-Mills potential with density dependent critical scale according to Eq. (3.52) is chosen. This is because with the polynomial form of the Polyakov-loop potential the Polyakov-loop is not bound at small temperatures and large densities when the potential is unquenched as is discussed in Sec. 4.2.

Figure 5.5 shows that the values of the chiral condensates at the first order phase transition are practically independent of the parametrisation the Polyakov-loop potential but the Polyakov-loop extension slightly strengthens the transition compared to the pure Quark-Meson model. Qualitatively, the values that the Polyakov loop takes in the minima along the phase transition line are similar but with quantitative differences. In general the Polyakov loop takes smaller values in both minima when the SU(3) group volume is considered.

As discussed in Sec. 5.3 to calculate the coarse-grained free energy and surface tension of the PQM model, the kinetic prefactor κ of the Polyakov-loop variables has to be determined. Dimensional arguments lead to the estimate $\kappa \simeq 0.9\,T_0$ as discussed above. Alternatively, it can be adjusted to the surface tension of pure Yang-Mills theory $\Sigma_{\rm YM} \simeq 0.02\,T_0^3$ [179, 261, 262]. For bubble nucleation with in the thin-wall approximation its dependence on the Polyakov-loop potential is

$$\Sigma_{\rm YM}\,(T) \;=\; \sqrt{2}\,\kappa \int_{\Phi_r^{(1)}}^{\Phi_r^{(2)}} {\rm d}\Phi_r\, \sqrt{2\,\mathcal{U}(\Phi_r;T)}\;. \tag{5.27}$$

The integral can be calculated for the individual parametrisations and this leads to the values for the kinetic parameter κ that are given in Table 5.1.
Figure 3.2 showed that the polynomial-logarithmic parametrisation is adjusted the best to the width of the barrier at the Yang-Mills phase transition of latest lattice calculations, $\Phi^{(2)} \simeq 0.35$ and its kinetic parameter fitted to the pure gauge surface tension is of the same order as the dimensional estimate. The logarithmic potential and the polynomial form with the parameters of Ref. [80] show a broader and higher barrier as is shown in Fig. 3.1 so that the parameter κ has to be smaller to get the same result for

Table 5.1.: Values of the kinetic parameter κ in the coarse-grained free energy and surface tension of the PQM model adjusted to the surface tension of pure Yang-Mills theory $\Sigma_{\rm YM} \simeq 0.02\,T_0^3$ [179, 261, 262] for the different parameterisations of the Polyakov-loop potential. Dimensional arguments lead to $\kappa \simeq 0.9\,T_0$.

	Poly-BNL	Poly-TUM	Log	Poly-Log
$\kappa\ [T_0]$	0.146	145	0.211	0.578

the surface tension. The height of the barrier of the potential calculated with the FRG is larger than that of the polynomial-logarithmic parametrisation as can be also seen in Fig. 3.1 so that for the true value of the kinetic parameter should hold $\kappa \lesssim 0.6\,T_0$.
A striking difference is the kinetic parameter of the polynomial potential with the parameters of Ref. [69] that is two to three orders of magnitude off scale compared to the other results. This is because the width and height of the barrier at the phase transition is significantly smaller with this potential as was discussed in the discussion of Figs. 3.1 and 3.2. Therefore, to compensate for this in the result for the surface tension in pure gauge theory, the kinetic parameter of the Polyakov loop has to be significantly larger.

But this has tremendous implications for the result of the surface tension of the PQM model as shows the inset of Fig. 5.6. When quarks and mesons are coupled to the Polyakov loop all parametrisations show similar values for the Polyakov loop at the phase transition as can be seen in Fig. 5.5. But the much larger kinetic parameter κ in Eq. (5.22) for the polynomial Polyakov-loop potential [69] that enters the surface tension (5.23) implies that $\Delta\Phi_{\rm r}$ determines the result of the surface tension and leads to a result that is off scale. The results for the surface tension along the coexistence line with the other Polyakov-loop potentials are similar to each other as is shown in Fig. 5.6.

For the results shown on the right of Fig. 5.6 the same kinetic parameter $\kappa \simeq 0.9\,T_0$ is chosen for all parametrisations of the Polyakov-loop potential. This implies that also the polynomial potential [69] leads to a result for the surface tension that is similar to that with the other Polyakov-loop potentials. On the other hand with this value for κ the result for the surface tension in Yang-Mills theory for the polynomial parameterisation [69] would be 161 times smaller than the result of lattice calculations [261, 262] and in effective matrix model calculations [179].
For the other Polyakov-loop potentials this choice of the kinetic prefactor of the Polyakov loop gives a larger weight to the jump of the Polyakov loop at the phase transition and Fig. 5.6 shows that than the results for the surface tension vary more at small temperatures where the differences in the Polyakov-loop coordinates is larger between the different parametrisations.

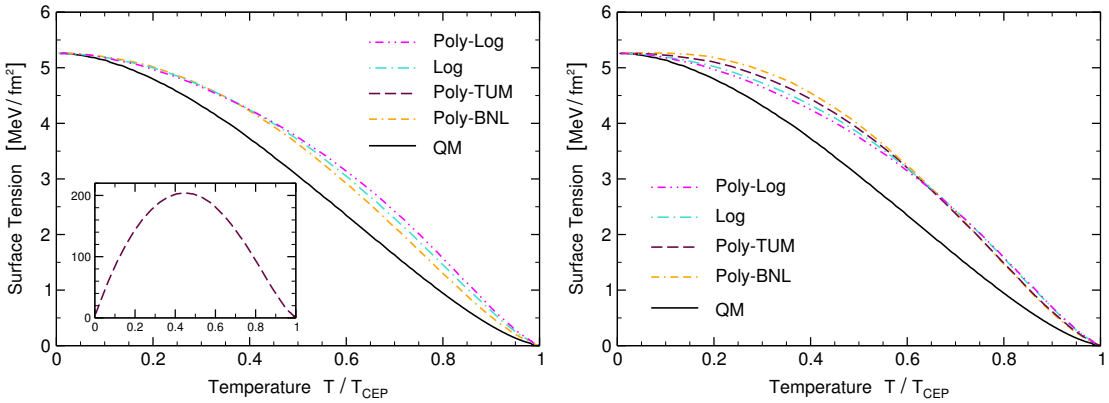

Figure 5.6.: Surface tension along the coexistence line for the different parametrisations of the Polyakov-loop potential. Compared are the results when the kinetic parameter κ is adjusted to the pure gauge surface tension (left), see Table 5.1 and with $\kappa = 0.9\,T_0$ from dimensional arguments (right).

5.4.3. Implications for proto-neutron stars, the early Universe and heavy ion collisions

The values of surface tension for the isospin symmetric $N_\mathrm{f} = 2 + 1$ PQM model found here have interesting implications for several physical scenarios. For example, compact stars can be considered as laboratories for nuclear matter at low temperatures and at such high densities that they may contain quark matter [22, 24]. Possible scenarios for the formation of quark matter in compact stars are old accreting neutron stars, proto-neutron stars after a supernova explosion or during the early postbounce evolution of core collapse supernovae [18,21]. Physical conditions and time scales in these cases imply equilibrium with respect to weak interactions and low electron fractions. Estimates from Ref. [98] show that a hadron-quark phase transition during the bounce phase of a core-collapse supernova can be dynamically suppressed if the surface tension of this phase interface is much larger than, say, 20 MeV/fm^2. The estimates from Refs. [264, 265] and the present work consistently point towards low values of the surface tension, which would be compatible with the formation of quark matter during the bounce. An observable signal would be a second peak in the neutrino signal dominated by the emission of antineutrinos and with a significant change in the energy of emitted neutrinos [18,246]. However, none of these calculations really takes into account realistic equations of state for supernova matter, which has to include not only scalar mesons, but also vector mesons, nucleons and, very importantly, leptons. A calculation of surface tension in such a complete model is a future task.

In the cosmological case, physical boundary conditions to describe the QCD phase transition in the early Universe include charge neutrality, equilibrium with respect to weak interactions and baryon and lepton asymmetries consistent with observations. Observations of the cosmic microwave background radiation and constraints from primordial nucleosynthesis require a tiny baryon asymmetry at relatively low temperatures

($T \lesssim 1\,\mathrm{MeV}$) [12]. In the standard scenario this observational constraint is extrapolated up to the scale of the QCD phase transition that is then a smooth crossover. In the scenario of little inflation [266], the Universe enters the QCD era with a very high quark density. As a result, the quark-gluon plasma (QGP) that fills the Universe cools down until it eventually crosses a first-order line of the phase diagram, becoming metastable. While the QGP is metastable, the conditions for a cosmic inflation can be met and the extra quark density becomes very diluted. Observational signals of this evolution include an enhancement of primordial density fluctuations on stellar up to galactic scales, production of galactic and extragalactic magnetic fields and a modification of the gravitational wave spectrum [13, 267]. At some point of the expansion, however, the phase transition from a QGP to hadronic matter must happen, most likely through bubble nucleation. In order to be effective, the baryon dilution required by the little inflation scenario needs to be long enough. This requires that the QGP remains metastable even for high degrees of supercooling, something that requires a very low nucleation rate and, therefore, a large value of surface tension. As we have discussed, however, the values of surface tension found with chiral models, including the study presented here, are relatively small and possibly do not allow the strong metastability required by the scenario of little inflation. However, also a large lepton asymmetry can drive the evolutionary path of the Universe towards larger quark chemical potentials [86].

In heavy ion collisions the phase boundary of hadronic and quark matter is, if at all, crossed twice. First, as formation of a quark gluon plasma in a hadronic gas and then as rehadronisation of the fireball. Complications in studying nucleation in heavy ion collisions are the short time scales and the finite size of the system. Additionally, the nucleation rate has to be considered in relation to the expansion time. These conditions can lead to the fact that the system stays in the metastable state close to the spinodal instability and that the dominant mechanism for phase conversion is the alternative scenario to homogenous nucleation, namely spinodal decomposition [94]. Nevertheless, the growth rate of fluctuations by spinodal instabilities is closely related to the surface tension [268, 269]. They can lead to observable signatures for the value of the surface tension found here [269]. Additionally, these fluctuations can be amplified by nucleation in the metastable region. The relatively small values of the surface tension found in the present study suggest a early nucleation of small quark-gluon plasma droplets at relatively modest energies like at FAIR's SIS 100 [270]. The details of rehadronisation leave their fingerprints on those observables that are sensitive to the life-time of the fireball. Weak supercooling favours the thermal freeze-out to happen in the hadronic phase with impact on particle yields and spectra [271] and a distinct hydrodynamic expansion pattern [94].

In summary, in this chapter a formalism was derived that allows to calculate an upper limit of the surface tension for bubble nucleation in the thin wall approximation in a model with more than one order parameter as e.g. in the PQM model. It was shown

that the $N_\mathrm{f} = 2 + 1$ PQM model yields results very similar to those of the two-flavour NJL and QM models, so that the influence of both the strange quark and the Polyakov loop at low temperatures is small. The conservative upper bound of $10\,\mathrm{MeV/fm^2}$ for the surface tension allows a quick hadron-quark phase conversion which implies interesting implications for several physical scenarios, be it heavy ion collisions, proto-neutron stars or the early Universe. The analysis revealed a shortcoming of a widely used Polyakov-loop potential, that of Ref. [69] that is incapable to describe Yang-Mills theory and full QCD at the same time.

6. Conclusions and Outlook

«Et dans 150 ans, on n'y pensera même plus
A ce qu'on a aimé, à ce qu'on a perdu,
... Alors souris.»
Raphaël Haroche

In this work, thermodynamical properties and the phase structure of strongly-interacting matter have been analysed in an improved framework of the Polyakov-loop–extended Quark-Meson model with $2+1$ constituent quark flavours. This effective low-energy model for strongly-interacting matter describes the generation of constituent-quark masses by spontaneous chiral symmetry breaking and is extended by an order parameter for colour confinement, the Polyakov loop, that is actually an order parameter for centre symmetry.

In the theoretical derivation of the framework, special emphasise was put on the generalisation to isospin-symmetry breaking and on the consideration that the in-medium effective potential of the model is in general not a real function of real variables. The effective potential has been rewritten in terms of real variables only, such that the real and imaginary parts of the potential could be separated. This allowed to discuss the relation between the imaginary part of the effective potential and the fermion sign problem and to compare ways how to circumvent this problem in effective models.

Furthermore, low-energy effective models include confinement only in a statistical manner via a phenomenological Polyakov-loop potential fitted to lattice data of Yang-Mills theory. Therefore, they lack the coupling of the matter sector to the gauge sector in QCD describing the confining dynamics. References [82–84] calculated non-perturbatively the Polyakov-loop potential for Yang-Mills theory and Refs. [36, 37] the QCD analogue taking into account the full back-coupling of the matter sector on the gauge degrees of freedom in a functional renormalisation-group approach, which is outlined in App. A. In Sec. 3.2.1 it was shown that the two potentials can be simply related by an appropriate rescaling of the temperature to mimic the effect of the quark backreaction on the gauge sector. This offered a simple and systematic approach to improve the Polyakov-loop potential of effective models from a pure gauge potential to the unquenched glue potential in full QCD.

Moreover, as another step beyond usual mean-field analyses not only quark quantum fluctuations at one-loop have been considered but the contribution of thermal meson

fluctuations to thermodynamics was taken into account.

The results of this improved 2+1 flavour Polyakov-loop–extended Quark-Meson model for the temperature dependence of the quark condensates, the Polyakov loop and thermodynamic observables at vanishing chemical potential have been compared to the results of latest non-perturbative lattice calculations [38–42]. This allowed to adjust the remaining parameters and to investigate the impact of the different ingredients of the presented framework and to test the robustness of the results by analysing parameter dependences.

The important improvement to achieve agreement with lattice data for the order parameters and thermodynamics proved to be the enhancement of the Polyakov-loop potential from a pure gauge potential to the unquenched glue potential in full QCD by applying Eqs. (3.58) and (3.56). Further ingredients for a reliable description of the chiral and (de)confinement phase transition with effective models showed to be the inclusion of the contribution (3.11) of fermionic quantum fluctuations and to consider the contribution of thermal meson fluctuations (3.21). The inclusion of meson and quark fluctuations beyond one loop with a renormalisation group framework changes the values of the parameters within their uncertainties for which best agreement with results of lattice calculations is achieved but would not further improve this agreement as was shown in Figs. 4.7 and 4.8.

A parameter-dependence of the results has been found, which cannot be ignored in a quantitative analysis. When varying the critical temperature of the Polyakov-loop potential and the σ-meson mass it was observed that a larger glue critical temperature has a similar effect on the results as a decrease of the mass of the σ-meson. The widely used, polynomial parametrisation of the Polyakov-loop potential with the parameter set of Ref. [69] showed to be the least suited to reproduce lattice data of Yang-Mills theory and full QCD. Only the parametrisations of the Polyakov-loop potential that respect the SU(3) group volume measure led to a satisfying agreement of all discussed observables with the results of lattice simulations. Further input to constrain the form of the potential or a potential from first-principal calculations are important to improve the reliability of results of effective models. One possibility is e.g. to work-in the height of the barrier and the difference of the potential at the minima in the metastable region of the QCD glue potential.
Another improvement on the parameter dependence of low-energy effective models would be the determination of the input parameters in the chiral sector, like the σ-meson mass from first-principle functional renormalisation-group flows.

Overall, the biggest impact on the nature of the transition at zero quark chemical potentials of the different ingredients and parameter dependences discussed, showed to have the unquenching of the Polyakov-loop potential.

With the parameters adjusted in order to reproduce lattice results at zero quark dens-

ities this setting constituted an adequate framework to investigate the phase structure of strongly-interacting matter at nonzero quark and isospin densities and to test the applicability of such a model at nonzero densities.

As well for the position of the transition line at non-vanishing densities unquenching the Polyakov-loop potential revealed the biggest effect, even if the backreaction of the quarks onto the gluons is considered as density independent. Using the quark-enhanced Polyakov-loop potential the chiral and (de)confinement transition remain linked at small temperatures and large quark chemical potentials. The biggest impact on the nature of the transition at large densities and small temperatures had nevertheless the fermionic vacuum fluctuations in the present study.

Even though considering the quark-enhanced Polyakov-loop potential proved to be decisive to find results for the phase structure at zero density that agree with results of lattice calculations, the curvature of the transition line of the Polyakov–Quark-Meson model with the unquenched Polyakov-loop potential remained larger than in non-perturbative functional and lattice calculations. The comparison of the isospin dependence of the curvature of the phase transition line with recent lattice data in Sec. 4.3 confirmed this conclusion that the model in its here presented form faces difficulties describing non-perturbative results for the transition temperature when one considers further medium-dependences besides the temperature such as non-vanishing quark chemical potential, isospin or magnetic field [243].
This entails that the medium dependence of the quark backreaction has to analysed in more detail and further ingredients to the effective model have to be considered, such as repulsive interactions by exchange of vector mesons and meson and quark fluctuations with the renormalisation-group flow.

Calculations at non-zero isospin density are performed with different pion masses in the literature. To correct for the effect of the pion mass onto the abscissae of the temperature-isospin phase diagram, the isospin chemical potential has been normalised by the individual pion masses. This removed a general offset between calculations with different pion masses and one could observe that in the range before the onset of pion condensation the curvature of the transition line is much more sensitive to the pion mass than to the number of quark flavours. A lower limit of the pseudo-critical temperature at nonzero isospin chemical potential for the case of 2+1 quark flavours and physical pion mass was presented as well as predictions on the isospin-density dependence of order parameters and thermodynamics for 2+1 quark flavours and physical quark masses

The investigation of the three dimensional temperature - isospin chemical potential - quark chemical potential phase diagram showed that it is important to consider the isospin of a system to determine the nature of the phase transition, especially at low temperatures and large quark chemical potential. This can affect a possible phase transition in the evolution of a supernova explosion.

These calculations can be extended by considering nonzero pion fields to include the possibility of pion condensation at larger isospin [11].

The careful circumvention of the fermion sign problem in a way that preserved the solutions of the equation of motion as minima of the effective potential allowed to derive a formalism to study homogeneous nucleation of bubbles in a first-order phase transition. An upper limit of the surface tension for bubble nucleation in the thin-wall approximation has been calculated. It was found that the Polyakov–Quark-Meson model with 2+1 quark flavours yields results similar to those of the two-flavour Quark-Meson model, so that the influence of both, the strange quark and the Polyakov loop at low temperatures is small. The conservative upper bound of $10\,\mathrm{MeV/fm^2}$ found for the surface tension allows a quick hadron-quark phase conversion. The implications of this result for several physical scenarios, be it heavy ion collisions, proto-neutron stars or the early Universe have been discussed.

The outcomes of these investigations motivate several applications and further extensions. They are discussed in the order of the occurrence of the related topics in the thesis.

- Further symmetries of QCD Lagrangian can be included to the presented framework such as scale symmetry which is related to the non-vanishing trace anomaly of gauge theory. This introduces a dilaton field as the order parameter of scale-symmetry breaking, representing a glueball. With this extension, one has to adjust the parameters of the dilaton potential and the Polyakov-loop potential to a combined description of the gauge sector via Polyakov loop and dilaton field. As well, the dilaton field enters to the adjustment of the parameters of the Dilaton–Quark-Meson model to vacuum properties.

- The parameter dependence of the Linear-σ potential (including a dilaton) can be constrained by determining the low-energy input parameters from first-principle flows.

- The situation of the description of the gauge sector via a phenomenological Polyakov-loop potential is very unsatisfying. One should further constrain the form of the potential by including more information of the FRG-QCD glue potential, e.g. about the separation of the minima and the hight of the barrier in the coexistence phase. Furthermore, more first-principle information on the slope of the potential at temperatures below its critical temperature, especially in the temperature range of the chiral and (de)confinement transition in the full model is required. At these temperatures, regions of the potential away from the minimum at the origin are probed but the available parametrisations are only adjusted to this single point.

- The sign problem of effective models that include gauge degrees of freedom should be solved beyond the lowest order approximation in order to search for an effective potential that possesses minima at non-vanishing quark chemical potential and that describes the expected order of the Polyakov-loop observables related to the free energy of a static quark and to that of a static antiquark, i.e. $\langle\bar{\Phi} - \Phi\rangle > 0$ at $\mu_\mathrm{q} > 0$.

- One should overcome the mixture that the Polyakov-loop potential is expressed as a function of $\langle\Phi\left[A_0\right]\rangle$ since it is fitted to lattice calculations that use this order parameter while the coupling of quarks to the gauge fields results in the use of $\Phi\left[\langle A_0\rangle\right]$ in the contribution of thermal quark fluctuations. This could be achieved by using the gauge field itself as order parameter instead of the Polyakov loop and by the application of a first-principle glue potential from functional calculations.

- At one-loop order, one should include the thermal meson fluctuations in the presented framework not only to thermodynamics but consider their contribution to the equations of motion consistently.

- In general, the presented investigations can be improved by considering the thermal and quantum fluctuations of quarks and mesons beyond one-loop order with the flow equation of the renormalisation group approach.

- In general, low-energy effective models contain only mesonic degrees of freedom to describe the confined phase. This is justifiable at vanishing and up to moderate quark chemical potential. But to capture the correct degrees of freedom in the low temperature and large quark chemical potential region of the phase diagram, baryons have to be included.

- Including the quark-backreaction on the gauge sector showed to have a big impact on the interrelation of the chiral and (de)confinement transition at non-vanishing chemical potential and these transitions remained linked even in the high quark-density and small temperature region of the phase diagram. This result is obtained ignoring any density dependence of the quark-backreaction. So, to confirm or reject this trend it is important to investigate a density dependence of the quark-backreaction on the gauge sector.

- It would be preferable to describe confinement in effective models beyond a statistical way. The too large curvature of the phase transition line along the quark chemical potential and isospin chemical potential axes found and the failure to reproduce inverse magnetic catalysis [243] indicate a need for improvement in this direction.

- Including repulsive vector interactions allows for an equation of state of quark matter that leads to a maximum mass of compact stars that is consistent with observations [10] and in Ref. [220] it was shown that these can lead to a slope of the

phase transition line at nonzero baryon chemical potential that corresponds to the data of lattice calculations. But on the other hand, it was shown in Refs. [221,222] that the results for quark number susceptibilities are in tension with lattice data for significant vector interactions. This shows that further investigations are required to include repulsive vector interactions properly to these models.

- In a continuation of the presented work, one can consider nonzero pion fields to include the possibility of pion condensation at non-vanishing isospin. This allows to investigate the phase structure and thermodynamics up to larger isospin chemical potential. In this regime latest lattice data for thermodynamics with nearly physical pion mass are available [46].

- One can compare the three-dimensional temperature - isospin chemical potential - quark chemical potential phase diagram for the scenario of vanishing net strangeness as it is the case in heavy ion collisions and for local β-equilibrium with respect to weak flavour-mixing interactions as in the case of supernovae and in the early universe which is presented here.

- The isospin dependence found for the nature of the phase transition in the high density, low temperature region of the phase diagram can be considered in the equation of state of quark stars and in the occurrence of a phase transition during the evolution of a supernova.

- One can extend the calculation of the surface tension and nucleation rate to the complete metastable region also away from the transition line, as well as over its hole extension of the first order region at nonzero isospin. This would provide further insight on nucleation of quark matter in dynamical environments.

- The presented framework is able to describe the result of the temperature dependence of the light and subtracted quark condensates of lattice calculations. But it fails to reproduce the decrease of the strange chiral condensate when increasing the temperature at zero density as seen on the lattice [42]. This calls for considering a medium dependence of the explicit chiral-symmetry breaking and axial-symmetry breaking.

- An ingredient of investigations of quarkonium suppression in a quark-gluon plasma formed in heavy-ion collisions is the expansion of the plasma itself [17, 272]. Here, the temperature and density dependence of quark and meson masses found in the presented framework can serve as an input.

- The Quark-Meson part of the model including the quark quantum-fluctuations and the thermal meson-fluctuation contribution to thermodynamics can be applied to calculate the equation of state of quark-star matter and to investigate the resulting mass-radius relation of these.

- The conditions in the early Universe can be included to the presented framework to elucidate the nature of the cosmological QCD phase transition at non-vanishing lepton number [86].

A. QCD with functional methods

Functional continuum methods are well suited for a non-perturbative study of the chiral and confining dynamics of QCD at finite temperature and density. In recent years, much progress in this direction has been made within the functional renormalisation group (FRG) approach to QCD [36,37]. Low-energy effective models emerge dynamically from the first-principle QCD-flow. The parameters of these models defined below a hadronic mass scale of $\sim 1\,\mathrm{GeV}$ can be extracted from a QCD RG-flow starting with the classical QCD action at a given high (perturbative) scale $\Lambda \gg \Lambda_{\mathrm{QCD}}$. This first-principle determination of the input parameters can be used to systematically remove the ambiguities of the low-energy effective models. For the Polyakov-loop–extended quark-meson model this is discussed in Refs. [4, 72, 76, 78]. Detailed QCD-related introductions and reviews to the functional-RG approach are e.g. Refs. [30–35, 37].

The QCD flow-equation of the effective action $\Gamma_k[\bar{A};\phi]$ in the background Landau-DeWitt gauge is [36, 37]

$$\begin{aligned}\partial_t \Gamma_k\left[\bar{A};\phi\right] &= \frac{1}{2}\,\mathrm{Tr}\left(G_k^{\mathrm{a}}\left[\bar{A};\phi\right]\partial_t R_k^{\mathrm{A}}\right) - \mathrm{Tr}\left(G_k^{\mathrm{c}}\left[\bar{A};\phi\right]\partial_t R_k^{\mathrm{c}}\right) - \\ &\quad - \mathrm{Tr}\left(G_k^{\mathrm{q}}\left[\bar{A};\phi\right]\partial_t R_k^{\mathrm{q}}\right) + \frac{1}{2}\mathrm{Tr}\left(G_k^{\mathrm{H}}\left[\bar{A};\phi\right]\partial_t R_k^{\mathrm{H}}\right)\ . \end{aligned} \tag{A.1}$$

Its diagrammatic representation is shown in Fig. A.1. The full field content of QCD of constituent quarks $(q, \bar{q})$, the corresponding hadrons (H) and the ghost $(c, \bar{c})$ and gluon $(A = \bar{A} + a)$ fields with a constant background $\bar{A}$ and a fluctuating part a is collected in $\phi = (a,\ c,\ \bar{c},\ q,\ \bar{q},\ H)$. The traces in Eq. (A.1) involve d-dimensional integrations over momenta or coordinates, respectively as well as summations over internal indices such

Figure A.1.: Partially bosonised version of the FRG flow-quation for QCD. The loops denote the gluon, ghost, quark and hadronic contributions, respectively. Lines with filled circles represent fully dressed field-dependent propagators $G_k\left[\bar{A};\phi\right]$ and crossed circles denote the regulator insertion $\partial_t R_k$. $t = \log k/\Lambda$ with the infrared momentum scale k and the references scale Λ. From Ref. [2].

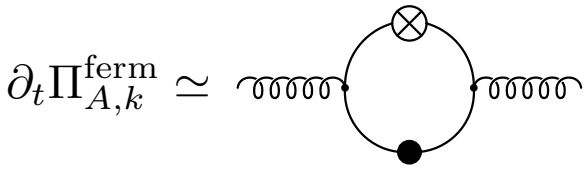

Figure A.2.: Quark polarisation contribution to the gluon propagator representing a contribution to the matter backcoupling. From Ref. [2].

as flavour, colour and Dirac indices. To the flow-equation enter the full field-dependent propagators

$$G_k^{\phi}\left[\bar{A};\phi\right](p,q) = \frac{1}{\Gamma_k^{(2)}\left[\bar{A};\phi\right] + R_k^{\phi}} \qquad \text{with} \qquad \Gamma_k^{(2)}\left[\bar{A};\phi\right] = \frac{\delta^2\,\Gamma_k}{\delta\phi(p)\,\delta\phi(q)}\,, \tag{A.2}$$

and the regulator functions R_k^{ϕ}. The momentum dependence of these is such that they act as a mass for small momenta and vanish for large momenta. Overall, they act as momentum-dependent additional mass-terms. The loops depicted in Fig. A.1 are intrinsically coupled to each other. In particular, there are contributions from the matter sector to the diagrams for the gluon propagator as the quark part of the gluonic vacuum polarisation as illustrated in Fig. A.2.

For temperatures below the chiral and (de)confinement phase transitions the glue dynamics decouples from the matter dynamics. In the Landau gauge this physical decoupling is realised simply by a mass gap in the gluon propagator, that is $k^2 G_k^{\mathrm{a}} \to 0$ for small momenta, see e.g. Ref. [273] and references therein. As the ghost-matter coupling is mediated by the gluon this decoupling extends to the full ghost-gluon dynamics and one is left with the flow equation of the dynamical matter-sector,

$$\partial_t\,\Gamma_k^{\mathrm{matter}}\left[\bar{A};\phi\right] \;=\; -\,\mathrm{Tr}\left(G_k^{\mathrm{q}}\left[\bar{A};\phi\right]\partial_t R_k^{\mathrm{q}}\right) + \frac{1}{2}\mathrm{Tr}\left(G_k^{\mathrm{H}}\left[\bar{A};\phi\right]\partial_t R_k^{\mathrm{H}}\right)\,, \tag{A.3}$$

which is depicted in Fig. A.3. Even though the glue-dynamics decouples for low temperatures, the gluonic background $\bar{A} = \langle A \rangle$ does play an important role. In the confining phase it screens the propagation of the quarks which confines them even statistically as discussed in Sec. 3.1, leaving aside the confining potential. The expectation value $\langle A \rangle$ is given by the solution of the QCD equations of motion which also requires the first part

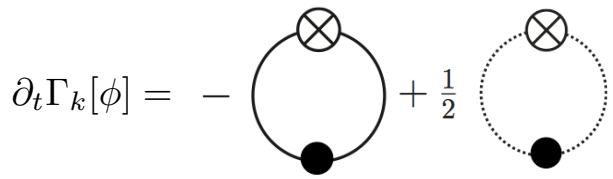

Figure A.3.: FRG flow for the matter sector of QCD. The loops denote the quark and hadronic contributions, respectively. From Ref. [2].

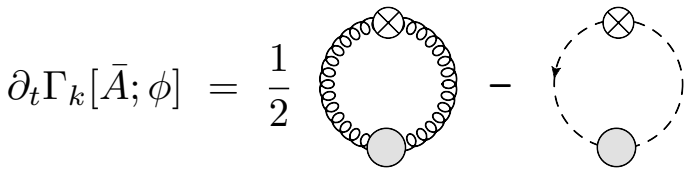

Figure A.4.: Functional flow for the gauge part of the effective action. From Ref. [2].

of the QCD flow (A.1),

$$\partial_t \Gamma_k^{\text{glue}}\left[\bar{A};\phi\right] \;=\; \frac{1}{2}\,\text{Tr}\left(G_k^{\text{a}}\left[\bar{A};\phi\right]\partial_t R_k^{\text{A}}\right) - \text{Tr}\left(G_k^{\text{c}}\left[\bar{A};\phi\right]\partial_t R_k^{\text{c}}\right)\,, \tag{A.4}$$

which is depicted in Fig. A.4. The fluctuation ϕ is evaluated at the equation of motion, $\phi = \bar{\phi}$. Therefore, the gluonic fluctuation background is vanishing, $\bar{a} = 0$ whereas the mesonic background leads to the running quark masses (2.53) that enter to the quark vacuum polarisation shown in Fig. A.2. The flow equation for the ghost-gluon sector can then be written as that of a glue potential, encoding the ghost-gluon dynamics in the presence of matter fields,

$$\partial_t \Gamma_k^{\text{glue}}\left[\bar{A};\phi\right] \;=\; \beta V \partial_t \mathcal{U}_{\text{glue}}\left[\langle A\rangle\right] \tag{A.5}$$

where V is the spatial volume and $\beta = 1/T$ the inverse temperature. Structurally, the flow of the gluonic background in QCD (A.4) resembles the pure Yang-Mills flow-equation,

$$\partial_t \Gamma_k^{\text{YM}}\left[\bar{A}; a=0, c=0, \bar{c}=0\right] \;=\; \beta V \partial_t \mathcal{U}_{\text{YM}}\left[\langle A\rangle\right] \tag{A.6}$$

which also has the pictorial form of Fig. A.4. The ghost and gluon propagators in Eq. (A.5), however, are those of QCD. In particular, the flow of the gluon propagator receives contributions from matter loops, e.g. the quark contribution to the vacuum polarisation in Fig. A.2. Based on this functional-RG approach Refs. [82–84] calculated the non-perturbative Polyakov-loop potential for SU(N_{c}) Yang-Mills theories and Refs. [36, 37] the QCD analogue taking into account the full backcoupling of the matter sector on the propagators of the gauge degrees of freedom via dynamical quark-gluon interactions [184–186].

As explained in Sec. 3.2, in low-energy effective models confinement is only included in a statistical manner via a phenomenological Polyakov-loop potential. This potential is fixed to the temperature dependence of the Polyakov loop and the thermodynamics of pure Yang-Mills theory as obtained in lattice simulations. Hence, it approximates the Polyakov-loop potential generated by pure gluodynamics, $\mathcal{U}_{\text{YM}}$ in Eq. (A.6). The coupling of the matter sector to the gauge sector is lost in such an approach which lacks the glue-matter dynamics to both the chiral as well as the (de)confinement physics. This entails that the glue potential of full QCD, $\mathcal{U}_{\text{glue}}$ in Eq. (A.5), encoding the gauge dynamics in the presence of matter fields, is replaced by a phenomenological Polyakov-loop potential $\mathcal{U}$.

A first step towards the inclusion of the backreaction of quarks on the gauge sector in low-energy effective models is to estimate the change of the transition temperature of the Polyakov-loop potential when going from Yang-Mills theory to QCD. This has been done in Ref. [72] by a perturbative estimate of the change of Λ_{QCD} when going from Yang-Mills theory to QCD based upon Refs. [185, 207].
To bring low-energy effective model studies even closer to (full) QCD, their Polyakov-loop potential $\mathcal{U}$ has to be replaced by the QCD glue potential $\mathcal{U}_{\mathrm{glue}}$, i.e. by the contribution stemming from the gauge degrees of freedom in the presence of dynamical quarks. It is therefore beneficial to amend these model calculations by utilising the available information on the QCD glue potential $\mathcal{U}_{\mathrm{glue}}$ and its Yang-Mills analogue $\mathcal{U}_{\mathrm{YM}}$. One can extract the relation of both potentials as discussed in Sec. 3.2.1 and apply it then to improve the Polyakov-loop potential $\mathcal{U}$ entering low-energy effective models, as shown in this thesis.

In the FRG-approach quantum and thermal fluctuations are self-consistently taken into account and hadronic states can be included successively within dynamical hadronisation [32, 184, 274, 275]. This technique describes the following physical mechanism. When lowering the RG-scale in the QCD flow-Eq. (A.1), strongly-bound quark correlations, i.e. quark-antiquark (mesons), diquark, and three-quark (baryons) correlations, will be dynamically created by the flow. These correlations can be parameterised in terms of mesonic, diquark and hadronic operators respectively, whereupon the diquark operators do not describe asymptotic states but only intermediate correlations. The respective coupling of the hadronic operators is dynamically enhanced by the quark-gluon fluctuations at higher scales, while it takes over the dynamics from the quark-gluon sector at lower scales, hence the name dynamical hadronisation. This fluctuation-triggered dynamical hadron creation within the QCD-flow avoids any double-counting problem since the respective couplings are created from the QCD input. The results of Refs. [36, 37] used in Sec. 3.2.1 were computed within the two-flavour approximation of QCD which takes into account the lowest mesonic multiplet, the σ-meson and the pions $\vec{\pi}$ in this way. Motivation for considering only these is that close to the phase boundary between the quark-gluon plasma phase and the hadronic phase and at not too large chemical potential mesonic degrees of freedom, and in particular the pion and σ-fluctuations, become important while baryonic fluctuations are considered as subleading at vanishing density.

The systematic embedding of low-energy effective models in first-principle FRG-QCD is the following. The background gluon-field $\bar{A}$ as well as the ghost- and gluon-fluctuation fields, $c, \bar{c}$ and a are simply spectators in Eq. (A.3). If setting these spectator fields to zero the flow equation (A.3) reduces to that of generic low-energy models of QCD. The respective models are then singled out by specifying the hadronic content of the flow.
In the Quark-Meson model truncation one considers that close to the phase boundary

between the quark-gluon plasma phase and the hadronic phase and at not too large chemical potential mesonic degrees of freedom, in particular the pion and σ-fluctuations, are important. This leads to a quark-meson flow-Eq. (A.3) with a constant temporal gauge-field background which defines the Polyakov-loop–extended Quark-Meson model [72, 76], including quantum and thermal matter fluctuations.
NJL-type truncations of the matter sector miss any hadronic loops and the full matter dynamics is described by the quark loop. This is a description of the low-energy matter dynamics of QCD purely in terms of quark correlation functions. Hence, it can only capture the correct QCD dynamics if the hadronic spectrum is taken into account via resonances in the scattering amplitudes of quarks.

In Eq. (A.3), the presence of a quark loop should not be confused with the presence of quarks as observable (asymptotic) states. The presence of this loop only states that quark loops are still present 'internally' and required to give a microscopic description of the interaction of the hadronic degrees of freedom. In the same spirit, gluon loops also play a role in the low-energy sector even though they do not represent observable (asymptotic) states in this regime as well. However, gluon loops govern the dynamics of the confinement order-parameter potential which in turn determines the background gluon-field entering Eq. (A.3) as discussed above.

B. Further Calculations and Results

Entropy and Energy density of Yang-Mills theory

In Polyakov-loop–extended constituent-quark models a phenomenological Polyakov-loop potential is used that is fixed to the temperature dependence of the Polyakov loop and the thermodynamics of pure Yang-Mills theory as obtained in lattice simulations. There are several parametrisations of the Polyakov-loop potential available in the literature with different parameter sets as presented in Sec. 3.2. The main text in Sec. 3.2 contains the comparison of the results of the different parametrisations with latest lattice calculations for the Polyakov loop, the pressure and the trace anomaly in Figs. 3.2, 3.3 and 3.4, respectively.
Other quantities to which the parameters of the potentials are adjusted to are the entropy density and energy density. The results for these are compared in Figs B.1 and B.2. The conclusions one can conclude from these are similar as these of Figs. 3.2, 3.3 and 3.4. The evolution of the centre symmetry breaking minimum in the polynomial potential of Ref. [69] lags behind the lattice data and the other potentials which scatter close around the lattice data and those potentials that include the Haar measure are the closest to the data points. The polynomial parametrisation of Ref. [80] fails to describe the high temperature convergence of the entropy density and energy density. Instead of converging towards the Stefan-Boltzmann limit it reaches a maximum and slightly decreases from there on. None of the parametrisations reproduces the discontinuity at the transition temperature exactly. The polynomial potential of Ref. [69] clearly underestimates it, while the other parametrisation slightly overshoot it but give the correct order of magnitude, especially the polynomial-logarithmic potential.

Structure constants of SU(3)

To the potential of the $N_\mathrm{f} = 3$ Linear-σ model in its general form (2.44) enter the structure constants of SU(3), d_{abc} and f_{abc}. They are given by

$$d_{ab0} = \sqrt{2/3}\,\delta_{ab}\,, \tag{B.1a}$$

$$d_{118} = d_{228} = d_{338} = -d_{888} = 1/\sqrt{3}\,, \tag{B.1b}$$

$$d_{448} = d_{558} = d_{668} = d_{778} = -1/(2\sqrt{3})\,, \tag{B.1c}$$

$$d_{146} = d_{157} = -d_{247} = d_{256} = d_{344} = d_{355} = -d_{366} = -d_{377} = 1/2\,, \tag{B.1d}$$

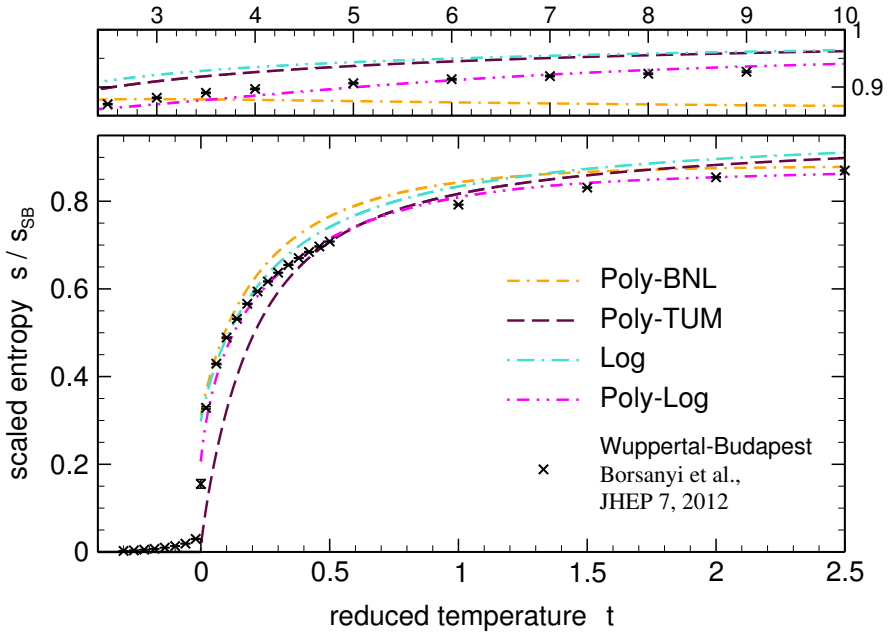

Figure B.1.: Scaled entropy density as a function of the reduced temperature in the pure-gauge sector for the different parametrisations of the Polyakov-loop potential, compared to corresponding lattice results taken from Ref. [203].

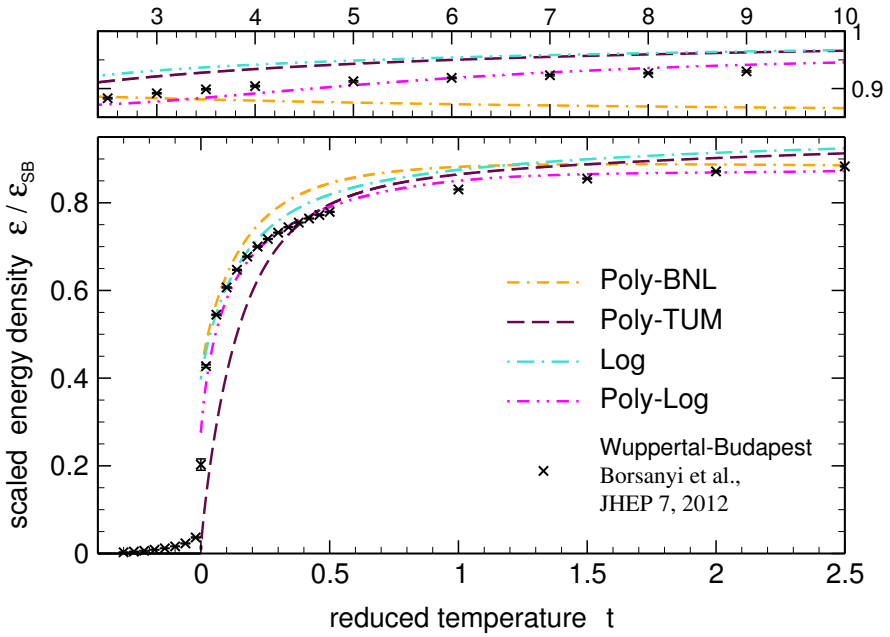

Figure B.2.: Scaled energy density as a function of the reduced temperature in the pure-gauge sector for the different parametrisations of the Polyakov-loop potential, compared to corresponding lattice results taken from Ref. [203].

and

$$
\begin{aligned}
f_{ab0} &= 0 \,, && \text{(B.2a)}\\
f_{123} &= 1 \,, && \text{(B.2b)}\\
f_{147} = -f_{156} = f_{246} = f_{257} = f_{345} = f_{367} &= 1/2 \,, && \text{(B.2c)}\\
f_{458} = f_{678} &= \sqrt{3}/2 \,, && \text{(B.2d)}
\end{aligned}
$$

These are symmetric or antisymmetric, respectively

$$
\{T_a, T_b\} = d_{abc} T_c \,, \qquad [T_a, T_b] = \mathrm{i} f_{abc} T_c \,. \tag{B.3}
$$

$T_a = \lambda_a/2$ are the generators of the group.

Derivatives of the Linear-σ potential $U(\sigma)$

The expectation value of a field is given by the absolute minimum of the effective potential. So the first derivative of the potential with respect to the field has to vanish. The derivatives of the potential of the Linear-σ model in its form in Eq. (2.50) are

$$
\begin{aligned}
\frac{\partial U}{\partial \bar{\sigma}_0} &= m^2 \bar{\sigma}_0 + \left(\lambda_1 + \frac{\lambda_2}{3}\right) \bar{\sigma}_0^3 + (\lambda_1 + \lambda_2)\left(\bar{\sigma}_3^2 + \bar{\sigma}_8^2\right) \bar{\sigma}_0 + \\
&\quad + \frac{\lambda_2}{\sqrt{2}} \left(\bar{\sigma}_3^2 \bar{\sigma}_8 - \frac{\bar{\sigma}_8^3}{3}\right) - \frac{c}{\sqrt{6}} \left(\bar{\sigma}_0^2 - \frac{\bar{\sigma}_3^2 + \bar{\sigma}_8^2}{2}\right) - h_0 \,, && \text{(B.4a)}\\
\frac{\partial U}{\partial \bar{\sigma}_3} &= m^2 \bar{\sigma}_3 + \left(\lambda_1 + \frac{\lambda_2}{2}\right) \bar{\sigma}_3^3 + \\
&\quad + \left[(\lambda_1 + \lambda_2)\, \bar{\sigma}_0^2 + \left(\lambda_1 + \frac{\lambda_2}{2}\right) \bar{\sigma}_8^2 + \sqrt{2} \lambda_2 \bar{\sigma}_0 \bar{\sigma}_8\right] \bar{\sigma}_3 + \\
&\quad + \frac{c}{\sqrt{3}} \left(\frac{\bar{\sigma}_0}{\sqrt{2}} - \bar{\sigma}_8\right) \bar{\sigma}_3 - h_3 \,, && \text{(B.4b)}\\
\frac{\partial U}{\partial \bar{\sigma}_8} &= m^2 \bar{\sigma}_8 + \left(\lambda_1 + \frac{\lambda_2}{2}\right) \bar{\sigma}_8^3 - \frac{\lambda_2}{\sqrt{2}} \bar{\sigma}_0 \bar{\sigma}_8^2 + \\
&\quad + \left[(\lambda_1 + \lambda_2)\, \bar{\sigma}_0^2 + \left(\lambda_1 + \frac{\lambda_2}{2}\right) \sigma_3^2\right] \bar{\sigma}_8 + \frac{\lambda_2}{\sqrt{2}} \bar{\sigma}_0 \bar{\sigma}_3^2 + \\
&\quad + \frac{c}{2\sqrt{3}} \left(\sqrt{2} \bar{\sigma}_0 \bar{\sigma}_8 - \bar{\sigma}_3^2 + \bar{\sigma}_8^2\right) - h_8 \,. && \text{(B.4c)}
\end{aligned}
$$

The Linear-σ potential can be given either in the basis of the condensates $\bar{\sigma}_0$, $\bar{\sigma}_3$ and $\bar{\sigma}_8$ as in Eq. (2.50) with the derivatives in Eqs. (B.4) or in the basis of the quark-flavour

condensates $\bar{\sigma}_\mathrm{u}$, $\bar{\sigma}_\mathrm{d}$ and $\bar{\sigma}_\mathrm{s}$ as in Eq. (2.56). Then the corresponding derivatives are

$$\begin{aligned}
\frac{\partial U}{\partial \bar{\sigma}_\mathrm{u}} &= \frac{m^2}{2}\bar{\sigma}_\mathrm{u} + \frac{\lambda_1}{4}\left[\bar{\sigma}_\mathrm{u}\left(\bar{\sigma}_\mathrm{u}^2 + \bar{\sigma}_\mathrm{d}^2\right) + 2\bar{\sigma}_\mathrm{u}\bar{\sigma}_\mathrm{s}^2\right] + \frac{\lambda_2}{4}\bar{\sigma}_\mathrm{u}^3 - \\
&\quad - \frac{c}{2\sqrt{2}}\bar{\sigma}_\mathrm{d}\bar{\sigma}_\mathrm{s} - \frac{h_\mathrm{ud}}{2}\,, \qquad \text{(B.5a)} \\
\frac{\partial U}{\partial \bar{\sigma}_\mathrm{d}} &= \frac{m^2}{2}\bar{\sigma}_\mathrm{d} + \frac{\lambda_1}{4}\left[\bar{\sigma}_\mathrm{d}\left(\bar{\sigma}_\mathrm{u}^2 + \bar{\sigma}_\mathrm{d}^2\right) + 2\bar{\sigma}_\mathrm{d}\bar{\sigma}_\mathrm{s}^2\right] + \frac{\lambda_2}{4}\bar{\sigma}_\mathrm{d}^3 - \\
&\quad - \frac{c}{2\sqrt{2}}\bar{\sigma}_\mathrm{u}\bar{\sigma}_\mathrm{s} - \frac{h_\mathrm{ud}}{2}\,, \qquad \text{(B.5b)} \\
\frac{\partial U}{\partial \bar{\sigma}_\mathrm{s}} &= m^2\bar{\sigma}_\mathrm{s} + \lambda_1\left[4\bar{\sigma}_\mathrm{s}^3 + 2\left(\bar{\sigma}_\mathrm{u}^2 + \bar{\sigma}_\mathrm{d}^2\right)\bar{\sigma}_\mathrm{s}\right] + \lambda_2\bar{\sigma}_\mathrm{s}^3 - \\
&\quad - \frac{c}{2\sqrt{2}}\bar{\sigma}_\mathrm{u}\bar{\sigma}_\mathrm{d} - h_\mathrm{s}\,, \qquad \text{(B.5c)}
\end{aligned}$$

and

$$\begin{aligned}
\frac{\partial^2 U}{\partial \bar{\sigma}_\mathrm{u}^2} &= \frac{m^2}{2} + \frac{\lambda_1}{4}\left(3\bar{\sigma}_\mathrm{u}^2 + \bar{\sigma}_\mathrm{d}^2 + 2\bar{\sigma}_\mathrm{s}^2\right) + \frac{3}{4}\lambda_2\bar{\sigma}_\mathrm{u}^2\,, \qquad \text{(B.6a)} \\
\frac{\partial^2 U}{\partial \bar{\sigma}_\mathrm{d}^2} &= \frac{m^2}{2} + \frac{\lambda_1}{4}\left(\bar{\sigma}_\mathrm{u}^2 + 3\bar{\sigma}_\mathrm{d}^2 + 2\bar{\sigma}_\mathrm{s}^2\right) + \frac{3}{4}\lambda_2\bar{\sigma}_\mathrm{d}^2\,, \qquad \text{(B.6b)} \\
\frac{\partial^2 U}{\partial \bar{\sigma}_\mathrm{s}^2} &= m^2 + 2\lambda_1\left[6\bar{\sigma}_\mathrm{s}^2 + \left(\bar{\sigma}_\mathrm{u}^2 + \bar{\sigma}_\mathrm{d}^2\right)\right] + 3\lambda_2\bar{\sigma}_\mathrm{s}^2\,, \qquad \text{(B.6c)} \\
\frac{\partial^2 U}{\partial \bar{\sigma}_\mathrm{d}\partial \bar{\sigma}_\mathrm{u}} &= \frac{\lambda_1}{2}\bar{\sigma}_\mathrm{u}\bar{\sigma}_\mathrm{d} - \frac{c}{2\sqrt{2}}\bar{\sigma}_\mathrm{s} = \frac{\partial^2 U}{\partial \bar{\sigma}_\mathrm{u}\partial \bar{\sigma}_\mathrm{d}}\,, \qquad \text{(B.6d)} \\
\frac{\partial^2 U}{\partial \bar{\sigma}_\mathrm{s}\partial \bar{\sigma}_\mathrm{u}} &= \frac{\lambda_1}{2}\bar{\sigma}_\mathrm{u}\bar{\sigma}_\mathrm{s} - \frac{c}{2\sqrt{2}}\bar{\sigma}_\mathrm{d} = \frac{\partial^2 U}{\partial \bar{\sigma}_\mathrm{u}\partial \bar{\sigma}_\mathrm{s}}\,, \qquad \text{(B.6e)} \\
\frac{\partial^2 U}{\partial \bar{\sigma}_\mathrm{s}\partial \bar{\sigma}_\mathrm{d}} &= \frac{\lambda_1}{2}\bar{\sigma}_\mathrm{d}\bar{\sigma}_\mathrm{s} - \frac{c}{2\sqrt{2}}\bar{\sigma}_\mathrm{u} = \frac{\partial^2 U}{\partial \bar{\sigma}_\mathrm{d}\partial \bar{\sigma}_\mathrm{s}}\,. \qquad \text{(B.6f)}
\end{aligned}$$

To see the effects introduced by isospin breaking it is convenient to separate the effect of the isospin-breaking condensate $\sigma_3 = (\sigma_\mathrm{u} - \sigma_\mathrm{d})/2$ from that of the average light quark condensate $\sigma_\mathrm{l} = (\sigma_\mathrm{u} + \sigma_\mathrm{d})/2$. The derivatives of this notation of the potential of the Linear-σ model (2.57) are

$$\begin{aligned}
\frac{\partial U}{\partial \bar{\sigma}_\mathrm{l}} &= m^2\,\bar{\sigma}_\mathrm{l} + \lambda_1\,\bar{\sigma}_\mathrm{l}\left(\bar{\sigma}_\mathrm{s}^2 + \bar{\sigma}_3^2\right) + \frac{2\lambda_1 + \lambda_2}{2}\bar{\sigma}_\mathrm{l}^3 + \frac{3}{2}\lambda_2\,\bar{\sigma}_\mathrm{l}\bar{\sigma}_3^2 - \\
&\quad - \frac{c}{\sqrt{2}}\,\bar{\sigma}_\mathrm{l}\bar{\sigma}_\mathrm{s} - h_\mathrm{l}\,, \qquad \text{(B.7a)} \\
\frac{\partial U}{\partial \bar{\sigma}_\mathrm{s}} &= m^2\,\bar{\sigma}_\mathrm{s} + \lambda_1\,\bar{\sigma}_\mathrm{s}\left(\bar{\sigma}_\mathrm{l}^2 + \bar{\sigma}_3^2\right) + (\lambda_1 + \lambda_2)\,\bar{\sigma}_\mathrm{s}^3 - \\
&\quad - \frac{c}{2\sqrt{2}}\,\left(\bar{\sigma}_\mathrm{l}^2 - \bar{\sigma}_3^2\right) - h_\mathrm{s}\,, \qquad \text{(B.7b)} \\
\frac{\partial U}{\partial \bar{\sigma}_3} &= m^2\,\bar{\sigma}_3 + \lambda_1\left(\bar{\sigma}_\mathrm{l}^2 + \bar{\sigma}_\mathrm{s}^2\right)\bar{\sigma}_3 + \frac{3}{2}\lambda_2\,\bar{\sigma}_\mathrm{l}^2\bar{\sigma}_3 + \frac{2\lambda_1 + \lambda_2}{2}\,\bar{\sigma}_3^3 + \\
&\quad + \frac{c}{\sqrt{2}}\,\bar{\sigma}_3\bar{\sigma}_\mathrm{s} - h_3\,. \qquad \text{(B.7c)}
\end{aligned}$$

Pseudoscalar decay constants

Two of the constants to which the parameters of mesonic potential of the PQM model are adjusted, are the pion decay constant f_π and kaon decay constant f_K. In general, the decay constants f_a corresponding to the pseudoscalar fields π_a follow from the partially conserved axial-vector current [60]

$$f_a = d_{aab}\bar{\sigma}_b \ . \tag{B.8}$$

Explicitly, these are

$$f_0 = d_{00b}\bar{\sigma}_b = \sqrt{\frac{2}{3}}\bar{\sigma}_0 \ , \tag{B.9a}$$

$$f_1 = f_2 = f_3 = d_{11b}\bar{\sigma}_b = \sqrt{\frac{2}{3}}\bar{\sigma}_0 + \frac{1}{\sqrt{3}}\bar{\sigma}_8 \ , \tag{B.9b}$$

$$f_4 = f_5 = d_{44b}\bar{\sigma}_b = \sqrt{\frac{2}{3}}\bar{\sigma}_0 + \frac{1}{2}\bar{\sigma}_3 - \frac{1}{2\sqrt{3}}\bar{\sigma}_8 \ , \tag{B.9c}$$

$$f_6 = f_7 = d_{66b}\bar{\sigma}_b = \sqrt{\frac{2}{3}}\bar{\sigma}_0 - \frac{1}{2}\bar{\sigma}_3 - \frac{1}{2\sqrt{3}}\bar{\sigma}_8 \ , \tag{B.9d}$$

$$f_8 = d_{88b}\bar{\sigma}_b = \sqrt{\frac{2}{3}}\bar{\sigma}_0 - \frac{1}{\sqrt{3}}\bar{\sigma}_8 \ . \tag{B.9e}$$

Derivatives of the quark masses with respect to the meson fields

To the equations of motion and meson masses enter the derivatives of the squared quark masses (2.52) with respect to the meson fields. The first order derivatives are summarised in the table below. They are given in the basis of the average light, strange and isospin-symmetry breaking condensate to illustrate the effect of isospin-symmetry breaking. All entries have the unit g^2.

	m_u^2	m_d^2	m_s^2
$\partial/\partial\sigma_0$	$(\bar{\sigma}_\mathrm{l} + \bar{\sigma}_3)/\sqrt{6}$	$(\bar{\sigma}_\mathrm{l} - \bar{\sigma}_3)/\sqrt{6}$	$\bar{\sigma}_\mathrm{s}/\sqrt{3}$
$\partial/\partial\sigma_3$	$(\bar{\sigma}_\mathrm{l} + \bar{\sigma}_3)/2$	$-(\bar{\sigma}_\mathrm{l} - \bar{\sigma}_3)/2$	0
$\partial/\partial\sigma_8$	$(\bar{\sigma}_\mathrm{l} + \bar{\sigma}_3)\,/\,(2\sqrt{3})$	$(\bar{\sigma}_\mathrm{l} - \bar{\sigma}_3)\,/\,(2\sqrt{3})$	$-2\bar{\sigma}_\mathrm{s}/\sqrt{3}$

The meson masses depend as well on the second order derivatives of the quark masses on the (pseudo-)scalar fields. These are given below and are as well in units of g^2.

	m_u^2	m_d^2	m_s^2
$\partial^2/\partial\sigma_0^2$	$1/3$	$1/3$	$1/3$
$\partial^2/\left(\partial\sigma_0\partial\sigma_3\right)$	$1/\sqrt{6}$	$-1/\sqrt{6}$	0
$\partial^2/\left(\partial\sigma_0\partial\sigma_8\right)$	$1/\left(3\sqrt{2}\right)$	$1/\left(3\sqrt{2}\right)$	$-\sqrt{2}/3$
$\partial^2/\partial\sigma_3^2$	$1/2$	$1/2$	0
$\partial^2/\left(\partial\sigma_3\partial\sigma_8\right)$	$1/\left(2\sqrt{3}\right)$	$-1/\left(2\sqrt{3}\right)$	0
$\partial^2/\partial\sigma_8^2$	$1/6$	$1/6$	$2/3$

Contributions of the mesonic potential $U\left(\bar{\sigma}\right)$ to the meson masses

The couplings and the axial-vector symmetry breaking coefficient of the mesonic potential are adjusted to meson masses in the vacuum. Equations (2.42) and (2.43) give the contributions of the mesonic potential to the scalar and pseudoscalar meson masses. For the vacuum expectation value $\bar{\phi} = \left(\lambda_0\bar{\sigma}_0 + \lambda_3\bar{\sigma}_3 + \lambda_8\bar{\sigma}_8\right)/2$ the contributions to the scalar-meson masses are

$$M_{s,00}^2 = m^2 - \sqrt{\frac{2}{3}}c\bar{\sigma}_0 + \left(3\lambda_1+\lambda_2\right)\bar{\sigma}_0^2 + \left(\lambda_1+\lambda_2\right)\left(\bar{\sigma}_3^2+\bar{\sigma}_8^2\right) \ , \tag{B.10a}$$

$$M_{s,03}^2 = \left[\frac{c}{\sqrt{6}} + 2\left(\lambda_1+\lambda_2\right)\bar{\sigma}_0 + \sqrt{2}\lambda_2\bar{\sigma}_8\right]\bar{\sigma}_3 \ , \tag{B.10b}$$

$$M_{s,08}^2 = \left[\frac{c}{\sqrt{6}} + 2\left(\lambda_1+\lambda_2\right)\bar{\sigma}_0 - \frac{\lambda_2}{\sqrt{2}}\bar{\sigma}_8\right]\bar{\sigma}_8 + \frac{\lambda_2}{\sqrt{2}}\bar{\sigma}_3^2 \ , \tag{B.10c}$$

$$\begin{aligned} M_{s,11}^2 = M_{s,22}^2 &= m^2 + \frac{c}{\sqrt{6}}\bar{\sigma}_0 - \frac{c}{\sqrt{3}}\bar{\sigma}_8 + \left(\lambda_1+\lambda_2\right)\bar{\sigma}_0^2 + \sqrt{2}\lambda_2\bar{\sigma}_0\bar{\sigma}_8 + \\ &\quad + \left(\lambda_1+\frac{\lambda_2}{2}\right)\left(\bar{\sigma}_3^2+\bar{\sigma}_8^2\right) \ , \end{aligned} \tag{B.10d}$$

$$\begin{aligned} M_{s,33}^2 &= m^2 + \frac{c}{\sqrt{6}}\bar{\sigma}_0 - \frac{c}{\sqrt{3}}\bar{\sigma}_8 + \left(\lambda_1+\lambda_2\right)\bar{\sigma}_0^2 + \sqrt{2}\lambda_2\bar{\sigma}_0\bar{\sigma}_8 + \\ &\quad + \left(\lambda_1+\frac{\lambda_2}{2}\right)\bar{\sigma}_8^2 + \left(3\lambda_1+\frac{3}{2}\lambda_2\right)\bar{\sigma}_3^2 \ , \end{aligned} \tag{B.10e}$$

$$M_{s,38}^2 = \left[-\frac{c}{\sqrt{3}} + \sqrt{2}\lambda_2\bar{\sigma}_0 + \left(2\lambda_1+\lambda_2\right)\bar{\sigma}_8\right]\bar{\sigma}_3 \ , \tag{B.10f}$$

$$\begin{aligned} M_{s,44}^2 = M_{s,55}^2 &= m^2 + \frac{c}{\sqrt{6}}\bar{\sigma}_0 - \frac{c}{2}\bar{\sigma}_3 + \frac{c}{2\sqrt{3}}\bar{\sigma}_8 + \left(\lambda_1+\lambda_2\right)\bar{\sigma}_0^2 + \\ &\quad + \left(\lambda_1+\frac{\lambda_2}{2}\right)\left(\bar{\sigma}_3^2+\bar{\sigma}_8^2\right) + \sqrt{\frac{3}{2}}\lambda_2\bar{\sigma}_0\bar{\sigma}_3 - \frac{\lambda_2}{\sqrt{2}}\bar{\sigma}_0\bar{\sigma}_8 \ , \end{aligned} \tag{B.10g}$$

$$\begin{aligned} M_{s,66}^2 = M_{s,77}^2 &= m^2 + \frac{c}{\sqrt{6}}\bar{\sigma}_0 + \frac{c}{2}\bar{\sigma}_3 + \frac{c}{2\sqrt{3}}\bar{\sigma}_8 + \left(\lambda_1+\lambda_2\right)\bar{\sigma}_0^2 + \\ &\quad + \left(\lambda_1+\frac{\lambda_2}{2}\right)\left(\bar{\sigma}_3^2+\bar{\sigma}_8^2\right) - \sqrt{\frac{3}{2}}\lambda_2\bar{\sigma}_0\bar{\sigma}_3 - \frac{\lambda_2}{\sqrt{2}}\bar{\sigma}_0\bar{\sigma}_8 \ , \end{aligned} \tag{B.10h}$$

$$
\begin{aligned}
M^2_{s,88} &= m^2 + \frac{c}{\sqrt{6}}\bar{\sigma}_0 + \frac{c}{\sqrt{3}}\bar{\sigma}_8 + (\lambda_1+\lambda_2)\,\bar{\sigma}_0^2 + \\
&\quad + \left(\lambda_1 + \frac{\lambda_2}{2}\right)\left(\bar{\sigma}_3^2 + 3\bar{\sigma}_8^2\right) - \sqrt{2}\lambda_2\bar{\sigma}_0\bar{\sigma}_8\,, \qquad \text{(B.10i)}\\
M^2_{s,ix} &= 0 \quad \text{for} \quad x \notin \{0,3,8\} \quad \vee \quad i \in \{0,3,8\}\,, \qquad \text{(B.10j)}\\
M^2_{s,ix} &= 0 \quad \text{for} \quad x \notin \{i\} \quad \vee \quad i \notin \{0,3,8\}\,. \qquad \text{(B.10k)}
\end{aligned}
$$

The contributions of the Linear-σ model to the pseudoscalar-meson masses are

$$
\begin{aligned}
M^2_{p,00} &= m^2 + \sqrt{\frac{2}{3}}c\bar{\sigma}_0 + \left(\lambda_1 + \frac{\lambda_2}{3}\right)\left(\bar{\sigma}_0^2 + \bar{\sigma}_3^2 + \bar{\sigma}_8^2\right)\,, \qquad \text{(B.11a)}\\
M^2_{p,03} &= \left[-\frac{c}{\sqrt{6}} + \frac{2}{3}\lambda_2\left(\bar{\sigma}_0 + \frac{\bar{\sigma}_8}{\sqrt{2}}\right)\right]\bar{\sigma}_3\,, \qquad \text{(B.11b)}\\
M^2_{p,08} &= \left[-\frac{c}{\sqrt{6}} + \frac{2}{3}\lambda_2\bar{\sigma}_0 - \frac{\lambda_2}{3\sqrt{2}}\bar{\sigma}_8\right]\bar{\sigma}_8 + \frac{\lambda_2}{3\sqrt{2}}\bar{\sigma}_3^2\,, \qquad \text{(B.11c)}\\
M^2_{p,11} = M^2_{p,22} &= m^2 - \frac{c}{\sqrt{6}}\bar{\sigma}_0 + \frac{c}{\sqrt{3}}\bar{\sigma}_8 + \left(\lambda_1 + \frac{\lambda_2}{3}\right)\bar{\sigma}_0^2 + \frac{\sqrt{2}}{3}\lambda_2\bar{\sigma}_0\bar{\sigma}_8 + \\
&\quad + \left(\lambda_1 + \frac{\lambda_2}{6}\right)\bar{\sigma}_8^2 + \left(\lambda_1 + \frac{3}{2}\lambda_2\right)\bar{\sigma}_3^2\,, \qquad \text{(B.11d)}\\
M^2_{p,33} &= m^2 - \frac{c}{\sqrt{6}}\bar{\sigma}_0 + \frac{c}{\sqrt{3}}\bar{\sigma}_8 + \left(\lambda_1 + \frac{\lambda_2}{3}\right)\bar{\sigma}_0^2 + \frac{\sqrt{2}}{3}\lambda_2\bar{\sigma}_0\bar{\sigma}_8 + \\
&\quad + \left(\lambda_1 + \frac{\lambda_2}{6}\right)\bar{\sigma}_8^2 + \left(\lambda_1 + \frac{\lambda_2}{2}\right)\bar{\sigma}_3^2\,, \qquad \text{(B.11e)}\\
M^2_{p,38} &= \left[\frac{c}{\sqrt{3}} + \frac{\lambda_2}{3}\left(\sqrt{2}\bar{\sigma}_0 + \bar{\sigma}_8\right)\right]\bar{\sigma}_3\,, \qquad \text{(B.11f)}\\
M^2_{p,44} = M^2_{p,55} &= m^2 - \frac{c}{\sqrt{6}}\bar{\sigma}_0 + \frac{c}{2}\bar{\sigma}_3 - \frac{c}{2\sqrt{3}}\bar{\sigma}_8 + \\
&\quad + \left(\lambda_1 + \frac{\lambda_2}{3}\right)\bar{\sigma}_0^2 + \left(\lambda_1 + \frac{\lambda_2}{2}\right)\bar{\sigma}_3^2 + \left(\lambda_1 + \frac{7}{6}\lambda_2\right)\bar{\sigma}_8^2 + \\
&\quad + \frac{\lambda_2}{\sqrt{6}}\bar{\sigma}_0\bar{\sigma}_3 - \lambda_2\left(\frac{\bar{\sigma}_0}{3\sqrt{2}} - \frac{2}{\sqrt{3}}\bar{\sigma}_3\right)\bar{\sigma}_8\,, \qquad \text{(B.11g)}\\
M^2_{p,66} = M^2_{p,77} &= m^2 - \frac{c}{\sqrt{6}}\bar{\sigma}_0 - \frac{c}{2}\bar{\sigma}_3 - \frac{c}{2\sqrt{3}}\bar{\sigma}_8 + \\
&\quad + \left(\lambda_1 + \frac{\lambda_2}{3}\right)\bar{\sigma}_0^2 + \left(\lambda_1 + \frac{\lambda_2}{2}\right)\bar{\sigma}_3^2 + \left(\lambda_1 + \frac{7}{6}\lambda_2\right)\bar{\sigma}_8^2 - \\
&\quad - \frac{\lambda_2}{\sqrt{6}}\bar{\sigma}_0\bar{\sigma}_3 - \frac{\lambda_2}{3\sqrt{2}}\bar{\sigma}_0\bar{\sigma}_8 - \frac{2}{\sqrt{3}}\lambda_2\bar{\sigma}_3\bar{\sigma}_8\,, \qquad \text{(B.11h)}\\
M^2_{p,88} &= m^2 - \frac{c}{\sqrt{6}}\bar{\sigma}_0 - \frac{c}{\sqrt{3}}\bar{\sigma}_8 + \left(\lambda_1 + \frac{\lambda_2}{3}\right)\bar{\sigma}_0^2 + \\
&\quad + \left(\lambda_1 + \frac{\lambda_2}{6}\right)\bar{\sigma}_3^2 + \left(\lambda_1 + \frac{\lambda_2}{2}\right)\bar{\sigma}_8^2 - \frac{\sqrt{2}}{3}\lambda_2\bar{\sigma}_0\bar{\sigma}_8\,, \qquad \text{(B.11i)}\\
M^2_{p,ix} &= 0 \quad \text{for} \quad x \notin \{0,3,8\} \quad \vee \quad i \in \{0,3,8\}\,, \qquad \text{(B.11j)}\\
M^2_{p,ix} &= 0 \quad \text{for} \quad x \notin \{i\} \quad \vee \quad i \notin \{0,3,8\}\,. \qquad \text{(B.11k)}
\end{aligned}
$$

Derivatives of the potential of thermal quark fluctuations with respect to the meson fields

To the in-medium masses of the mesons contribute besides the mesonic potential and the quark quantum fluctuations also the thermal quark fluctuations. For the QM model the derivatives of the thermal quark fluctuation potential with respect to the meson fields are given in Ref. [66] but for the PQM model they are not yet available in the literature and a are derived as follows. The first order derivative of the thermal quark fluctuation potential (3.12) with respect to the (pseudo-)scalar fields is

$$\begin{aligned}\frac{\partial\Omega_{\mathrm{q\bar{q}}}^{\mathrm{th}}}{\partial\varphi_a} = 3\sum_f \int \frac{\mathrm{d}^3k}{(2\pi)^3}\,\frac{m_{f,a}^2}{E_f}\,\times \\ \times\left\{\frac{e^{-(E_f-\mu_f)/T}}{[\dots]_f}\,\left[\Phi + 2\bar{\Phi}e^{-(E_f-\mu_f)/T} + e^{-2(E_f-\mu_f)/T}\right] + \right. \\ \left. + \frac{e^{-(E_f+\mu_f)/T}}{[\dots]_{\bar{f}}}\,\left[\bar{\Phi} + 2\Phi e^{-(E_f+\mu_f)/T} + e^{-2(E_f+\mu_f)/T}\right]\right\}\,, \quad \text{(B.12)}\end{aligned}$$

where the square brackets contain the arguments of the logarithms in Eq. (3.12). The contributions of thermal quark fluctuations to the squared meson masses can then be displayed as

$$\begin{aligned}\frac{\partial^2\Omega_{\mathrm{q\bar{q}}}^{\mathrm{th}}}{\partial\varphi_a\partial\varphi_b} = 3\sum_f \int \frac{\mathrm{d}^3k}{(2\pi)^3}\left\{\left(\frac{m_{f,ab}^2}{E_f} - \frac{m_{f,a}^2 m_{f,b}^2}{2E_f^3}\right)\{\dots\} - \frac{m_{f,a}^2 m_{f,b}^2}{2\,T E_f}\,\times\right. \\ \times\left\{\frac{e^{-(E_f-\mu_f)/T}}{[\dots]_f}\,\times\right. \\ \times\left[-\frac{3e^{-(E_f-\mu_f)/T}\,[\dots]_{f,1}^2}{[\dots]_f} + 2e^{-(E_f-\mu_f)/T}\left(\bar{\Phi} + e^{-(E_f-\mu_f)/T}\right) + [\dots]_{f,1}\right] + \\ + \frac{e^{-(E_f+\mu_f)/T}}{[\dots]_{\bar{f}}}\,\times \\ \left.\left.\times\left[-\frac{3e^{-(E_f+\mu_f)/T}\,[\dots]_{\bar{f},1}^2}{[\dots]_{\bar{f}}} + 2e^{-(E_f+\mu_f)/T}\left(\Phi + e^{-(E_f+\mu_f)/T}\right) + [\dots]_{\bar{f},1}\right]\right\}\right.\,, \\ \text{(B.13)}\end{aligned}$$

where the square brackets $[\dots]_{f,1}$ and $[\dots]_{\bar{f},1}$ abbreviate the square brackets in Eq. (B.12) and the empty braces contain the content of the braces in Eq. (B.12).

List of Figures

Bibliography

[1] B. W. Mintz, R. Stiele, R. O. Ramos, and J. Schaffner-Bielich, "Phase Diagram and Surface Tension in the 3-flavor Polyakov-Quark-Meson Model," *Phys. Rev.* **D 87** (2013) 036004, arXiv:1212.1184 [hep-ph].

[2] L. M. Haas, R. Stiele, J. Braun, J. M. Pawlowski, and J. Schaffner-Bielich, "Improved polyakov-loop potential for effective models from functional calculations," *Phys. Rev.* **D 87** (Apr, 2013) 076004, arXiv:1302.1993 [hep-ph].

[3] R. Stiele, E. S. Fraga, and J. Schaffner-Bielich, "Thermodynamics of (2+1)-flavor strongly interacting matter at nonzero isospin," *Phys. Lett.* **B 729** (2014) 72–78, arXiv:1307.2851 [hep-ph].

[4] T. K. Herbst, M. Mitter, J. M. Pawlowski, B.-J. Schaefer, and R. Stiele, "Thermodynamics of QCD at vanishing density," arXiv:1308.3621 [hep-ph].

[5] R. Stiele, L. M. Haas, J. Braun, J. M. Pawlowski, and J. Schaffner-Bielich, "QCD thermodynamics of effective models with an improved Polyakov-loop potential," *PoS* **ConfinementX** (2012) 215, arXiv:1303.3742 [hep-ph].

[6] B. W. Mintz, R. Stiele, R. O. Ramos, and J. Schaffner-Bielich, "Nucleation of quark matter in the PQM model," *AIP Conf. Proc.* **1520** (2012) 370–372.

[7] R. Stiele and J. Schaffner-Bielich, "The QCD Phase Transition at finite Isospin," *PoS* **ConfinementX** (2012) 333.

[8] T. K. Herbst, M. Mitter, J. M. Pawlowski, B.-J. Schaefer, and R. Stiele, "Exploring the Phase Structure and Thermodynamics of QCD," *PoS* **QCD-TNT-III** (2014) 030, arXiv:1401.1735 [hep-ph].

[9] T. Beisitzer, R. Stiele, and J. Schaffner-Bielich, "Supernova Equation of State with an extended SU(3) Quark-Meson Model." in preparation.

[10] A. Zacchi, R. Stiele, and J. Schaffner-Bielich, "Compact stars in a SU(3) Quark-Meson-Model." in preparation.

[11] A. Zacchi, R. Stiele, E. S. Fraga, and J. Schaffner-Bielich work in progress.

[12] D. Boyanovsky, H. de Vega, and D. Schwarz, "Phase transitions in the early and the present universe," *Ann. Rev. Nucl. Part. Sci.* **56** (2006) 441–500, arXiv:hep-ph/0602002 [hep-ph].

[13] T. Boeckel and J. Schaffner-Bielich, "A little inflation at the cosmological QCD phase transition," *Phys. Rev.* **D 85** (2012) 103506, arXiv:1105.0832 [astro-ph.CO].

[14] T. Boeckel, S. Schettler, and J. Schaffner-Bielich, "The Cosmological QCD Phase Transition Revisited," *Prog. Part. Nucl. Phys.* **66** (2011) 266–270, arXiv:1012.3342 [astro-ph.CO].

[15] Y. Hama, R. P. Andrade, F. Grassi, J. Socolowski, Otavio, T. Kodama, *et al.*, "3D relativistic hydrodynamic computations using lattice-QCD-inspired equations of state," *Nucl. Phys.* **A 774** (2006) 169–178, arXiv:hep-ph/0510096.

[16] P. Romatschke, "New Developments in Relativistic Viscous Hydrodynamics," *Int. J. Mod. Phys.* **E 19** (2010) 1–53, arXiv:0902.3663 [hep-ph].

[17] R. Marty and J. Aichelin, "Molecular dynamics description of an expanding $q/\bar{q}$ plasma with the Nambu–Jona-Lasinio model and applications to heavy ion collisions at RHIC and LHC energies," *Phys. Rev.* **C 87** (2013) 034912, arXiv:1210.3476 [hep-ph].

[18] I. Sagert, T. Fischer, M. Hempel, G. Pagliara, J. Schaffner-Bielich, *et al.*, "Signals of the QCD phase transition in core-collapse supernovae," *Phys. Rev. Lett.* **102** (2009) 081101, arXiv:0809.4225 [astro-ph].

[19] T. Fischer, I. Sagert, G. Pagliara, M. Hempel, J. Schaffner-Bielich, *et al.*, "Core-collapse supernova explosions triggered by a quark-hadron phase transition during the early post-bounce phase," *Astrophys. J. Suppl.* **194** (2011) 39, arXiv:1011.3409 [astro-ph.HE].

[20] Y. Suwa, T. Takiwaki, K. Kotake, T. Fischer, M. Liebendörfer, *et al.*, "On the Importance of the Equation of State for the Neutrino-Driven Supernova Explosion Mechanism," *Astrophys. J.* **764** (2013) 99, arXiv:1206.6101 [astro-ph.HE].

[21] H.-T. Janka, "Explosion Mechanisms of Core-Collapse Supernovae," *Ann. Rev. Nucl. Part. Sci.* **62** (2012) 407–451, arXiv:1206.2503 [astro-ph.SR].

[22] F. Weber, "Strange quark matter and compact stars," *Prog. Part. Nucl. Phys.* **54** (2005) 193–288, arXiv:astro-ph/0407155 [astro-ph].

[23] J. Schaffner-Bielich, I. Sagert, M. Hempel, G. Pagliara, T. Fischer, *et al.*, "Astrophysical Implications of the QCD phase transition," *PoS* **CONFINEMENT8** (2009) 138, arXiv:0903.0991 [astro-ph.SR].

[24] J. Schaffner-Bielich, "Strangeness in Compact Stars," *Nucl. Phys.* **A 835** (2010) 279–286, arXiv:1002.1658 [nucl-th].

[25] B. Muller and J. L. Nagle, "Results from the relativistic heavy ion collider," *Ann. Rev. Nucl. Part. Sci.* **56** (2006) 93–135, arXiv:nucl-th/0602029 [nucl-th].

[26] B. Muller, J. Schukraft, and B. Wyslouch, "First Results from Pb+Pb collisions at the LHC," *Ann. Rev. Nucl. Part. Sci.* **62** (2012) 361–386, arXiv:1202.3233 [hep-ex].

[27] M. Bleicher, M. Nahrgang, J. Steinheimer, and P. Bicudo, "Physics Prospects at FAIR," *Acta Phys. Polon.* **B 43** (2012) 731–740, arXiv:1112.5286 [hep-ph].

[28] B. Friman, C. Höhne, J. Knoll, S. Leupold, J. Randrup, *et al.*, "The CBM physics book: Compressed baryonic matter in laboratory experiments," *Lect. Notes Phys.* **814** (2011) 1–980.

[29] **NICA Collaboration, MPD Collaboration** Collaboration, V. Kekelidze, A. Kovalenko, I. Meshkov, A. Sorin, and G. Trubnikov, "NICA at JINR: New prospects for exploration of quark-gluon matter," *Phys. Atom. Nucl.* **75** (2012) 542–545.

[30] D. F. Litim and J. M. Pawlowski, "On gauge invariant Wilsonian flows," arXiv:hep-th/9901063 [hep-th].

[31] J. Berges, N. Tetradis, and C. Wetterich, "Nonperturbative renormalization flow in quantum field theory and statistical physics," *Phys. Rept.* **363** (2002) 223–386, arXiv:hep-ph/0005122 [hep-ph].

[32] J. M. Pawlowski, "Aspects of the functional renormalisation group," *Annals Phys.* **322** (2007) 2831–2915, arXiv:hep-th/0512261 [hep-th].

[33] H. Gies, "Introduction to the functional RG and applications to gauge theories," *Lect. Notes Phys.* **852** (2012) 287–348, arXiv:hep-ph/0611146 [hep-ph].

[34] B.-J. Schaefer and J. Wambach, "Renormalization group approach towards the QCD phase diagram," *Phys. Part. Nucl.* **39** (2008) 1025–1032, arXiv:hep-ph/0611191 [hep-ph].

[35] J. Braun, "Fermion Interactions and Universal Behavior in Strongly Interacting Theories," *J. Phys.* **G 39** (2012) 033001, arXiv:1108.4449 [hep-ph].

[36] J. Braun, L. M. Haas, F. Marhauser, and J. M. Pawlowski, "Phase Structure of Two-Flavor QCD at Finite Chemical Potential," *Phys. Rev. Lett.* **106** (2011) 022002, arXiv:0908.0008 [hep-ph].

[37] J. M. Pawlowski, "The QCD phase diagram: Results and challenges," *AIP Conf. Proc.* **1343** (2011) 75–80, arXiv:1012.5075 [hep-ph].

[38] **Wuppertal-Budapest Collaboration** Collaboration, S. Borsanyi *et al.*, "Is there still any T_c mystery in lattice QCD? Results with physical masses in the continuum limit III," *JHEP* **1009** (2010) 073, arXiv:1005.3508 [hep-lat].

[39] S. Borsanyi, G. Endrodi, Z. Fodor, A. Jakovac, S. D. Katz, *et al.*, "The QCD equation of state with dynamical quarks," *JHEP* **1011** (2010) 077, arXiv:1007.2580 [hep-lat].

[40] A. Bazavov, T. Bhattacharya, M. Cheng, C. DeTar, H. Ding, *et al.*, "The chiral and deconfinement aspects of the QCD transition," *Phys. Rev.* **D 85** (2012) 054503, arXiv:1111.1710 [hep-lat].

[41] **HotQCD Collaboration** Collaboration, A. Bazavov, "The QCD equation of state with 2+1 flavors of Highly Improved Staggered Quarks (HISQ)," *Nucl. Phys.* **A 904-905** (2013) 877c–880c, arXiv:1210.6312 [hep-lat].

[42] A. Bazavov and P. Petreczky, "On the Polyakov loop in 2+1 flavor QCD," *Phys. Rev.* **D 87** (2013) 094505, arXiv:1301.3943 [hep-lat].

[43] J. Kogut and D. Sinclair, "The Finite temperature transition for 2-flavor lattice QCD at finite isospin density," *Phys. Rev.* **D 70** (2004) 094501, arXiv:hep-lat/0407027 [hep-lat].

[44] P. de Forcrand, M. A. Stephanov, and U. Wenger, "On the phase diagram of QCD at finite isospin density," *PoS* **LAT2007** (2007) 237, arXiv:0711.0023 [hep-lat].

[45] P. Cea, L. Cosmai, M. D'Elia, A. Papa, and F. Sanfilippo, "The critical line of two-flavor QCD at finite isospin or baryon densities from imaginary chemical potentials," *Phys. Rev.* **D 85** (2012) 094512, arXiv:1202.5700 [hep-lat].

[46] W. Detmold, K. Orginos, and Z. Shi, "Lattice QCD at non-zero isospin chemical potential," *Phys. Rev.* **D 86** (2012) 054507, arXiv:1205.4224 [hep-lat].

[47] G. Bali, F. Bruckmann, G. Endrodi, Z. Fodor, S. Katz, *et al.*, "The QCD phase diagram for external magnetic fields," *JHEP* **1202** (2012) 044, arXiv:1111.4956 [hep-lat].

[48] G. Bali, F. Bruckmann, G. Endrodi, Z. Fodor, S. Katz, *et al.*, "QCD quark condensate in external magnetic fields," *Phys. Rev.* **D 86** (2012) 071502, arXiv:1206.4205 [hep-lat].

[49] G. Bali, F. Bruckmann, G. Endrodi, F. Gruber, and A. Schaefer, "Magnetic field-induced gluonic (inverse) catalysis and pressure (an)isotropy in QCD," *JHEP* **1304** (2013) 130, arXiv:1303.1328 [hep-lat].

[50] F. Bruckmann, G. Endrodi, and T. G. Kovacs, "Inverse magnetic catalysis and the Polyakov loop," *JHEP* **1304** (2013) 112, arXiv:1303.3972 [hep-lat].

[51] P. de Forcrand and O. Philipsen, "The Chiral critical line of N(f) = 2+1 QCD at zero and non-zero baryon density," *JHEP* **0701** (2007) 077, arXiv:hep-lat/0607017 [hep-lat].

[52] C. DeTar and U. Heller, "QCD Thermodynamics from the Lattice," *Eur. Phys. J.* **A 41** (2009) 405–437, arXiv:0905.2949 [hep-lat].

[53] K. Fukushima and C. Sasaki, "The phase diagram of nuclear and quark matter at high baryon density," *Prog. Part. Nucl. Phys.* **72** (2013) 99–154, arXiv:1301.6377 [hep-ph].

[54] Y. Nambu and G. Jona-Lasinio, "Dynamical Model of Elementary Particles Based on an Analogy with Superconductivity. 1.," *Phys. Rev.* **122** (1961) 345–358.

[55] Y. Nambu and G. Jona-Lasinio, "Dynamical Model of Elementary Particles Based on an Analogy with Superconductivity. II," *Phys. Rev.* **124** (1961) 246–254.

[56] M. Gell-Mann and M. Levy, "The axial vector current in beta decay," *Nuovo Cim.* **16** (1960) 705.

[57] M. Lévy, "Currents and symmetry breaking," *Nuovo Cim.* **52** (1967) 23.

[58] J. Berges, D. Jungnickel, and C. Wetterich, "Two flavor chiral phase transition from nonperturbative flow equations," *Phys. Rev.* **D 59** (1999) 034010, arXiv:hep-ph/9705474 [hep-ph].

[59] B.-J. Schaefer and H.-J. Pirner, "Renormalization group flow and equation of state of quarks and mesons," *Nucl. Phys.* **A 660** (1999) 439–474, arXiv:nucl-th/9903003 [nucl-th].

[60] J. T. Lenaghan, D. H. Rischke, and J. Schaffner-Bielich, "Chiral symmetry restoration at nonzero temperature in the SU(3)(r) x SU(3)(l) linear sigma model," *Phys. Rev.* **D 62** (2000) 085008, arXiv:nucl-th/0004006 [nucl-th].

[61] O. Scavenius, A. Mocsy, I. Mishustin, and D. Rischke, "Chiral phase transition within effective models with constituent quarks," *Phys. Rev.* **C 64** (2001) 045202, arXiv:nucl-th/0007030 [nucl-th].

[62] J. Braun, K. Schwenzer, and H.-J. Pirner, "Linking the quark meson model with QCD at high temperature," *Phys. Rev.* **D 70** (2004) 085016, arXiv:hep-ph/0312277 [hep-ph].

[63] A. Mocsy, I. Mishustin, and P. Ellis, "Role of fluctuations in the linear sigma model with quarks," *Phys. Rev.* **C 70** (2004) 015204, arXiv:nucl-th/0402070 [nucl-th].

[64] B.-J. Schaefer and J. Wambach, "The Phase diagram of the quark meson model," *Nucl. Phys.* **A 757** (2005) 479–492, arXiv:nucl-th/0403039 [nucl-th].

[65] E. S. Bowman and J. I. Kapusta, "Critical Points in the Linear Sigma Model with Quarks," *Phys. Rev.* **C 79** (2009) 015202, arXiv:0810.0042 [nucl-th].

[66] B.-J. Schaefer and M. Wagner, "The Three-flavor chiral phase structure in hot and dense QCD matter," *Phys. Rev.* **D 79** (2009) 014018, arXiv:0808.1491 [hep-ph].

[67] P. N. Meisinger and M. C. Ogilvie, "Chiral symmetry restoration and Z(N) symmetry," *Phys. Lett.* **B 379** (1996) 163–168, arXiv:hep-lat/9512011 [hep-lat].

[68] K. Fukushima, "Chiral effective model with the Polyakov loop," *Phys. Lett.* **B 591** (2004) 277–284, arXiv:hep-ph/0310121 [hep-ph].

[69] C. Ratti, M. A. Thaler, and W. Weise, "Phases of QCD: Lattice thermodynamics and a field theoretical model," *Phys. Rev.* **D 73** (2006) 014019, arXiv:hep-ph/0506234 [hep-ph].

[70] E. Megias, E. Ruiz Arriola, and L. Salcedo, "Polyakov loop in chiral quark models at finite temperature," *Phys. Rev.* **D 74** (2006) 065005, arXiv:hep-ph/0412308 [hep-ph].

[71] S. Roessner, C. Ratti, and W. Weise, "Polyakov loop, diquarks and the two-flavour phase diagram," *Phys. Rev.* **D 75** (2007) 034007, arXiv:hep-ph/0609281 [hep-ph].

[72] B.-J. Schaefer, J. M. Pawlowski, and J. Wambach, "The Phase Structure of the Polyakov–Quark-Meson Model," *Phys. Rev.* **D 76** (2007) 074023, arXiv:0704.3234 [hep-ph].

[73] B.-J. Schaefer, M. Wagner, and J. Wambach, "Thermodynamics of (2+1)-flavor QCD: Confronting Models with Lattice Studies," *Phys. Rev.* **D 81** (2010) 074013, arXiv:0910.5628 [hep-ph].

[74] V. Skokov, B. Stokic, B. Friman, and K. Redlich, "Meson fluctuations and thermodynamics of the Polyakov loop extended quark-meson model," *Phys. Rev.* **C 82** (2010) 015206, arXiv:1004.2665 [hep-ph].

[75] V. Skokov, B. Friman, E. Nakano, K. Redlich, and B.-J. Schaefer, "Vacuum fluctuations and the thermodynamics of chiral models," *Phys. Rev.* **D 82** (2010) 034029, arXiv:1005.3166 [hep-ph].

[76] T. K. Herbst, J. M. Pawlowski, and B.-J. Schaefer, "The phase structure of the Polyakov–quark-meson model beyond mean field," *Phys. Lett.* **B 696** (2011) 58–67, arXiv:1008.0081 [hep-ph].

[77] B. Schaefer and M. Wagner, "QCD critical region and higher moments for three flavor models," *Phys. Rev.* **D 85** (2012) 034027, arXiv:1111.6871 [hep-ph].

[78] T. K. Herbst, J. M. Pawlowski, and B.-J. Schaefer, "On the phase structure and thermodynamics of QCD," *Phys. Rev.* **D 88** (2013) 014007, arXiv:1302.1426 [hep-ph].

[79] J. O. Andersen, R. Khan, and L. T. Kyllingstad, "The chiral phase transition and the role of vacuum fluctuations," arXiv:1102.2779 [hep-ph].

[80] O. Scavenius, A. Dumitru, and J. Lenaghan, "The K / pi ratio from condensed Polyakov loops," *Phys. Rev.* **C 66** (2002) 034903, arXiv:hep-ph/0201079 [hep-ph].

[81] P. M. Lo, B. Friman, O. Kaczmarek, K. Redlich, and C. Sasaki, "Polyakov loop fluctuations in SU(3) lattice gauge theory and an effective gluon potential," *Phys. Rev.* **D 88** (2013) 074502, arXiv:1307.5958 [hep-lat].

[82] J. Braun, H. Gies, and J. M. Pawlowski, "Quark Confinement from Color Confinement," *Phys. Lett.* **B 684** (2010) 262–267, arXiv:0708.2413 [hep-th].

[83] J. Braun, A. Eichhorn, H. Gies, and J. M. Pawlowski, "On the Nature of the Phase Transition in SU(N), Sp(2) and E(7) Yang-Mills theory," *Eur. Phys. J.* **C 70** (2010) 689–702, arXiv:1007.2619 [hep-ph].

[84] L. Fister and J. M. Pawlowski, "Confinement from Correlation Functions," *Phys. Rev.* **D 88** (2013) 045010, arXiv:1301.4163 [hep-ph].

[85] D. J. Schwarz and M. Stuke, "Does the CMB prefer a leptonic Universe?," *New J. Phys.* **15** (2013) 033021, arXiv:1211.6721 [astro-ph.CO].

[86] D. J. Schwarz and M. Stuke, "Lepton asymmetry and the cosmic QCD transition," *JCAP* **0911** (2009) 025, arXiv:0906.3434 [hep-ph].

[87] D. Son and M. A. Stephanov, "QCD at finite isospin density," *Phys. Rev. Lett.* **86** (2001) 592–595, arXiv:hep-ph/0005225 [hep-ph].

[88] K. Fukushima and Y. Hidaka, "A Model study of the sign problem in the mean-field approximation," *Phys. Rev.* **D 75** (2007) 036002, arXiv:hep-ph/0610323 [hep-ph].

[89] A. Dumitru, R. D. Pisarski, and D. Zschiesche, "Dense quarks, and the fermion sign problem, in a SU(N) matrix model," *Phys. Rev.* **D 72** (2005) 065008, arXiv:hep-ph/0505256 [hep-ph].

[90] S. Roessner, T. Hell, C. Ratti, and W. Weise, "The chiral and deconfinement crossover transitions: PNJL model beyond mean field," *Nucl. Phys.* **A 814** (2008) 118–143, arXiv:0712.3152 [hep-ph].

[91] J. S. Langer and L. A. Turski, "Hydrodynamic Model of the Condensation of a Vapor near Its Critical Point," *Phys. Rev.* **A 8** (1973) 3230–3243.

[92] L. P. Csernai and J. I. Kapusta, "Nucleation of relativistic first order phase transitions," *Phys. Rev.* **D 46** (1992) 1379–1390.

[93] M. Gleiser, G. C. Marques, and R. O. Ramos, "On the evaluation of thermal corrections to false vacuum decay rates," *Phys. Rev.* **D 48** (1993) 1571–1584, arXiv:hep-ph/9304234 [hep-ph].

[94] O. Scavenius, A. Dumitru, E. Fraga, J. Lenaghan, and A. Jackson, "First order chiral phase transition in high-energy collisions: Can nucleation prevent spinodal decomposition?," *Phys. Rev.* **D 63** (2001) 116003, arXiv:hep-ph/0009171 [hep-ph].

[95] A. Bessa, E. Fraga, and B. Mintz, "Phase conversion in a weakly first-order quark-hadron transition," *Phys. Rev.* **D 79** (2009) 034012, arXiv:0811.4385 [hep-ph].

[96] I. Bombaci, P. K. Panda, C. Providencia, and I. Vidana, "Metastability of hadronic compact stars," *Phys. Rev.* **D 77** (2008) 083002, arXiv:0802.1794 [astro-ph].

[97] I. Bombaci, D. Logoteta, P. Panda, C. Providencia, and I. Vidana, "Quark matter nucleation in hot hadronic matter," *Phys. Lett.* **B 680** (2009) 448–452, arXiv:0910.4109 [astro-ph.SR].

[98] B. Mintz, E. Fraga, G. Pagliara, and J. Schaffner-Bielich, "Nucleation of quark matter in protoneutron star matter," *Phys. Rev.* **D 81** (2010) 123012, arXiv:0910.3927 [hep-ph].

[99] R. Landua, "Teilchenphysik 2," in *German Teachers Programme*, CERN. October, 2013. https://indico.cern.ch/event/200520/session/1/contribution/63/material/slides/0.pdf.

[100] G. Ecker, "The colourful world of quarks and gluons I: The shaping of quantum chromodynamics," *PoS* **ConfinementX** (2012) 344.

[101] T. K. Herbst, "Polyakov loop dynamics with the renormalization group," Master's thesis, Karl-Franzens-Universität Graz, 2009.

[102] J. Kapusta and C. Gale, "Finite-temperature field theory: Principles and applications,".

[103] H. Geiger and E. Marsden, "On a diffuse reflection of the -particles," *Proc. Roy. Soc.* **82** (1909) 495–500.

[104] E. Rutherford, "The scattering of alpha and beta particles by matter and the structure of the atom„" *Phil. Mag.* **21** (1911) 669–688.

[105] E. Rutherford, "Nuclear constitution of atoms," *Royal Society of London Proceedings Series A* **97** (Jul, 1920) 374–400.

[106] J. Chadwick, "Possible Existence of a Neutron," *Nature* **129** (1932) 312.

[107] H. Yukawa, "On the interaction of elementary particles," *Proc. Phys. Math. Soc. Jap.* **17** (1935) 48–57.

[108] V. F. Hess, "Über Beobachtungen der durchdringenden Strahlung bei sieben Freiballonfahrten," *Physikalische Zeitschrift* **13** (1912) 1084–1091.

[109] D. Perkins, "Nuclear Disintegration by Meson Capture," *Nature* **159** (1947) 126–127.

[110] C. Lattes, G. Occhialini, and C. Powell, "Observations on the tracks of slow mesons in photographic emulsions. 1," *Nature* **160** (1947) 453–45.

[111] C. Lattes, G. Occhialini, and C. Powell, "Observations on the tracks of slow mesons in photographic emulsions. 2," *Nature* **160** (1947) 486–492.

[112] E. Gardner and C. Lattes, "Production of Mesons by the 184-Inch Berkeley Cyclotron," *Science* **12** (March, 1948) 270–271.

[113] W. Heisenberg, "Über den Bau der Atomkerne. 1," *Z. Phys.* **77** (1932) 1–11.

[114] W. Heisenberg, "Über den Bau der Atomkerne. 2," *Z. Phys.* **78** (1932) 156–164.

[115] E. Wigner, "On the Consequences of the Symmetry of the Nuclear Hamiltonian on the Spectroscopy of Nuclei," *Phys.Rev.* **51** (1937) 106–119.

[116] T. Nakano and K. Nishijima, "Charge Independence for V-particles," *Prog. Theor. Phys.* **10** (1953) 581–582.

[117] K. Nishijima, "Charge Independence Theory of V Particles," *Prog. Theor. Phys.* **13** (1955) 285–304.

[118] M. Gell-Mann, "The interpretation of the new particles as displaced charge multiplets," *Nuovo Cim.* **4** (April, 1956) 848–866.

[119] Y. Ne'eman, "Derivation of strong interactions from a gauge invariance," *Nucl. Phys.* **26** (1961) 222–229.

[120] M. Gell-Mann *California Institute of Technology Synchrotron Laboratory Report CTSL-20* (1961) .

[121] M. Gell-Mann, "Symmetries of baryons and mesons," *Phys. Rev.* **125** (1962) 1067–1084.

[122] M. Gell-Mann, "A Schematic Model of Baryons and Mesons," *Phys. Lett.* **8** (1964) 214–215.

[123] G. Zweig, "An SU(3) model for strong interaction symmetry and its breaking. Version 1," *CERN-TH* **401** (1964) .

[124] G. Zweig, "An SU(3) model for strong interaction symmetry and its breaking. Version 2," *CERN-TH* **412** (1964) .

[125] R. P. Feynman, "Very high-energy collisions of hadrons," *Phys. Rev. Lett.* **23** (1969) 1415–1417.

[126] R. Feynman, "The behavior of hadron collisions at extreme energies," *Conf. Proc.* **C 690905** (1969) 237–258.

[127] R. Feynman, "Partons," *Conf. Proc.* **C 700414** (1970) 773–813.

[128] J. Bjorken and E. A. Paschos, "Inelastic Electron Proton and gamma Proton Scattering, and the Structure of the Nucleon," *Phys. Rev.* **185** (1969) 1975–1982.

[129] R. E. Taylor, "Nucleon form-factors above 6 GeV," in *Electron and Photon Interactions at High Energy*, p. 78. 1967.

[130] C. Boley, J. Elias, J. Friedman, G. Hartmann, H. Kendall, *et al.*, "Experimental Search for a Heavy Electron," *Phys. Rev.* **167** (1968) 1275–1279.

[131] E. D. Bloom, D. Coward, H. DeStaebler, J. Drees, G. Miller, *et al.*, "High-Energy Inelastic e p Scattering at 6-Degrees and 10-Degrees," *Phys. Rev. Lett.* **23** (1969) 930–934.

[132] O. Greenberg, "Spin and Unitary Spin Independence in a Paraquark Model of Baryons and Mesons," *Phys. Rev. Lett.* **13** (1964) 598–602.

[133] M. Han and Y. Nambu, "Three Triplet Model with Double SU(3) Symmetry," *Phys. Rev.* **139** (1965) B1006–B1010.

[134] H. Fritzsch and M. Gell-Mann, "Current algebra: Quarks and what else?," *eConf* **C 720906V2** (1972) 135–165, arXiv:hep-ph/0208010 [hep-ph].

[135] H. Fritzsch, M. Gell-Mann, and H. Leutwyler, "Advantages of the Color Octet Gluon Picture," *Phys. Lett.* **B 47** (1973) 365–368.

[136] **PLUTO Collaboration** Collaboration, C. Berger *et al.*, "Jet Analysis of the Υ (9.46) Decay Into Charged Hadrons," *Phys .Lett.* **B 82** (1979) 449.

[137] **PLUTO Collaboration** Collaboration, C. Berger *et al.*, "Evidence for Gluon Bremsstrahlung in e+ e- Annihilations at High-Energies," *Phys. Lett.* **B86** (1979) 418.

[138] **PLUTO Collaboration** Collaboration, C. Berger *et al.*, "A Study of Multi-Jet Events in e+ e- Annihilation," *Phys. Lett.* **B97** (1980) 459.

[139] J. Bjorken and S. Glashow, "Elementary Particles and SU(4)," *Phys. Lett.* **11** (1964) 255–257.

[140] S. Glashow, J. Iliopoulos, and L. Maiani, "Weak Interactions with Lepton-Hadron Symmetry," *Phys. Rev.* **D 2** (1970) 1285–1292.

[141] **SLAC-SP-017 Collaboration** Collaboration, J. Augustin *et al.*, "Discovery of a Narrow Resonance in e+ e- Annihilation," *Phys. Rev. Lett.* **33** (1974) 1406–1408.

[142] **E598 Collaboration** Collaboration, J. Aubert *et al.*, "Experimental Observation of a Heavy Particle J," *Phys. Rev. Lett.* **33** (1974) 1404–1406.

[143] M. Kobayashi and T. Maskawa, "CP Violation in the Renormalizable Theory of Weak Interaction," *Prog. Theor. Phys.* **49** (1973) 652–657.

[144] S. Herb, D. Hom, L. Lederman, J. Sens, H. Snyder, *et al.*, "Observation of a Dimuon Resonance at 9.5-GeV in 400-GeV Proton-Nucleus Collisions," *Phys. Rev. Lett.* **39** (1977) 252–255.

[145] **CDF Collaboration** Collaboration, F. Abe *et al.*, "Observation of top quark production in $\bar{p}p$ collisions," *Phys. Rev. Lett.* **74** (1995) 2626–2631, arXiv:hep-ex/9503002 [hep-ex].

[146] **D0 Collaboration** Collaboration, S. Abachi *et al.*, "Search for high mass top quark production in $p\bar{p}$ collisions at $\sqrt{s} = 1.8$ TeV," *Phys. Rev. Lett.* **74** (1995) 2422–2426, arXiv:hep-ex/9411001 [hep-ex].

[147] **Particle Data Group** Collaboration, J. Beringer *et al.*, "Review of Particle Physics (RPP)," *Phys. Rev.* **D 86** (2012) 010001.

[148] Fermilab Visual Media Services, "05-0440-01D.hr.jpg." `http://www-visualmedia.fnal.gov/VMS_Site/gallery/stillphotos/2005/0400/05-0440-01D.hr.jpg`.

[149] D. J. Gross and F. Wilczek, "Ultraviolet Behavior of Nonabelian Gauge Theories," *Phys. Rev. Lett.* **30** (1973) 1343–1346.

[150] D. Gross and F. Wilczek, "Asymptotically Free Gauge Theories. 1," *Phys. Rev.* **D 8** (1973) 3633–3652.

[151] D. Gross and F. Wilczek, "Asymptotically Free Gauge Theories. 2," *Phys. Rev.* **D 9** (1974) 980–993.

[152] H. D. Politzer, "Reliable Perturbative Results for Strong Interactions?," *Phys. Rev. Lett.* **30** (1973) 1346–1349.

[153] H. D. Politzer, "Asymptotic Freedom: An Approach to Strong Interactions," *Phys. Rept.* **14** (1974) 129–180.

[154] C.-N. Yang and R. L. Mills, "Conservation of Isotopic Spin and Isotopic Gauge Invariance," *Phys. Rev.* **96** (1954) 191–195.

[155] R. Hagedorn, "Statistical thermodynamics of strong interactions at high-energies," *Nuovo Cim. Suppl.* **3** (1965) 147–186.

[156] N. Cabibbo and G. Parisi, "Exponential Hadronic Spectrum and Quark Liberation," *Phys. Lett.* **B 59** (1975) 67–69.

[157] A. M. Polyakov, "Thermal Properties of Gauge Fields and Quark Liberation," *Phys. Lett.* **B 72** (1978) 477–480.

[158] L. Susskind, "Lattice Models of Quark Confinement at High Temperature," *Phys. Rev.* **D 20** (1979) 2610–2618.

[159] K. Kajantie, C. Montonen, and E. Pietarinen, "Phase Transition of SU(3) Gauge Theory at Finite Temperature," *Z. Phys.* **C 9** (1981) 253.

[160] J. Engels, F. Karsch, and H. Satz, "The High Temperature Behavior of Lattice QCD With Fermions," *Phys. Lett.* **B 113** (1982) 398.

[161] N. Itoh, "Hydrostatic Equilibrium of Hypothetical Quark Stars," *Prog. Theor. Phys.* **44** (1970) 291.

[162] J. C. Collins and M. Perry, "Superdense Matter: Neutrons Or Asymptotically Free Quarks?," *Phys. Rev. Lett.* **34** (1975) 1353.

[163] G. Chapline and M. Nauenberg, "Asymptotic Freedom and the Baryon-Quark Phase Transition," *Phys. Rev.* **D 16** (1977) 450.

[164] GSI Helmholtzzentrum für Schwerionenforschung, "quark-gluon-phasendiagramm_01." http://www.gsi.de/uploads/pics/quark-gluon-phasendiagramm_01.png.

[165] B.-J. Schaefer and M. Wagner, "On the QCD phase structure from effective models," *Prog. Part. Nucl. Phys.* **62** (2009) 381, arXiv:0812.2855 [hep-ph].

[166] T. Beisitzer, "Supernova Equation of State with an extended SU(3) Polyakov Quark-Meson Model," Master's thesis, University of Heidelberg, 2012.

[167] S. Klevansky, "The Nambu-Jona-Lasinio model of quantum chromodynamics," *Rev. Mod. Phys.* **64** (1992) 649–708.

[168] R. D. Pisarski, "Quark gluon plasma as a condensate of SU(3) Wilson lines," *Phys. Rev.* **D 62** (2000) 111501, arXiv:hep-ph/0006205 [hep-ph].

[169] J. Greensite, "The Confinement problem in lattice gauge theory," *Prog. Part. Nucl. Phys.* **51** (2003) 1, arXiv:hep-lat/0301023 [hep-lat].

[170] C. Vafa and E. Witten, "Restrictions on Symmetry Breaking in Vector-Like Gauge Theories," *Nucl. Phys.* **B 234** (1984) 173.

[171] E. Megias, E. Ruiz Arriola, and L. Salcedo, "Dimension two condensates and the Polyakov loop above the deconfinement phase transition," *JHEP* **0601** (2006) 073, arXiv:hep-ph/0505215.

[172] F. Marhauser and J. M. Pawlowski, "Confinement in Polyakov Gauge," arXiv:0812.1144 [hep-ph].

[173] N. Weiss, "The Effective Potential for the Order Parameter of Gauge Theories at Finite Temperature," *Phys. Rev.* **D 24** (1981) 475.

[174] D. J. Gross, R. D. Pisarski, and L. G. Yaffe, "QCD and Instantons at Finite Temperature," *Rev. Mod. Phys.* **53** (1981) 43.

[175] N. Weiss, "The Wilson Line in Finite Temperature Gauge Theories," *Phys. Rev.* **D 25** (1982) 2667.

[176] B. Svetitsky, "Symmetry Aspects of Finite Temperature Confinement Transitions," *Phys. Rept.* **132** (1986) 1–53.

[177] C. Sasaki and K. Redlich, "An Effective gluon potential and hybrid approach to Yang-Mills thermodynamics," *Phys. Rev.* **D 86** (2012) 014007, arXiv:1204.4330 [hep-ph].

[178] M. Ruggieri, P. Alba, P. Castorina, S. Plumari, C. Ratti, *et al.*, "Polyakov Loop and Gluon Quasiparticles in Yang-Mills Thermodynamics," *Phys. Rev.* **D 86** (2012) 054007, arXiv:1204.5995 [hep-ph].

[179] A. Dumitru, Y. Guo, Y. Hidaka, C. P. K. Altes, and R. D. Pisarski, "Effective Matrix Model for Deconfinement in Pure Gauge Theories," *Phys. Rev.* **D 86** (2012) 105017, arXiv:1205.0137 [hep-ph].

[180] D. Diakonov, C. Gattringer, and H.-P. Schadler, "Free energy for parameterized Polyakov loops in SU(2) and SU(3) lattice gauge theory," *JHEP* **1208** (2012) 128, arXiv:1205.4768 [hep-lat].

[181] K. Fukushima and K. Kashiwa, "Polyakov loop and QCD thermodynamics from the gluon and ghost propagators," *Phys. Lett.* **B 723** (2013) 360–364, arXiv:1206.0685 [hep-ph].

[182] H. Reinhardt and J. Heffner, "The effective potential of the confinement order parameter in the Hamilton approach," *Phys. Lett.* **B 718** (2012) 672–677, arXiv:1210.1742 [hep-th].

[183] K. Kashiwa and Y. Maezawa, "Quark back reaction to deconfinement transition via gluon propagators," arXiv:1212.2184 [hep-ph].

[184] H. Gies and C. Wetterich, "Universality of spontaneous chiral symmetry breaking in gauge theories," *Phys. Rev.* **D 69** (2004) 025001, arXiv:hep-th/0209183 [hep-th].

[185] J. Braun and H. Gies, "Chiral phase boundary of QCD at finite temperature," *JHEP* **0606** (2006) 024, arXiv:hep-ph/0602226 [hep-ph].

[186] J. Braun, "The QCD Phase Boundary from Quark-Gluon Dynamics," *Eur. Phys. J.* **C 64** (2009) 459–482, arXiv:0810.1727 [hep-ph].

[187] B. Svetitsky and L. G. Yaffe, "Critical Behavior at Finite Temperature Confinement Transitions," *Nucl. Phys.* **B 210** (1982) 423.

[188] T. Banks and A. Ukawa, "Deconfining and Chiral Phase Transitions in Quantum Chromodynamics at Finite Temperature," *Nucl. Phys.* **B 225** (1983) 145.

[189] U. S. Gupta and V. K. Tiwari, "Revisiting the Phase Structure of the Polyakov-quark-meson Model in the presence of Vacuum Fermion Fluctuation," *Phys. Rev.* **D 85** (2012) 014010, arXiv:1107.1312 [hep-ph].

[190] S. Chatterjee and K. A. Mohan, "Including the Fermion Vacuum Fluctuations in the $(2+1)$ flavor Polyakov Quark Meson Model," *Phys. Rev.* **D 85** (2012) 074018, arXiv:1108.2941 [hep-ph].

[191] J. Polonyi, "Lectures on the functional renormalization group method," *Central Eur. J. Phys.* **1** (2003) 1–71, arXiv:hep-th/0110026 [hep-th].

[192] B.-J. Schaefer, "Fluctuations and the QCD Phase Diagram," *Phys. Atom. Nucl.* **75** (2012) 741–743, arXiv:1102.2772 [hep-ph].

[193] L. von Smekal, "Universal Aspects of QCD-like Theories," *Nucl. Phys. Proc. Suppl.* **228** (2012) 179–220, arXiv:1205.4205 [hep-ph].

[194] D. Parganlija, P. Kovacs, G. Wolf, F. Giacosa, and D. H. Rischke, "Meson vacuum phenomenology in a three-flavor linear sigma model with (axial-)vector mesons," *Phys. Rev.* **D 87** (2013) 014011, arXiv:1208.0585 [hep-ph].

[195] V. Dexheimer and S. Schramm, "Chiral Symmetry Restoration and Deconfinement to Quark Matter in Neutron Stars," *Nucl. Phys. Proc. Suppl.* **199** (2010) 319–324, arXiv:0910.1312 [astro-ph.SR].

[196] V. Dexheimer and S. Schramm, "A Novel Approach to Model Hybrid Stars," *Phys. Rev.* **C 81** (2010) 045201, arXiv:0901.1748 [astro-ph.SR].

[197] T. Hell, *Modeling the Thermodynamics of QCD*. PhD thesis, Technische Universität München, July, 2010.

[198] M. Gross, J. Bartholomew, and D. Hochberg, "SU(N) Deconfinement Transition and the N State Clock Model,".

[199] J. Langelage, S. Lottini, and O. Philipsen, "Centre symmetric 3d effective actions for thermal SU(N) Yang-Mills from strong coupling series," *JHEP* **1102** (2011) 057, arXiv:1010.0951 [hep-lat].

[200] O. Kaczmarek, F. Karsch, P. Petreczky, and F. Zantow, "Heavy quark anti-quark free energy and the renormalized Polyakov loop," *Phys. Lett.* **B 543** (2002) 41–47, arXiv:hep-lat/0207002 [hep-lat].

[201] G. Boyd, J. Engels, F. Karsch, E. Laermann, C. Legeland, *et al.*, "Thermodynamics of SU(3) lattice gauge theory," *Nucl. Phys.* **B 469** (1996) 419–444, arXiv:hep-lat/9602007 [hep-lat].

[202] P. M. Lo, B. Friman, O. Kaczmarek, K. Redlich, and C. Sasaki, "Probing Deconfinement with Polyakov Loop Susceptibilities," *Phys. Rev.* **D 88** (2013) 014506, arXiv:1306.5094 [hep-lat].

[203] S. Borsanyi, G. Endrodi, Z. Fodor, S. Katz, and K. Szabo, "Precision SU(3) lattice thermodynamics for a large temperature range," *JHEP* **1207** (2012) 056, arXiv:1204.6184 [hep-lat].

[204] E. Witten, "Current Algebra Theorems for the U(1) Goldstone Boson," *Nucl. Phys.* **B 156** (1979) 269.

[205] J. Schechter, "Effective Lagrangian with Two Color Singlet Gluon Fields," *Phys. Rev.* **D 21** (1980) 3393–3400.

[206] R. Gomm, P. Jain, R. Johnson, and J. Schechter, "Scale anomaly and the scalars," *Phys. Rev.* **D 33** (1986) 801.

[207] J. Braun and H. Gies, "Running coupling at finite temperature and chiral symmetry restoration in QCD," *Phys. Lett.* **B 645** (2007) 53–58, arXiv:hep-ph/0512085 [hep-ph].

[208] F. Karsch and H. Wyld, "Complex Langevin Simulation of the SU(3) Spin Model With Nonzero Chemical Potential," *Phys. Rev. Lett.* **55** (1985) 2242.

[209] M.-P. Lombardo, "An Introduction to lattice QCD at nonzero temperature and density," arXiv:hep-lat/0210040 [hep-lat].

[210] J. Weber, S. Diehl, T. Kuske, and M. Wagner, "An introduction to lattice hadron spectroscopy for students without quantum field theoretical background," arXiv:1310.1760 [hep-lat].

[211] H. Rothe, "Lattice gauge theories: An Introduction," *World Sci. Lect. Notes Phys.* **43** (1992) 1–381.

[212] T. DeGrand and C. E. Detar, *Lattice methods for quantum chromodynamics.* World Sci., 2006.

[213] A. Zacchi, "Ein drei flavor Quark-Meson Modell für kompakte Sterne," Master's thesis, Goethe Universität Frankfurt, June, 2013.

[214] G. Eichmann, R. Alkofer, C. Fischer, A. Krassnigg, and D. Nicmorus, "Baryons in and beyond the quark-diquark model," *AIP Conf. Proc.* **1374** (2011) 617–620, arXiv:1010.0206 [hep-ph].

[215] M. Oettel, *Baryons as relativistic bound states of quark and diquark.* PhD thesis, Tübingen University, 2000. arXiv:nucl-th/0012067 [nucl-th].

[216] D. Ebert and T. Jurke, "Effective chiral meson - baryon Lagrangian from path integral hadronization of a quark diquark model," *Phys. Rev.* **D 58** (1998) 034001, arXiv:hep-ph/9710390 [hep-ph].

[217] A. Buck, R. Alkofer, and H. Reinhardt, "Baryons as bound states of diquarks and quarks in the Nambu-Jona-Lasinio model," *Phys. Lett.* **B 286** (1992) 29–35.

[218] C. S. Fischer, L. Fister, J. Luecker, and J. M. Pawlowski, "Polyakov loop potential at finite density," arXiv:1306.6022 [hep-ph].

[219] G. Endrodi, Z. Fodor, S. Katz, and K. Szabo, "The QCD phase diagram at nonzero quark density," *JHEP* **1104** (2011) 001, arXiv:1102.1356 [hep-lat].

[220] N. M. Bratovic, T. Hatsuda, and W. Weise, "Role of Vector Interaction and Axial Anomaly in the PNJL Modeling of the QCD Phase Diagram," *Phys. Lett.* **B 719** (2013) 131–135, arXiv:1204.3788 [hep-ph].

[221] J. Steinheimer and S. Schramm, "The problem of repulsive quark interactions - Lattice versus mean field models," *Phys. Lett.* **B 696** (2011) 257–261, arXiv:1005.1176 [hep-ph].

[222] J. Steinheimer and S. Schramm, "Constraining the vector interaction strength of QCD," arXiv:1401.4051 [nucl-th].

[223] E. Fraga, L. Palhares, and C. Villavicencio, "Quark mass and isospin dependence of the deconfining critical temperature," *Phys. Rev.* **D 79** (2009) 014021, arXiv:0810.1060 [hep-ph].

[224] L. Palhares, E. Fraga, and C. Villavicencio, "Mass and chemical asymmetry in QCD matter," *Nucl. Phys.* **A 820** (2009) 287C–290C, arXiv:0810.2742 [hep-ph].

[225] D. Toublan and J. Kogut, "Isospin chemical potential and the QCD phase diagram at nonzero temperature and baryon chemical potential," *Phys. Lett.* **B 564** (2003) 212–216, arXiv:hep-ph/0301183 [hep-ph].

[226] M. Frank, M. Buballa, and M. Oertel, "Flavor mixing effects on the QCD phase diagram at nonvanishing isospin chemical potential: One or two phase transitions?," *Phys. Lett.* **B 562** (2003) 221–226, arXiv:hep-ph/0303109.

[227] A. Barducci, R. Casalbuoni, G. Pettini, and L. Ravagli, "A Calculation of the QCD phase diagram at finite temperature, and baryon and isospin chemical potentials," *Phys. Rev.* **D 69** (2004) 096004, arXiv:hep-ph/0402104.

[228] L.-y. He, M. Jin, and P.-f. Zhuang, "Pion superfluidity and meson properties at finite isospin density," *Phys. Rev.* **D 71** (2005) 116001, arXiv:hep-ph/0503272 [hep-ph].

[229] D. Ebert and K. Klimenko, "Gapless pion condensation in quark matter with finite baryon density," *J. Phys.* **G 32** (2006) 599–608, arXiv:hep-ph/0507007.

[230] D. Ebert and K. Klimenko, "Pion condensation in electrically neutral cold matter with finite baryon density," *Eur. Phys. J.* **C 46** (2006) 771–776, arXiv:hep-ph/0510222.

[231] J. O. Andersen and L. Kyllingstad, "Pion Condensation in a two-flavor NJL model: the role of charge neutrality," *J. Phys.* **G 37** (2009) 015003, arXiv:hep-ph/0701033 [hep-ph].

[232] H. Abuki, R. Anglani, R. Gatto, M. Pellicoro, and M. Ruggieri, "The Fate of pion condensation in quark matter: From the chiral to the real world," *Phys. Rev.* **D 79** (2009) 034032, arXiv:0809.2658 [hep-ph].

[233] X. Kang, M. Jin, J. Xiong, and J. Li, "The influence of magnetic field on the pion superfluidity and phase structure in the NJL model," arXiv:1310.3012 [hep-ph].

[234] K. Kamikado, N. Strodthoff, L. von Smekal, and J. Wambach, "Fluctuations in the quark-meson model for QCD with isospin chemical potential," *Phys. Lett.* **B 718** (2013) 1044–1053, arXiv:1207.0400 [hep-ph].

[235] T. Sasaki, Y. Sakai, H. Kouno, and M. Yahiro, "QCD phase diagram at finite baryon and isospin chemical potentials," *Phys. Rev.* **D 82** (2010) 116004, arXiv:1005.0910 [hep-ph].

[236] R. Cavagnoli, D. P. Menezes, and C. Providência, "Phase structure of hadronic and Polyakov-loop extended NJL model at finite isospin density," arXiv:1307.2112 [nucl-th].

[237] H. Ueda, T. Z. Nakano, A. Ohnishi, M. Ruggieri, and K. Sumiyoshi, "QCD phase diagram at finite baryon and isospin chemical potentials in Polyakov loop extended quark meson model with vector interaction," *Phys. Rev.* **D 88** (2013) 074006, arXiv:1304.4331 [nucl-th].

[238] D. Toublan and J. B. Kogut, "The QCD phase diagram at nonzero baryon, isospin and strangeness chemical potentials: Results from a hadron resonance gas model," *Phys. Lett.* **B 605** (2005) 129–136, arXiv:hep-ph/0409310 [hep-ph].

[239] J. O. Andersen, "Pion and kaon condensation at finite temperature and density," *Phys. Rev.* **D 75** (2007) 065011, arXiv:hep-ph/0609020 [hep-ph].

[240] T. Xia, L. He, and P. Zhuang, "Three-flavor Nambu–Jona-Lasinio model at finite isospin chemical potential," *Phys. Rev.* **D 88** (2013) 056013, arXiv:1307.4622 [hep-ph].

[241] G. Bali, P. Bruns, S. Collins, M. Deka, B. Glasle, *et al.*, "Nucleon mass and sigma term from lattice QCD with two light fermion flavors," *Nucl. Phys.* **B 866** (2013) 1–25, arXiv:1206.7034 [hep-lat].

[242] A. Dumitru, D. Roder, and J. Ruppert, "The Quark mass dependence of T(c) in QCD: Working up from m = 0 or down from m = infinity?," *Phys. Rev.* **D 70** (2004) 074001, arXiv:hep-ph/0311119 [hep-ph].

[243] E. Fraga, B. Mintz, and J. Schaffner-Bielich, "A search for inverse magnetic catalysis in thermal quark-meson models," arXiv:1311.3964 [hep-ph].

[244] T. Fischer, D. Blaschke, M. Hempel, T. Klahn, R. Lastowiecki, *et al.*, "Core collapse supernovae in the QCD phase diagram," *Phys. Atom. Nucl.* **75** (2012) 613–620, arXiv:1103.3004 [astro-ph.HE].

[245] N. Nishimura, T. Fischer, F.-K. Thielemann, C. Frohlich, M. Hempel, *et al.*, "Nucleosynthesis in core-collapse supernova explosions triggered by a quark-hadron phase transition," *Astrophys. J.* **758** (2012) 9, arXiv:1112.5684 [astro-ph.HE].

[246] B. Dasgupta, T. Fischer, S. Horiuchi, M. Liebendorfer, A. Mirizzi, *et al.*, "Detecting the QCD phase transition in the next Galactic supernova neutrino burst," *Phys. Rev.* **D 81** (2010) 103005, arXiv:0912.2568 [astro-ph.HE].

[247] J. Langer, "Statistical theory of the decay of metastable states," *Annals Phys.* **54** (1969) 258–275.

[248] J. D. Gunton, M. San Miguel, and P. S. Sahni, "The Dynamics of First Order Phase Transitions," in *Phase Transitions and Critical Phenomena*, Domb, C. and Lebowitz J., ed., vol. 8, pp. 269–466. Academic Press, London, 1983.

[249] J. W. Cahn and J. E. Hilliard, "Free Energy of a Nonuniform System. I. Interfacial Free Energy," *Journal of Chemical Physics* **28** (1958) 258–267.

[250] J. W. Cahn and J. E. Hilliard, "Free Energy of a Nonuniform System. III. Nucleation in a Two-Component Incompressible Fluid," *Journal of Chemical Physics* **31** (1959) 688–699.

[251] S. R. Coleman, V. Glaser, and A. Martin, "Action Minima Among Solutions to a Class of Euclidean Scalar Field Equations," *Commun. Math. Phys.* **58** (1978) 211.

[252] M. Gleiser and R. O. Ramos, "Thermal fluctuations and validity of the one loop effective potential," *Phys. Lett.* **B 300** (1993) 271–277, arXiv:hep-ph/9211219 [hep-ph].

[253] R. O. Ramos, "Subcritical fluctuations at the electroweak phase transition," *Phys. Rev.* **D 54** (1996) 4770–4779, arXiv:hep-ph/9607417 [hep-ph].

[254] S. R. Coleman, "The Fate of the False Vacuum. 1. Semiclassical Theory," *Phys. Rev.* **D 15** (1977) 2929–2936.

[255] J. Callan, Curtis G. and S. R. Coleman, "The Fate of the False Vacuum. 2. First Quantum Corrections," *Phys. Rev.* **D 16** (1977) 1762–1768.

[256] S. Coleman, *Aspects of Symmetry.* Cambridge University Press, Cambridge, England, 1988.

[257] D. Kashchiev, *Nucleation: Basic Theory with Applications.* Butterworth Heinemann, New York, 2000.

[258] H. Vehkamaeki, *Classical Nucleation Theory in Multicomponent Systems.* Springer, New York, 2006.

[259] A. D. Linde, "Decay of the False Vacuum at Finite Temperature," *Nucl. Phys.* **B 216** (1983) 421.

[260] E. J. Weinberg, "Vacuum decay in theories with symmetry breaking by radiative corrections," *Phys. Rev.* **D 47** (1993) 4614–4627, arXiv:hep-ph/9211314 [hep-ph].

[261] B. Beinlich, F. Karsch, and A. Peikert, "SU(3) latent heat and surface tension from tree level and tadpole improved actions," *Phys. Lett.* **B 390** (1997) 268–274, arXiv:hep-lat/9608141 [hep-lat].

[262] B. Lucini, M. Teper, and U. Wenger, "Properties of the deconfining phase transition in SU(N) gauge theories," *JHEP* **0502** (2005) 033, arXiv:hep-lat/0502003 [hep-lat].

[263] R. Rajaraman, *Solitons And Instantons. An Introduction To Solitons And Instantons In Quantum Field Theory.* North-Holland, Amsterdam, 1982.

[264] L. F. Palhares and E. S. Fraga, "Droplets in the cold and dense linear sigma model with quarks," *Phys. Rev.* **D 82** (2010) 125018, arXiv:1006.2357 [hep-ph].

[265] M. B. Pinto, V. Koch, and J. Randrup, "The Surface Tension of Quark Matter in a Geometrical Approach," *Phys. Rev.* **C 86** (2012) 025203, arXiv:1207.5186 [hep-ph].

[266] T. Boeckel and J. Schaffner-Bielich, "A little inflation in the early universe at the QCD phase transition," *Phys. Rev. Lett.* **105** (2010) 041301, arXiv:0906.4520 [astro-ph.CO].

[267] S. Schettler, T. Boeckel, and J. Schaffner-Bielich, "Imprints of the QCD Phase Transition on the Spectrum of Gravitational Waves," *Phys. Rev.* **D 83** (2011) 064030, arXiv:1010.4857 [astro-ph.CO].

[268] J. Randrup, "Phase transition dynamics for baryon-dense matter," *Phys. Rev.* **C 79** (2009) 054911, arXiv:0903.4736 [nucl-th].

[269] J. Steinheimer and J. Randrup, "Spinodal amplification of density fluctuations in fluid-dynamical simulations of relativistic nuclear collisions," *Phys. Rev. Lett.* **109** (2012) 212301, arXiv:1209.2462 [nucl-th].

[270] J. I. Kapusta, A. P. Vischer, and R. Venugopalan, "Nucleation of quark - gluon plasma from hadronic matter," *Phys. Rev.* **C 51** (1995) 901–910, arXiv:nucl-th/9408029 [nucl-th].

[271] L. Csernai and I. Mishustin, "Fast hadronization of supercooled quark - gluon plasma," *Phys. Rev. Lett.* **74** (1995) 5005–5008.

[272] P. Gossiaux, R. Bierkandt, and J. Aichelin, "Tomography of a quark gluon plasma at RHIC and LHC energies," *Phys. Rev.* **C 79** (2009) 044906, arXiv:0901.0946 [hep-ph].

[273] C. S. Fischer, A. Maas, and J. M. Pawlowski, "On the infrared behavior of Landau gauge Yang-Mills theory," *Annals Phys.* **324** (2009) 2408–2437, arXiv:0810.1987 [hep-ph].

[274] H. Gies and C. Wetterich, "Renormalization flow of bound states," *Phys. Rev.* **D 65** (2002) 065001, arXiv:hep-th/0107221 [hep-th].

[275] S. Floerchinger and C. Wetterich, "Exact flow equation for composite operators," *Phys. Lett.* **B 680** (2009) 371–376, arXiv:0905.0915 [hep-th].

Acknowledgements

„Ich grüße alle und den Rest der Welt“
Spider Murphy Gang

I am deeply grateful to Bruno Werneck Mintz for waking up my passion for the topic and for an inspiring collaboration. I thank him for his support of my research stay at the Department for Theoretical Physics at the Physics Institute of the Federal University of Rio de Janeiro and I am much obliged to him and his wife Natalie for their hospitality in Rio.

I am very thankful to Eduardo S. Fraga for a fruitful collaboration, for many valuable discussions and for showing me how to tackle physics questions the smart way. I am much obliged to him for his support of my research stay at the Department for Theoretical Physics at the Physics Institute of the Federal University of Rio de Janeiro and his hospitality. I thank him for the discussions about my future in science and for his support of the very same.

Jan M. Pawlowski earns a big thanks for giving me the possibility to participate in some of his research and for giving me insight into the exciting science of applying functional methods to QCD. I thank him for many valuable discussions and his support.

Of course a unique thanks goes to Jürgen Schaffner-Bielich for giving me the opportunity to do this research and for all the discussions we had. I am very grateful to him that he made it possible for me to participate in conferences, workshops and schools. As well, I thank him for his support of my scientific career.

I thank Lisa M. Haas, Tina Katharina Herbst and Mario Mitter for valuable collaborations. I am thankful to them that they shared their knowledge with me and for the valuable discussions we have.

For collaboration on our common publications I give sincere thanks to Jens Braun, Rudnei O. Ramos and Bernd-Jochen Schaefer.
My special thanks go to Leonard Fister, Letícia F. Palhares and Nils Strodthoff for valuable discussions.

For the good time in Jürgen's working group I thank Thomas Beisitzer, Tillmann Boeckel, Debarati Chatterjee, Thorben Graf, Matthias Hempel, Marget Maly, Giuseppe Pagliara, Irina Sagert, Simon Schettler, Simon Weissenborn and Andreas Zacchi.
I am thankful to Giuseppe Colucci, Thorben Graf, Anja Habersetzer, Achim Heinz and Stanislaus Janowski for having a good time at Frankfurt University and our coffee breaks. Thorben earns a special thanks for the fuel of innumerable coffees that helped

me to get through finishing this thesis.
For showing me the beauty of the marvellous Rio de Janeiro during my research stay I thank Anderson Kendi Kohara.

I am very grateful to Carsten Greiner for giving me the chance to gain experience in teaching and for his support.
For his support of my scientific career I am indebted to Sascha Vogel.
I thank Joerg Aichelin, Eduardo S. Fraga, Takeshi Kodama and Bernd-Jochen Schaefer for their approval of my scientific achievements that gave and gives me confidence.

I am much obliged to Jürgen Berges for his acceptance of being reviewer of my thesis and sincere thanks are given to him, Eva Grebel and Klaus Reygers for building with Jürgen Schaffner-Bielich the examination committee of my disputation.

For their manifold, valuable support I thank the secretaries and administration of the Institutes for Theoretical Physics in Heidelberg and Frankfurt, of the Heidelberg Graduate School of Fundamental Physics (HGSFP) and of the Helmholtz Graduate School for Hadron and Ion Research (HGS-HIRe for FAIR).
I thank the Graduate Program for Hadron and Ion Research (GP-HIR), the Gesellschaft für Schwerionenforschung (GSI), the Frankfurt Institute for Advanced Studies (FIAS) and the Helmholtz Graduate School for Hadron and Ion Research (HGS-HIRe for FAIR) for their funding and financial support.

Special thanks goes to my brother, Holger for his passion for physics that called my curiosity and I thank my parents for their valuable, manifold support.
To end with a personal note, I thank my Upper-Bavarian homeland for the strength and serenity it mediates.

Affidavit according to § 8 of the doctoral degree regulations of the Combined Faculty of Natural Sciences and Mathematics

This thesis I have submitted entitled 'On the Thermodynamics and Phase Structure of Strongly-Interacting Matter in a Polyakov-loop–extended Constituent-Quark Model' is my own work.

I have only used the sources indicated and have not made unauthorised use of services of a third party. Where the work of others has been quoted or reproduced, the source is always given.

I have not yet presented this thesis or parts thereof to a university as part of an examination or degree.

I confirm that the declarations made above a correct.

I am aware of the importance of a sworn affidavit and the criminal prosecution in case of a false or incomplete affidavit.

I affirm that the above is the absolute truth to the best of my knowledge and that I have not concealed anything.

Heidelberg, 2014-02-17